Performance-Based Assessment of Road Design Elements using LiDAR Technology: Towards Adopting a Safe System Approach

by

Suliman Ali Gargoum

A thesis submitted in partial fulfillment of the requirements for the degree of

Doctor of Philosophy

in

Transportation Engineering

Department of Civil and Environmental Engineering
University of Alberta

ABSTRACT

The adoption of a safe system approach is seen by many as a critical element to achieving the aims of vision zero (i.e., eliminating fatalities and serious injuries on roads). Unlike in traditional approaches, in a safe system approach it is acknowledged that road users are humans who are prone to make errors and that the result of those errors should not be a serious injury or fatality. Accordingly, a safe system approach adopts a human-centric design philosophy whereby human fallibility and human vulnerability must be understood and integrated into the design of all elements of road infrastructure.

Despite it being introduced more than two decades ago, efforts to integrate the safe system philosophy into national highway design guides have been limited. In fact, there is no information in design guides on the extent to which a road designed to meet minimum design requirements is able to handle driver demand. Furthermore, the safety impacts of meeting or deviating from recommended design standards are also unknown. Despite this lack of information, roads are still built to meet standards recommended in design guides. Safety problems occur on those roads and are often addressed by introducing certain countermeasures, which sometimes include geometric changes to a road's alignments. Although those countermeasures are often effective in improving safety on the existing highways, they do not address the root cause of the problem. In other words, the fact that deficiencies in recommended design standards might have contributed to certain safety problems on the existing highways is often neglected when new roads are designed. New roads are usually designed to meet the same standards as existing roads, which results in the same safety problems. This contradicts the core principles of a safe system approach where it is required that safety problems and the systems failure to accommodate driver demand are understood and integrated into the design process.

To address this problem, this thesis proposes the adoption of a performance-based design (PBD) approach whereby links between driver capabilities, safety performance, and geometric design elements on existing roads are first established when formulating design requirements for new facilities. One obstacle to the adoption of such an approach is the challenges associated with surveying information about geometric design elements of roads on a large scale. Therefore, the first phase of this thesis focuses on the development of novel algorithms that facilitate large-scale extraction and assessment of different geometric elements on highways scanned using mobile

Light Detection and Ranging (LiDAR) technology. In particular, the first phase focuses on the development, testing, and validation of algorithms for (i) extraction and slope estimation of road cross-sections, (ii) the detection and the extraction of attributes of horizontal alignments, (iii) the inventory and clearance assessment of overhead assets, and (iv) the assessment of sight distances. The developed algorithms are fully automated and facilitate assessment of the aforementioned features along entire highway corridors in an efficient and accurate manner.

The second phase of the thesis focuses on conducting a performance-based assessment of stopping sight distance (SSD) requirements on highways. The performance-based assessment is conducted deterministically and probabilistically with the aims of (i) developing an understanding of the underlying links between demand for sight distance, geometric integrity, and safety performance on existing highways, and (ii) developing a framework for future studies interested in conducting a performance-based assessment of other geometric design elements. The assessment is conducted on over 40km of crash prone highways in Alberta where available sight distance is first quantified and then assessed against deterministically defined, and stochastically simulated driver demand. Among other findings, the assessment revealed that a significant proportion of the analyzed highways did not satisfy the SSD requirements of up to 70% of the driving population. These finding indicate the importance of adopting a probabilistic performance-based approach, which integrates driver capabilities and anticipated safety performance when designing new highway facilities.

In addition to facilitating performance-based assessment of highway geometric elements, algorithms developed in this thesis can be used for efficient network-level asset management as well as for the assessment of structural integrity of geometric elements on roads.

PREFACE

Work presented in this thesis is either published or is under-review for publication in various journals in the areas of transportation engineering, civil engineering, and remote sensing.

PAPERS PUBLISHED

1. **Gargoum et al.** (2018) "*A Fully Automated Approach to Extract and Assess Road Cross Sections from Mobile Lidar Data*" IEEE Transactions in Intelligent Transportation Systems. <u>Accepted December 2017</u>.
2. **Gargoum et al.** (2018) "*Automated Extraction of Horizontal Curve Attributes using LiDAR Data*" Transportation Research Record: Journal of the Transportation Research Board, <u>Accepted October 2017</u>.
3. **Gargoum et al.** (2018) "*Assessment of Stopping and Passing Sight Distance on Highways Using Mobile LiDAR Data.*" Journal of Computing in Civil Engineering, <u>Accepted October 2017</u>.
4. **Gargoum et al.** (2018) "*Automated Assessment of Vertical Clearance on Highways Scanned Using Mobile LiDAR Technology*" Journal of Automation in Construction. <u>Accepted August 2018</u>.
5. **Gargoum et al.** (2018) "*Network-Level Clearance Assessment Using LiDAR to Improve the Reliability and Efficiency of Issuing Over-Height Permits on Highways*" Transportation Research Record: Journal of the Transportation Research Board, <u>Accepted October 2017</u>.
6. **Gargoum et al.** (2018) "*Available Sight Distance on Existing Highways: Meeting Stopping Sight Distance Requirements of an Ageing Population*" Accident Analysis & Prevention, <u>Accepted January 2018</u>.

PAPERS UNDER REVIEW

7. **Gargoum** & El-Basyouny (2019) "*A Literature Synthesis of LiDAR Applications in Transportation: Feature Extraction and Geometric Assessments of Highways*", <u>Under Review</u>.
8. **Gargoum** & El-Basyouny (2019) "*Analysing the Ability of Crash Prone Highways to Handle Stochastically Modelled Driver Demand for Stopping Sight Distance*", <u>Under Review</u>.
9. **Gargoum** & El-Basyouny (2019) "*Impacts of Point Cloud Density Reductions on Extracting Road Geometric Features from LiDAR data*", <u>Under Review</u>.

Dedicated To My Parents

Salma El-Feituri & Ali Gargoum

... و قل ربي ارحمهما كما ربياني صغيرا ...

ACKNOWLEDGEMENTS

TABLE OF CONTENTS

LIST OF FIGURES

LIST OF TABLES

LIST OF ABBREVIATIONS

AASHTO: American Association of State Highway and Transportation Officials

ADA: Americans with Disabilities Act

ALS: Aerial Laser Scan

ASD: Available Sight Distance

AT: Alberta Transportation

AV: Autonomous Vehicles

CSRS: Canadian Spatial Reference System

CS: Cross slopes

DBD: Displacement Based Design

DBSCAN: Density-Based Spatial Clustering of Application with Noise

DMI: Distance Measurement Indicators

DSM: Digital Surface Model

DTM: Digital Terrain Model

EB: Eastbound

FHWA: Federal Highway Administration

GVF: Gradient Vector Flow

HD: Height Difference

HSM: Highway Safety Manual

IDW: Inverse Distance Weighted Interpolation

IMU: Inertial Measurement Unit

kNN: k-Nearest Neighbour

LDH: Local Descriptor Histograms

MARS: Multivariate Adaptive Regression Splines

MHD: Maximum Height Difference

MLS: Mobile Laser Scan

NAD83: North American Datum 1983

NB: Northbound

NCHRP: National Cooperative Highway Research Program

PBD: Performance Based Design

PC: Point of Curvature

PCA: Principle Component Analysis

PDF: Probability Density Function

PI: Point of Intersection

PRT: perception reaction time

PT: Point of Tangency

RFIP: Roadside Feature Inventory Program

ROI: Region of Interest

SB: Southbound

SS: Side slopes

SSD: Stopping Sight Distance

T: Tangent

TAC: Transportation Association of Canada

TIN: Triangular Irregular Network

TRB: Transportation Research Board

V2I: Vehicle to Infrastructure

WB: Westbound

1 INTRODUCTION

1.1 BACKGROUND & MOTIVATION

1.1.1 THE SAFE SYSTEM APPROACH

The past decade has seen a significant number of transportation agencies shift their strategy towards adopting Vision Zero. Vision Zero originated in Sweden two decades ago with the aims of completely eliminating fatalities and serious injuries on roads. The vision is an expression of the ethical imperative that the cost of mobility should not be the loss of life or serious injury to any road user [1].

Despite those aspirational aims and continuous efforts to improve road safety, collision statistics in many developed countries show that the downward trend in fatalities observed in the late 1970s and 80s due to major legislative changes including the introduction of seatbelts started to level out in the past two decades, as illustrated in Figure 1. This indicates that, while effective in reducing a significant proportion of serious collisions in the past, conventional countermeasures including the introduction of seatbelt legislation must be supplemented with more innovative and informed techniques to maximize the chances of completely eliminating fatalities and serious injuries on roads.
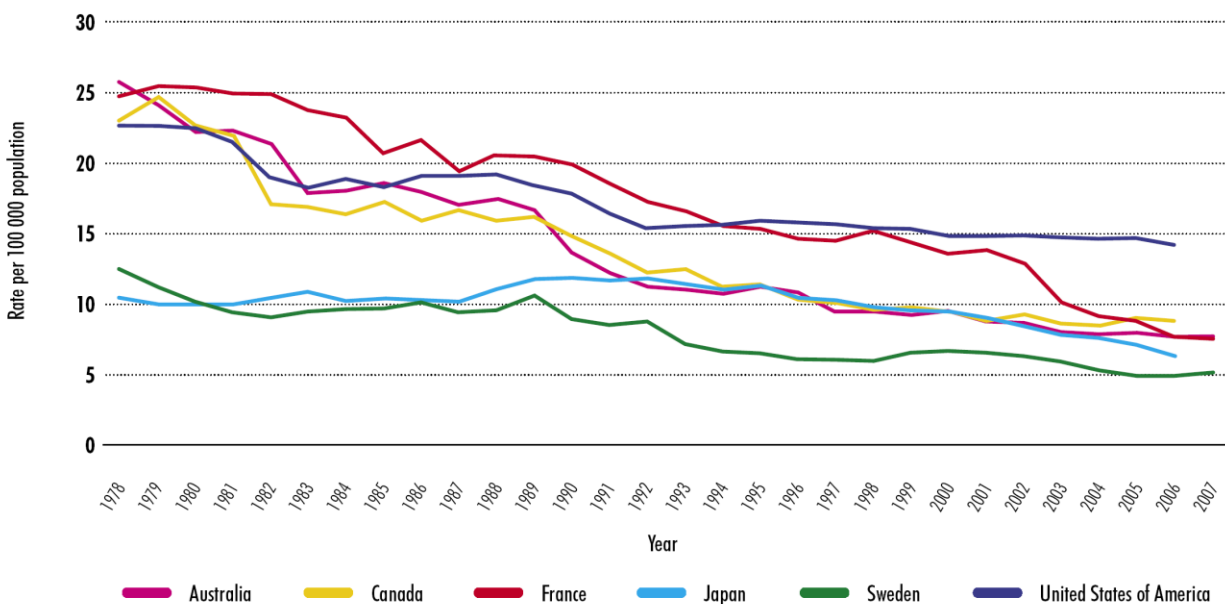
Figure 1: Fatality Trends in Developed Countries[2]

Many researchers and road safety experts agree that a critical element to achieving the aims of Vision Zero is the adoption of a Safe System Approach [3-5]. In a Safe System Approach, the key principle of designing any roadway facility is to take human fallibility and vulnerability into account [4,6]. Although effective management of traffic safety includes managing the 3E's of traffic safety (Engineering, Enforcement, and Education), experts have recently shifted the attention from blaming drivers for safety problems, to designing systems that are able to accommodate driver limitations. To that end, roads are designed in a manner that caters to driver capabilities and one that is more forgiving of human error. Contrary to the conventional design approach, where highways are designed based on predefined guidelines that have been set several decades ago, a safe system approach, in principle, would require understanding limitations of drivers and formulating design standards to accommodate those limitations [6].

Although the Safe System Approach was introduced more than two decades ago, efforts to integrate its principles into national roadway design guides have been limited. The next few sections describe the current highway design process and the means through which it could be transformed into a performance-based process that is consistent with the principles of the safe system approach.

1.1.2 *Traditional Geometric Design*

In current practice, geometric design of highways is regulated by a set of policies, standards, and provisions recommended in national design guides. In the US the national design guide titled "A Policy on Geometric Design of Highways and Streets" is published by the American Association of State Highway and Transportation Officials (AASHTO) [7]. Similarly, the "Geometric Design Guide for Canadian Roads" by the Transportation Association of Canada (TAC) governs design on Canadian highways [8]. In fact, many jurisdictions across North America and the world have developed local design guides to regulate the design process on local highways. The province of Alberta, for instance, published the first version of its local guide for the design of Albertan Highways in 1995 [9]. The value of local design guides lies in their ability to supplement national guides with information that takes local conditions into consideration.

Design guides consist of recommendations, specifications, and mathematical procedures developed to assist Engineers in selecting design values for different geometric elements on a highway [7-9]. Whether it is for the construction of new facilities, reconstruction, resurfacing or

rehabilitation of existing facilities, design guides represent a valuable resource for engineers and designers. Such guides are essential to the uniformity and consistency of highway design. Moreover, the recommended standards are also set to help promote safe and efficient operation of traffic on roads.

Although, design guides are developed with some consideration to safety, the guidelines do not provide much information on the anticipated safety performance on roads designed to meet the recommended standards. Consequently, it is unclear how safe a road that meets minimum design guidelines might be. Moreover, there is also a lack of information in design guides on whether a road designed to meet recommended standards satisfies the demands[1] of the driving population. This is extremely concerning, particularly when considering potential changes in population demographics that may affect the capabilities of the average driving population.

The lack of such information is, in part, due to the means through which content is added to and removed from national guides. According to Hauer [10], some of the content added to design guides is based on successful practice, common sense, and expert judgment. Despite the importance of such factors, they do not explicitly account for road user capabilities, neither do they account for safety performance on roads. As a result, Hauer [11] concludes that the safety on roads designed to meet guidelines is unpremeditated.

In an attempt to distinguish the difference between the presumable level of safety achieved by meeting recommendations in design guides and the actual level of safety measured using data observed on roads, Hauer [12] defines two types of safety in highway design, namely, Nominal and Substantive safety. Nominal safety is defined as a measure of whether a roadway, design alternative, or design element, meets minimum design criteria. In contrast, Substantive safety provides a statistically reliable assessment of safety performance.

It is worth noting here that the recent edition of the AASHTO design guide does refer users to the Highway Safety Manual (HSM) as a source of information on the Substantive safety impacts of design. Similarly, the TAC design guide contains some information about Safety Performance Functions for some geometric elements. In fact, since its introduction in 2010, the HSM has been a valuable resource for engineers interested in comparing the safety performance of design

---

[1] "Driver Demand" is used to refer to driver capabilities and limitations as opposed to their desires.

alternatives. However, the HSM does not provide much information on the ability of different design alternatives to accommodate the capabilities of the driving population. Moreover, the HSM does not account for potential interactions between design elements or the relationship between meeting complex design requirements and safety [13]. For instance, while the HSM might be used to compare the safety performance of changing lane width on a road from 11 to 12ft, information on the safety impacts of meeting, or deviating from, standards recommended for other design elements such as stopping sight distance requirements, is limited [13].

Despite the introduction of the HSM, there remains a clear disconnect between information documented in geometric design guides and the actual safety performance of design. Design guides still fail to reveal the safety consequences of meeting, or even deviating from, standards recommended in the guides [14]. Furthermore, there does not seem to be a framework or a process for updating design recommendations to account for research on safety performance on roads or potential changes in road user capabilities, which are elements critical to the adoption of a safe system approach.

In a recent report by the National Cooperative Highway Research Program (NCHRP) updating the design criteria for Passing Sight Distance (PSD) on two-lane highways in AASHTO's design policy, Harwood and Sun [15] write *"These …. criteria have remained virtually unchanged since they were incorporated in the 1954 version of the policy. The 1954 policy used criteria based on a summary report of extensive field observations of passing maneuvers made between 1938 and 1941. Surveys conducted in 1971 and 1978 found that AASHTO values for PSD were conservative, except at passing vehicle speeds above 105 km/h (65 mph). While the vehicle fleet has changed dramatically over the past 50 years, the PSD values in the Green Book remain unchanged."*

Similar to PSD, information in the 4th Edition of AASHTO's roadside design guide, published in 2011, on clear zones was added to the guide in 1977 and has not changed since. What is more concerning is that when referring to recommendations on clear zone design the guide acknowledges that the information and the recommendations *"…are based on limited empirical data that were extrapolated to provide information for a wide range of conditions"[7].* Unfortunately, this issue is not limited to PSD and clearzone design alone but something common in design guides.

In summary, existing design guides lack information on (i) the extent to which roads designed to meet recommended design standards are able to accommodate road users and their abilities, and (ii) the safety impacts of failure to accommodate those capabilities. This lack of information means that accounting for human fallibility when designing new facilities is not possible. Instead, newly constructed facilities are often designed to meet the same recommendations as existing roads, which often result in the same safety problems.

1.1.3 EVIDENCE-BASED DESIGN APPROACH

The shift towards designing forgiving highways that account for human fallibility hinges on adopting a performance-based design approach whereby links between road user's and their capabilities, substantive safety, and design elements on existing highways are established and integrated into initial stages of the design process. Performance-Based Design (PBD) is often described as an approach where design criteria are expressed in terms of achieving a set of performance objectives [16]. In highway design, the ultimate objective is minimizing failure (i.e.,, minimizing collision frequency and severity). This is achieved by understanding road user capabilities and their limitations and designing roads that are able account for those limitations.

One way in which PBD differs from conventional design is that, instead of designing different elements of a highway using preset standards, design requirements are first linked to performance metrics. Design standards are then updated based on their ability to serve the existing population at the desired level of performance. In other words, the standards used in a particular design are formulated based on the anticipated demand and the chances of failure under that demand [16].

Adopting such an approach depends heavily on the existence of three pieces of information: (i) observations of driver behavior, (ii) safety performance records on highways, and (iii) information on the geometric attributes and roadside asset on existing highway infrastructure. Over the past few years, transportation agencies and police departments have been successful in creating a rich database of collision information that accurately reflect the level of safety on roadways. Similarly, attributes of driver behavior such as speeds on a road segment could be collected by monitoring traffic dynamics on highways. In contrast to collision records and driver behaviour, information about highway infrastructure and the geometric attributes of different road features is very sparse, and rarely reflects existing conditions. This is particularly true in the case of complex design elements such as available sight distance on a highway and microscopic elements such as attributes

of horizontal curves or road slopes along a highway corridor. Surveying these geometric attributes requires extended site visits where the presence of crew on the road is necessary. This is a tedious and time consuming process that exposes crew to serious risks, particularly at locations of both high traffic volume and speeds [17]. Considering the size of highway networks in North America, it is extremely challenging to manually survey and inventory attributes of roads using conventional tools.

This lack of information on geometric attributes of roads has placed constraints on researchers looking to perform safety assessments of different roadway infrastructure elements. For instance, in their work assessing the impacts of roadside design on safety, Lee and Mannering [18] describe the lack of information on roadside assets as a "chronic lack of data" that has represented an obstacle to attempts to develop statistical models relating roadside features to collision frequency and severity. According to Hauer [10], the lack of information about design elements and the high costs associated with making adjustments to those elements is one reason why, when investigating the causes of safety problems, focus is often placed on events that happened on the scene and in the build up to the collisions instead of design attributes. Events that occur in the buildup to a collision are seen as causes preventable by human action while design problems are seen as secondary causes since they happened in the distant past and changing them would be extremely costly [10].

One tool which has the potential to help overcome the challenges associated with conventional surveying practice, if properly utilized, is mobile Light Detection and Ranging (LiDAR) remote sensing technology. Unlike traditional surveying, mobile LiDAR scanning produces an accurate 3D point cloud of a road's environment while travelling at highway speeds. This causes minimal disruption to traffic and significantly reduces data collection time. Moreover, since a 3D point cloud of the entire highway is captured, the same dataset can be used to accurately measure multiple geometric elements on a highway. Consequently, given the appropriate processing tools, mobile LiDAR datasets could be used to create a comprehensive province-wide dataset where all details about geometric elements on highways are stored in a single database.

1.1.4 USING LiDAR FOR INFRASTRUCTURE ASSESSMENT

The recent surge in computing power and the high accuracy of datasets collected using LiDAR technology (a form of Remote Sensing) has led many agencies to consider using the technology

for assessing different elements of transportation infrastructure [19,20]. In a recent review on the potential of LiDAR in transportation by the National Cooperative Highway Research Program (NCHRP), LiDAR was described as a technology that has the *"… promise of transforming the way in which transportation agencies plan, design, construct and maintain their highway networks*" [21].

LiDAR data is collected using scanning systems that are equipped with laser scanners, sensors, Global Navigation Satellite System (GNSS) receivers, and inertial measurement units (IMU). The laser scanners constantly emit light beams at surrounding objects and, based on the properties of the reflected beams, compute the exact position of the point off which each beam reflects. Constant scanning of objects around the scanners creates a 3D point cloud of known positional coordinates such as that seen in Figure 2. In Mobile Laser Scanning (MLS), scanners are mounted on vehicles, which travel along the highway of interest capturing highly detailed positional information of the roadway [22].
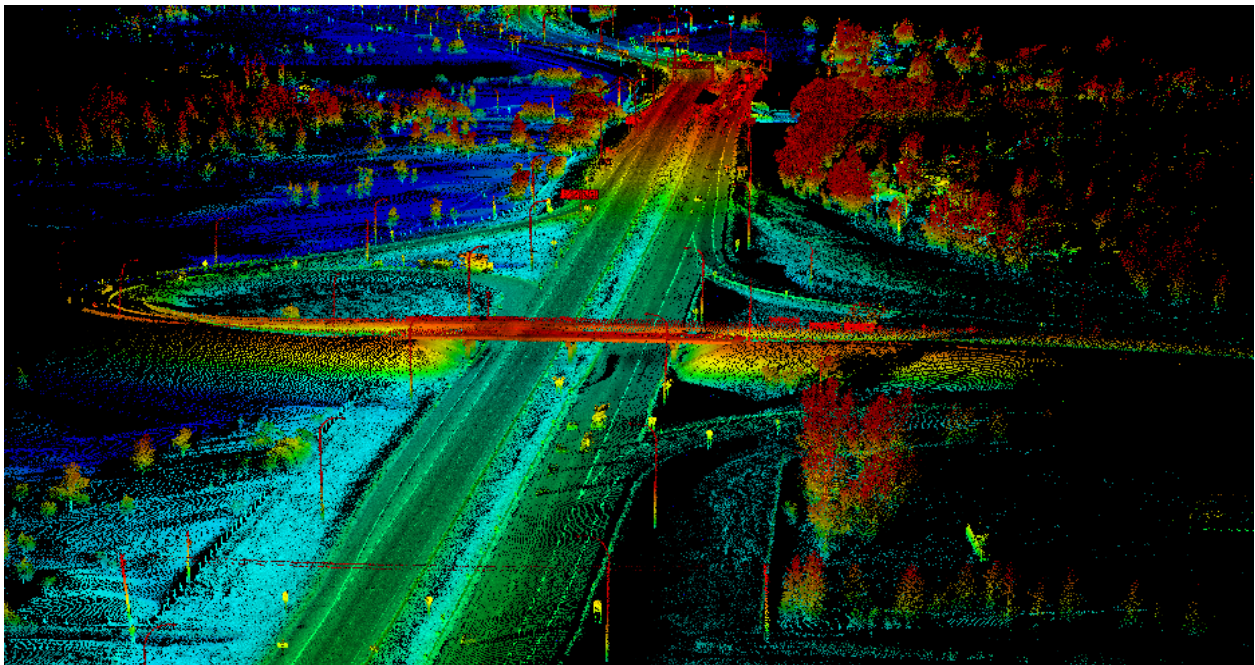
Figure 2: LiDAR Highway

According to many experts, the ability to use LiDAR as an alternative to traditional surveying tools depends on the development of new applications that facilitate the extraction of information from LiDAR point cloud datasets in an efficient manner [23]. In a recent study comparing the efficiency of using different techniques including field inventory, photo-logs, aerial photograph,

and laser scanning (aerial, mobile, and terrestrial) for surveying data required for the HSMs safety prediction models, Jalayer, et al. [24] concluded that mobile LiDAR had the potential to replace all other extraction techniques if more efficient processing and feature extraction methods were developed.

Although many agencies have been considering using LiDAR for transportation applications, research in this area has been fairly limited. Based on the results of a review conducted by the NCHRP in 2013, it was concluded that there was a lack of research on "how" information can be extracted from LiDAR [21]. The report states that "*Generally, most information related to MLS use is from presentations at conferences or short web articles that do not go into detail regarding the work performed.*"

In the past few years research in this area has gained some momentum with particular focus on utilizing LiDAR for the inventory of traffic signs and other pole-like objects [25-32]; however, less focus has been placed on the extraction and assessment of geometric attributes of roads. Even studies that do exist in this capacity suffer from many limitations including the large amount of manual input required when processing the datasets [33-35]. Manual processing demonstrates the feasibility of extracting information from LiDAR while also eliminating the safety risks associated with traditional surveying; however, such procedures are still tedious and time consuming, particularly when network level assessment of microscopic design elements is desired. This failure to fully utilize LiDAR datasets for transportation applications has been primarily attributed to the lack of expertise [21].

In fact, despite entire PhD dissertations being dedicated to feature extraction from LiDAR in the past, not much of that work has focused on the extraction of geometric design elements from LiDAR. Instead, the focus has been on the extraction of on road features such as lane markings and road edges. For instance, Haiyan [36] focuses on the extraction of road edges, lane markings, and pavement cracks from mobile LiDAR data. Similarly, Kumar [37], also dedicated his PhD work to the extraction of road edges, lane markings, and road roughness from LiDAR. In another PhD dissertation, Ai [38] focused his efforts on the extraction of traffic sign information from MLS while also assessing their conditions and establishing links between intensity measurements and sign retro-reflectivity. Huang [39], combined LiDAR information with other sensing technology to develop algorithms for lane detection as part his PhD dissertation, although the

application was developed to assist lane keeping technology within autonomous vehicles, as opposed to mapping elements of road infrastructure. Lu [40] also developed an algorithm for lane marking detection for Autonomous vehicles by combining information extracted from LiDAR and other sensors.

Based on a thorough review of literature conducted as part of this thesis, it was identified that only a handful of studies were found on using LiDAR to perform sight distance assessments [41,42], extract attributes of horizontal curves[34], and extract road cross section information [35,43] from LiDAR. Furthermore, these studies suffer from many limitations. In the case of cross section extraction, for instance, even the few studies that do exist in the literature are limited to the extraction of cross slopes. Similarly, work on sight distance assessments suffer from a number of limitations including the inability to account for overhanging objects, which biases the assessment results. Further discussion of the existing studies and their limitations is provided in Chapter 2 of the thesis.

Research conducted in this thesis aims to overcome the aforementioned limitations by developing algorithms that would help automatically assess and extract critical geometric design elements of highway from LiDAR. Specifically, the first phase of this thesis focuses on extracting elements of a road's vertical and horizontal alignments as well as slope and clearance information. This is done with the aim of providing tools that can be utilized to conduct a performance-based assessment of critical design elements, as demonstrated in the second phase of the thesis.

1.2   PROBLEM STATEMENT

In conventional design, a road is built to meet design standards recommended in design guides, despite the lack of information on whether or not such requirements satisfy the needs of the driving population and without any information on safety consequences of the failure to do so. The road goes into operation and safety problems arise. Addressing those safety problems is often achieved by introducing certain countermeasures on the highway as illustrated in Figure 3. Although countermeasures are effective in addressing the problems on the existing highway, they do not address the issue on newly designed roads. In other words, despite the fact that design deficiencies might have contributed to safety problems that occurred on the existing highway, new roads are still designed to meet the same standards, which results in similar safety problems.
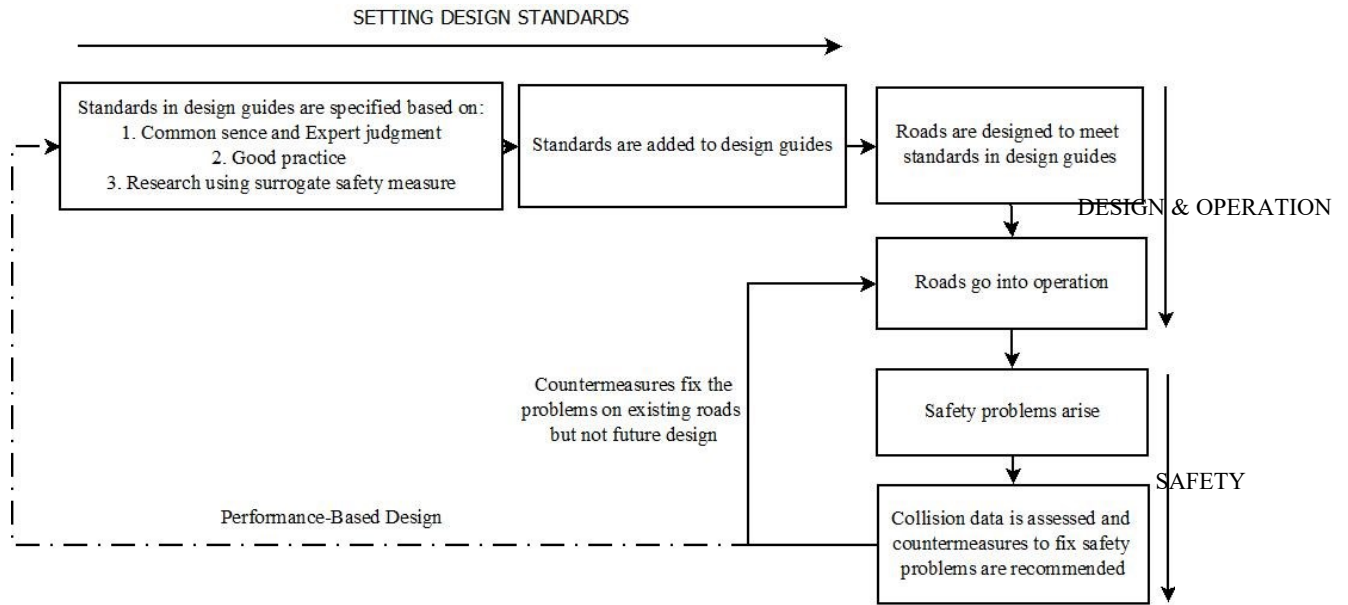
Figure 3: Proposed Design Framework

This is similar to a physician treating the symptoms of a disease but not the actual root-cause. While treating the symptoms might provide temporary relief (i.e., address the problems on existing roads), lessons are not learned from previous experience when designing new facilities due to the disconnect between safety performance and recommended design standards, as illustrated by the dashed line in Figure 3. This naïve approach results in designers constantly falling into the same pitfalls every time.

"A believer should not be stung (by something) out of the same hole twice." – Prophet Mohammed PBUH[2]

Despite the lack of a direct connection between performance on existing roads and design standards, and despite the failure to learn from past experiences, drastic improvements in safety are expected. In fact, the failure to understand the demands of the driving populations (i.e., their abilities) and the consequent failure to integrate those demands into the design of new facilities completely contradicts the core principle of the safe system approach, where it is required that roads are designed to accommodate road user fallibility and human vulnerability.

To overcome such a problem, this thesis proposes the adoption of a performance-based design (PBD) approach. In PBD, design standards are formulated to accommodate the anticipated road

---

[2] PBUH: Peace Be Upon Him

user demand, the ability of existing road infrastructure to handle that demand is then investigated and the impacts of this on safety performance are understood. This ensures that standards used to design new highways account for the issues experienced on existing highways. It is worth noting here that adopting such an approach will not completely eliminate all collisions since poor design is not the only cause of collisions, many collisions are caused by simple driver negligence. Nonetheless, poor design is definitely one major contributing factor that is often ignored.

In fact, the 2011 version of AASHTO's Design Guide advocates the adoption of a performance-based design (PDB) approach, which indicates that even entities responsible for developing design guides acknowledge the importance of migrating towards such an approach. Adopting a PBD approach would help create a framework whereby lessons learned from the interaction between road users and the existing roadway infrastructure can be fed back into the design process as illustrated in Figure 3.

Before PBD can be adopted, however, an efficient method that facilitates large scale assessment of the geometric attributes on existing road infrastructure is required. One way in which this could be achieved is using mobile LiDAR technology. LiDAR datasets collected in mobile laser scans consist of rich point clouds that can be utilized for efficient network-level assessment of road infrastructure, nevertheless, this requires the development of algorithms and processes that facilitate such practice, which is the aim of the first phase of this thesis.

1.3   OBJECTIVES

The ultimate goal of this thesis is to facilitate the adoption of a performance-based design approach whereby a sound connection road user demand, substantive safety, and design elements of road infrastructure could be established. Meeting such a goal requires meeting multiple objectives which are detailed in the next few paragraphs. In addition, the workflow of the research conducted in this thesis is also summarized in Figure 4.

1.3.1   *PHASE I (ALGORITHM DEVELOPMENT AND VALIDATION)*

- Assessing the performance of geometric design elements on existing highways hinges on the development of tools that can be used to efficiently survey those attributes. Accordingly, Phase I of this thesis focuses on developing algorithms for that cause. The research utilizes tools of linear algebra, planimetry, machine learning, and statistical

science to develop a set of novel algorithms that facilitate automated extraction and assessment of critical road design elements on highways scanned using LiDAR technology. Novel automated algorithms are developed for:

- o The extraction of ***road cross sections*** at regular intervals along a highway corridor and the estimation of their slopes. The limited research that exists on the extraction of cross sections from LiDAR datasets suffers from multiple limitations, including the dependence on lane marking information to define the extents of the road and the inability to assess side slopes. The novel algorithm proposed in this thesis adopts *k*-means clustering and Multivariate Adaptive Regression Splines (MARS) to account for detecting end point of cross sections, which facilitates automated estimation of cross and side slope along an entire highway corridor.

- o The detection of ***horizontal alignments*** (simple curves) along a highway corridor and the measurements of their attributes. Unlike the single study that attempted extraction of horizontal curve attributes from LiDAR in the literature, the method proposed in this thesis is fully automated and does not require manual input. Moreover, the proposed method is developed to extract multiple attributes including curve endpoints, deflection angle, curve length, and tangent length, as opposed to focusing on curve radii, which has been the case for most existing studies.

- o The detection, classification of ***overhead assets***, and clearance assessment at those assets. Research in this area is limited to assessing clearance at isolated bridge scans obtained using static LiDAR scanning, which, despite increasing the accuracy of the assessments, does not help increase the efficiency. The novel method proposed in this thesis utilizes machine learning search algorithms to detect overhead assets and assess their clearance. Moreover, statistical kurtosis-balancing is used to classify detected assets, which facilitates large scale inventory, classification, and clearance assessment at bridges and non-bridges on an entire highway corridor.

- o The extraction and assessment of ***available sight distance*** along a highway corridor under different observer and target orientations. Unlike existing work in this area, the algorithms proposed in this thesis utilize mobile LiDAR datasets for the assessment of sight distance. Moreover, the algorithm is fully automated and

accounts for the existence of overhanging objects through applying voxel-based ground segmentation of the data. This ensures that available sight distance along an entire corridor could be estimated in an efficient and accurate manner.

- Once the extraction and assessment algorithms were developed, the algorithms were validated. This was done by testing the algorithms of LiDAR data collected on multiple highway segments in Alberta, Canada. The aim here was to assess the accuracy and the repeatability of the developed algorithms and to ensure that they could be used for large scale assessment of road geometric attributes.

- To further assess the robustness of the proposed algorithms and to develop an understanding of how point cloud density could impact the quality of information extracted from LiDAR, sensitivity analysis of impacts of point cloud density on the quality of the information extracted was also conducted for all four applications. Despite the importance of such information, to the best of the author's knowledge, no study to date has assessed the impacts of reducing point density on the quality of information extracted from LiDAR point clouds for transportation applications. This is true even for features where a significant amount of research exists in the literature such as the extraction of traffic signs from LiDAR.
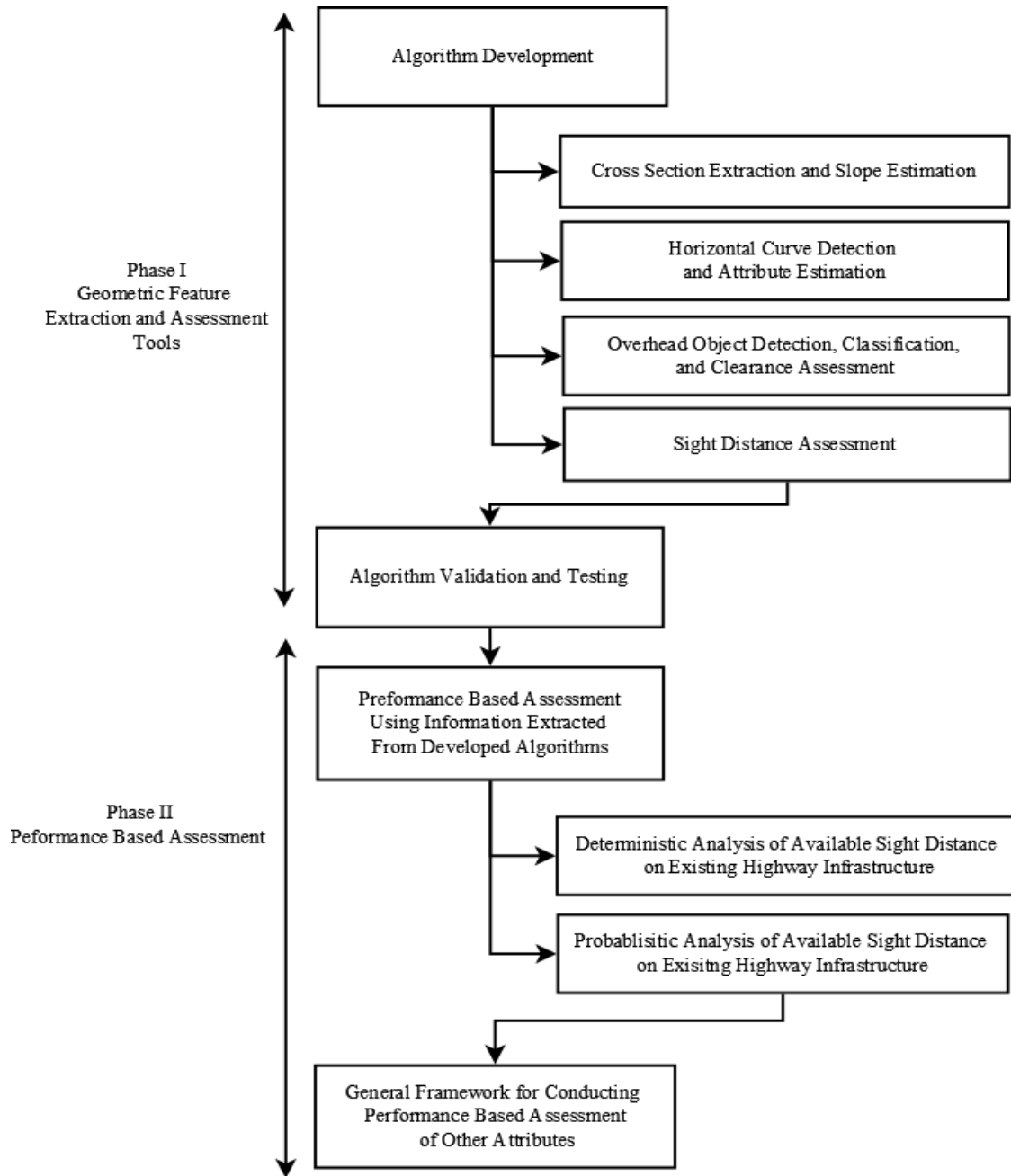
Figure 4: Thesis Workflow

1.3.2 *PHASE II (PERFORMANCE-BASED ASSESSMENT)*

- After the algorithms were developed, tested, and validated, the next objective of the thesis was to investigate the means by which the information extracted from the developed algorithms could be utilized to conduct a performance-based assessment of geometric elements. For this purpose, the focus was placed on a single design element, namely,

stopping sight distance. Two different approaches for conducting a performance-based assessment were projected:

- o The first type of assessment was a deterministic multi-level assessment, whereby different levels of driver demand for stopping sight distance were defined based on the outputs of previous research. The sight distance assessment algorithm was used to quantify sight distance available along over 40km of crash-prone rural highways in Alberta and the performance of the highways under different levels of demand was assessed.

- o The second type of assessment was a probabilistic assessment whereby, demand for stopping sight distance (SSD) was modelled stochastically. One significant limitation of existing design guides is the assumption that driver behavior is deterministic. Unfortunately, this assumption is inaccurate and results in roads being designed to accommodate the needs of a certain class of drivers without much information on the proportion of drivers who fall under that class. To overcome this issue, Monte Carlo Simulation models were developed to model driver demand for stopping sight distance on each of the test highways. A performance-based assessment was then conducted on a similar set of highways to those assessed in the deterministic assessment; however, in the probabilistic assessment it was possible to identify the proportion of drivers impacted by limitations in SSD.

- The aim of the performance-based assessments conducted in this phase of this thesis was twofold: (i) develop an understanding the underlying links between demand for stopping sight distance, geometric integrity, and safety performance on existing highways, and (ii) develop a framework for future studies interested in conducting a performance-based assessment of other geometric elements, while highlighting the differences between conducting a deterministic and a probabilistic assessment.

1.4 THESIS STRUCTURE

The remainder of this thesis is divided into eleven different chapters. Details of the topics covered in each chapter are described below:

Chapter 2 provides a thorough literature review of the applications of LiDAR data in transportation. This includes details of the different algorithms that have been developed to date, the main limitations of research in this area, and the gaps that need to be filled by more research.

- A version of this chapter has been submitted for a potential journal publication under the following title:

  Gargoum & El-Basyouny (2017). "*A Literature Synthesis of LiDAR Applications in Transportation: Feature Extraction and Geometric Assessments of Highways*", Under Review.

Chapter 3 introduces the reader to LiDAR data. This includes information about LiDAR data collection mechanism, the different scanners used to collect data, the accuracy of data acquired using LiDAR technology, and the cost effectiveness of using LiDAR for transportation applications. The chapter also provides details of the scanning system used to collect data for this thesis and describes properties of the dataset compiled for use in this research effort.

Chapter 4, 5, 6, and 7 provide details of the four different algorithms that were developed to perform geometric feature extraction on LiDAR highways. Each chapter includes a detailed description of the extraction pipeline of the proposed algorithm, the results of testing the proposed method on a selection of highways segments, and a thorough discussion of the strengths and weakness of the proposed method.

- Chapter 4 is dedicated to the extraction of road cross sections along LiDAR highways. Furthermore, the chapter also includes information on the algorithm proposed for the measurement of the cross slopes and side slopes at those cross sections.
  - A version of Chapter 7 has been published in the *IEEE Journal of Transactions on Intelligent Transportation Systems*:

    Gargoum et al., (2018) "*A Fully Automated Approach to Extract and Assess Road Cross Sections from Mobile LiDAR Data*" *IEEE Transactions in Intelligent Transportation Systems*. Accepted December 2017.
- Chapter 5 is dedicated to the detection and the extraction of features of horizontal curves on LiDAR highways.

- o A version of this Chapter has published in *Transportation Research Record the Journal of Transportation Research Board*:

    Gargoum et al., (2018). "*Automated Extraction of Horizontal Curve Attributes Using LiDAR Data*" Transportation Research Record: Journal of the Transportation Research Board, <u>Accepted October 2017</u>.

- Chapter 6 is dedicated to the inventory, mapping, and clearance assessment of overhead objects along LiDAR highways.

    - o A version of this Chapter has been published in the *Journal of Automation in Construction*:

        Gargoum et al., (2018). "*Automated Assessment of Vertical Clearance on Highways Scanned Using Mobile LiDAR Technology*" *Journal of Automation in Construction*. <u>Accepted August 2018</u>.

- Chapter 7 is dedicated to the extraction and assessment of available sight distance on LiDAR highways.

    - o A version of this Chapter has been published in the *ASCE Journal of Computing in Civil Engineering*:

        Gargoum et al., (2018) "*Assessment of Stopping and Passing Sight Distance on Highways Using Mobile LiDAR Data.*" Journal of Computing in Civil Engineering, <u>Accepted October 2017</u>.

Chapter 8 explores the impacts of reducing the point cloud density on the quality and accuracy of information extracted from LiDAR using the algorithms prosed in Chapters 4 through 7. The LiDAR point cloud density is first reduced to several different levels using stratified random sampling. Information is then extracted at different levels of point density and the results obtained at the different levels are compared and discussed.

- o A version of this Chapter is being reviewed for a potential journal publication under the following title:

    Gargoum & El-Basyouny (2019) "*Impacts of Point Cloud Density Reductions on Extracting Road Geometric Features from LiDAR data*", <u>Under Review</u>.

Chapter 9 is dedicated to conducting a deterministic performance-based assessment of sight distance. The chapter utilizes the sight distance assessment algorithm proposed in Chapter 7 to

evaluate the sight distance available on the test highways. The performance of the test highway segments under different levels of demand are then evaluated and the results and their implications are discussed.

- o A version of this Chapter has published in the *Journal of Accident Analysis and Prevention*:

  Gargoum et al., (2018). "*Available Sight Distance on Existing Highways: Meeting Stopping Sight Distance Requirements of an Ageing Population*" Accident Analysis and Prevention, <u>Accepted January 2017</u>.

Chapter 10 is dedicated to the stochastic performance-based assessment of sight distance. The first part of the chapter includes details of the Monte Carlo simulation and the process of modelling stopping sight distance demands. The consequent sections include an assessment of the ability of test segments to handle the demand and the safety performance expected at different levels of demand. The closing sections of the chapter include a discussion of the results, their implications, and a framework that summarizes the performance-based design approach proposed in this thesis.

- o A version of this Chapter is being reviewed for a potential journal publication under the following title:

  Gargoum and El-Basyouny (2019). "*Analysing the Ability of Crash Prone Highways to Handle Stochastically Modelled Driver Demand for Stopping Sight Distance*", Under Review.

Chapter 11 includes a summary of the research conducted in this thesis, a discussion of the contributions of this work to the state of the art, and a discussion of avenues through which future research could extend work presented in this thesis.

2 LITERATURE REVIEW

2.1 DEVIATING FROM RECOMMENDED DESIGN STANDARDS

Despite the lack of information between recommended standards and safety existing design guides do require following a thorough process in cases where deviating from design standards is required. Such cases are referred to as design exceptions that can be initiated at any stage of a project. The TAC design guide recommends that in cases where deviations from recommended standards are desired the deviations are supported with appropriate engineering judgment, quantitative analysis, and good, consistent documentation of the reason for the decision. The guide also requires that mitigating strategies are considered and implemented [8].

TAC guidelines describes the process summariesed in Figure 5 as a *"good design exception process"* [8]. When evaluating the impacts of deviating from design requirements the guide requires that impacts from all perspectives are considered. This includes safety, economic, environmental, societal, operational, and cultural impacts. The guide also recommend a set of mitigation strategies that may be considered in cases where deviations are necessary. For instance, if deviations from stopping sight distance standards are required the guide recommends considering speed advisory plaques, more lighting, and adjustments to the road's cross sectional elements.
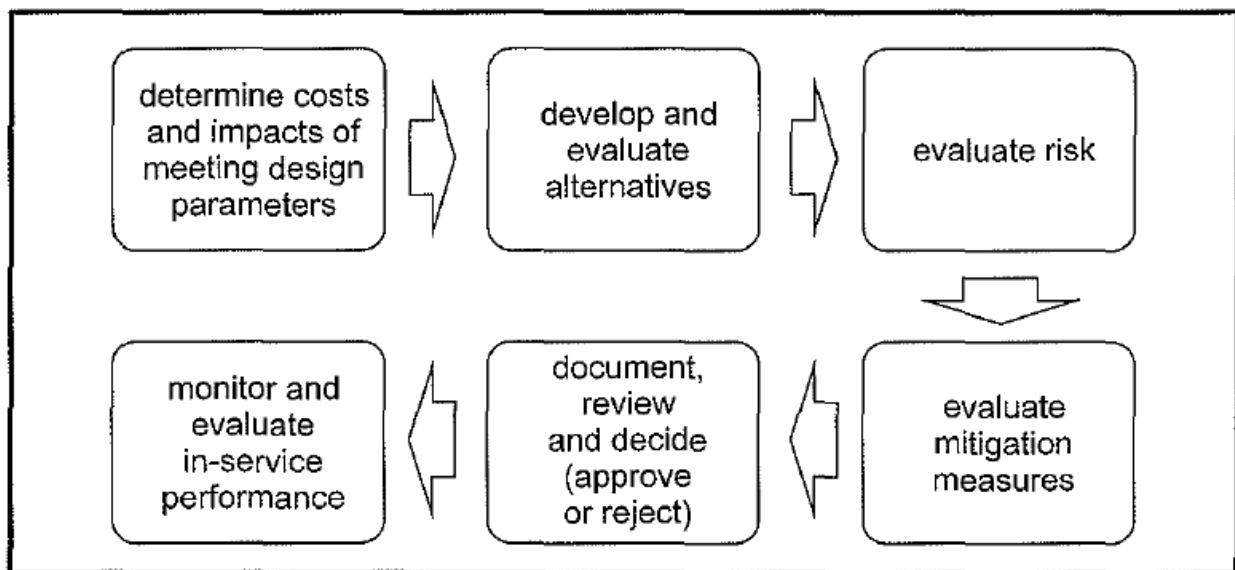
Figure 5: Design Exception Process[8]

19

The TAC guide acknowledges that conducting a comprehensive assessment for deviations in any design elements may not be practical and, as a result, it only requires that such assessment is conducted for 12 critical design elements including Stopping Sight Distance, Vertical Clearances, Cross Slopes, and Superelevations. While such recommendations are valuable, the assumption that recommended design standards yield safe design and that evaluations are only required when deviating from those standards is unreasonable.

2.2   PERFORMANCE BASED DESIGN

2.2.1   DEFINITION AND ADOPTION

The concept of Performance Based Design (PBD) dates to the 1980s when it was first introduced in Seismic Design. The literature includes many different definitions for PBD with many studies defining it as a general philosophy in which design criteria are expressed in terms of achieving stated performance objectives when the designed structure is subject to a certain level of demand [16,44]. PBD has also been defined as a method that relates structural performance to design process by eliminating intrinsic uncertainties [45].

Despite the differences in definitions, there is an agreement that PBD encompasses a wider design scope that results in more predictable performance over a full range of demand. The unique features of PBD allow designers to consider different hazard levels along with different functional classifications [46]. In seismic design, the field where PBD was first introduced, PBD made it possible for designers to relate post-earthquake structural performance to engineering design standards and parameters. In other words, design requirements were formulated based on the level of damage (performance) accepted after an earthquake. This made it possible for engineers to design structures that could sustain a certain level of damage (known to designers) without losing serviceability.

Since its adoption, a substantial amount of research has been done on the means through which PBD could be adopted in seismic design [47-49]. Most of the seismic PBD approaches available in literature adopt the displacement based design (DBD) method developed by Priestley, et al. [50] where a structure is designed for a target maximum displacement under a specified design earthquake [47]. However, other approaches also exist and vary in terms of the performance metrics they use, the different hazard levels they consider, and the means by which performance is predicted. As a result, Leelataviwat, et al. [51] describe PBD as not a single design method but

an actual framework for optimal design. The Pacific Earthquake Engineering Research (PEER) Center developed a probabilistic methodology for seismic PBD in which the performance assessment and design processes were broken down into elements that can be studied in a rigorous and consistent manner [52].

2.2.2 PBD IN HIGHWAY ENGINEERING

In the past few years, transportation and highway engineering entities such as the Transportation Research Board (TRB) and the Federal Highway Administration (FHWA) have shown interest in adopting the concept of PBD in highway geometric design [53,54]. Ray, et al. [53] defines PBD as a principles-focused approach that examines the outcomes of design decisions as the primary measure of thier effectiveness. It is also viewed as an approach that provides the means to support flexible design solutions or elements to adapt to unique project needs. PBD is seen as a tool that would provide designers with the flexibility to deviate from design standards in cases where "*designing to full standards is not feasible*" (i.e., not economically feasible) and where deviation does not have any impacts on safety. Unfortunately, as already noted in this thesis, there is no evidence that designing a road to meet recommended standards is the most effective way to achieve a specific level of performance. Whether it results in standards that are more stringent or less stringent, there is an agreement that PBD is an approach that will promote informed decision making.
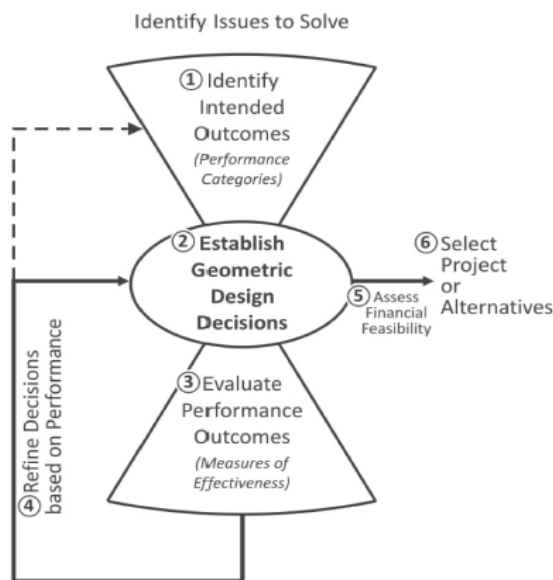
Figure 6: Framework [53]

21

As part of efforts to promote the adoption of PBD, the NCHRP recently published a report that provides a general framework for entities interested in adopting the design approach [53]. The report does not demonstrate how the relationship between design elements and performance metrics can be established, however, it does provide a general strategy of the entire design process. The report defines three different stages in the design process illustrated in Figure 6, namely; (i) identifying intended outcomes, (ii) establishing geometric design decisions, and (iii) evaluating performance outcomes.

According to the report, in the first stage, the aim is to define the project-level objectives and clarify the key performance measures, including transportation performance measures (e.g., improving safety and mobility). The second stage involves defining quantitative performance measures that act as a proxy for the project's objectives; these measures are related to geometric design elements by performing iterative geometric sensitivity tests and selecting an alternative based on the results of the tests. The ability of the proposed design in achieving project objectives is evaluated in the third stage.

Geometric sensitivity used in the second stage of the design process is defined as the process whereby the impacts of deviations from recommended geometric design standards on performance measures are studied. Despite this step being the most critical step to the whole PBD process, the report acknowledges that, in many cases, geometric design sensitivity is expected but is not supported by any research to date.

Segment Geometric Elements/Characteristics	Accessibility	Mobility	Quality of Service	Reliability	Safety
Shoulder width(s) and composition	● ◇	● *	● *	□ *	● *
Shoulder type(s)	● ◇	● x	● x	□ ◇	● *
Lane & shoulder cross slopes	—	—	—	□ x	● x
Superelevation	—	● x	● x	□ ◇	● *
Roadside design features	● x	● x	● x	□ x	● *
Roadside barriers	● ◇	● *	● *	□ ◇	● *
Minimum horizontal clearances	● ◇	● *	● *	□ ◇	● *
Minimum sight distance	● x	● x	● x	□ x	● x
Maximum grade(s)	□ ◇	□ *	□ *	□ ◇	□ *
Minimum vertical clearances	● ◇	□ x	□ x	□ x	□ x
Vertical alignment(s)	—	● *	● *	□ *	● *
Bridge cross section	● ◇	● *	● *	□ *	● *
Bridge length/termini	—	—	—	□ ◇	● *
Rumble strips	● ◇	—	—	□ x	● *

● = expected direct effect
□ = expected indirect effect
— = expected not to have an effect
* = relationship can be directly estimated by existing performance prediction tools
◇ = relationship can be indirectly estimated using more than one existing tool
x = relationship cannot be estimated by existing tools

Figure 7: Geometric Sensitivity [53]

The report provides a list of different geometric elements and the potential relationships between those elements and a set of performance measures. The information, seen in Figure 7, also includes information on whether or not a relationship could be studied using existing tools. Three important elements that the report highlights as elements which cannot be linked to performance metrics using existing tools are (i) sight distances, (ii) vertical clearances, and (iii) cross-sectional slopes. As a result, research in the first phase of this thesis focuses developing efficient extraction tools that can be used in the assessment of those critical features.

In summary, although the concept of PBD in transportation engineering has been promoted in recent years, research to facilitate the implementation of such a concept (i.e., research on he means by which geometric elements could be surveyed and work addressing the relationships between design elements and performance metrics) has been limited. Apart from the NCHRP report, where the focus is on developing a project-level framework for PBD in highway engineering, to date,

there has been hardly any research in this area. Although this is reasonable considering the FHWA only started promoting the idea in the past four years, more research is clearly required in this area. This includes research developing tools for large-scale assessment of geometric elements on road infrastructure to facilitate the assessment, as well as research to establish a connection between design elements and performance on Highways.

2.3 APPLICATIONS OF LiDAR IN TRANSPORTATION & HIGHWAY ENGINEERING

One technology that has huge potential in facilitating efficient assessment of highway infrastructure is LiDAR remote sensing technology. Data collected using LiDAR scanners consists of closely spaced points with known positional data and intensity information as illustrated in Figure 8. In Mobile Laser Scanning, data collection equipment is mounted on a truck that travels through a highway creating a 3D point cloud image of the entire road segment. The high point density of such datasets enables the extraction and the assessment of multiple geometric features on highways at a high level of accuracy without the need to conduct long site visits.
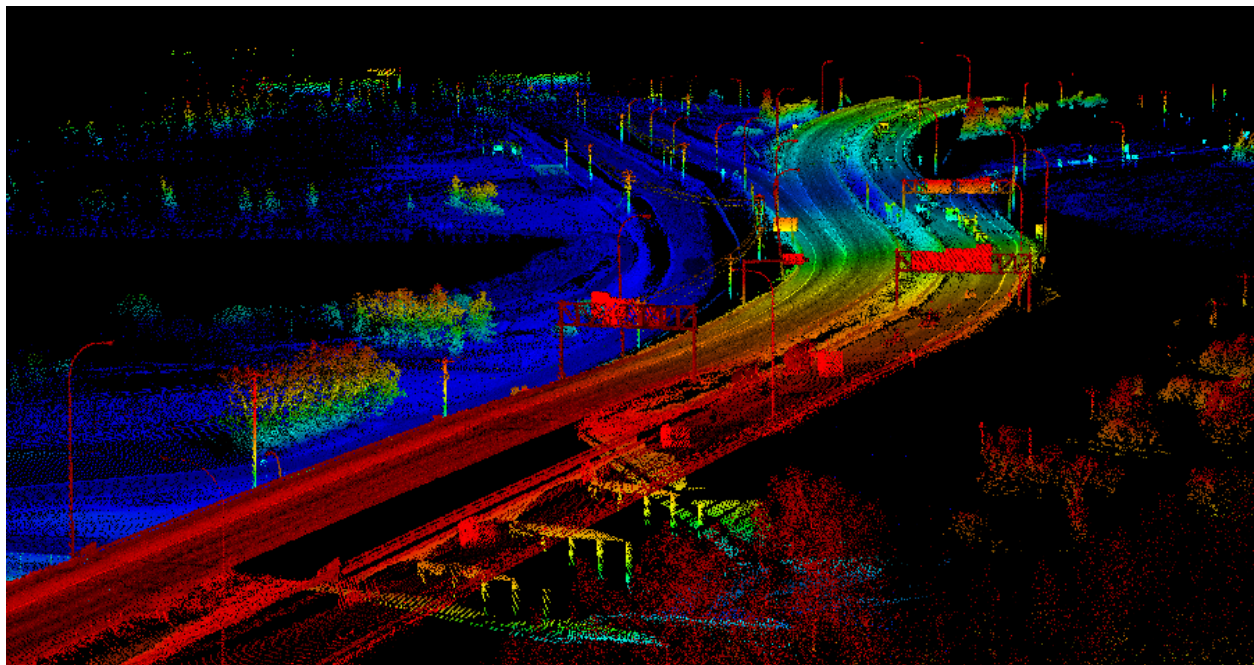
Figure 8: LiDAR point cloud highway (colour-coded by elevation, varying vertical alignment)

The next few sections provide a thorough review of the previous attempts to extract information about transportation infrastructure from LiDAR dataset. The challenges associated with the extraction processes and the gaps that exist in the literature are all highlighted. The studies

reviewed include research using LiDAR to extract (i) on-road information, (ii) roadside information, and (ii) geometric features.

2.3.1   ON-ROAD INFORMATION (LANE MARKINGS, EDGES, AND CURBS)

Extracting lane markings, curbs and road edges from LiDAR data has been heavily explored in previous research. Zhou and Deng [55] proposed a three-step procedure to detect curbstones in airborne LiDAR datasets. The first step involves identifying points where there is an abrupt change in height. The maximum height difference (MHD) within the neighborhood is then computed between midpoints of high and low points on either ends of the height jump. These points are arranged into a sequence to obtain a polygonal chain describing the approximate curbstone location and all points near the chain are then fitted to a sigmoidal function to increase the accuracy. The final step involves closing gaps between nearby and collinear segments. The authors compared the results obtained from Aerial Laser Scanning (ALS) to information obtained using GPS and Mobile Laser Scanning (MLS). The results revealed that completeness[3] varied between 53% and 92% from ALS on the different test segments. Accuracy for ALS was slightly higher than that of MLS (54% to 83%). The failure to achieve 100% rates was attributed partially to parked cars blocking curbs.

Zhang [56] attempted real time extraction of a road's surface and edges from LiDAR data. The data was first decomposed into elevation signals and signals projected on the ground plane. Elevation-based filtering was then performed to identify a road candidate region, and pattern recognition techniques were used to determine whether the candidate region was a road segment. After that, line representation of the projected signals on the ground plane were identified and compared to a simple road model in the top-down view to determine whether the candidate region is a road segment with its edges. The authors state that the algorithm detects most road points, road-curb points, and road-edge points correctly with false positive and false negative rates of 0.83% and 0.55% respectively.

Serna and Marcotegui [57] attempted curb extraction by mapping point clouds into range images. Ground-non ground segmentation was then performed using the λ-flat zones algorithm. Finally, the height and elongation criteria were used to select curb candidates and Bézier curves were used

---

[3] Defined in Section 6.3.4 of the thesis

to reconnect close curbs. The proposed method was tested using datasets collected in France and the Netherlands with results showing completeness rates ranging from 54 to 65% and correctness[4] ranging from 91 to 95%. In another algorithm by McElhinney, et al. [58] road edges were extracted in two stages. The first stage involved extracting the cross sections of the data. These cross sections were then fitted to 2D cubic splines and those lines were analyzed based on intensity, pulse width, slope and proximity to vehicle to identify road edges. The algorithm was tested on two urban road segments. The paper did not include discussion of the results; however, the authors acknowledge that their algorithm requires further refinement and improvements.

Jaakkola, et al. [59] attempted detecting road markings and curbstone information from LiDAR with the aid of image processing techniques. The authors first modelled the road's surface as a triangulated irregular network (TIN). Classification of the road into curbs and markings involved segmentation using thresholding combined with morphological operations applied to elevation and intensity images. Success rates of around 80% were reported for the classification of curbstones, zebra crossings, and parking space lines.

Kumar, et al. [60] also attempted extraction of road edges using image segmentation techniques. The authors used a combination of Gradient Vector Flow (GVF) and Balloon Parametric Active Contour models to perform the extraction. The algorithm involved converting the LiDAR images into 2D raster surfaces based on elevation, reflectance, and pulse width attributes. Edge boundaries of the raster surfaces were then formed using hierarchical thresholding (limits noise) and canny edge detection (determines boundaries). A snake curve was then used to construct road segments that would intersect with LiDAR road data points. The developed technique was tested on three 50m road sections. The road sections were segmented into multiple sub-sections and the edge extraction was accurate in all but two instances. Inaccuracy was attributed to a low point density on one edge of the road compared to the other. In another study, Kumar, et al. [61] extended their work on road edge extraction to extract lane markings. The authors performed range dependent thresholding to the LiDAR intensity values and used binary morphological operations to obtain lane marking information. Similar to edge extraction, the authors started by converting the data into 2D range and intensity raster surfaces before both thresholding and applying morphological operations. For incomplete road markings (i.e., locations where markings had rubbed off), linear

---

[4] Defined in section 6.3.4 of the thesis

dilation was used to fill in the gaps. Markings were extracted over seven road sections covering 150m. Of 93 road markings, 80 markings were correctly detected. The undetected markings were attributed to low point density and low intensity. In addition to the false negatives, 13 false positives were detected. These false positives were on road sections where the road edges were inaccurately identified.

Guan, et al. [62], also developed an algorithm to extract lane markings using range dependent thresholding and the application of morphological operations. The authors first proposed a curb-based procedure to extract the roads surface by slicing the LiDAR data into blocks perpendicular to the road's trajectory. Within each block, differences in elevation are used to classify points into layers and to identify road edges (curbs). Once the road surface was extracted, geo-referenced intensity images of the LiDAR points were generated using Inverse-Distance-Weighted interpolation (IDW). The IDW rasterizes the road surface based on the reflectivity of points and their proximity to the central point on the road. The final step of the extraction procedure involved using density-dependent multi-threshold segmentation to filter out lane markings and the application of closing morphological operations to remove noise and fill gaps within extracted lane markings. The algorithm was applied on two datasets covering 168m of roadway length. Three sub-segments of those two roadways were used to assess the accuracy of the algorithms. This was done by manually comparing the results of the sub-segments to the ground truth. The authors reported success rates of 0.96 and 0.83 for completeness and correctness, respectively.

In Thuy and León [63], the lane detection process started by plotting the Probability Density Function (PDF) for the reflectivity observations of all data points. Since most points fall on the road's surface, the maximum observation in PDF was assumed to correspond to the reflectivity of the roadway. Once that was identified, a dynamic threshold was calculated based on the maximum of the reflectivity PDF to distinguish and improve the contrast between the road surface points and lane markings. A threshold value was chosen based on the standard deviation. Values estimated for the road surface were subtracted from the histogram within a one-sigma interval. The mean value was recalculated and used as the threshold for image binarization. A Canny filter (edge detection algorithm) was applied to the binary image for better lane detection. Although the developed algorithm was tested, not much discussion is provided on the results of the lane detection.

Yan, et al. [64] proposed a scanline-based method to extract road markings from LiDAR. After processing the data and removing outlying observations, the proposed algorithm involved ordering LiDAR points sequentially by timestamp. Points were then organized into scan lines based on scanner angle with the aim of increasing the efficiency of data processing. Seed road points were extracted based on Height Difference (HD) between trajectory data and the road surface. Seed points were used to extract the full road points. This was done by fitting a line through the seed point and all other points along the scan line using moving least squares and only retaining points which fall within a certain threshold of the line. Road points were then classified based on intensity into asphalt points and road marking points. Intensity values were smoothed by a dynamic window median filter to reduce noise and road markings were extracted using the Edge Detection and Edge Constraints (EDEC) method, which measures abrupt changes in intensity along a scan line. Testing was conducted on 3 segments in Beijing, China, ranging in length from 70 to 100m. Average completeness and correctness rates of 0.96 and 0.93, respectively were achieved.

2.3.2 ROADSIDE INFORMATION

2.3.2.1 TRAFFIC SIGNS

Traffic sign inventory has been the most common application for which LiDAR dataset have been utilized in the past few years. The extraction pipelines[5] proposed vary among different studies; however, in general, success rates have been satisfactory.

In one of the earliest studies that dealt with traffic sign inventory from LiDAR, Chen, et al. [65] attempted automated extraction of signs along a 600m road segment in Chicago. The technique used in the study involved filtering the data based on a user-defined distance from the sensor, a certain sensor angle interval, and intensity. Data clustering was then performed whereby points were placed onto a grid, and a threshold was defined to retain grids with a higher point density only; the grids were also subject to geometric filtering of the different clusters. The authors provide no information about the percentage of signs accurately extracted, however, they did state that the detection rates were satisfactory.

In more recent work, Vu, et al. [66] attempted real time identification and classification of traffic signs (i.e., detection and classification of signs while the probe vehicle travels along the road

---

[5] A *pipeline* in computer science is a term used to describe a set of data processing elements connected such that the output of one element is the input of the next one

collecting LiDAR data). The authors used onboard sensors including a sensor platform equipped with GPS/IMU, 3D LiDAR, and a vision sensor. Data points were first filtered based on intensity after projecting the LIDAR data onto images to obtain what the authors call a Virtual Scan Image. The range between high intensity planes was checked and only planes with a spacing of more than 1m were retained. Principle Component Analysis (PCA) was then used to determine alignment of planes, and only planes aligned along the road were retained. The main limitation of this study was that the extraction procedure was only applied on a controlled test track; hence, its performance in a dynamic environment is unknown. Real-time traffic sign detection was also attempted in [55]. In this study, LiDAR point cloud data was converted into camera pixel images. The regions of interest were then identified and classified using colour characteristics of the images. Success rates ranging from 84 to 96% were reported depending on whether the sign was in the range of the data collection vehicle.

Weng, et al. [67] used mobile LiDAR data collected on Huandao road in Xiamen, China, to detect and classify traffic signs. The detection procedure involved filtering the point cloud by intensity, hit count, elevation, and height. A minimum of 70 points was chosen as a threshold for hit count, a minimum elevation of 2m, and a minimum sign height of 0.4m were also predefined. The success rate of detection was not discussed, but it is mentioned that some false positives such as billboard signs were detected.

Ai and Tsai [68] also filtered their data based on intensity and hit count when extracting traffic signs from LiDAR. In addition, the authors used elevation and offset values specified in the Manual for Uniform Traffic Control Devices for further filtering of the point cloud. To find the optimal threshold value for each parameter, an initial value was chosen, then a sensitivity sweeping procedure was used to optimize the thresholds, minimizing false-negatives and false-positives. Trimble T3D analyst software was used for automatic sign detection. The algorithm was tested on road segments in Indiana with a 94% detection rate achieved and 6 false-positives for I-95 highway, and a 91.4% success rate with 7 false-positives on 37th street. There were also four cases of false-negatives which were attributed to either poor retro-reflectivity, insufficient height, and/or a sign being obstructed by other objects.

The algorithm proposed by Landa and Prochazka [69] also employed intensity filters to the point cloud data when extracting traffic signs. Euclidean distance was used for preliminary clustering.

Further filtering of clusters was achieved based on point per cluster density, elevation, and height. A 93 success rate was reported in the study with the authors attributing missed signs to low point density. In a different study, Wu, et al. [70] combined intensity filters with PCA to detect vertical planes where traffic signs exist in a LiDAR point cloud of a highway. On-image sign area detection was implemented by projecting the 3D points of each traffic sign onto a 2D image region that represents the traffic sign. Success rates were not discussed in the study.

Soilán, et al. [32] started their detection process by removing points more than 20m away from the laser scanner. The ground surface was converted to a raster grid to remove ground point from the dataset. An intensity filtering based on a Gaussian mixture model was then applied to remove low intensity points that remained in the dataset. Density based clustering was used to group signs into different sets and a PCA filter was used to distinguish sign clusters from posts. The method was applied to an urban road and a highway segment in Spain, achieving success rates of 86.1% and 92.8% for the urban road and highway, respectively. The study attributed false positives to planar metallic surfaces and pedestrians dressed in reflective clothing.

Riveiro, et al. [25] followed a similar procedure to Soilán, et al. [32] applying intensity filters to the point cloud while also using Gaussian mixture models to further filter the data. A similar procedure was also used for the clustering and PCA was used to remove false positive clusters (clusters with curvature). The methodology was tested in Brazil, Spain, and Portugal with success rates ranging from 80% to 90% depending on the road type and the type of sign extracted.

2.3.2.2 *OTHER ROADSIDE OBJECTS*

Previous studies have attempted to extract roadside objects including lamp posts, trees, and utility poles from LiDAR. Such objects can have huge effects on the severity of runoff the road crashes. In fact, pole-like fixed objects are associated with the highest percentage of severe accidents on highways [71]. Thus, their existence and proximity to the road must be identified for effective roadside management.

The purpose of pole-like object extraction in the literature ranged from inventory of roadside furniture and analyzing the placement of objects for roadside design, to improving the positional information for autonomous driving application.

Recent work by Zheng, et al. [72] proposed a technique to automatically extract street lighting poles from mobile LiDAR. The authors first used a piecewise elevation histogram segmentation method to remove ground points. After that, a new graph-cut-based segmentation method was introduced to extract the street lighting poles from each cluster obtained through a Euclidean distance clustering algorithm. In addition to the spatial information, the street lighting pole's shape and the point's intensity information were also considered to formulate an energy function. Finally, a Gaussian-mixture-model-based method was introduced to recognize the street lighting poles from the candidate clusters. The proposed approach was tested on several point clouds collected by different mobile LiDAR systems. Experimental results showed that the proposed method achieved detection rates of up to 90%.

Teo and Chiu [26] proposed the use of coarse-to-fine approach to extract pole-like objects from mobile LiDAR. Specifically, the extraction framework involved (i) data processing, where data trajectories were re-organised into different road elements and building facades were filtered out of the point cloud, (ii) coarse-to-fine segmentation, whereby pole-like objects were detected at an aggregate voxel scale before detecting them at the point scale for final inventory. Testing revealed that the proposed method was effective in detecting pole-like objects with at a rate of 90%. The authors attributed false negatives to object occlusion and false positives to complex environment.

Lehtomäki, et al. [30] proposed a scan-line-based algorithm to extract pole-like objects from mobile LiDAR. In scanline LiDAR data, poles will exist as sweeps (i.e., curved group of points) in each scanline. Point groups, which are on top of each other in adjacent scan lines, were clustered and clusters that constituted the same pole were merged using PCA. A cluster was defined as part of a pole-like object if it met specific geometric properties. The algorithm was tested on a 450m straight and flat section and the authors reported a 77.7% detection rate and 81.0% correctness rate. False positives included pillars in buildings and different wall structures. Lamp posts were found to be the easiest to detect with a detection rate of 93% as compared to traffic signs and tree trunks with 73.3% and 76.1% detection rates, respectively. For objects that were not detected, the authors attributed this to an insufficient number of data points or objects being obstructed from the view of the scanner.

Pu, et al. [73] presented a method to classify LiDAR point clouds into three categories: ground surface, objects on the ground, and objects off the ground. Additionally, objects on the ground are

classified into detailed groups such as traffic signs, trees, building walls, barriers, and utility poles. A surface growing algorithm taken from Vosselman, et al. [74] was employed to determine the points representing the ground surface. To detect poles, the common feature of a vertical principal axis was used. Objects were divided into quartiles based on their height and the third quartile (measured from the lowest elevation point of a given cluster) is chosen for further analysis. This helps omit objects such as bushes and trees when classifying on ground objects into poles and non-poles. The authors reported an 87% success rate for detecting pole-like objects using their procedure. Lower detection rates were reported for traffic signs (61%) and trees (64%).

The procedure proposed by El-Halawany and Lichti [28] to extract poles started by organizing the point cloud using a *KD* tree data structure. A 2D density-based segmentation was performed using a density-based clustering algorithm (DBSCAN), which finds clusters of high density in local neighbourhoods. The proximity threshold in the DBSCAN search was defined based on utility pole radius of 25cm. The output of the clustering was then used in a vertical region growing procedure to extract upright objects starting from the lowest elevation object detected in the previous step as the seed for the vertical regions. To merge different vertical segments that were close enough to be considered part of the same object, segment merging was based on the horizontal distance between centroids of the vertical regions grown in the previous step. Objects were then classified using several criteria including object height range, the surface normal direction, and the largest normalized eigenvalue. The algorithm was tested using data collected on three urban streets ranging in length from 103 and 768m with a reported processing time of 4-6 hours. The average detection rate was 86% for the three segments and the accuracy was 97%.

Yan, et al. [64] proposed a four-step procedure to extract poles and towers from LiDAR. The method involved ground filtering, unsupervised clustering, classification, and data cleaning. Filtering the ground surface from the LiDAR point cloud was done based on the statistical distribution of the points (assuming normality of ground points). This allows for a statistical skewness balancing algorithm to be applied to the height attribute to differentiate ground and non-ground points. The paper then uses DBSCAN to cluster the height-normalized non-ground points. Each cluster was then classified into one of five types of poles based on a set of defined decision rules. The final stage involved using least square circle fitting algorithms on the lower 10 to 20 percent portion of the pole structure to eliminate ground points from the extracted pole object. The

proposed algorithm was tested on an urban site in Toronto, Ontario, resulting in a 91% detection rate for five types of light poles and towers.

Wu, et al. [75] propose a voxel-based method for identification of street trees from LiDAR. The method involved voxelization, calculating values of voxels, searching and marking neighbourhoods, extracting potential trees, and using morphological parameters to eliminate pole-like objects other than trees. It is worth noting that the voxel layer that fell 1.2-1.4m above the ground was used to begin the neighbourhood marking and searching to extract trees. The proposed algorithm was tested on two 300m long flat urban street segments with less than one-meter difference in elevation, hence, height normalization with respect to ground surface was not required. This resulted in a completeness and correctness of over 98% in detection.

Cabo, et al. [27] also proposed an automatic voxel-based extraction of pole-like objects from mobile LiDAR. The data was first voxelized to reduce data size for processing and each horizontal layer of the voxel grid was analyzed and segmented separately. The segments were then merged to form the selected 3D features. The 2D analysis was carried out to identify pole-like candidates in three stages: segmentation of connected horizontal elements, selection of elements greater than maximum area criteria, and selection of elements by isolation criteria. Both the second and third stages were based on the assumptions that poles have a relatively small cross-sectional area and are isolated. The results provide a set of segments associated with a Z coordinate of a candidate part of a pole. The third step involved connecting all voxel elements that share a face, edge or vertex among all elevation layers. A minimum vertical height was set for connected groups to differentiate pole-like objects. The algorithm was successfully tested on four sites with an average completeness of 92.3% and a correctness of 83.8%.

Lehtomäki, et al. [76] proposed an automated voxel-based method for detection and classification of roadside objects in a mobile LiDAR point cloud. The proposed method involved isolating non-ground points from the point cloud, object segmentation, segment classification, and object location estimation. The authors used connected component labelling to perform object segmentation. Feature descriptors calculated from voxels making up a segmented object include local descriptor histograms (LDHs), spin images, and general shape and point distribution attributes in order to apply machine learning techniques for object classification. The paper was successful in extracting and classifying trees, lamp posts, traffic signs, cars, pedestrians, and

advertising boards. The authors tested their algorithm on a 900-m-long stretch of road in a suburban area in Espoo, Finland. In general, the authors report between 66.7% and 94.3% recall for the six defined object classes.

2.3.3   GEOMETRIC DATA EXTRACTION AND ASSESSMENTS

In general, the use of LiDAR in the assessment of geometric features and elements of roads has received less attention by researchers than traffic signs, lane markings, and other roadside objects. In this section, a thorough review is conducted of the work that has been done in this area. The review focuses on design elements that have standards recommended for them in design guides. These include sight distance, superelevation, grades, horizontal and vertical alignments, and other elements of geometric design.

2.3.3.1   ROAD CROSS SECTION INFORMATION

Design guides are full of recommendations governing the design cross sectional elements, due to their importance in the safe and efficient operation of roads. Despite that, a limited number of studies have attempted extracting such features from LiDAR.

Tsai, et al. [35] developed an algorithm which can be used to extract cross slopes of roads from mobile LiDAR data. First, the laser scanner was oriented at a specific beam angle and beam distance. Cross section information was then extracted for the region of interest (ROI) that perpendicularly bisects the roads trajectory. The depth of the ROI is user-defined and bounded by lane markings on the edges. The authors recommend that lane markings are extracted from the LiDAR dataset using an algorithm proposed in a different study. Once the desired ROI was extracted, its cross slopes were estimated using linear regression. To identify the appropriate depth for the ROI, the authors ran a sensitivity analysis on the data. The analysis revealed that length of ROI should be 2ft to achieve adequate cross slope estimates. In addition to the sensitivity analysis, the authors tested the proposed algorithm in a controlled environment to assess its accuracy and repeatability. The authors found that the proposed algorithm yielded results within 0.28% of the digital level measurements.

In another recent paper that considered extracting road cross sectional elements, Holgado-Barco, et al. [43] proposed an algorithm that can be used to determine slopes, lane widths and number of lanes on a segment from mobile LiDAR images. The algorithm involved road segmentation where

the road surfaces were extracted using an adaptive height threshold and scanner angle. After extracting the road surface, intensity-based data filtering was employed to obtain lane marking information. A geometric filter was applied to lane markings to remove false positives and PC A was used to connect discontinuous lines. Distances between lines were then used as a proxy measure for lane width and shoulder widths. Slope differences were also measured based on the difference in elevation between lines. The proposed technique was tested on two motorways (400m and 1km) in Spain. Comparing multiple extractions on each motorway, the authors found that only slight variations in the extracted information existed. Variations in shoulder width along the same segment were attributed to the existence of vehicles, which obstructed the view of the scanner.

Although not with the intention of extracting road slopes, Lato, et al. [77] used mobile LiDAR to assess cut-slopes along transportation corridors. The study's aim was to detect rock hazards falling off slopes along road corridors. Multiple mobile laser scans were compared to identify potential rock movement. The measurements were extracted using 3D metrology software PolyWorks. The authors concluded that the assessment was effective in the detection of small rock block release (sub 15cm). Embankment slope instability was also assessed by Miller, et al. [78], however, the authors used static terrestrial laser scans to test for slope failure and extract slope features. The slope deformation and failure were examined at two locations. The study found that, for both sites, the detection of minor changes, such as soil creep and surface runoff was possible using the laser scans, however, vegetation was found to be a confounding factor to detection. The authors used a least squares surface matching algorithm to filter out the vegetation, which resulted in detection of change at a centimetric precision level.

2.3.3.2 ALIGNMENT INFORMATION

The design of vertical and horizontal alignments on roadways is also governed by multiple guidelines. This includes the standards recommended for the length of the vertical crest and sag curves, vertical grades, the radii of horizontal curves, superelevations and spiral transitions. Obtaining such information about design elements is an extremely tedious process that requires long site visits; as a result, transportation agencies limit surveying such information to locations where the information is desperately needed to apply changes to the design of the road. The next few paragraphs review the research that has been done to explore the potential to extract such information from LiDAR point clouds.

Vertical Alignments

One of the earliest studies that worked on the collection of vertical alignment information from LiDAR data was a project led by Iowa's Department of Transport (DOT) just over a decade ago [79]. The authors used least squares regression analysis to estimate the elevation of points along the centerline of a highway. The boundaries of the 100ft road segments (road edges) were first manually defined in ArcGIS by drawing polygons around the location of interest. The midpoints of the edges were used as the centerlines of the road segments and multiple linear regression analysis was used to estimate the elevation of points along the proposed centerline. The predictors of the regression model were (i) the lateral distance of a LiDAR point from the centerline and (ii) the longitudinal distance along the segment from its origin. The regression coefficients of the two independent variables (lateral distance to the centerline and longitudinal distance to the centerline) represented the cross slope and the grade of the segment, respectively. The study found that the estimated grade and slope attributes both deviated significantly from field survey measurements, particularly for cross slopes. This led the authors to conclude that collecting LiDAR data for those purposes alone was not cost effective.

In other work, Zhang and Frey [80], used a similar technique to that proposed in [79] to estimate vertical grade information. One difference between the two studies is that Zhang and Frey [80] used road width information to define road edges and a map of the road to estimate the location of the centerline. The paper also used regression analysis to estimate the grade of the road with the authors reporting a level of accuracy of up to 5%. One major limitation of this study and the one by Souleyrette, et al. [79] is that the segments for which grade estimation is attempted need to be straight segments (i.e., estimation was not possible for segments with great deviations in the horizontal alignment of the road). This led authors to select segments that were short enough so that the curvature was not significant. The segments, however, had to belong to have enough points for the regression analysis and meet the normality assumption.

Dawkins [81] used LiDAR data to validate road profile extracted using a vehicle suspension model, although the author does not provide many details on how the profile was estimated using LiDAR. It is likely that the paper traced the path of the data collection vehicle and used the elevations of the point cloud points along that line to produce the profile. However, this is not explicitly discussed in the paper.

Wu, et al. [82] used LiDAR data to compute the elevation of the road surface. In this process, 3D cloud point data was projected onto vertical planes defined by the trajectory of the vehicle collecting the LiDAR data. The points along the profile were segmented using the Douglas-Peucker algorithm, which connects points within the vertical planes to produce a line segment representing one portion of road's profile. Since the aim of the analysis was not to extract the vertical profile of the road segment, the authors do not provide any discussion of the level of accuracy achieved.

Han, et al. [83] used a photogrammetric approach to extract information about road profiles. The authors used a laser module to measure the distance between the onboard sensors in the data collection vehicle and the road surface. This information was linked to the image coordinates. To identify the profile at a certain location, image coordinates corresponding to the real space coordinates of that location were identified along with the elevation information.

In a recent paper, Higuera de Frutos and Castro [84] proposed a method for the reconstruction of road vertical profiles using GNSS data collected along a road's centreline. The aim of the study was to automatically acquire information about different elements of a road's vertical profile including grades and parabolic curve details using the points collected along its centreline. The first step of the procedure involved classification of points along the profile into grade points, parabolic curve points, or border points, and clustering points based on their type. Analytic expressions were then estimated for the set of points between borders before calculating integrals of those expressions to obtain the models for the elements of the longitudinal profile. The proposed method was tested on rural highways in Spain with the authors reporting a mean error of less than 8cm when estimating the geometric elements of a road's vertical profile.

Although not automated procedures, Di Mascio, et al. [85] and Baass and Vouland [86] also used GNSS data to extract vertical profile information on roads. In Baass and Vouland [86], the authors classified segments of the profile into tangents or parabolic curves based on the rate of change in slope. To ensure that different components of road profiles were aligned to one another, the authors used special constrained regression procedures. The proposed method was tested on rural roads in Quebec, Canada, with authors reporting an average error of 15 cm and a maximum error of 1.5 m. It is worth noting that, although GNSS data is not necessarily collected as part of a LiDAR scan,

such information is acquired by all MLS systems. Therefore, procedures proposed in the above-listed papers do apply to datasets collected using LiDAR scanning systems.

Horizontal Alignments

Previous research on the extraction of horizontal curve attributes has followed three different directions. The extraction using Graphical Information Systems (GIS) [87,88], GPS data [89,90], and photogrammetric techniques [91]. Despite the high accuracy of LiDAR datasets, attempts to use them in the extraction of horizontal curve attributes have been limited.

Holgado-Barco, et al. [34] is one of a few studies that attempted the extraction of horizontal alignment information from LiDAR. The semi-automatic method proposed in the paper involved segmenting, parametrizing, and filtering the point cloud. In the segmentation stage, points tracing the road's trajectory (lane markings) were filtered out. These points were then classified into curved and straight segments based on changes in azimuth and curvature between consecutive points. The outputs were classified into three segment types straight segments (if zero curvature is detected), circular arcs (in case of constant curvature) and clothoids (if curvature varies across consecutive points). After detecting the curves, radii and the transition lengths were estimated. The proposed algorithm was tested on simulated data and data collected on a Spanish highway. Comparing results obtained from the algorithm to those estimated by an experienced topographer, errors in length of up to 3.8m (2.0%) for circular arcs and 5.6m (0.4%) for circular radius were reported. When testing on the simulated segment the errors were 0.3m (0.1%) and 0.9m (1.1%) for arc radius and length, respectively.

Kim, et al. [92] explored the measurement of several geometric features from LiDAR data including horizontal curves and vertical profiles. The paper does not provide details of the extraction procedure; however, it is claimed that the extraction of horizontal and vertical alignments as well as cross sectional slopes was achieved. According to the authors, horizontal alignment extraction involved splitting the data into straight and curved segments using the Douglas and Peucker simplification algorithm while cross sectional information was estimated using the least squares method. Test data was collected on a 1km long highway in China. When comparing between finally extracted elements and ground truth the authors claim that the extraction procedure yielded almost the same values as ground truth when considering

construction errors. The paper concludes that the extraction of road information from LiDAR images is more efficient than traditional manual methods.

Sight Distance Assessment

In recent years, researchers have realized the value of using LiDAR data in sight distance assessments. Although in theory, designing curves based on the minimum stopping sight distance requirements ensures that this distance is available at any point along the curve; the assumptions associated with the estimation procedure and certain project constraints (financial or practical) mean that there may be locations along a highway where minimum requirements are not met. Moreover, scheduled maintenance activities such as road resurfacing could affect the original alignment of the highway causing potential limitations in sight distance. The addition of roadside structures, such as buildings or trees, may also limit the available sight distance in the post-construction stage.

In early work, Khattak and Shamayleh [33] explored the feasibility of assessing stopping and passing sight distance on highways using aerial LiDAR data. Aerial LiDAR data was collected along Iowa Highway 1. The data was imported into ArcGIS to create a TIN surface of the highway. The surface was then visually inspected and potentially problematic locations (i.e., locations with potential limitations in sight distance) were marked. The Line of Sight tool (in ArcView) was then used to verify limitations in sight distance (SD) at the set locations identified in the previous step. The authors found 10 locations where sight distance was limited, a result that was validated using data from the field.

Castro, et al. [42] adopted a slightly different approach to their assessment. The method involved the creation of a Digital Terrain Model (DTM) raster of the point cloud. This DTM was combined observer input information for the computation of Viewsheds. Viewsheds denote areas on the raster that are visible to the observer. All visible areas are converted into polygons and then intersected with a vehicle trajectory obtained from GPS. The distance between the observer and the closest intersection between the trajectory and the viewshed was taken as the available sight distance. The sight distances obtained were compared to values given by highway design software, Trivium. Although statistical analysis showed no significant difference between the results, there were locations where the design software reported shorter sight distances. This was attributed to

the Trivium software being more effective that the proposed algorithm in detecting obstructions on vertical curves.

In a move to improve the efficiency of sight distance assessments on LiDAR highways, Castro, et al. [41] attempted to increase the level of automation in the assessment using ArcGIS tools. The first step involved using aerial LiDAR data to create a DTM of the highway. The visibility of multiple target points from a single observer was then assessed using ArcGIS tools. Once an obstruction was detected, the available sight distance was recorded as the distance between the observer point and the last visible point. The obtained sight distances were compared to those found in other work [42] using Kolmogorov-Smirnov and Wilcoxon tests revealed no significant differences.

In a different study, Castro, et al. [93] attempted to show differences in accuracy between DTM (bare ground) and the Digital Surface Model (DSM) also known as TIN surfaces when extracting sight distance information from LiDAR. The paper used both mobile and aerial data for two DSMs. Kolmogorov–Smirnov and Mann–Whitney–Wilcoxon tests were employed to assess the differences in sight distance outputs using the two surface models. The results showed a significant difference between all three surfaces. Specifically, DSMs were found to have shorter sight distances than DTMs, which lead the authors to conclude that more obstructions can be detected using the DSM. Comparisons between the aerial and mobile DSMs showed that mobile DSMs had a greater density, which allows for a higher DSM resolution, leading to a more accurate representation of the environment.

Tsai, et al. [94], was one of few studies that attempted analyzing sight distance at intersections from LiDAR data. Although the authors do not assess sight distance per se, they propose a manual method that can be used to detect obstructions at an intersection by analyzing aerial LiDAR data. The first step in the procedure involved offsetting GPS points representing the road's centreline so that they trace the centerlines of the travel lanes on the major and minor roads. Based on the type of control at the intersection and posted speeds on the intersecting roads, the authors determined the dimensions and the edges sight triangle, which must be kept clear of any obstructions. The triangle was overlaid onto a DSM created using the LiDAR data and LiDAR market software was used to perform a plane of sight analysis between the observer and all target points. This process yeilded a raster grid of visible and nonvisible cells, which are overlaid on the sight triangle, and

sight distance was computed based on the outcomes. The authors highlighted the importance of removing overhanging objects such as cables from the LiDAR data before performing the assessment since those objects result in false obstructions when creating surface models. The obstruction information obtained using the proposed method was compared to field data collected at an intersection. The authors concluded that the proposed technique was effective in determining 92% of obstructions. This outperformed normal on-site line of sight assessment which was only effective in detecting 64% of obstructions. Missed obstructions were often objects that were present between consecutive lines of sight.

2.3.3.3   VERTICAL & LATERAL CLEARANCE

Another application for LiDAR in transportation engineering is for the assessment of clearances, particularly vertical clearance. Various techniques have been used to conduct vertical clearance assessment on highways, one of which is through using LiDAR data. Although some municipalities still use manual methods such as theodolites and total stations, other digitized devices have recently been adopted. For instance, many DOTs use digital measuring rods and electronic measuring devices [95], similarly, clearance assessment using photolog data has also been previously attempted [96].

Liu, et al. [97], proposed a method to assess clearance at bridges using static terrestrial LiDAR scans of a bridge. The authors developed an algorithm where scanned ground points are automatically matched to bridge deck points that fall within a certain margin of the vertical plane perpendicular to the ground surface. The algorithm loops through all points until all points on the ground surface are matched to points on the bridge deck. Although this technique increases the likelihood of determining the actual minimum clearance beneath a bridge, static LiDAR scanning means that disruptions to traffic and safety concerns still exist. Moreover, network level analysis is still not possible since the technique involves conducting site visits and scanning each bridge on the network individually.

Puente, et al. [98] used mobile LiDAR data in the assessment of vertical clearance in tunnels. The authors propose a semi-automated algorithm where cross sections along the trajectory of the tunnel are first extracted and used to measure the clearance. The method involved using lane markings to define the edges of the travel lanes at which the clearance must be evaluated. The edges were then matched with the points on the roof of the tunnel and the cross section of the tunnel was defined

using convex hull before measuring the clearance. Although the results were positive, with a relative error between ground truth and detected clearance not exceeding 1 % for most cross sections, the algorithm was only used to assess a portion of the point cloud data with the authors citing loading time as the main reason testing was not conducted on the full point cloud.

It is worth noting that a few studies have also attempted utilizing LiDAR point cloud data for structural assessment of bridges. See, for example, [99-102].

2.3.4   DISCUSSION AND LIMITATIONS

As evident from the review, there seems to be a growing appreciation for the potential value of LiDAR in transportation. However, the majority of existing research has focused on using LiDAR in the inventory of roadside objects, such as poles and signs, and on-road features, such as lane markings and road edges. One reason these applications have attracted more interest than others is that mapping such features is important for autonomous vehicle applications. Moreover, most of the research conducted in this area has been conducted by experts in the fields of computer science and geomatics, who are not particularly concerned with design elements of transportation infrastructure.

The review clearly highlights the need for more research, particularly on the extraction of road geometric elements from LiDAR. There is currently a lack of studies attempting the extraction of cross-sectional elements, horizontal and vertical alignment data and clearance information. In fact, despite the high quality and accuracy of LiDAR data, particularly that obtained using mobile laser scanning, there is also a lack of studies attempting geometric and safety assessment of highways using LiDAR point clouds.

With regards to the geometric design elements considered in this thesis, the review shows that, just like other geometric elements, there is a lack of studies proposing the extraction and assessment of those elements. Moreover, even studies that do exist suffer from several limitations. For instance, sight distance assessment has been attempted on LiDAR highways in a few studies; however, methods proposed in previous studies are limited in many aspects. One major limitation common in all studies that have explored sight distance assessment on LiDAR is that they do not account for the existence of overhanging objects. This results in biased estimates when creating the digital surface models of the highway, which, in turn, bias the sight distance assessment results [103]. Another common issue with sight distance assessment in previous studies is that almost all

those studies used aerial LiDAR when developing their assessment methods [33,41]. Although useful for urban planning applications, the top-down nature of aerial LiDAR scans and the low point density of those scans compared to mobile datasets means that not all obstructions are accurately represented in the point cloud. This also affects the accuracy of the sight distance assessment. Moreover, the lower point density in aerial scans results in datasets where the sizes are manageable from a processing perspective, hence, using mobile scans represents a unique set of challenges including potentially longer processing times. It is also worth noting that in previous studies, testing was mostly conducted on a single segment, which raises some concerns about the repeatability of the extraction procedures. The manual element in some of the extraction procedures is also a concern since it restrains the ability to perform large-scale assessments of sight distance on a highway network.

Attempts to extract cross sectional elements and profile information from LiDAR data are also limited. Just like sight distance assessments, attempts that do exist suffer from some common limitations. The majority of the algorithms that do exists for the extraction of cross slopes from LiDAR assume prior knowledge of lane marking information. While using lane marking information might be helpful, extracting such information requires prepossessing of the datasets, moreover, the quality of lane markings on rural roads might be poor and undetectable. In fact, lane markings might not even exist on some rural highways which makes the procedure limited to a specific set of highways where lane markings are sharply defined. Another common limitation of the two studies that have explored cross section extraction from LiDAR is that they only attempt the extraction of cross slope information. To the best of the author's knowledge, no study to date has attempted the extraction of side slopes from LiDAR. This has often been attributed to the high vegetation, typically present in the ditches, posing huge challenges to the extraction process.

Extraction of horizontal curve attributes from LiDAR data has also been lacking in the literature. In the only paper that exists in this capacity, the extraction process is not fully automated, and it also involves extraction of lane marking information. Moreover, the focus in the paper is on curve length and radius without any attempts to extract other features of curves such as deflection angle, end points of curves and chord length. In fact, the focus on radii and curve length is also a limitation of studies that use non-LiDAR techniques to extract horizontal curve attributes. Other

disadvantages of non-LiDAR methods include the low point density, which results in the inaccurate estimation of curve attributes.

Another application developed in this thesis for which research has been extremely limited is the detection and clearances assessment of overhead objects. To the best of the author's knowledge, no study, to date, has attempted the automated detection (i.e., inventory) of overhead assets on highways. In the few studies that do exist in this area, clearance assessment is conducted on static LiDAR scans of bridges. Although such techniques might help minimize human error associated with conventional tools while also reducing the length of site visits, they do not help increase the efficiency of the assessment process, since each bridge must still be scanned individually. In fact, road closure is still required to perform such scans since the LiDAR equipment is often placed on tripods to collect data at a specific bridge. Another limitation of research in this area is that, despite the ability of LiDAR scans to capture different overhead objects including power lines and overhead signs, previous research seems limited to using the technology for assessing clearance at bridges only.

In summary, despite the growing interest in research on the extraction of different features from LiDAR in recent years, the review shows that more work is still required to fully utilize the true value of the technology. The review shows that potential for more research exists regardless of the application; however, there is a clear lack of research on utilizing LiDAR for the extraction and assessment of geometric design elements.

3   LIGHT DETECTION AND RANGING (LIDAR)

3.1   LiDAR Technology

Light Detection and Ranging (LiDAR) is an optical remote sensing technology that uses light rays to collect positional information about surrounding objects. LiDAR scanning can be airborne or terrestrial. Terrestrial LiDAR scans can be either static, where scanning equipment is mounted on a tripod; or mobile, where scanning equipment is mounted on a data collection truck. The most common approach to collect LiDAR for transportation applications is MLS, since road features can be captured with a high level of detail using this method [22]. In fact, the ability of MLS to capture a highly detailed representation of the entire roadway environment in a single survey pass gives it the edge over other remote sensing techniques such as photogrammetry and satellite imaging. Although such sensors often provide accurate scans of a road's environment, the level of detail captured or the area covered by sensors is often low. This means that the scans can only be used to extract or assess some features and not others. For instance, while it may be possible to use a low density ALS to assess sight distances, using the same dataset to extract information about road cross sections would not be possible.
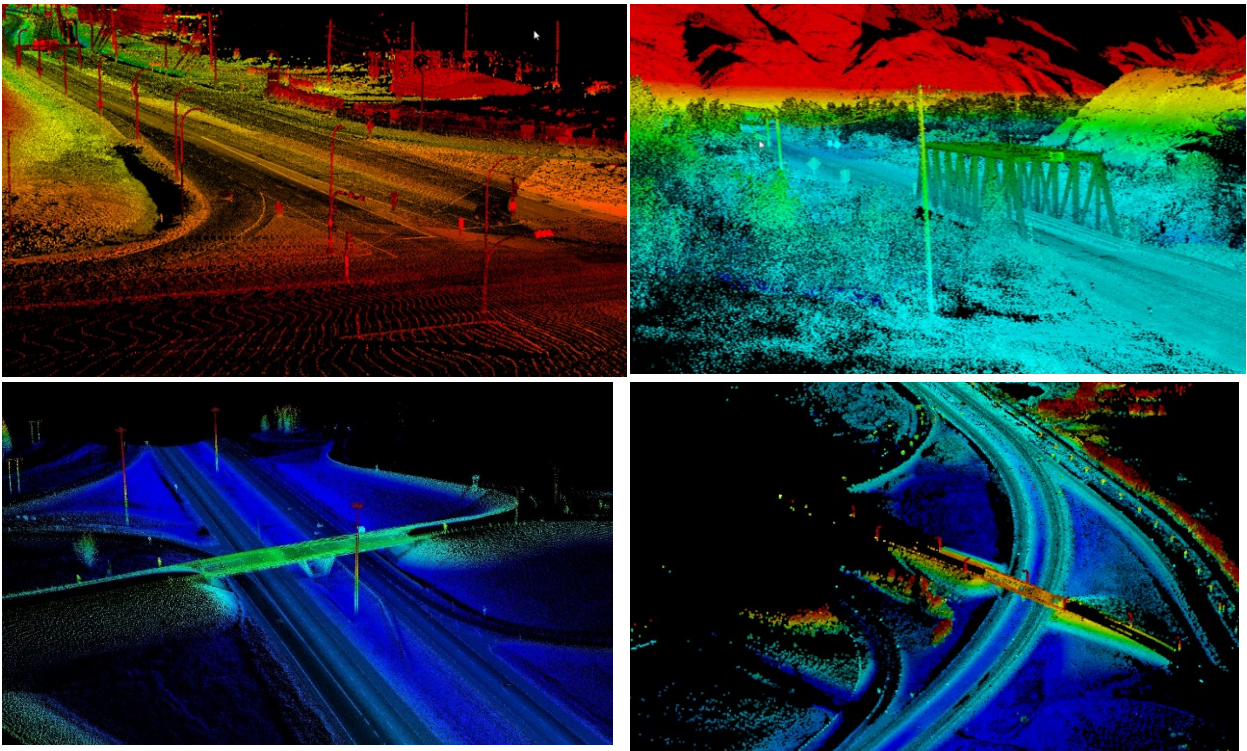
Figure 9: LiDAR point cloud data collected in Alberta

As already noted, in MLS vehicles mounted with laser scanning equipment travel along the highway of interest while constantly scanning the surrounding terrain; this results in a dense cloud of closely spaced points representing the surrounding infrastructure, as illustrated in Figure 9. This section describes the different components of a typical laser scanning system while providing a detailed description of the data collection process through which a 3D point cloud of LiDAR is assembled. The section also includes a brief description of the RIEGL VMX-450, which is the laser scanning system used to collect data for this thesis.

3.2   SYSTEM ARCHITECTURE AND LiDAR WORKING PRINCIPLES

3.2.1   SCANNING SYSTEM COMPONENTS

The system architecture of a basic laser scanning system consists of a dual frequency real-time kinematic GNSS, an Inertial Measurement Unit (IMU), and a laser scanner. Most scanning systems are also equipped with wheel-mounted Distance Measurement Indicators (DMI) and digital cameras. In addition to the sensors and the cameras, the system is also equipped with a data logging computer and a control system that integrates all sensors into a single system and facilitates data storage. It is worth noting here that, although many scanning systems used today are equipped digital cameras to supplement the LiDAR point clouds, datasets used in this thesis only consist of point cloud data with no images. Accordingly, the procedures developed in this thesis depend solely on the point clouds to extract the geometric attributes and perform the assessments.

Each component of the scanning system serves a specific purpose: the GNSS and IMU sensors provide accurate positional information of the scanning system as the LiDAR scanning truck travels along a highway corridor. Specifically, the GNSS system provides information related to the position (latitude, longitude), time and velocity of the scanning system. The IMU, on the other hand, is equipped with a microcomputer unit and a module of accelerometers and gyroscopes. The IMU records altitude information (i.e., heading, roll, and pitch) of the data collection vehicle as it travels along the highway corridor of interest. The DMI acts as a tracking system measuring the distance travelled to supplement information obtained by the GNSS and the IMU in cases where there is a lapse in the satellite signal. In addition, since the DMI is wheel mounted, it can sense positions when then data collection truck is static and, hence, helps reduce duplication in the LiDAR point cloud in those situations [17]. Figure 10 shows a typical laser scanning system and

the data collection truck on which it is mounted. It is important to point out here that the scanning system can be mounted on any vehicle to conduct the surveys.

Figure 10: Multi-Function Pavement Surface Profiling Vehicle (Left), VMX-450 MLS System (Right).

3.2.2 DATA COLLECTION PROCESS

A laser scanning system collects data through the laser scanners emitting light beams at surrounding objects. The light pulse emitted from the sensor, hits the target object and then gets reflected back to the scanner, based on the properties of the reflected beam and the position of the laser scanning system (obtained from the GNSS, IMU and DMI), the relative position of point off which the laser beam was reflected is computed. In addition, based on the amount of energy in the reflected beam, the scanning system also stores information about the intensity of the target point. The intensity reading is a measure of the strength of the reflected laser pulse, which is calculated based on the pulse wavelength. The strength of the return varies depending on the reflectivity and the composition of the surface object reflecting the laser pulse.

The data collection mechanism varies depending on whether the laser scanners are Time of Flight (TOF) or Phase-Based Scanners [104]. In case of TOF scanners such as the RIEGL VMX-450 used in this research, the scanner computes the position based on the reflection time. The time it takes for the emitted beam to hit the target point and reflect back to the scanner along the same trajectory is measured and, given the speed of light, the distance between the scanner and the target object is computed using the time-of-flight principle calculation shown in Equation 1.

$$d = \frac{\Delta t \times c}{2} \tag{1}$$

where d denotes the distance from the scanning system to the target point on the scanned object, Δt is the difference in time between the time the beam is emitted and the time of acquisition, and

c is the speed of light. The time difference must be divided by 2, since the light beam travels the measured distance twice.

In case of phase-based scanners, distance is computed based on the change in wavelength of the reflected beam as opposed to the time of flight.

During the scanning process, thousands of beams per second are transmitted from the laser scanner, with the aid of rotating mirrors, this results in millions or, in some cases, billions of distance measurements to surrounding surfaces [105]. Relative position information of the scanned object can then be determined based on the distance between the object and the scanner (*d*), and the positional information of the scanner obtained from the GNSS equipment as seen in Figure 11. The position of each point (*p*) in the mapping coordinate system (M) is computed as follows:

$$
\begin{bmatrix} P_x \\ P_y \\ P_z \end{bmatrix} = \begin{bmatrix} X_{GNSS} \\ Y_{GNSS} \\ Z_{GNSS} \end{bmatrix}^M + R_{IMU}^M(\varpi,\varphi,\kappa) \times \left(R_S^{IMU}(\Delta\varpi,\Delta\varphi,\Delta\kappa) \bullet r_{P'}^S(ad) + \begin{bmatrix} L_X \\ L_Y \\ L_Z \end{bmatrix}_S^{IMU} - \begin{bmatrix} L_X^{\frac{G}{I}} \\ L_Y^{\frac{G}{I}} \\ L_Z^{\frac{G}{I}} \end{bmatrix}_{GNSS}^{IMU} \right) \tag{2}
$$

where

$P_X; P_Y; P_Z$ denotes the Location of the target P in the mapping frame.

$X_{GNSS}; Y_{GNSS}; Z_{GNSS}$ denote the Location of GNSS antenna in the mapping frame.

$R^M{}_{IMU}$ denotes the rotation matrix between the mapping frame (M) and the IMU

ω, φ, κ represent the roll, pitch and yaw angles, respectively, measured by the IMU.

$R^{IMU}{}_S$ denotes the rotation matrix between the laser scanner (S) and IMU,

$r^S{}_P(ad)$ is the relative position vector of Point P in the laser scanner coordinate system. a and d denote scan angle and range measured, respectively.

L_X, L_Y, L_Z denote the lever-arm offsets from the navigation and IMU origin to the laser scanner origin determined by system calibration or measurement.

$L_X^{G/I}, L_Y^{G/I}, L_Z^{G/I}$ denote lever-arm offsets from the IMU origin to the GNSS origin determined by system calibration or measurement.
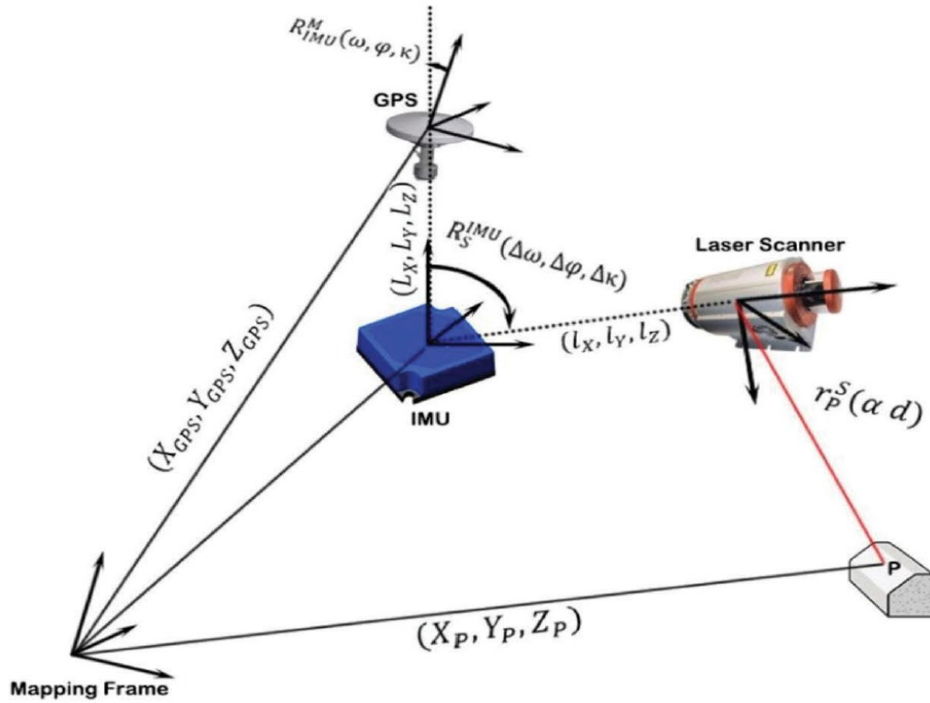
Figure 11: LiDAR Scanning [104]

3.3   RIEGL VMX-450 SCANNING SYSTEM

3.3.1   SYSTEM SPECIFICATIONS

The laser scanning system used to collect data for this thesis, commercially known as the RIEGL VMX-450, is depicted in Figure 12. The VMX-450 is equipped with two VQ-450 scanners that are symmetrically configured on the left and right sides, pointing toward the rear of the vehicle at a heading angle of approximately 145°. The VQ-450 scanner has a scan frequency of up to 550 Hz, which means a single survey pass is sufficient to yield a highly dense point cloud of the surrounding environment [104]. The scan speed of VQ-450 is 400 lines per second resulting in a scan rate of 1.1 million points per second for two laser scanners, a precision of 5mm and an accuracy of 8mm [106]. It is worth noting here that the relative and the absolute accuracy of the IMU/GNSS unit are 10mm and 20-50mm, respectively. The density of the points on a scanned object depends on the range, and the speed of the data collection truck, however, provincial surveys conducted at 90km/h result in LiDAR point densities on the pavement surface ranging from 150 to 1000 points/m^2 [107][6].

---

[6] Average point density and the factors impacting point density are discussed in Chapter 8 of the thesis

Data collected along a given highway is saved in multiple files in *.LAS* format with each file representing a certain segment along the highway. Data used in this thesis was segmented every 4km (i.e., each *.LAS* file contains the point cloud of a 4km section of a specific highway corridor). Due to the high point density of the data, the size of the 4km segment file could reach over 500 MB, hence, the segmentation is done to ensure that the file size is manageable.
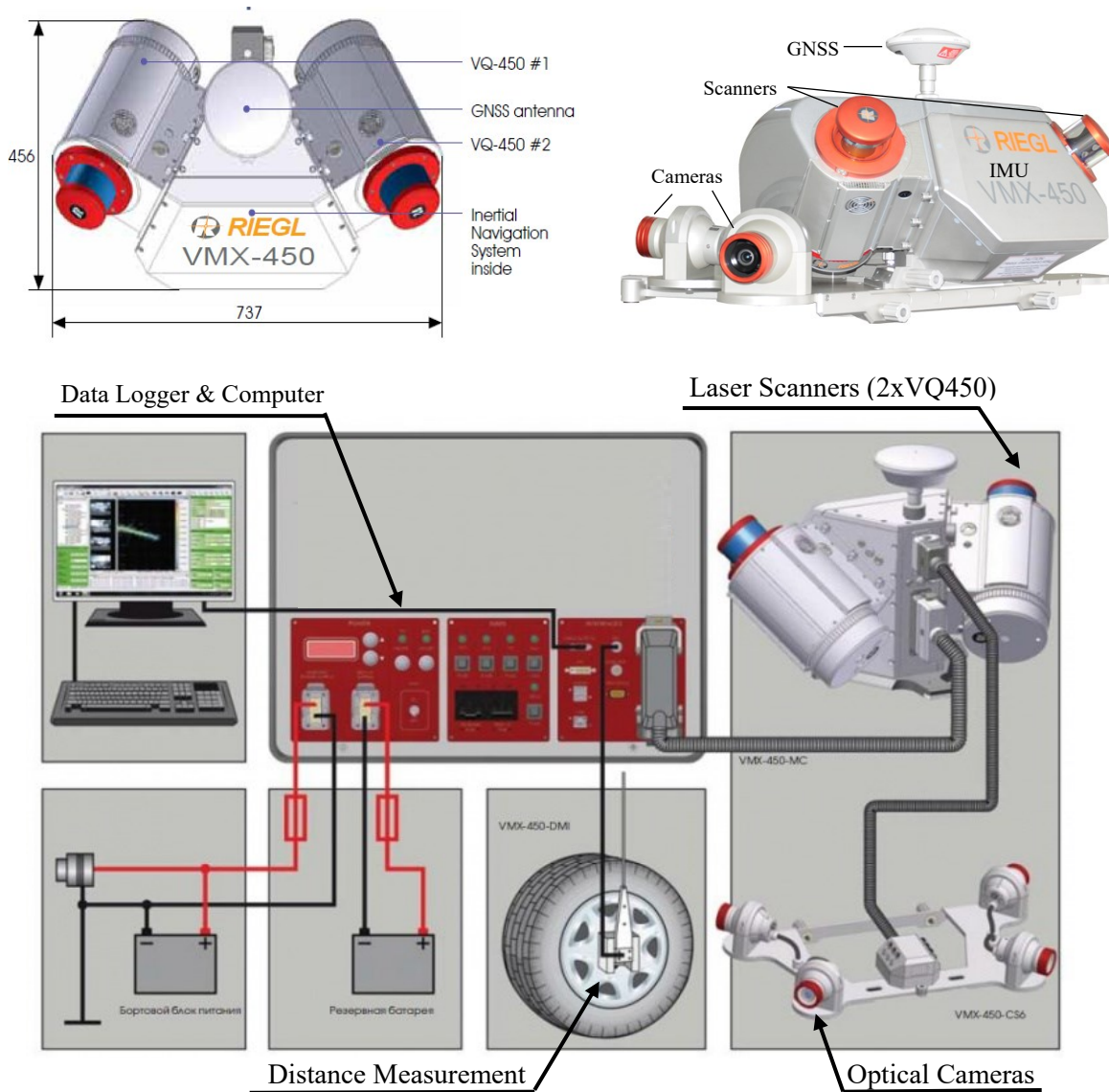
Figure 12: RIEGL VMX-450 Scanner Components

3.3.2 EQUIPMENT COST

Similar to most high-end mobile LiDAR scanning systems, the REIGL VMX 450 is costly equipment to acquire. In general, an MLS system could cost anywhere between $80,000 and

$700,000, depending on the specifications and the hardware included in the system[108]. Despite those high costs, LiDAR equipment is extremely cost effective when properly utilized.

In a recent study, Yen, et al. [17] conducted a comprehensive cost-benefit analysis of using mobile LiDAR technology in the management of Highway infrastructure. The authors only considered three applications in their assessment, namely, roadside feature inventory program (RFIP), bridge clearance measurement, and Americans with Disabilities Act (ADA)–feature inventory. The authors used information on the historical and current expenditures associated with these three applications at two western state DOTs (Washington State Department of Transportation and the California Department of Transportation) and compared that to the costs of using mobile LiDAR technology for the same applications.

The authors concluded that *"the benefits and cost savings from the bridge-clearance operations alone can outweighs the higher cost and produce higher savings"[17].* The study found that, although savings might not be apparent in the first cycle of data collection and inspections, savings could range from $1.3 million to $6.1 million after as low as three data-collection cycles. These conclusions are reached while only considering three applications for the technology. Moreover, the assessment did not include the indirect (intangible) benefits from using the technology such as the safety benefits, the higher data-collection speed, and higher data accuracy associated with using MLS.

In fact, even in the NCHRP review of LiDAR applications in transportation, DOT's surveyed on the top factors delaying the adoption of the technology, the majority of DOTs were more concerned about the lack of technical expertise required to process the datasets and the size and complexity of datasets as opposed to the cost of the equipment [21]. Funding ranked fifth on the list of 11 factors included in the survey.

Finally, the fact that LiDAR has become a critical sensor in most Autonomous Vehicle (AV) systems means that in the future data could be collected passively by AV as they navigate their way through the highway infrastructure, which could significantly reduce the data collection costs.

4   CROSS SECTION EXTRACTION AND SLOPE ESTIMATION

4.1   BACKGROUND

A road's cross-sectional elements are integral to the safe operation of a highway. In fact, an entire chapter (Chapter C) in Alberta's Highway Design guide is dedicated to recommendations governing the design of road cross sectional elements. Similarly, Chapter 4 of the AASHTO design guide is also entirely dedicated to cross section design.

Cross and side slopes are critical cross-sectional elements that have a significant role in highway design. Reducing the risks of safety hazards, such as hydroplaning, Cross slopes ensure speedy water drainage off roads. Similarly, designing a road's side slopes in a forgiving manner ensures that errant vehicles involved in potential run-off-the-road collisions, which account for approximately a third of all fatal crashes on highways [109,110], have a higher chance of recovery. Information about slopes is also critical to assessing a road's lateral clearance, roadside design, and vertical clearances. Identifying locations of ineffective slopes in order to be able to take corrective action in a timely manner is important to the safety and efficiency of highway operation.

Settlement, cracking, rutting due to traffic load, and soil movement are all environmental phenomenon that cause slopes to become ineffective. Therefore, regular assessment of slope conditions is required. Accordingly, most transportation agencies require that cross slopes and side slopes are constantly reviewed for compliance with current design standards. Transportation agencies require that field verification of such attributes is conducted, particularly if suspicion of deficiencies in road slopes exist [111]. Nonetheless, collecting such information on highways can be extremely challenging.

The manual procedures used to measure cross slopes are unsafe, time consuming, and labor intensive. Despite that, total stations and manual digital levels such as those shown in Figure 13 are still commonly used by DOTs for slope measurements [112,113]. These methods require field engineers to physically place equipment on the pavement surface to obtain the measurements. Furthermore, such procedures also require that traffic control is placed at locations where the assessment is intended causing major disruption to traffic; in fact, on most highways lane closures are only permitted during early morning hours [114], which means that authorities only have limited time to carry out their measurements. All these issues make highway surveyor-occupied

measurements of cross sectional attributes within travel lanes almost impossible, especially on highways with heavy traffic volumes and high speeds [114]. These problems are aggravated when cross section assessment is required on multiple locations along a highway or when network-level assessment of slopes on multiple highways is required. Although cross slope information could be obtained using IMU, side slope information could not be captured using such systems. Even for cross slopes, large-scale extraction of slopes on multiple lanes is more effective using a MLS system since, in a single pass, the system is able to capture a range of up to 800m which covers multiple lanes. Moreover, data collected in MLS could be used for the extraction for multiple roadway features limiting the number of site visits required even for other features and roadway design elements.

Figure 13: Road Slope Measurements Using Digital Level

For slope evaluation on a long road segment, most transportation agencies require that a Full Digital Terrain Model (DTM) of the roadway's width to be generated based on data from field visits or photogrammetric tools. The DTM is then used to estimate cross sectional information at 100ft intervals. If generating a DTM from the entire roadway is not practical, some guidelines recommend that the roadway limits where cross slopes are potentially out of tolerance (i.e., locations where there is suspicion of ineffective slopes) are first determined and DTMs are only generated for these limits [111]. While different transportation agencies follow slightly different procedures for slope assessments, most procedures are not practical when assessment is required on a long segment or when a network-level assessment is required. Although the use of photogrammetric techniques and GPS data are more efficient compared to the use of manual digital levels, these techniques also suffer from certain limitations. Using GPS data to estimate slope information on roads requires collecting multiple observations to achieve higher accuracy, which

is time consuming. Similarly, the accuracy of data obtained from photogrammetric techniques is often limited by the quality of the images, which can be impacted by environmental factors such sun angle [115].

The burden associated with such assessments could be alleviated if a procedure is developed to extract cross sections and their slopes from LiDAR point clouds. Unlike other mapping techniques, LiDAR creates a highly accurate 360^0 dense point cloud of a highway such as that seen in Figure 14, which means that millimeter-level accuracy in slope measurements on roads could be achieved.
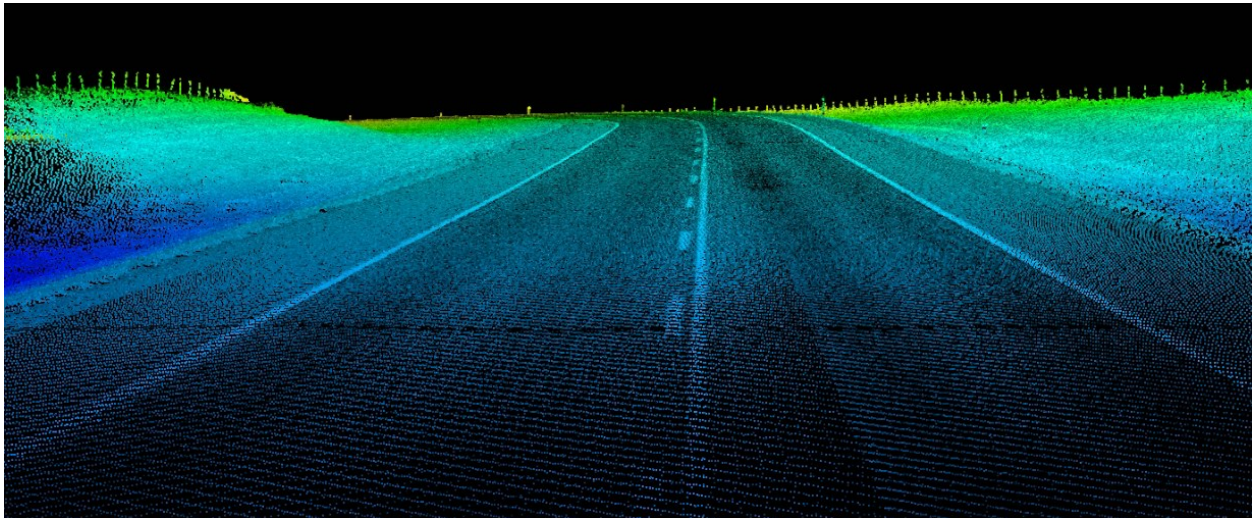
Figure 14: LiDAR 3D Point Cloud Data

As already highlighted in Chapter 2, not many studies have attempted extracting cross sectional slopes from LiDAR. Even the few studies that do exist in this area concentrate on extracting cross slopes of roads with almost no attention to side slopes [35,43]. In terms of the actual extraction procedure, most studies require prior knowledge of lane markings and, in some cases, lane widths in order to define the end points of slopes [35,43]. While this might not be a major issue on most roads, extracting lane marking information extends the duration of the extraction process, moreover, the quality of lane markings on some rural roads might have degraded limiting the extraction capabilities.

The novel algorithm proposed in this chapter overcomes the aforementioned limitations to facilitate automated cross section extraction from LiDAR point cloud data in a highly efficient and accurate manner. The proposed algorithm involves defining vectors that intersect the road's axis. Points within proximity of the vectors are then extracted from the point cloud representing the roads cross section. Multivariate Adaptive Regression Splines and *k*-means clustering are used to

identify points of change in slope on the extracted cross section, and linear regression is used to estimate the slopes.

The extraction algorithm is tested on different highway segments in the province of Alberta where multiple cross sections were extracted along each highway and the slope information was estimated. For validation purposes, the slope estimates were compared to slope information obtained by Alberta Transportation (AT) in separate surveys.

4.2 EXTRACTION ALGORITHM

This section includes a detailed description of the extraction algorithm developed in this chapter for the extraction of cross sections.

The cross-section extraction algorithm starts with defining position vectors and using them to create equally spaced trajectory vectors along the road's profile. Vectors normal to the trajectory are then constructed and the points within certain distance of a plane parallel to the normal vectors are extracted. These points represent the road's cross section at the location of the normal vector. The cross section is rotated and cleaned up, removing erroneous observations including outlying points and roadside vegetation. After that, k-means clustering and MARS are used to identify knots (i.e., points of inflection or change in slope). Finally, linear regression is used to estimate the slopes between the knots, which represent the cross slopes and side slopes of the extracted cross section. Details of each step in the algorithm are provided in the next few paragraphs.
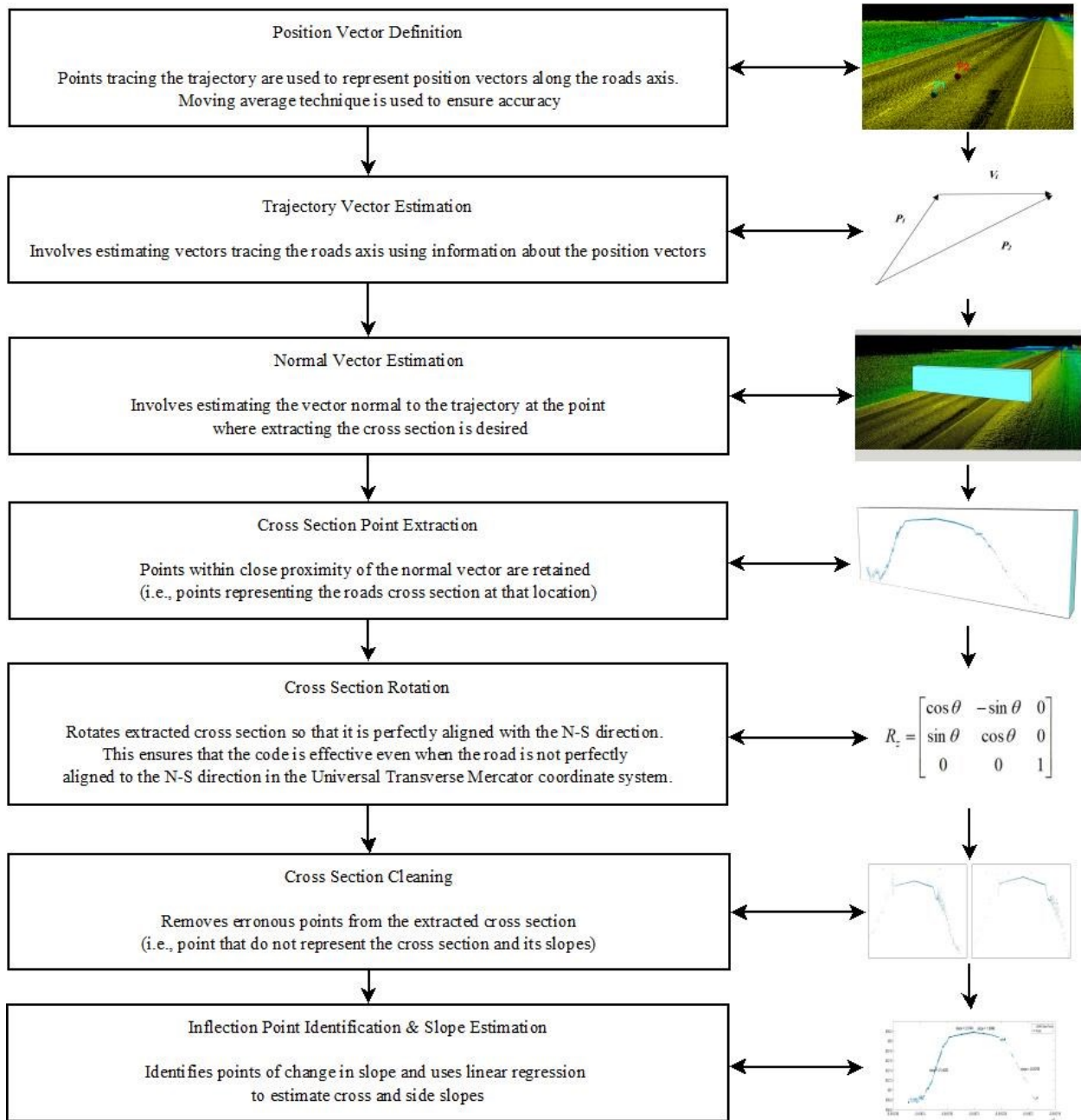
Figure 15: Cross Section Extraction Pipeline[7]

4.2.1 TRAJECTORY DEFINITION & TRAJECTORY VECTOR CREATION

The first step of the extraction involves defining points parallel to the road's centreline, which trace the roads trajectory and cover the entire segment (known as the position vectors). To obtain

---

[7] More information about the extraction algorithm is provided in the next few paragraphs

the position vectors, the point cloud was filtered based on scanner angle. Points that fell within the Nadir plane of the laser scanner (i.e., points that lie right below the scanner) were filtered out to represent the position vectors.

Although the position vectors are a very good representation of the road's axis, occasional deviation in points exist due to the changes in the yaw angle of the data collection vehicle. To ensure that these deviations did not impact the accuracy of the extraction, the moving average technique was used to estimate the new position vector (P_j) based on the positions of a set of three consecutive position vectors ($i = 1$ to m) as follows:

$$P_j = \frac{\sum_{i=1}^{m} P_i}{m} \tag{3}$$

The average position of three points is used to define the position vectors representing the end points of each trajectory vector.
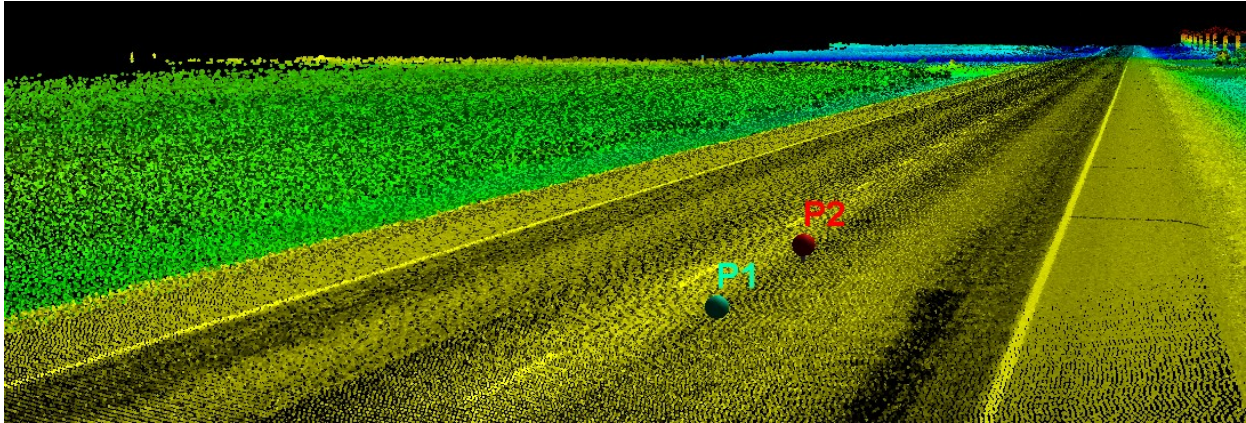
Figure 16: Position Vectors

Let $\widehat{P_1}$ be the position vector defining the start-point of the trajectory vector. Similarly let $\widehat{P_2}$ represent the position vector representing the end-point of the trajectory vector. In that case, the trajectory vector ($\hat{V}_i$) at a point i along the road can be defined as follows:

$$\hat{V}_i = \hat{P}_2 - \hat{P}_1 \tag{4}$$

Where, $\hat{P}_1 = \begin{bmatrix} x_1 \\ y_1 \\ z_1 \end{bmatrix}$ and $\hat{P}_2 = \begin{bmatrix} x_2 \\ y_2 \\ z_2 \end{bmatrix}$, hence $\hat{V}_i$ can be rewritten as follows:

57

$$\hat{V}_i = \begin{bmatrix} x_2 \\ y_2 \\ z_2 \end{bmatrix} - \begin{bmatrix} x_1 \\ y_1 \\ z_1 \end{bmatrix} = \begin{bmatrix} x_2 - x_1 \\ y_2 - y_1 \\ z_2 - z_1 \end{bmatrix} \qquad (5)$$

Multiple trajectory vectors ($i = 1$ to n) are defined between each pair of consecutive position vectors. The number of trajectory vectors defined depends on the length of each and the length of the segment analyzed, which is predefined by the user. For cross section extraction, 5m long trajectory vectors are recommended (i.e.,, the set of position vectors representing P_1 and P_2 are chosen to be 5m apart). Although this parameter can be altered by the user, the vectors should not be too long since this will create a poor representation of the roads profile on curved segments. To ensure that 5m vectors were sufficient to replicate the road's profile, sensitivity analysis was run on the data. The results of the analysis are presented in Section 4.3 of this Chapter.

4.2.2 NORMAL VECTOR DEFINITION

Once the trajectory vectors are defined the next step is to estimate the normal vector of the point at which the desired cross section is to be extracted. The normal vector (N_i) for each trajectory (V_i) can be estimated as follows:

$$N_i = \begin{bmatrix} v_y & -v_x & v_z \end{bmatrix} \qquad (6)$$

where, v_x, v_y, and v_z are the components of the trajectory vector (V_i).

After estimating the normal vector at every point i along the road, these vector are then shifted to the midpoint of the trajectory vector using a translation vector T_i so that the cross section is extracted at the midpoint of each trajectory vector V_i.

4.2.3 CROSS-SECTION POINT EXTRACTION AND ROTATION

The cross section extraction process involves extracting points that are within acceptable proximity of a plane that is parallel to the normal vector and perpendicularly intercepts roads centerline as seen in Figure 17. The dimensions of the plane are predefined by the user however, in cases where the algorithm is to be applied to a two-lane undivided highway a width in the region of 24m should be sufficient for capturing all cross slopes and side slopes. As for the depth of the cross section (i.e., the dimension of the plane that runs parallel to the road's centerline), this depends on the density of the LiDAR point cloud. If the point cloud density is high, a cross section depth of 0.2m was found to be sufficient to obtain accurate estimates of road slopes in previous work [35]. In fact, the sensitivity analysis of the depth parameter conducted in this thesis (Section 4.3 of this

chapter) reveals that even a depth of 0.05m is sufficient. Similarly, using a depth of up to 0.4m does not seem to add much value to the accuracy of the slope estimates.
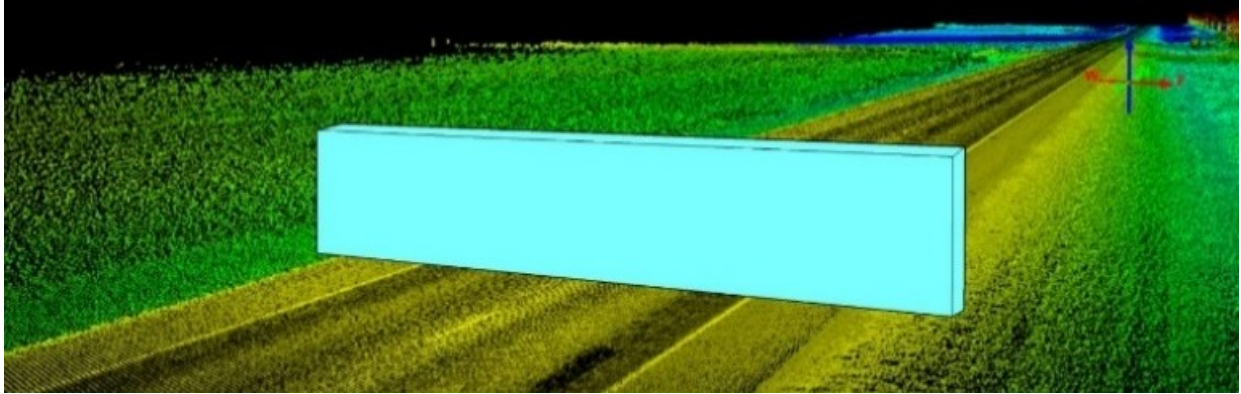
Figure 17: Cross Section Plane

The distance between each point and the normal plane is calculated using the cross product. The process involves looping through all points in the LiDAR point cloud and measuring their proximity to the normal plane. Points that satisfy proximity requirements are saved and exported as a *csv*.

To ensure that the extraction is applicable regardless of the orientation of the road, rotation of the extracted cross section around the global z-axis was essential. The rotation matrix (R_z) in Equation 7 is used to transform all points in the extracted cross section to a north-south orientation. In other words, the road centerline for all segments is rotated to run along the y-axis of the Universal Transverse Mercator (UTM) grid. This rotation helps avoid distortion when plotting the cross sections and ensures that filters used in the cross section cleanup stage (section 4.2.4) are applicable regardless of the roads profile's orientation on the UTM grid. The rotation also helps distinguish the side of the road for which slope estimates are obtained.

$$R_z = \begin{bmatrix} \cos\theta & -\sin\theta & 0 \\ \sin\theta & \cos\theta & 0 \\ 0 & 0 & 1 \end{bmatrix} \tag{7}$$

where, θ is the rotation angle which depends on the azimuth of the trajectory vector (V_i).

4.2.4 CROSS-SECTION CLEANUP

Although cross section extraction is achieved at this stage, the extracted cross sections typically contain erroneous points and outlying observations that impact the accuracy of slope estimates. Therefore, the extracted cross sections had to be cleaned up, which is achieved in two stages. An

intensity-based filter is first applied to the cross section and any remaining outliers are omitted using a statistically defined buffer region.

For most cross sections, the majority of erroneous points represented the vegetation on the side of the road (such as grass, trees, and shrubs). Vegetation is highly reflective to light rays, hence, points representing vegetation typically have high intensity values. Consequently, cross section points with the highest intensity are removed. Only 10% of the data is removed since excluding more points could potentially cause the elimination of points on the road's surface.

Intensity based filtering removes a significant portion of the noise, however, other outliers with low intensity might still exist. These low intensity points could be clusters of dust, vehicles or even point clusters due to multipath errors. To remove those points a buffer zone is used to outline areas where it is impossible for cross section points to exist. The right and left most bounds of the buffer zone are defined as follows:

$$if \ x_i > \bar{x} + 1.25\sigma_{\bar{x}} \ and \ z_i > \bar{z} + 0.1\sigma_{\bar{z}},$$
$$then \ (x_i, z_i) \ is \ an \ outlier$$

Similarly,

$$if \ x_i < \bar{x} - 1.25\sigma_{\bar{x}} \ and \ z_i > \bar{z} + 0.1\sigma_{\bar{z}},$$
$$then \ (x_i, z_i) \ is \ an \ outlier$$

where, x_i and z_i denote the x-coordinate and z-coordinate of the cross section point (i), respectively; $\bar{x}$ and $\bar{z}$ denote the average x-coordinate and z-coordinate of all cross section points, respectively; and $\sigma_{\bar{x}}$ and $\sigma_{\bar{z}}$ represent the standard deviation of the x-coordinate and z-coordinate of all cross section points, respectively.

Figure 18 shows the cross section before and after cleaning. The figure shows that the clean up process is effective in removing a large portion of the vegetation on the sides while retaining points on the road's surface. It is worth noting here that the regions further down the side slopes were not included in the buffer zone filter since there was a high risk of losing point on the bare ground at those locations.
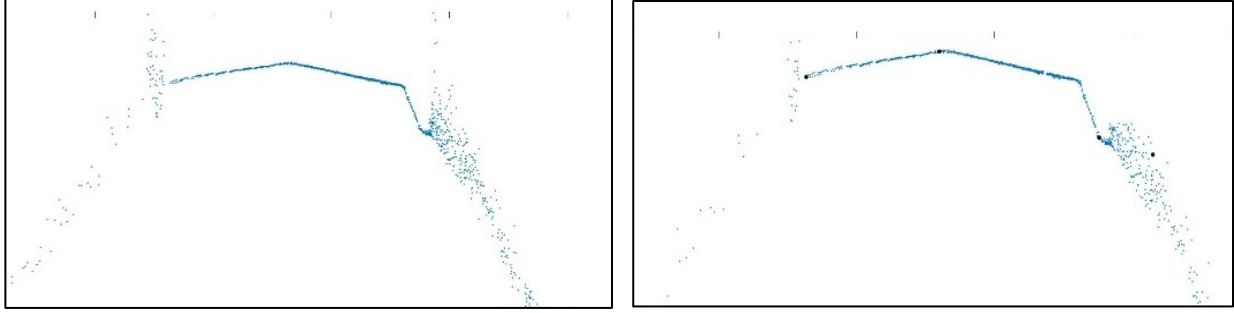
(a) Before Clean Up
(b) After Clean Up

Figure 18: Cross Section Clean Up

4.2.5 KNOT IDENTIFICATION

Since the proposed method is fully automated, it is assumed that the lane dimensions are unknown. Thus, points of inflection (change in slope) must be determined automatically. A two-step procedure is proposed for this cause: (i) Cross section clustering using k-means, and (ii) break point estimation using MARS.

4.2.5.1 K-MEANS CLUSTERING

k-means is an unsupervised learning algorithm used for clustering data. It works on assigning *n* data points to *k* clusters whereby each observation is assigned to the cluster with the nearest mean. Mathematically, the algorithm works on minimizing a squared error objective function. The algorithm aims to minimize the following objective function:

$$J = \sum_{j=1}^{k}\sum_{i=1}^{n}\left\|x_i^{j} - c_j\right\|^2 \tag{8}$$

Where, $\left\|x_i^{j} - c_j\right\|^2$ is a distance measure between observation x_i and the centroid of the cluster c_j. This is an indication of the distance of n points from their cluster centres.

In this Chapter Euclidian Distance was used as the measure to cluster different parts of the cross section. Four different clusters ($k = 4$) are specified since it is desired to break the cross section into two parts either side of the road's crown (to estimate cross slopes) and two parts in the ditch of the road (to estimate side slopes).
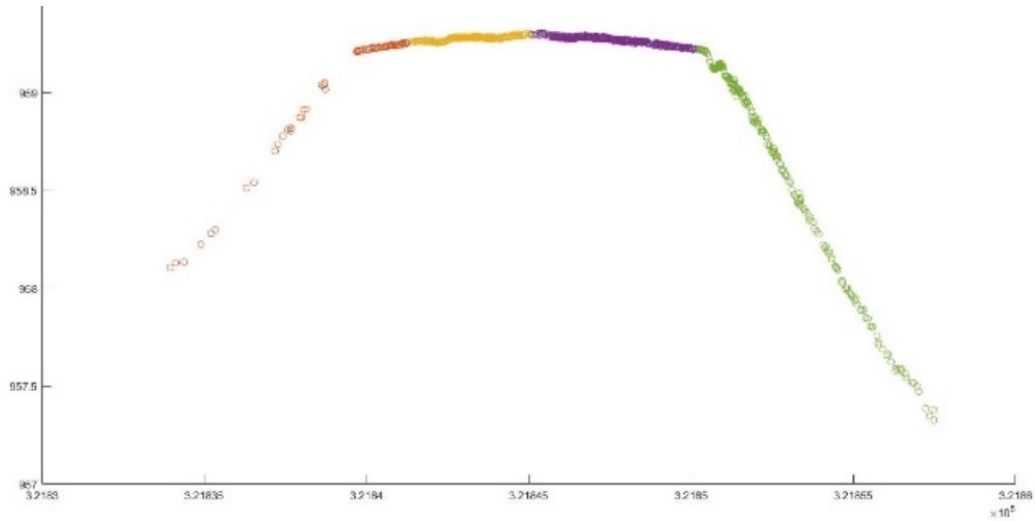
(a)   Clustering Results
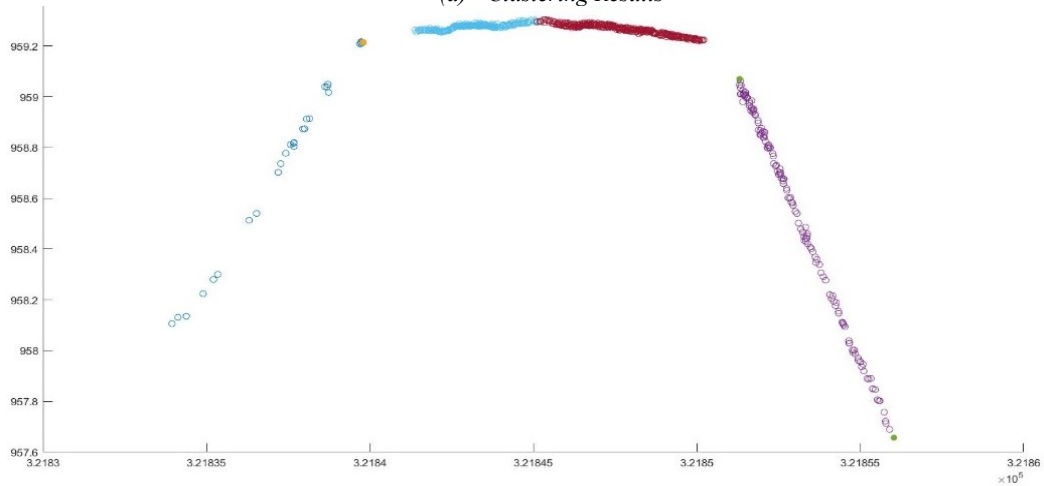
(b)   Change Point detected using MARS
Figure 19: Inaccurate Assignment k-means

Although the *k*-means is effective in accurately breaking up the cross section into four portions that accurately represented the crown and the sides of the road in most cases, occasional inaccurate assignments of point on the side slope to the cross slope and vice versa could occur as illustrated in Figure 19a. To overcome this, MARS is used to identify any break points where changes in slope between points in the same cluster were detected. It is worth noting here that using the MARS regression without clustering is possible, however, MARS is extremely sensitive to the existence of outlying points, hence, developing a MARS model for the entire cross section reduces the likelihood of accurately detecting the break points.

62

4.2.5.2 MARS REGRESSION

MARS is a form of piecewise linear regression introduced by Friedman [116]. MARS extends product spline basis functions such that the basis functions and their parameters, including knot locations, are determined automatically. In other words, MARS is a non-parametric regression technique that automatically detects and models non-linearity in data. The general notation for the MARS model is denoted as follows

$$f(x) = \sum_{i=1}^{n} c_i B_i(x) \tag{9}$$

where, *B(x)* is a basis function that can take the form of a constant or a hinge function.

A hinge function takes one of the following functional forms

$$\max(0, x - c) \tag{10}$$

$$\max(0, c - x) \tag{11}$$

where x is the independent variable and c is a constant which is also known as the knot.

It is worth noting that MARS uses modified recursive partitioning to adjust the coefficient values to best fit the data. This enables the automated selection of values for the knot variables of the hinge functions. These knots are the points of change in slope, which are required to estimate the slopes of the cross section.

4.2.6 SLOPE ESTIMATION

After identifying the knots on the cross section, cross slopes and side slopes could then be estimated. Points between each pair of consecutive knots are linearly regressed to estimate the slopes. Although cleaning up the cross sections removes a high portion of the noise, for some segments where high vegetation exists on the side of roads, some outliers may still exist.

The cross section and slope estimation algorithm detailed in the past few paragraphs were coded entirely in MATLAB. The code that utilizes the *earth* package in in **R** statistical software v3.3.1 was used to run the MARS regression [117]. To ensure full automation the *R* code was embedded into MATLAB.

4.3   SENSITIVITY ANALYSIS

Before testing the proposed algorithm, it was important to perform sensitivity analysis of the user-defined parameters in the extraction algorithm. The parameters discussed in this section are cross section depth and trajectory vector length.

4.3.1   CROSS SECTION DEPTH

To understand the impacts of the cross-section depth on slope estimates, 20 different slopes (including cross and side slopes) were estimated at the same station while changing the depth of the extracted cross section on one of the test highways. Figure 20 a and b show the results of the sensitivity analysis for cross slopes and side slopes, respectively. As seen in the figures, changing the depth of the cross section had limited effects on the slope estimates. In fact, there are also no common trends in the relationship between depth and slope estimates, which indicates that the minor differences are due to random error in the observations. This observation is reasonable considering the high point density on the road surface. The high point density means that even with a depth of 5cm, enough points are extracted along the roads cross sections, which ensures accurate slope estimates.
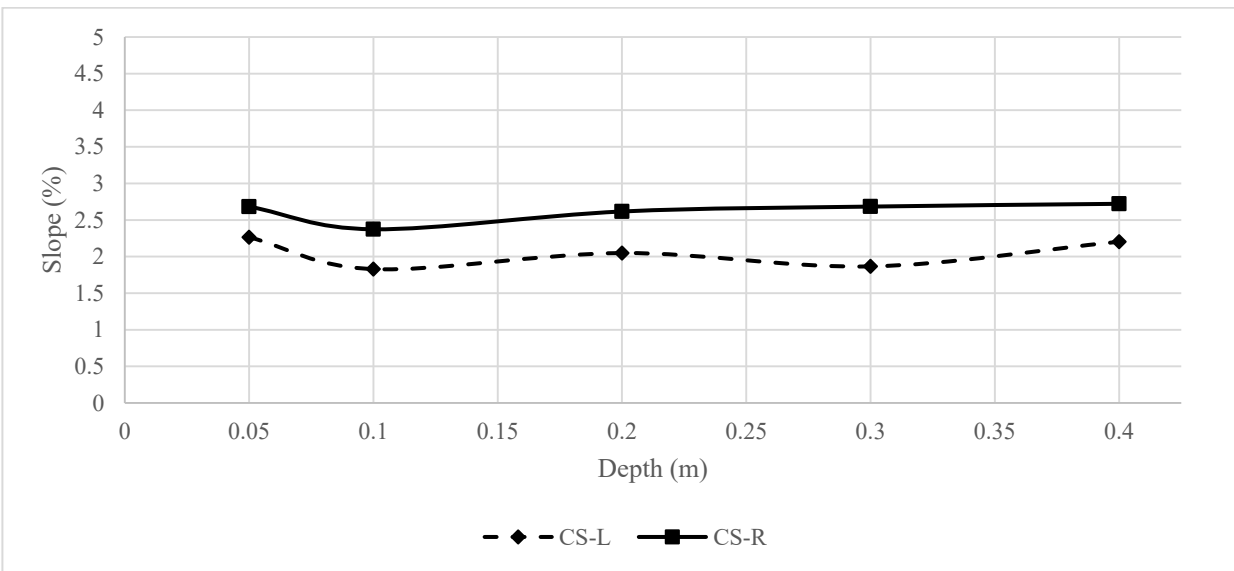
(a)   Cross Slopes Left and Right
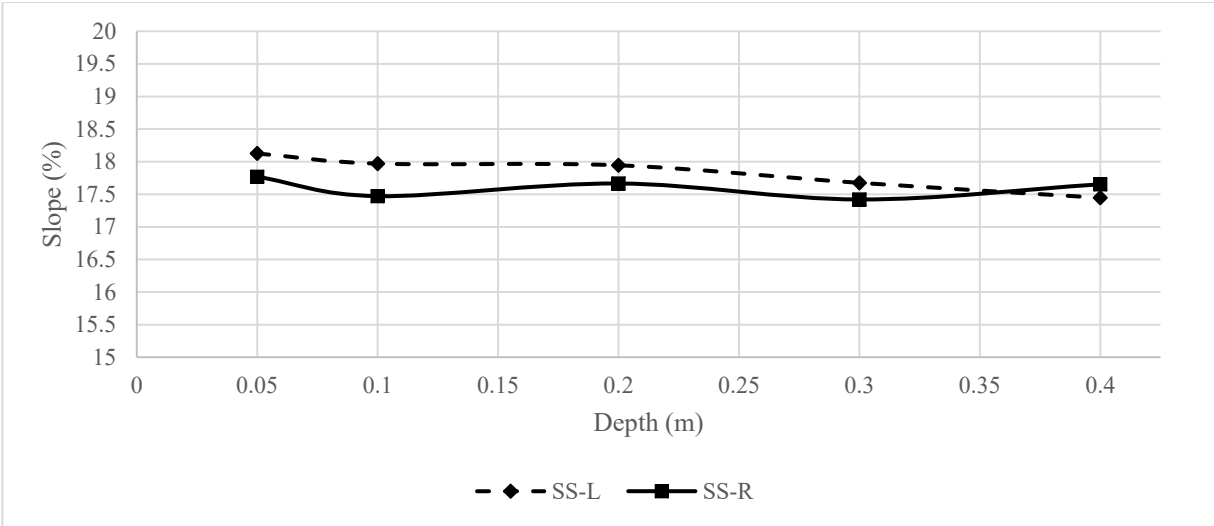
(b) Side Slopes Left and Right
Figure 20: Sensitivity Analysis of Cross Section Depth

4.3.2 LENGTH OF TRAJECTORY VECTORS

As already indicated, the length of trajectory vectors (or the spacing between the two position vectors used to estimate the trajectory vector) is user defined. However, the length should be specified while ensuring that the vectors are short enough to accurately replicate the road's profile, yet not too short to avoid capturing oscillations in the vehicle's yaw angle as actual changes in alignment. To identify whether the 5m length for the trajectory vectors was sufficient, sensitivity analysis was run on a LiDAR highway segment with a curve. This was done by estimating the change in azimuth between consecutive vectors at different vector lengths. The outputs of the analysis, as illustrated in Figure 21, show that 5m vectors were indeed the most effective since the change in azimuth between consecutive vectors is minimized at a length of 4-5m.
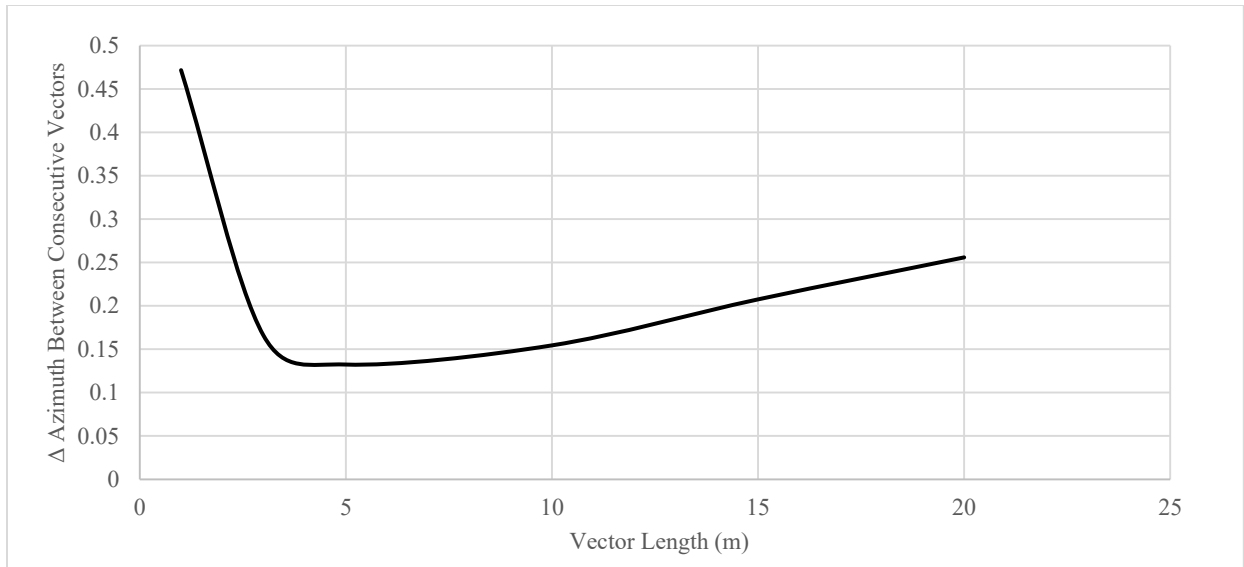
Figure 21: Sensitivity Analysis for Trajectory Vector Length

4.4   TEST DATA

4.4.1   DATA COLLECTION

As previously discussed, data used in this thesis was collected by AT using the RIEGL VMX-450 laser scanning system. More information on the capabilities of the REIGL VMX-450 are presented in Chapter 3 of this thesis. It is worth noting here that, the impacts of point density on the extraction of cross sections and their slopes are discussed in Chapter 8 of this thesis where a comprehensive assessment is performed.

Cross slopes estimated using the proposed method were compared to slope data stored in AT's Database. The information collected by AT was obtained in GPS surveys. Unfortunately, detailed information about how the slope information was collected by AT was not available, however, AT did provide information about the accuracy of a typical GPS survey. In a typical GPS survey the latitude and longitude coordinates are measured in degrees expressed as a minimum of 7-decimal real value in reference to the North American Datum 1983 Canadian Spatial Reference System (NAD83 CSRS) using the GSD95 Canadian geoid model for orthometric heights. Although measuring slopes on a road segment is not affected by absolute accuracy (i.e.,, the global accuracy of the points is not an issue when measuring slopes as long as they are accurate relative to one another), absolute accuracy of GPS data is also relatively high with horizontal errors being bounded by a circle of 0.625m radius 95% of the time. Similarly, the vertical coordinate is accurate to within 0.875m radius 95% of the time. Unlike GPS, digital level data was not available within

AT's database and, hence, it was not possible to compare the extracted information to digital level data.

4.4.2 TEST SEGMENTS

The extraction algorithm proposed in this Chapter was tested on two different highway segments in Alberta. The two highways (Highway 53 and Highway 36) are shown in Figure 22 and Figure 23, respectively.

Highway 53 is a two-lane undivided highway in central Alberta. The highway intersects Highway 2 just north of the City of Red Deer. The analyzed segment on Highway 53 lies slightly east of Highway 2 and extends a length of 4km. The segment falls between Highway 2 and Highway 21. Some variations in the road's vertical alignment exist along the analyzed segment. In contrast, no variations in horizontal alignment exist. Vegetation in the roadside area is moderate to high, with trees planted on the roadside at some locations. No interchanges or major intersections exist on the analyzed segment, however, access to local roads is provided.
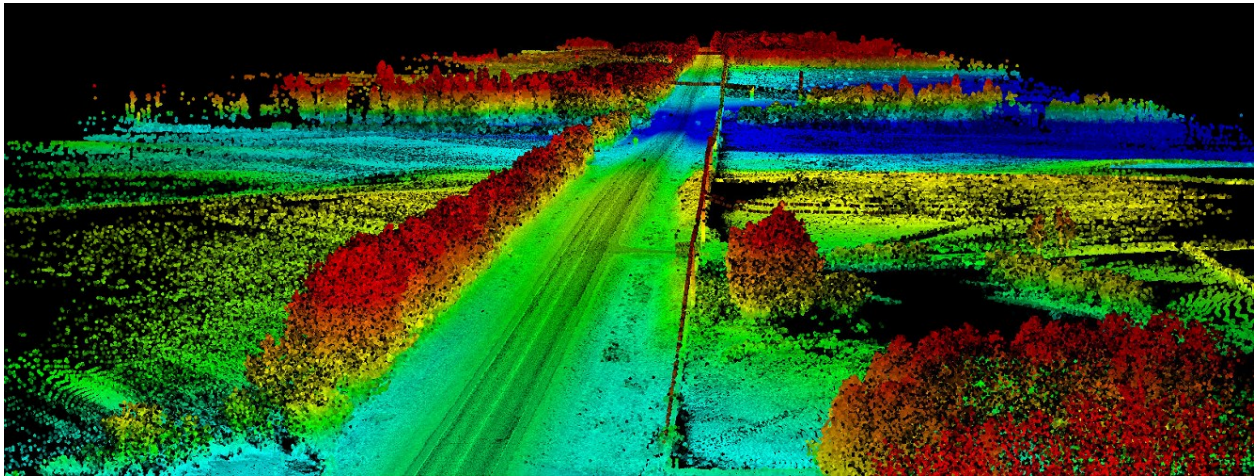
Figure 22: Test Segment on Highway 53
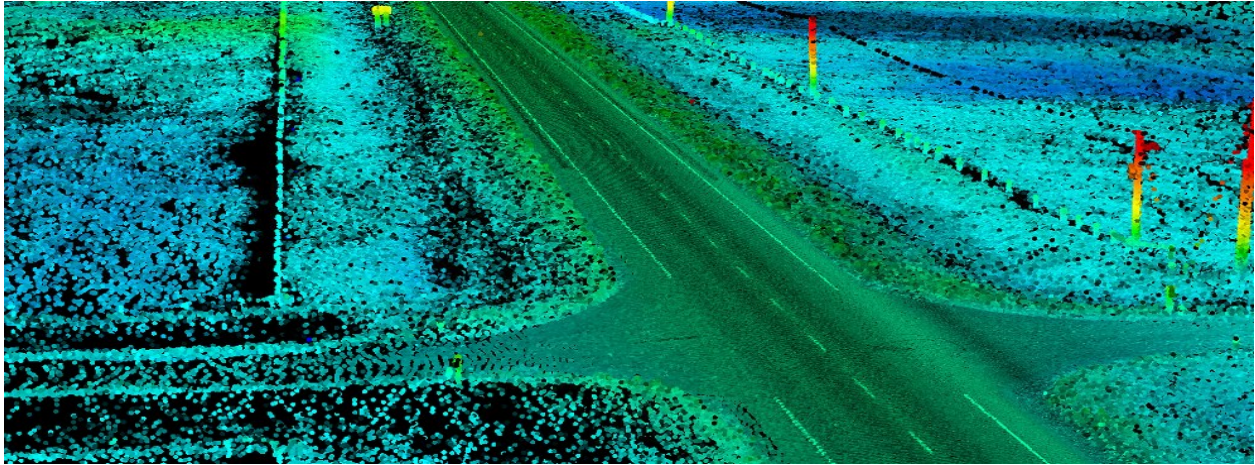
Figure 23: Test Segment on Highway 36

Highway 36 is a two-lane undivided highway in Alberta. The analyzed segment of Highway 36 was a 2km segment northeast of Drumheller. In general, vegetation is relatively low on this segment and the roadside area is relatively clear. The vertical alignment along the segment varies slightly and the speed limit on the road is 100 km/h. No major intersections or interchanges exist on the segment; however, the segment is accessible through local service roads.

4.5   RESULTS AND DISCUSSION

To test the algorithm proposed in this chapter, it was used to extract cross sections and estimate slopes on multiple highway segments in Alberta. Testing was conducted by importing a laser scan on of the test highway into the algorithm, which then outputted a set of points representing the cross section as well as slope estimates at a predefined station, or set of stations. The results presented in this section are those obtained from testing the algorithm on Highways 53 and 36.

Table 1 and Table 2 show slope information extracted at multiple stations along the LiDAR highways. Furthermore, Figure 24 and Figure 25 show LiDAR points representing the extracted cross sections at a selection of stations along the two highways. Slopes shown in the Table 1 and Table 2 are shown in decimal degrees while the slopes shown in Figure 24 and Figure 25 are in percent. The Figures show that the developed algorithms were extremely effective in extracting the road's cross sections. The knot locations are also highlighted on the figures with the end points, midpoint and the points of change in slope all estimated at a reasonable level of accuracy. The next few paragraphs discuss the slope estimates obtained on the two test highways.

4.5.1 CROSS SLOPES

Cross sections were extracted every 100m for a 1km stretch on each test highway, which demonstrates the value of the proposed algorithm in performing network level assessment of slopes on a highway segment. The cross slopes fell around the expected range of 1% to 2% on both segments (see Table 1 and Table 2). This range is the standard used in the Alberta Highway design guide for Asphalt Concrete Pavement highways [118].

Table 1: Slope Estimates Highway 53

Station (m)	SS Left (WB)[*]	CS Left (WB)[*]	CS Right (EB)[*]	SS Right (EB)[*]
21700	0.216	0.010	-0.032	-0.157
21800	0.201	0.010	-0.026	-0.135
21900	0.180	0.010	-0.023	-0.140
22000	0.222	0.011	-0.024	-0.149
22100	0.199	0.013	-0.022	-0.163
22200	0.244	0.011	-0.024	-0.173
22300	0.216	0.015	-0.025	-0.197
22400	0.237	0.014	-0.025	-0.156
22500	0.179	0.010	-0.026	-0.177
22600	0.217	0.014	-0.020	-0.203
22700	0.215	0.020	-0.019	-0.209
Mean	0.211	0.013	-0.024	-0.169
SD	0.020	0.003	0.003	0.025

Table 2: Slope Estimates Highway 36

Station (m)	SS Left (SB)[*]	CS Left (SB)[*]	CS Right (NB)[*]	SS Right (NB)[*]
25200	0.177	0.024	-0.025	-0.277
25300	0.162	0.018	-0.026	-0.309
25400	0.206	0.026	-0.027	-0.278
25500	0.176	0.019	-0.026	-0.152
25600	0.129	0.019	-0.026	-0.151
25700	0.128	0.019	-0.027	-0.252
25800	0.105	0.015	-0.028	-0.129
25900	0.137	0.018	-0.028	-0.183
Mean	0.153	0.020	-0.027	-0.217
SD	0.033	0.003	0.001	0.070

[*]Units are in decimal degrees, negative denotes opposite direction
CS: Cross Slope, SS: Side Slope
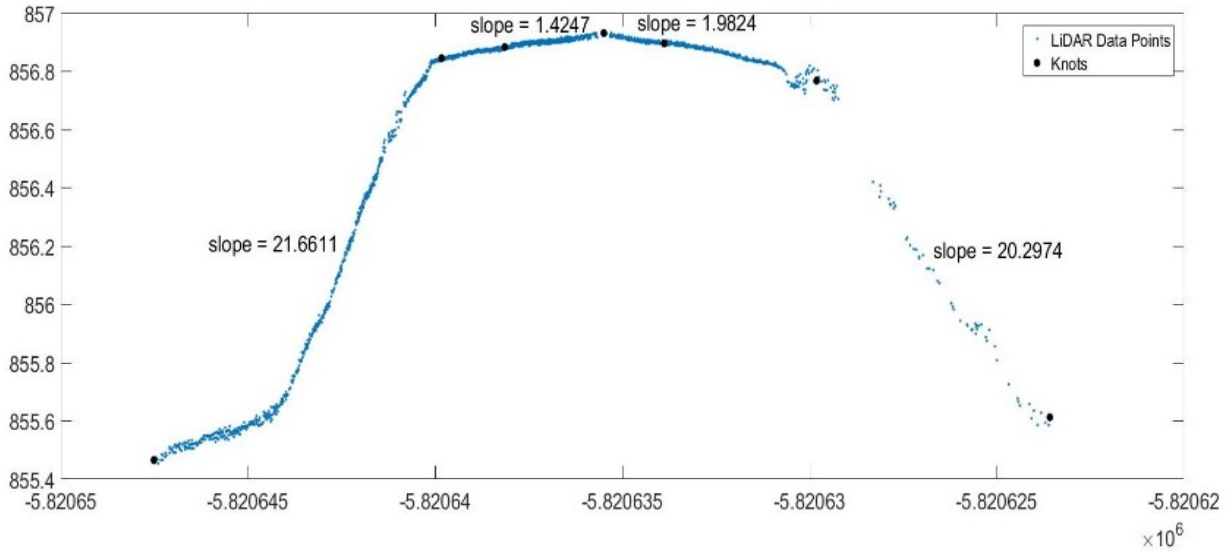
(a) Highway 53 Station 22600m
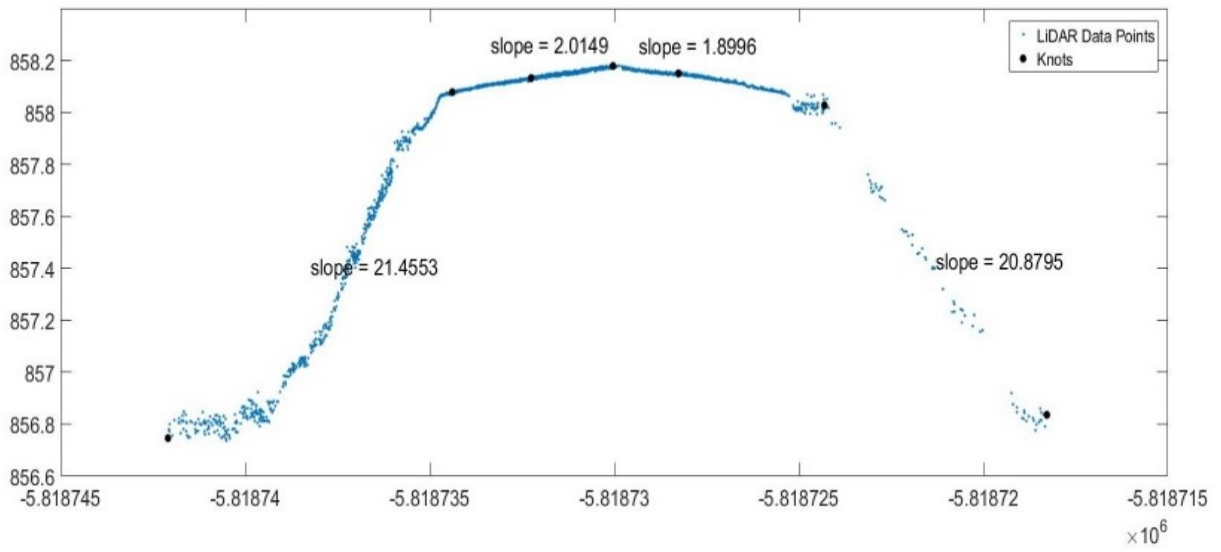
(b) Highway 53 Station 22700
Figure 24: Extracted Cross Sections Highway 53 (axes are in meters, slopes are in %)
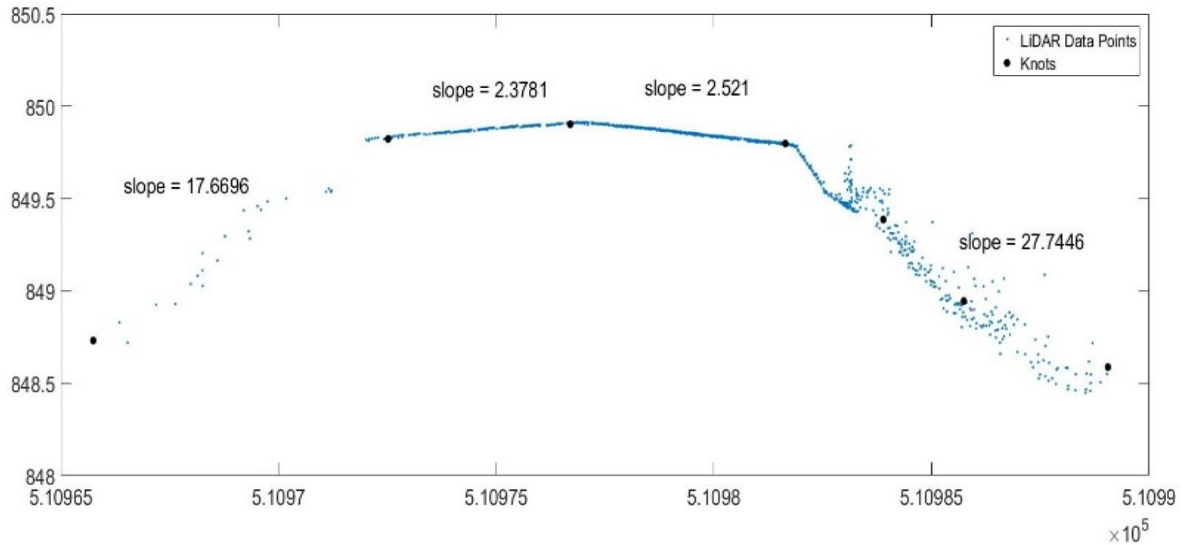
(a)   Highway 36 Station 25200m
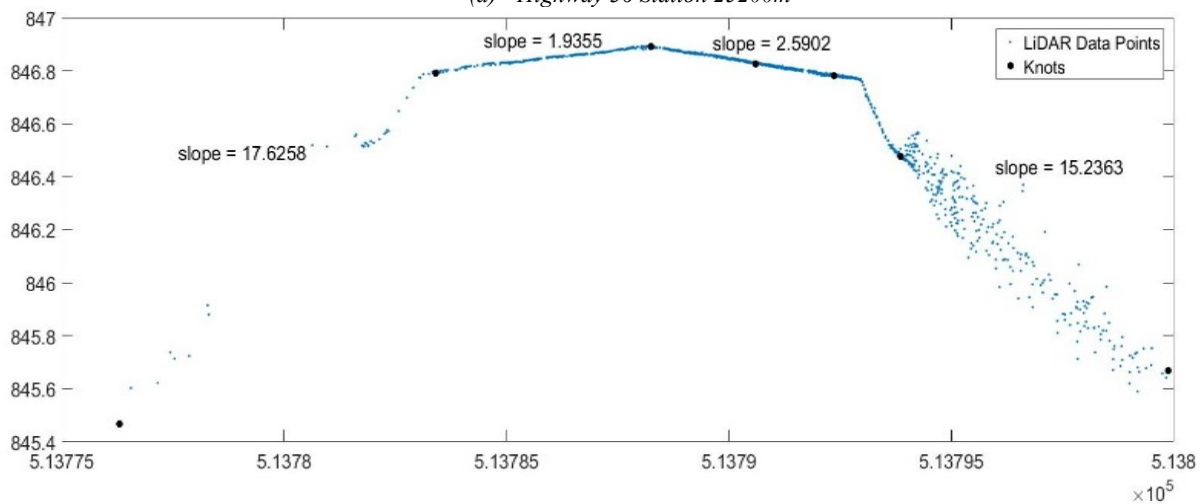
(b)   Highway 36 Station 25500m
Figure 25: Extracted Cross Sections Highway 36 (axes are in meters, slopes are in %)

Although slopes are not expected to be constant along a highway segment, significant variation in slopes is not expected either, unless that was intended in the design stage. Therefore, the fact that there was no major variation in cross slopes along the corridor is positive finding. The standard deviation of cross slopes along the 1km stretch for both travel approaches on both segments did not exceed 0.3%. These slight variations are expected given imperfections during the construction stage. In fact, it is worth noting that the instrument precision for a digital level ranges between 0.05% and 0.2% depending on the slope angle [119], hence, it is unlikely that a digital level would capture the difference in cross slopes obtained from the LiDAR assessment. In other words a digital level (due to the low precision of the instrument) would not be able to capture the slope differences at different points along the segment obtained using the MLS.

71

Alberta's design guide doesn't provide a range of allowable cross slopes before the need for corrective action. In contrast to that, the TAC design guide expects cross slopes to range between 1.5 and 3% for slopes that are not superelevated on a 100km/h highway [120]. If the cross slopes are not within the acceptable range, corrective action, which often includes replacing the full pavement layer at the defected region, might be required[121]. If the aforementioned criterion were to be applied to the test segments presented in this case study, no corrective action would be required since all cross slopes fall within the acceptable range on both test segments.

As already noted in section 4.1.1, the cross slopes extracted using the proposed algorithm from mobile LiDAR scans were compared to data estimated in other surveys and stored in ATs database to ensure both estimates were within range of one another. Figure 26 shows bar charts demonstrating the comparison where only slight variations in the slope exists. For eastbound (EB) direction on Highway 53 (Figure 26d) the average difference between slopes obtained from the LiDAR and the GPS is <0.001 decimal degrees (0.097%). Similarly, for the westbound (WB) direction (Figure 26c) the average difference was 0.0022 (0.22%). For Highway 36 the northbound (NB) direction (Figure 26b), the average difference was <0.001 (0.08%) while for the Southbound (SB) direction (Figure 26a) the difference was 0.0017 (0.17%). Although differences in slope between LiDAR and GPS exist at individual stations, the aggregate results are consistent. Differences at individual stations could be attributed to LiDAR detecting pavement degradation at those locations due to its high precision. Overall, depending on the location and the slope, percent differences ranged from 0.0001% to 0.4% for the 38 cross slopes estimated (19 stations, 2 travel approaches). These numbers are in line with findings of previous studies that performed cross slope extraction from LiDAR. In work by Tsai, et al. [35], the percent difference ranged from 0.01% to 0.3% for the 15 cross slopes extracted. In the paper by Holgado-Barco, et al. [122], the percent difference ranged from 0.024% to 0.094% for the 12 cross slopes extracted. Holgado-Barco, et al. [43] did not compare their results to any ground truth measurements. Despite the numbers being consistent, it is important to emphasize that different studies were conducted under different circumstances, using different tools and on different roads. Hence, the numbers reported here are only meant to provide the reader with a sense of what the percentages looked like in other studies. The intent is not to perform an absolute comparison between the different methods since

this is not possible unless the algorithms are tested on the same highway segment. That being said, the proposed algorithm does improve on previous studies through (i) full automation of the extraction process, which has significant impacts on the efficiency of performing network-level cross section assessments (ii) the extraction of side slopes in addition to cross slopes, something that has not been achieved to date in the literature, and (iii) the extraction of slope information independent of lane marking information, which helps increase the efficiency and the robustness of the extraction process.

(a)   Highway 36 Left Cross Slope (Southbound)

(b)   Highway 36 Right Cross Slope (Northbound)

(c)   Highway 53 Left Cross Slope (Westbound)

(d)   Highway 53 Right Cross Slope (Eastbound)
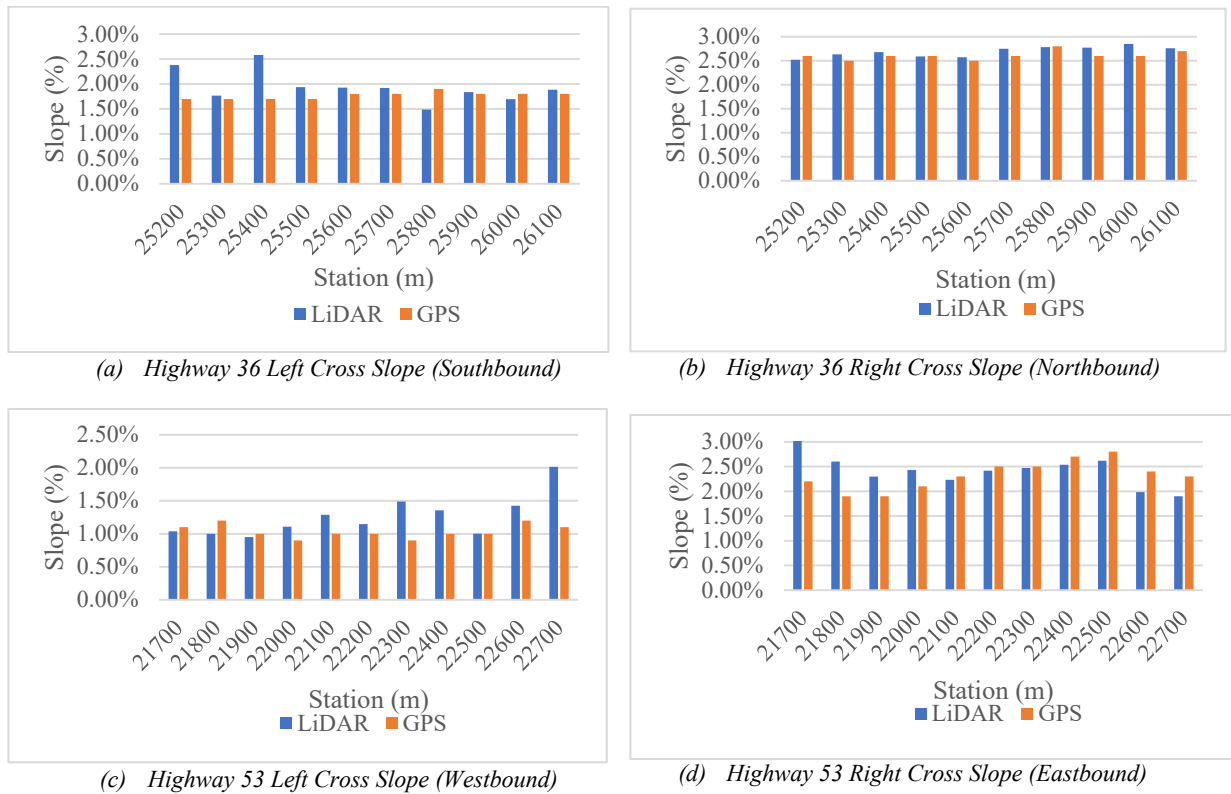
Figure 26: Cross Slope Comparison (LiDAR vs GPS)

One important observation on both segments is that the cross slopes are flatter on the WB direction (Highway 53) and the SB direction (Highway 36). On average, cross slopes on the WB direction of Highway 53 is 1.3% while the cross slopes on the EB direction is 2.4%. Likewise, the average cross slopes on the SB direction of Highway 36 was 2% while it was 2.7% for the NB direction. Similar observations were reached when comparing the GPS data from the two sides.

4.5.2   SIDE SLOPES

The proposed algorithm was also effective in estimating SS. In case of SS, the Alberta Design Guide requires that slope are not steeper than a 4:1(25%) [118]. The steepest side slope estimated

on the Highway 53 segment was 4.1:1 at station 22200. All other side slope along the segment were flatter than 4:1 (i.e., recoverable slopes). This implies that, in case a vehicle runs off the road, the slopes are forgiving enough to allow the driver to regain control (i.e., recover). Therefore, if an assessment were to be conducted on Highway 53, the side slope would not require corrective action since they satisfy minimum safety requirements. It is worth noting that high vegetation on Highway 53 did not impact side slope estimates. Unlike Highway 53, Highway 36 had side slope that were as steep as 3.5:1. This was observed between stations 25200 and 25400. Hence, further investigation and possible corrective action might be required in this region. In contrast to the cross slopes, the side slope on Highway 53 were flatter on the EB travel direction. For side slopes, the WB direction averages a 4.7:1 slope while the EB direction the average side slope is 5.9:1.

4.5.3   PROCESSING TIME, CHALLENGES, AND RECOMMENDATIONS

In addition to the high accuracy obtained using the proposed method, efficiency is also high. For Highway 53, a 4km LiDAR segment containing 31.7 million points, the entire procedure including knot identification, slope estimation, and plotting took 60.09''. Similarly, the extraction algorithm on Highway 36, which contained 15.5 million points, only took 31.3" per cross section. The high efficiency of the proposed algorithm helps overcome challenges associated with network-level estimation and assessment of slopes.

Despite the high accuracy and high efficiency achieved, some challenges did exist. The main challenge is that the MARS regression used to identify knots on the cross section is extremely sensitive to the density of the LiDAR points. More noise in the extracted cross section result in the MARS regressions identifying knots which do not correspond to actual changes in slope (i.e., false positives). Cleaning up the cross section using the intensity filter and splitting different portions of the cross section using the *k*-means algorithm significantly reduces the likelihood of such an issue, hence the importance of this stage. In the assessment conducted in this thesis, the maximum number of false positives identified on a single cross section was two false positives (i.e., only two inaccurate knots). In fact, some of those knots are identified in the middle of a slope, thus, the only impact they have on the results is that two accurate estimates are obtained for the same slope.

Another observation worth noting is that, the density of the points on one side of the road is always higher than the other. This is expected when LiDAR is collected in a single survey pass since the

74

density of LiDAR points is a function of the proximity of objects to the scanner. Thus, point density for the slope closer to the travelled approach is higher. Although, this had no impact on the results obtained in this thesis, it could be a source of concern if lower density scanners are used. Another source of variation in point density is the type of scanning system used. The higher the scan rate and point density, the higher the reliability of the slope estimates. Readers interested in how the algorithm would perform at lower point density are referred to Chapter 8 of this thesis.

4.6   SUMMARY & CONCLUSIONS

This Chapter of the thesis proposes a novel algorithm for the extraction of cross-sectional elements of roads scanned using LiDAR. The algorithm is highly efficient and fully automated, which facilitates timely assessment of slopes of highways on a network-level. This helps officials identify locations of ineffective slopes and take corrective action in a proactive manner (i.e.,, before any safety problems occur). The proposed algorithm was tested on two different highway segments in Alberta, Canada, where 38 different cross slope and side slope measurements were obtained. The results show that the algorithm is effective in estimating cross and side slopes of roads at a high level of precision and accuracy. Although cross slope extraction has been explored in previous research, most procedures require the use of lane marking information to perform such extraction. This makes the extraction difficult on road where lane markings have degraded or where markings do not exist. This study also demonstrates the possibility of extracting side slope from LiDAR at a high level of accuracy and at regions of high vegetation. To the best of the author's knowledge, no paper has considered the extraction of side slope information from LiDAR data before, with most studies citing high roadside vegetation as the reason why such extraction is extremely challenging.

5 HORIZONTAL CURVE DETECTION AND ATTRIBUTE ESTIMATION

5.1 BACKGROUND

Horizontal alignments on highways are designed to ensure that drivers travelling at the speed limit of the road can safely negotiate the curve. Curves with sharp radii or inadequate superelevations could result in drivers losing control of their vehicles increasing the risk of overturning or skidding off the highway. In fact, statistics show that approximately one-fourth of fatalities on highways occur on horizontal curves [123]. As a result, design guidelines dictate that curve radius and other attributes on a curve meet specific requirement. Minimum curve radius is estimated as a function of the road's design speed, the superelevation of the road, and a coefficient of friction, which is used as a proxy of the amount of friction the pavement provides. If the radius on a curve drops below the minimum radius estimated in design equations, the likelihood of a driver safely negotiating the curve reduces significantly.

Despite all efforts to construct road alignments in accordance with design guidelines, budget limitations, site imperfections, as well as maintenance and resurfacing mean that deviations from design plans often occur. Hence, it is essential to survey horizontal curves and their geometric attributes after construction and throughout the service life of a road to ensure that they meet design requirements. Obtaining such information in an efficient manner helps authorities take timely corrective action in cases where design limitations exist. Obtaining information about attributes of horizontal curves is also essential to the development of operating speeds models. These models are often used to predict operating speeds on roads based on a road's geometry. The prediction is then used to set a safe speed limit that is consistent with the road's geometry. In the realm of connected vehicle technology and vehicle to infrastructure (V2I) communications, curve warning systems also require that curve information be readily available and get efficiently communicated to drivers in real-time, ergo, the importance of having an efficient method to obtain such information in an accurate manner. The knowledge of curve geometry is also essential for autonomous driving at locations where lane marking information might not be sufficient to guide the vehicle through a curve.

Regardless of the reason, surveying the attributes of horizontal alignments on roads is an integral step to efficient management of road infrastructure. Nonetheless, manual methods to collect such

information such as the chord offset method and compass method are time consuming, labour intensive and prone to human error [124]. As a result, transportation agencies have been looking for more efficient alternatives to obtain such information, which include the use of GPS data. The literature shows that there have been multiple attempts to extract curve attributes using GIS platforms, with the majority of the work focusing on using GPS data specifically to estimate such attributes [87,88,90,125,126]. Although using GPS data has helped overcome the burden associated with site visits and manual data collection methods, the low density of points collected in GPS surveys and the low accuracy sometimes result in poor estimates of the horizontal alignment geometry. Furthermore, most studies that have attempted using GPS data to estimate curve attributes focus on estimating curve radii alone without much information on how other attributes could be extracted[88,126].

Figure 27: LiDAR Point Cloud Showing Horizontal Curve

This Chapter addresses some of the limitations of using GPS data for estimating curve attributes by proposing a novel algorithm to extract horizontal alignment attributes on highways scanned using mobile LiDAR technology. In addition to overcoming the limitations associated with using GPS data, the high point density of LiDAR datasets helps use the same dataset to measure other geometric attributes of curves such as sight distance and allowable horizontal sight offset. Furthermore, LiDAR also allows for the estimation of curve geometry at different approaches on a roadway or different lanes on an approach, something that is not possible using single path GPS data. Despite being rich in the information they carry (see Figure 27), the review conducted in Chapter 2 of this thesis revealed that only a single study had attempted the extraction of horizontal

alignment information from LiDAR[34]. Furthermore, the method proposed in that study was not fully automated.

The method proposed in this Chapter works by automatically detecting and measuring attributes of horizontal curves on LiDAR highways. The proposed algorithm uses changes in azimuth of vectors aligned along the road's axis to estimate the locations of horizontal curves. Once the points of curvature (PC) and tangency (PT) are defined for a particular curve, the algorithm uses linear regression of the tangents connecting the curve to locate the point of intersection (PI). The PC and PT are then re-estimated. The final step involves locating the centre of the curve. Once this is identified, the curve's radius, deflection angle, length and chord length are all estimated. The proposed algorithm was tested on two mobile LiDAR datasets. Moreover, to verify the accuracy of the proposed algorithm, it was also tested on a simulated data generated using AutoCAD Civil 3D.

5.2   EXTRACTION ALGORITHM

The algorithm proposed in this study is divided into multiple stages, which are summarized in Figure 28 and detailed in the next few subsections.
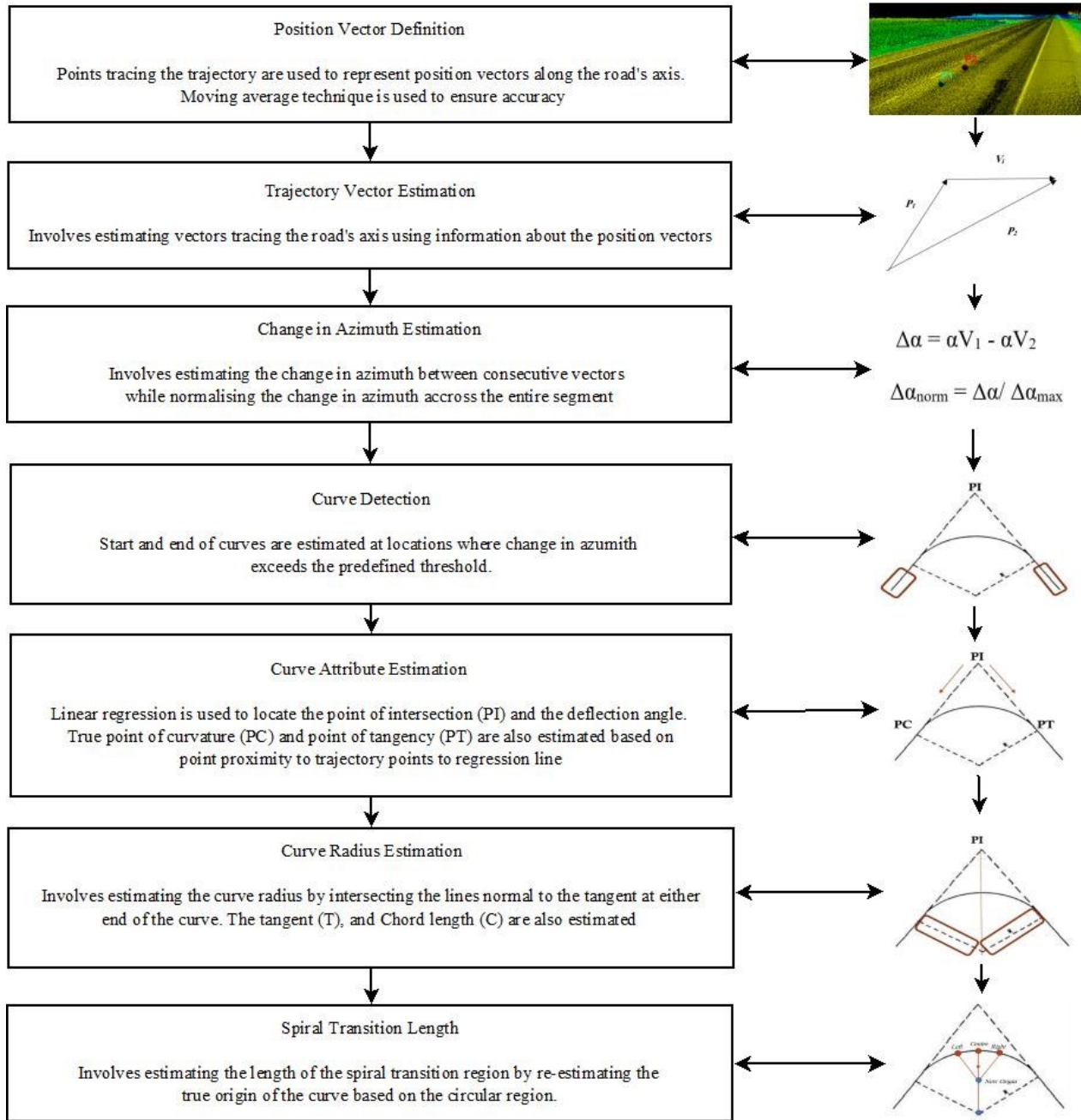
Figure 28: Horizontal Curve Extraction Pipeline

5.2.1 TRAJECTORY VECTOR DEFINITION

The first step of the extraction process involves defining trajectory vectors. The process used to obtain the vectors has already been discussed in Chapter 4, section 4.2.1 of this thesis. In this Chapter, 20m long trajectory vectors were used (i.e., the set of position vectors representing P_1 and P_2 are chosen to be 20m apart). This parameter can be altered by the user depending on the curve sharpness expected on a particular segment. For detection of smooth curves and higher spacing is recommended, while for sharp curves even a spacing of less than 5m may be sufficient.

5.2.2 CURVE DETECTION

For curve detection, the algorithm loops through all the trajectory vectors and compares the difference in the azimuth between consecutive vectors. If the change in azimuth exceeds a predefined threshold then this point is assumed to mark the start or the end of a curve. In order to ensure that the threshold for detecting a curve is effective for all curves on a particular segment, the difference in azimuth between consecutive points is normalized based on the local change in azimuth. This is done by dividing change in azimuth for each pair of consecutive trajectory vectors by the maximum change in azimuth detected within a range of 15 vectors. Let αV_1 and αV_2 represent the azimuth of two consecutive trajectory vectors V_1 and V_2 respectively, in this case $\Delta\alpha$, which is the change in azimuth, can be calculated as follows:

$$\Delta\alpha = \alpha V_1 - \alpha V_2 \tag{12}$$

The normalized change in azimuth ($\Delta\alpha_{norm}$) can be computed as follows

$$\Delta\alpha_{norm} = \Delta\alpha / \Delta\alpha_{max} \tag{13}$$

where $\Delta\alpha_{max}$ denotes the highest change in azimuth detected on the local region within a segment.

To distinguish the beginning of a curve from its end the code checks the change in azimuth of the pervious pair of points, if that does not exceed the threshold the point is a start point, otherwise it is the end of the curve. Furthermore, to ensure that the curve does indeed start at a particular point where a change in azimuth is detected, the code requires that the change is persistent (i.e., the change in azimuth is sustained for a particular length). This is done to minimize the possibility of detecting short changes in azimuth due to data collection inaccuracies as horizontal curves (i.e., minimize false positives).

5.2.3 FEATURE IDENTIFICATION

Once the whereabouts of the curves are identified, its geometric elements can be estimated, however, before that is done it is essential to accurately identify the defining points of the curve including the point of intersection (PI), the point of curvature (PC), and point of tangency (PT).

5.2.3.1 POINT OF INTERSECTION

To estimate PI, the algorithm uses a set of points before reaching the candidate start point of the curve and another set of points after passing the candidate end point of the curve as indicated in Figure 29 a. Linear regression equations are then developed for the two tangents. The algorithm then finds PI of the curve by intersecting those equations. The deflection angle is also estimated by calculating the difference in azimuth between the lines.

5.2.3.2 POINT OF CURVATURE AND TANGENCY

Although, the code identifies candidate locations for the start and end of each curve, these points are not always accurate. The true PC and PT could be a few points before or ahead of the location identified based on change in azimuth. Therefore, more accurate estimate for the beginning and end of the curve are estimated by minimizing the difference in northings estimated using the regression equation and those obtained from the LiDAR, which trace the road's axis. The code starts at PI and moves towards both PC and PT until the difference in northings drops below a specific threshold, as illustrated in Figure 29 b. Once that point is reached the new locations of PC and PT are defined.
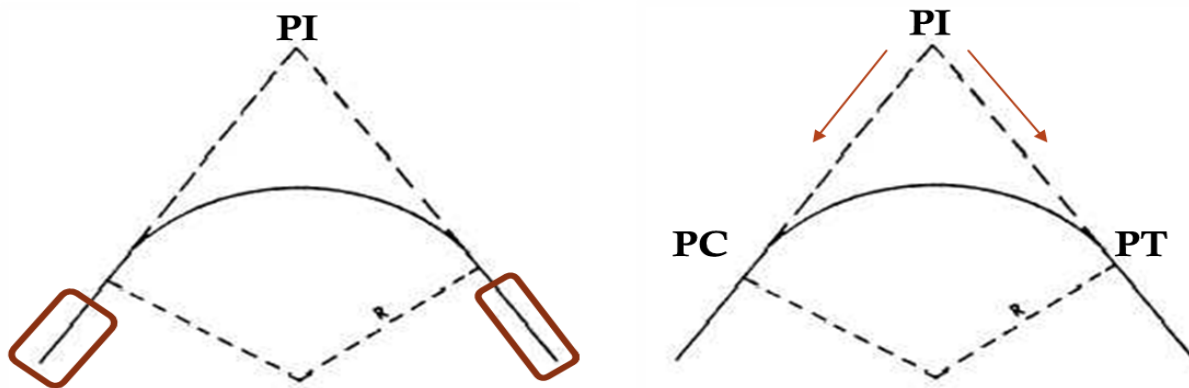
(a)   Developing Regression Equations to Locate PI   (b)   Locating Accurate PC and PT
Figure 29: PI, PC and PT Estimation

5.2.3.3 CURVE TANGENT, RADIUS AND CHORD LENGTH

The tangent of the curve (T) is estimated by calculating the Euclidean distance between PI and both PC and PT. It is expected that, for a symmetric curve, the estimates for T obtained from either side of the curve are almost equal.

To identify the radius of the curve, the normal line for each of the two tangent lines previously developed using regression is estimated. The lines are estimated such that they pass through PC and PT of the curve. The intersection point of the two lines, which represent the origin of the curve is then located as evident in Figure 30. After locating the origin of the curve, the radius is measured by finding the Euclidean distance between PC/PT and the origin (i.e., the intersection point). Moreover, the chord length is also measured by finding the Euclidean distance between PC and PT.
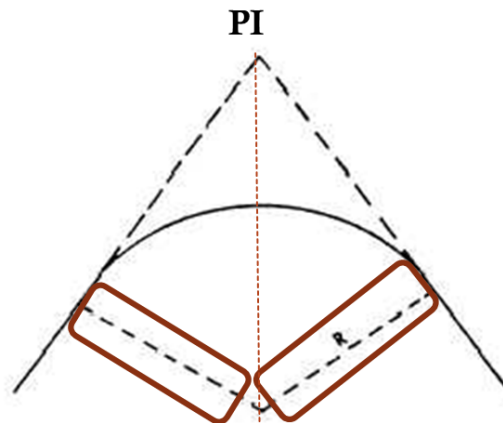
Figure 30: Locating the Curve's Origin and Measuring its Radius

5.2.4   SPIRAL TRANSITION DETECTION

In an attempt to identify whether the curve includes spirals or not, a separate procedure is proposed. In this procedure, the first step is to locate the centre point along the curve's arch between PC and PT, once this point is located, a point beyond (right) and preceding (left) the centre point which fall on the curve and are within 25% of the distance between the centre point and the end points are located as shown in Figure 31.
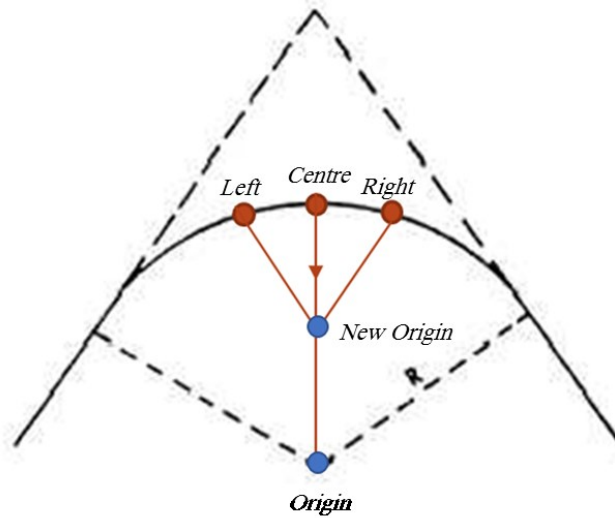
Figure 31: Left and Right Points with 25 Percent of the Centre of the Curve

After identifying the three points *left*, *right* and *centre*, the code calculates the distance between each of the three as well as points along the line that connect the centre of the curve and its origin, as illustrated in Figure 31. The code loops through multiple points along that line until the radii are equal in length. The idea here is that spiral curves are detected when estimated radii are different in length or estimated centers of curvature do not coincide

The code is written such that it would minimize the difference between the three radii. Once the difference meets an acceptable threshold defined by the user, the code outputs the coordinates of proposed origin of the circular curve and provides an estimate for the circular radii in case a spiral exists. It is worth noting here that the entire algorithm was coded in MATLAB.

5.3   TEST DATA

The proposed algorithm was tested (i) mobile LiDAR scans of existing highways and (ii) curves generated in AutoCAD Civil 3D. The next few paragraphs provide information on the two LiDAR segment and the Civil 3D data. More information on the laser scanner used to collect the LiDAR data and its capabilities are found in Chapter 3 of this thesis.

5.3.1   TEST SEGMENTS

The two highway segments on which the algorithm was tested are shown in Figure 32. Curve detection is based on changes in azimuth, which are typically high for sharp curves and low for mild curves. Therefore, to ensure that the algorithm is accurate enough in detecting even the

mildest of curves, testing was conducted on segments where existing curves had a very large radius (i.e., curves were not sharp).
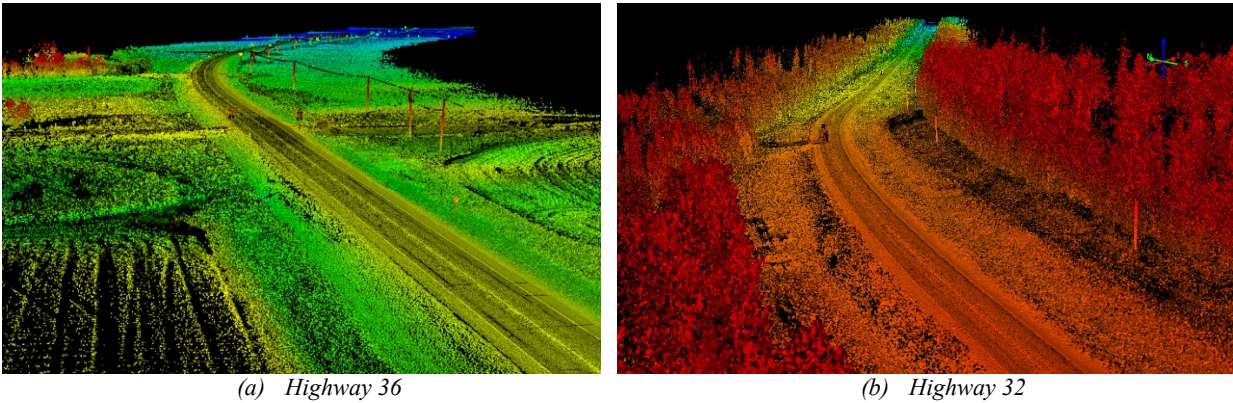
Figure 32: Point Cloud Data at Test Highways

The first segment used was a 4km segment on Highway 36. The segment is a two-lane undivided rural road with a speed limit of 100km/h located in the southern region of Alberta, southeast of the city of Lethbridge. The segment includes a single horizontal curve at the north-most part of analyzed section. The roadside area is relatively clear with very low vegetation with only slight variations in vertical alignment.

The other LiDAR segment was also a 4km segment; however, this segment was located on Highway 32. The segment is located in Central Alberta northwest the City of Edmonton. This segment is also a two-lane undivided rural road with a 100km/h speed limit and includes a single horizontal curve. Unlike Highway 36, vegetation is relatively high on this portion of Highway 32 as evident in Figure 32 b.

5.3.2   CIVIL 3D DATA

In addition to the two LiDAR highway segments, the algorithm was also tested on curved segments of known geometric features created in AutoCAD Civil 3D. This was done to verify the accuracy of the proposed algorithm since the attributes of those curves were well known and more reliable than information on as-builts of the LiDAR segments. Information on as-builts was not always up to date and, in some cases, did not represent existing conditions. Moreover, some information about the curves was missing from the as-builts and had to be calculated based on other attributes. Two different curves were drawn in Civil 3D one was a simple circular curve (Civil 3D Curve I) and the other was a curve with spiral transitions at either end (Civil 3D Curve II). After drawing the curves in Civil 3D, a high density of points was generated along each of the curves using the

"Along Line/Curve" tool under the "Create Points Miscellaneous" tab. The points were generated such that the point spacing was similar to that of the trajectory points filtered out of the LiDAR point cloud (6pts/m). These points were then used to create the trajectory vectors required for the curve detection and attribute estimation, as already detailed in section 5.2 of this chapter.

5.4 RESULTS AND DISCUSSION

Table 3 and Table 4 shows the results of running the algorithm on the segments. The table shows the information about all curve attributes including Radii, Deflection Angle, Arc Length, and Tangent Length for each of the test segments. For the LiDAR segments, Table 4 shows information obtained from the as-builts provided by AT and information estimated using the proposed algorithm. It is worth noting that as-built information was only available for Highway 32. Similarly, for the Civil 3D segments, Table 3 shows the actual attributes used to draw the curves in Civil 3D and the information obtained from the proposed algorithm. For all three curves, the tables also show the absolute difference in the two measurements (Actual vs Experimental) for each of the attributes. Moreover, the percent difference is also computed and shown in the tables.

In terms of the actual detection, the results show that the algorithm was successful in automatically detecting all the curves on the four test segments. In fact, the algorithm was also able to detect a second curve towards the end of the Highway 36 segment, however, the attributes of this curve were not measured (not listed in table) since only a portion of the curve was captured on the analyzed LiDAR segment.

The results also reflect the high accuracy achieved when estimating curve attributes using the proposed algorithm. For the three curves where reference measurements were available, the average percent difference between measurements obtained from the code and other measurements was less than 2.25% for all the attributes.

For Civl 3D Curve I, the percent difference between the measured and the actual attributes of the curve range from 0.33% to 1.2% for each of the attributes. For Civil 3D Curve II, the differences range from 0.92% to 2.1%. It is worth noting here that the values obtained from the algorithm and recorded in Table 3 are for the curve including spiral curve transitions (i.e., they are not attributes of the circular portion of the curve).

85

In case of the LiDAR highway, where as-built data was available, the result accuracy was also high. On Highway 32, the percent difference between the results obtained using the proposed algorithm and the information read off the as-built drawings ranged between 0.7% and 4.6%. The highest difference of 4.6% (54 m) was recorded when estimating the radius of the curve. In contrast, the smallest difference 0.7% was for the arc length 8.27m and the deflection angle of the curve 0.34^0. Recall that a 20m position vector spacing was used, hence, a difference of 54m could be a matter of the code being inaccurate by one or two points when locating the PC and PT of the curve.

Table 3: Test Results on Civil 3D Curves

	Civil 3D Curve				Civil 3D Spiral Curve			
	Actual	Detected	Difference (m)	%Diff	Actual	Detected	Difference (m)	%Diff
Radius (m)	2000	1976	24	1.20	1000	1009.2	9.2	0.92
Deflection Angle (degrees)	90	89.12	0.88	0.98	90	88.9	1.1	1.23
Length (m)	3141.5	3131.0	10.5	0.33	1570.8	1603.8	33.1	2.10
Tangent Length (m)	2000	1985	15	0.75	1000	1004.9	4.9	0.49

Table 4: Test Results on LiDAR-Detected Curves

	Highway 36				Highway 32			
	As-built	Detected	Difference (m)	%Diff	As-built	Detected	Difference (m)	%Diff
Radius (m)	N/A	1955.3	N/A	N/A	1164.3	1218.3	54.02	4.6
Deflection Angle (degrees)	N/A	24.28	N/A	N/A	52.1	51.7	0.34	0.7
Length (m)	N/A	838.8	N/A	N/A	1134.5	1126.2	8.27	0.7
Tangent Length (m)	N/A	398.5	N/A	N/A	579.2	571.2	8	1.4
Chord Length (m)	N/A	810.4	N/A	N/A	1021.7	1064.9	43.2	4.2

In case of Highway 36, although no as-built data was available to assess the accuracy of the results, further analysis on the curve data revealed that the curve was not symmetric and that a spiral transition existed on one end of the curve. The code was able to detect this difference when estimating the tangent (T) of the curve. Two different estimates were obtained either side of the curve (on all the other curves the estimates either side were very close). To verify the existence on a spiral transition on one end of the curve the azimuth change diagram seen in Figure 33 was plotted. It is noted on the figure that at one end of the curve (2200m) the change in the azimuth is

linear while on the other end it is nonlinear (2950m). This proves the existence of a spiral transition at the nonlinear and not the other.
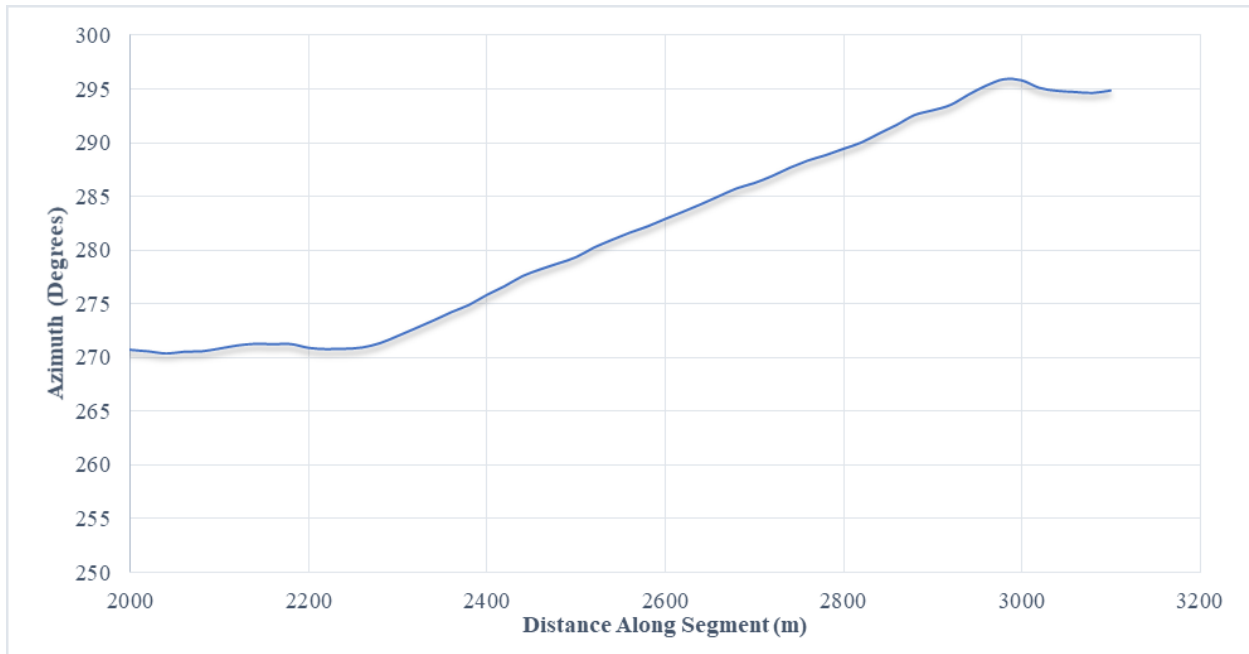
Figure 33: Change in Azimuth Along Highway 36 (no change denotes straight segment; linear change denotes curved segment; nonlinear change denotes spiral transition)

5.4.1   PROCESSING TIME, CHALLENGES, AND RECOMMENDATIONS

As demonstrated by the results, the proposed algorithm is highly accurate in detecting curves and estimating their attributes. Furthermore, the algorithm is also able to detect curves and measure their attributes in a highly efficient manner. Running the code on multiple segments revealed that curve detection and attribute estimation for a 4km LAS file can take anywhere between 8" and 13".

One limitation in the proposed algorithm lies in its ability to distinguish spiral transitions from circular curves depends on the spacing used to estimate the vectors in the initial stage. As already mentioned, testing was conducted on segments where existing curves had a very large radius (i.e.,, curves were not very sharp). In order for the algorithm to be able to detect curves of very large radius, sensitivity analysis revealed that a position vector spacing of 20m had to be used. This ensures that the change in azimuth between consecutive vectors is sharp enough for the curve to be detected. While this is essential to the detection process, it does not help when the aim is to detect spiral transitions. Since spiral transitions are often relatively short compared to the total

length of the curve's arc, a lower point spacing is required to distinguish the radius of the circular portion of a curve from the radius of the curve including the spirals.

Although the algorithm is effective in estimating attributes of simple horizontal curves, more work to distinguish simple curves from spirals. Future work could also consider supplementing the algorithm with a portion that would estimate horizontal sight offset on existing curves.

5.5　SUMMARY & CONCLUSIONS

This Chapter proposes an algorithm which can be used to automatically detect and measure the attributes of horizontal curves on highways sensed using LiDAR technology. The proposed algorithm involves assessing changes in the azimuth between consecutive trajectory vectors aligned to the road's axis to detect the presence of horizontal curves on a highway segment. The PC, PT, and PI for each curve are then identified using regression analysis and the origin of the curve is located to measure its radius. The code also measures the length of the curve and the length of its chord. The algorithm was tested using LiDAR data collected on two highway segments in the Province of Alberta as well as two curves created in Civil 3D. Testing revealed that the code was successful in detecting all curves on a highway segment. Moreover, the attributes of those curves were estimated with a high degree of accuracy. The proposed algorithm can be used to survey curves in a more efficient manner. This helps reduce the burden associated with conventional surveying tools.

6 OVERHEAD OBJECT EXTRACTION & CLEARANCE ASSESSMENT

6.1 BACKGROUND

It is common practice for transportation agencies to keep inventory information about all overhead assets on a highway, including bridges, power lines and overhead signs. Moreover, vertical clearance information at those objects must also be obtained to ensure that minimum clearance requirements are met. In fact, current bridge management practice includes a routine inspection phase where a diagnosis of the current state of the structure is obtained [127-129]. Clearance information is collected periodically as part of those bridge inspection procedures, since structural degradation and environmental conditions might cause changes to minimum clearance at overhead assets on highways. Such problems should be addressed in a timely manner to avoid potential collisions.

Vertical clearance information at both bridges and power lines is also essential to agencies responsible for issuing overheight permits for oversized vehicles. The efficiency and accuracy in which such information could be obtained helps significantly improve the effectiveness of routing oversized vehicles on a highway network. In contrast, inaccurate clearance information could result in the risk of collisions or significant delays to the routing program and hectic maintenance costs in cases of bridge strikes [130].

Bridge strikes are a common problem all around the world[131]. In the US, the Federal Highway Administration ranks damage due to bridge-vehicle collision as the third most common cause of bridge failure[132]. Similarly, statistics from Bejing, China, show that 20% of damage to bridges is caused by bridges being struck by overheight vehicles[133]. In the UK, national statistics show that a vehicle strikes a railway bridge every four and a half hours[131]. In California, the rate of bridge strikes average a single strike per month[17]. Figure 34, generated in work by [134] shows bridge strike statistics in the US during the period between 2005 and 2008[134]. Although the number of strikes varies significantly across different regions, places like Missouri experience, on average, over 400 strikes a year.

Figure 34: Bridge Strike Statistics in the US (2005-2008)[134]

Although bridge strikes might not represent a significant portion of the total number of collisions, repairing the damage caused by bridge-vehicle collisions can pose a significant financial burden on transportation agencies. For instance, the Texas DOT reports that each bridge strike incident costs an average $180,000 USD to repair[131].

In addition to helping agencies issue overheight permits to oversized vehicles, clearance information at bridges and power lines is also critical to agencies responsible for designating high-load corridors where clearance is expected to exceed a certain margin along the entire highway (9m in Alberta). These corridors have significant impact on freight transportation within and across different provinces and are critical to economic prosperity.

Unfortunately, in current surveying practice conducting clearance assessment is a time consuming, labour intensive, and financially demanding exercise that requires both road closure and surveyors to be on-site as illustrated in Figure 35. This makes network-wide assessments of all overhead assets extremely challenging, particularly in places like the Province of Alberta in Canada where

a large highway network (31,000km) exists with approximately 4,500 bridge structures and tens of thousands of power lines and overhead signs [135]. A network of this size forces officials to set priorities when managing assets on their highways. In case of bridges, this is achieved by prioritizing structures which are in a critical condition or focusing on structures located on primary highways when performing structural assessments and inspections [136].

Figure 35: Manual Clearance Assessment [128,137]

Considering the fact that around 40% of the bridges currently in use in Canada and the US were built over 50 years ago [138], a significant number of these structures are approaching critical conditions and require timely strengthening, rehabilitation, or replacement[139,140]. Unfortunately, given the limitations of existing data collection techniques, assessing clearances at all those structures simultaneously is not feasible; accordingly, municipalities have started considering alternative methods. Although some municipalities still use manual methods, such as theodolites and total stations, others have shifted to using more digitized tools such as digital measuring rods and electronic measuring devices [95]. Photolog data and static Light Detection and Ranging (LiDAR) scans have also been considered in recent years [96,97]. One common issue with all the aforementioned methods is that they are all static tools. Hence, while they could help improve the accuracy of clearance assessments by minimizing the sources of human error, they are not able to improve the efficiency of clearance assessments process. As a result, disruptions to traffic and the safety of personnel on the site are still common concerns. Moreover, network-level analysis (i.e., assessing a large selection of bridges on the network efficiently) is still a challenge.
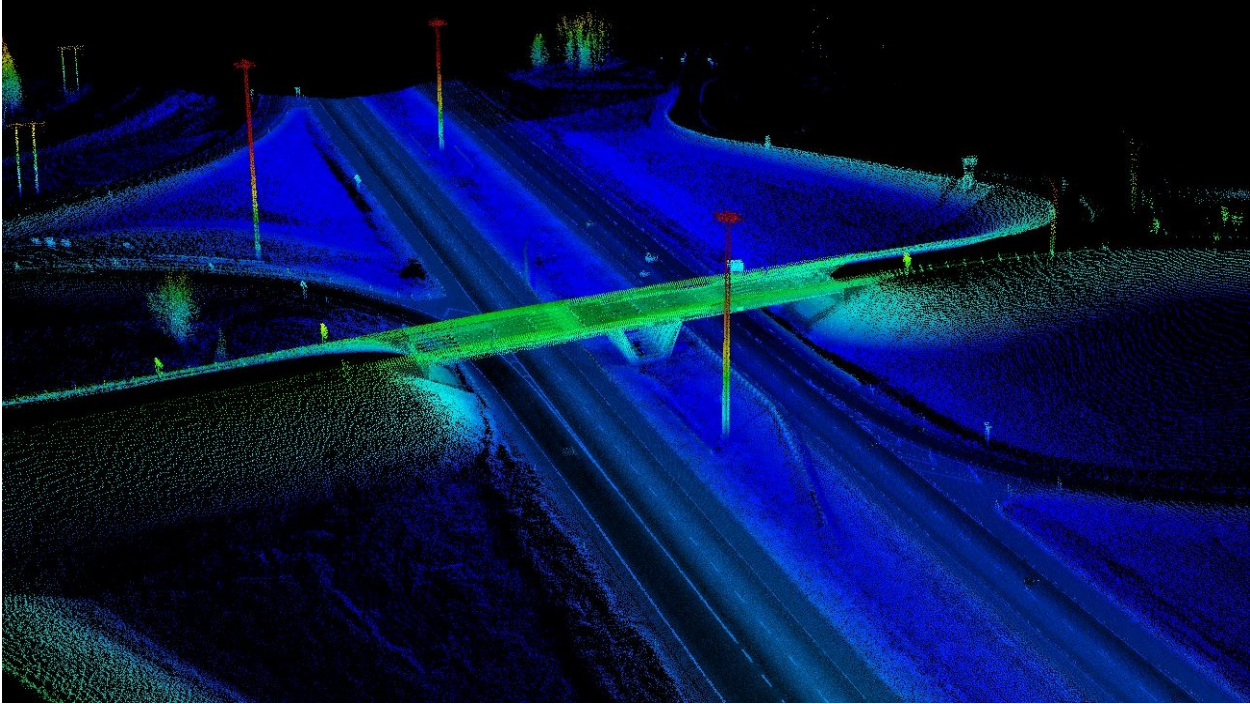
Figure 36: Point Cloud Highway Showing a Bridge Structure

Mobile LiDAR data, unlike static LiDAR scans, is collected by vehicles while travelling at highway speeds. Moreover, only a single pass is required to produce a highly detailed map of road infrastructure including bridges, as seen in Figure 36. Despite those advantages, research on assessing vertical clearance using mobile LiDAR data has been extremely scarce. As evident by the review presented in Chapter 2, even the few studies that do exist in the literature are limited to assessing clearances using static LiDAR scans of bridges. To the best of the authors' knowledge, no study, to date, has attempted assessing clearance at bridges, using mobile LiDAR data. In fact, even the assessment of clearance at other overhead objects such as power lines and overhead signs (see Figure 37) using mobile LiDAR has not been attempted in previous work. Furthermore, the automated detection (i.e., inventory) of bridges on highways using mobile LiDAR has not been explored either.

To address the aforementioned gaps, this Chapter proposes a novel algorithm that can automatically detect, classify, and measure vertical clearance of all overhead objects on a highway corridor in an efficient and accurate manner using mobile LiDAR data. This provides transportation agencies with information that could help them reduce the risk of potential bridge strikes through efficient routing of oversized vehicles on the highway network and through timely intervention to address structural imperfections. Since incorporating new technologies into

protocols requires validation, the accuracy and repeatability of the algorithms was tested on three different highway segments including a 242km corridor.
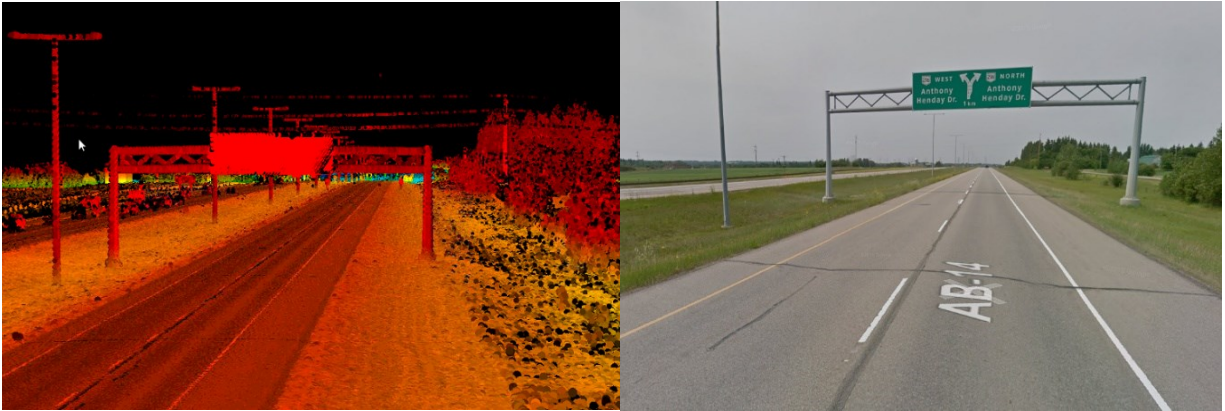
(a) Overhead Sign
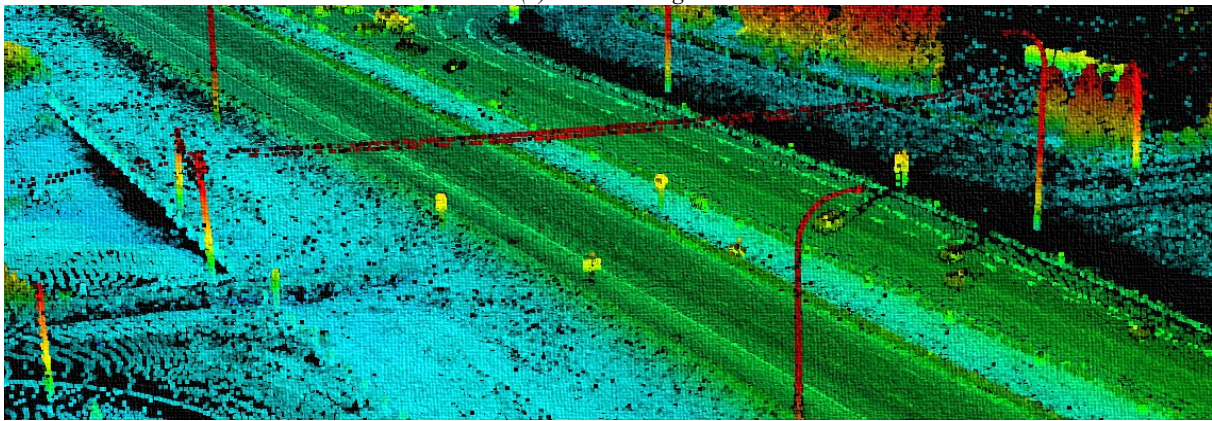
(b) Power line Cable
Figure 37: Overhead Objects

6.2   EXTRACTION ALGORITHM

The algorithm proposed for extracting vertical clearance involves detecting and classifying overhead structures while obtaining an estimate of their vertical clearance. After that a detailed assessment of vertical clearance is performed at the detected overhead objects. The next few paragraphs provide a detailed description of the different steps in the extraction algorithm. Moreover, the workflow is also summarized in the Figure 38.

.

```
                    ┌─────────────────────────────┐
                   ╱  3D Point Cloud Highway Loading ╱
                  └─────────────────────────────┘
                                │
                                ▼
                    ┌─────────────────────────────┐
                    │     Trajectory Generation    │
                    └─────────────────────────────┘
                                │
                                ▼
                    ┌─────────────────────────────┐
                    │    Point Cloud Voxelisation  │
                    └─────────────────────────────┘
                                │
                                ▼
                    ┌─────────────────────────────┐
                    │ Non-ground Point Segmentation│
                    └─────────────────────────────┘
                                │
                                ▼
                    ┌─────────────────────────────┐
                    │   Overhead Object Detection  │
                    └─────────────────────────────┘
                                │
                                ▼
                    ┌─────────────────────────────┐
                    │       Object Clustering      │
                    └─────────────────────────────┘
                                │
                                ▼
                        ◇ Object Classification ◇
                         ╱                    ╲
                        ▼                      ▼
                  ┌──────────┐          ┌──────────┐
                  │  Bridge  │          │Non-bridge│
                  └──────────┘          └──────────┘
                        │                      │
                        ▼                      │
     ┌─────────────────────────────────┐       │
     │Detailed Clearance Assessment Across Span│ │
     └─────────────────────────────────┘       │
                        │                      │
                        ▼                      ▼
                  ╱Clearance Estimate╱   ╱Clearance Estimate╱
```
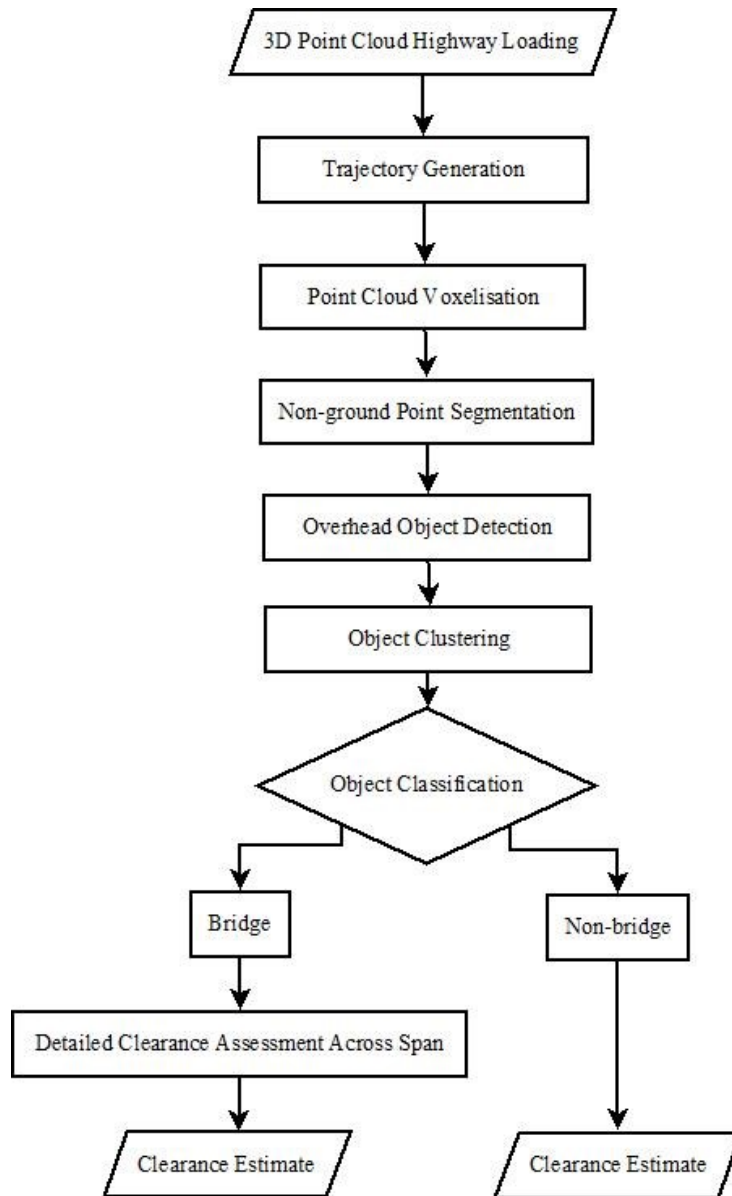
Figure 38: Algorithm Workflow

6.2.1 OVERHEAD STRUCTURE DETECTION

Detection of overhead structures before measuring their clearance is essential when a network-wide assessment of vertical clearance is desired, or when agencies are only interested in inventorying the number of overhead structures that exist on a highway segment. The aim is to minimize the need for user input and to automatically provide information about of the locations where overhead structures exist. Once this is achieved, a detailed assessment of vertical clearance can be performed if desired.

94

6.2.1.1 TRAJECTORY DEFINITION

The first step of the detection process involves defining points parallel to the road's axis that trace the road's trajectory and cover the entire road segment. As already discussed in Section 4.2.1, points that fall in the Nadir plane of the laser scanner were filtered out of the LiDAR point cloud to represent the points parallel to the road's axis.

It is worth noting here that the trajectory points extracted in this stage do not need to trace the centreline of the road or the lane. The only requirement is that the points run parallel to the road's axis and extend throughout the length of the entire segment. The location of the trajectory points is only significant if the detection of objects that overhang from the side of the road is desired. If the detection of such objects is desired, it is recommended that the trajectory points are offset into the desired lane before running the remainder of the detection algorithm.

6.2.1.2 POINT CLOUD SEGMENTATION

Once the trajectory points are defined, the next step is to segment the point cloud whereby points that potentially represent overhead objects are filtered out of the remainder of the LiDAR point cloud. In brief, the segmentation procedure involves voxelisation of the LiDAR point cloud and dynamically filtering points that potentially represent overhead objects from the remainder of the point cloud. Voxelisation is the process of discretizing the LiDAR point cloud into three dimensional voxels of a certain size, similar to two-dimensional pixels in a normal two-dimensional image as illustrated in Figure 39.
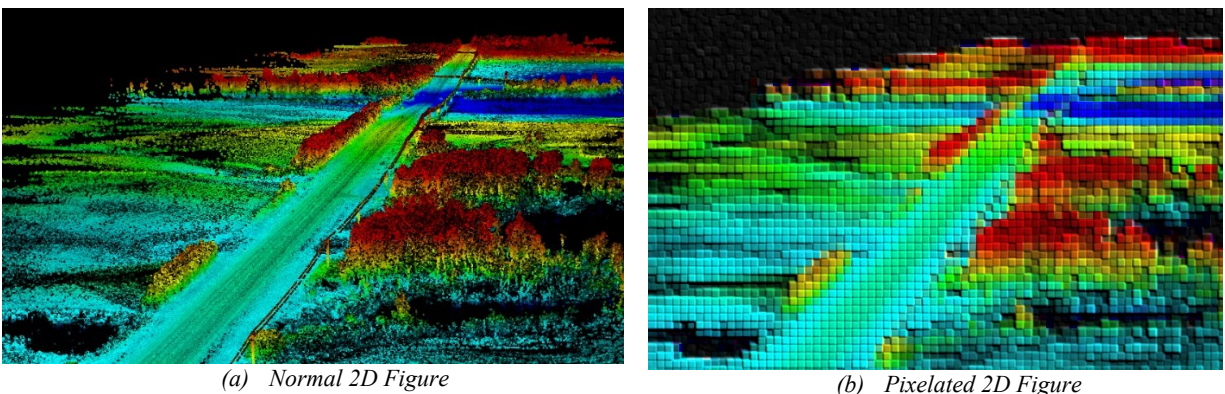
(a)   Normal 2D Figure   *(b)   Pixelated 2D Figure*
Figure 39: Pixelated Figure of a LiDAR Highway

Mathematically, voxelization can be expressed as follows. Let v(i, j, k) denote a voxel and v(I, J, k) denote all voxels in layer k *as* illustrated in Figure 40. If V represents the voxel grid system consisting of K layers, then the V can be defined as the union of all voxel layers:

$$V = \bigcup_{k=0}^{K} k \qquad (14)$$

The voxelization of each point in the point cloud is performed based on the spatial coordinates of the point. A point $P(x, y\ z)$ is assigned to a voxel $v(i, j, k)$ as follows. If $\varDelta x, \varDelta y,$ and $\varDelta z$ denote the dimensions of a single voxel cell (v) in the x, y and z directions and $x_0, y_0,$ and z_0 denote the origin of the voxel grid (V), then the ID of the voxel, $v(i, j, k)$, in which the point $P(x, y, z)$ falls can be computed as follows:

$$i = \frac{\text{int}(x - x_0)}{\Delta_x} \qquad (15)$$

$$j = \frac{\text{int}(y - y_0)}{\Delta_y} \qquad (16)$$

$$k = \frac{\text{int}(z - z_0)}{\Delta_z} \qquad (17)$$

Where, int(.) denotes the integer portion of the arithmetic operation between parentheses.
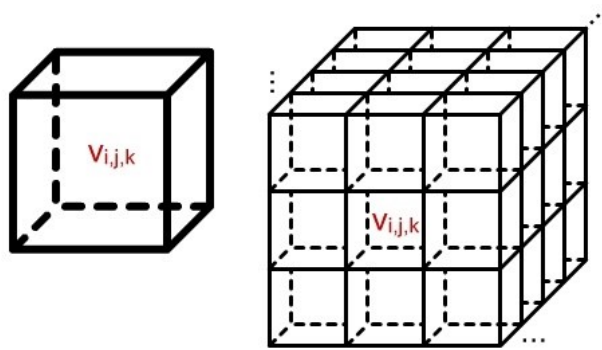
Figure 40: Voxel Representation [141]

The dimensions of the voxel are user defined. For best overall results, it is recommended that voxel dimensions be defined based on the laser scanner properties. Since the data scanned in this thesis was collected in scanlines that are approximately 20cm apart, a similar cell size for voxelization was used. This choice also enables efficient creation of 3D images within the limits of 16GB of RAM.

After discretizing the LiDAR point cloud into a 3D voxel grid, the data was segmented based on the elevation of each point from the road surface. This was done to isolate points representing potential overhead objects from the remainder of the point cloud.

To account for variations in the vertical alignment along the highway, the threshold was applied dynamically (i.e., a different reference point on the pavement surface was used to classify points depending on where the point is located along the road segment). The reference point for each point in the point cloud was the closest voxel in the trajectory voxel chain shown in Figure 41.
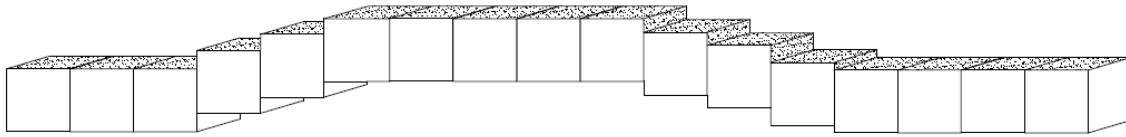
Figure 41: Side View of the Trajectory Voxel Chain Tracing the Road's Axis Along Pavement Surface

To achieve this, a k-nearest neighbour (kNN) search was conducted for each point in the point cloud. kNN is a supervised machine learning algorithm that is used for nonparametric classification purposes. The algorithm is effective in identifying patterns in big datasets in an efficient manner, this is particularly, true when dealing with low dimensional datasets. Another advantage of using kNN is that it makes no assumptions about the characteristics of the training dataset.

The algorithm works by assigning information from the nearest pattern to the target pattern x', for which a label is sought. When the kNN algorithm is used to search for the nearest neightbour and identify its location in space, that label becomes the coordinates of the nearest pattern. To identify the nearest neightbour, a similarity measure must be defined in the data space; for a data space of q dimensions $\mathbf{R}^q$ the Minkowski metric (p-norm) is employed as follows:

$$\left\| x' - x_j \right\|^p = \left(\sum_{i=1}^{q} \left| (x_i)' - (x_i)_j \right|^p \right)^{1/p} \tag{18}$$

Where, x_j represents the set of data points in the training dataset. It is worth noting that the metric estimated in Equation 18 reduces to Euclidian distance measure when $p = 2$ (which is the similarity measure used in this thesis).

To classify points or label points similar to their kNN, the algorithm works on developing a Voronoi cell around each data point of the training dataset and labels any data point that falls within that cell with a similar label as its neighbours. In case of k>1, the algorithm then aggregates the Voronoi cell to form a Voronoi tessellation that helps in the classification. In this thesis, k=1 is used since only a single nearest neighbour is sought for each point.

Once the closest voxel for every point is identified, the elevation difference between each point and the trajectory voxel is then computed. Points that have an elevation difference that is more than a specific threshold are then classified as potential overhead object candidates and are retained for the object detection step in section 6.2.1.3. The classification threshold is user defined depending on where the split is desired. A 3m threshold was used since this retains all points representing overhead structures while minimizing the search space for the object-detection step as evident in Figure 42.
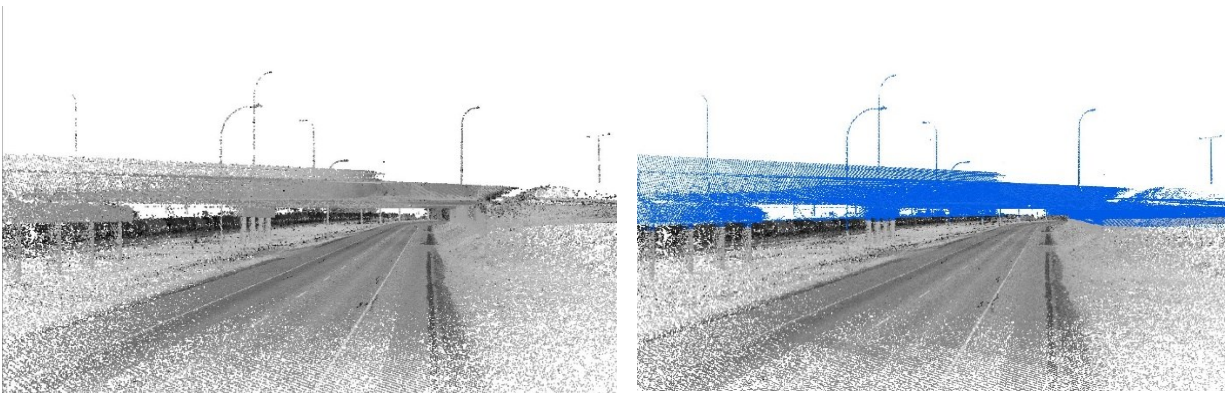
(a)   Full LiDAR Road Segment   *(b)   Highlighted Overhead-Object Candidate Points*

Figure 42: Point Cloud Segmentation

6.2.1.3   OBJECT DETECTION

The third step of the detection process involves matching the trajectory data with the overhead object candidate points obtained in the previous step to locate the overhead structures. At every point along the defined trajectory, a nearest neighbour classifier was also used to locate any

overhead structures above the trajectory point [142]. As displayed in Figure 43, the aim is to search for the overhead point nearest to the trajectory point on the ground.
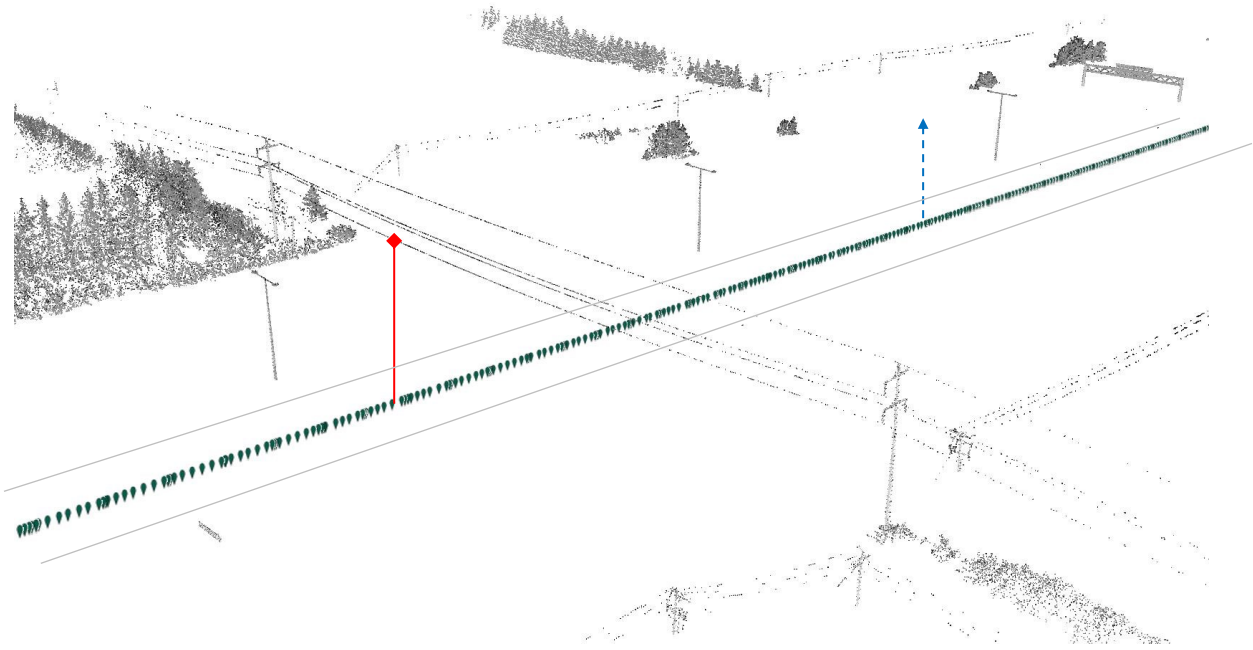
Figure 43: Overhead Object Detection (No overhead points exist above the trajectory points at the dashed arrow upstream the segment, therefore, no overhead object is detected. For the solid line overhead points representing a power line exist above the trajectory pin and hence, an overhead object is detected).

The algorithm loops through all trajectory points (pins shown in Figure 43) and returns a list of points for which an overhead match was found. For instance, for the dashed arrow in Figure 43, no overhead points exist above the trajectory points, therefore, no overhead object is detected. However, for the solid line, overhead points representing a power line exist above the trajectory pin and hence, the code identifies this as a location where an overhead structure does exist. The code also computes the difference in elevation between the overhead point and the point on the road's surface (i.e., the trajectory point). This estimate is used as a preliminary estimate of the clearance at that locations.

For overhead objects that have a limited thickness, and as a result, a low point density (along the road's axis) (<3 points), an additional check is conducted to ensure that the detected overhead points are indeed part of an overhead object and not random points representing noise. This is done by assessing the existence of points within the lateral vicinity of the detected point. Specifically, a

search is conducted for points that were closest to the detected overhead point in the lateral direction (i.e., the direction perpendicular to the road's axis), as shown in Figure 44.
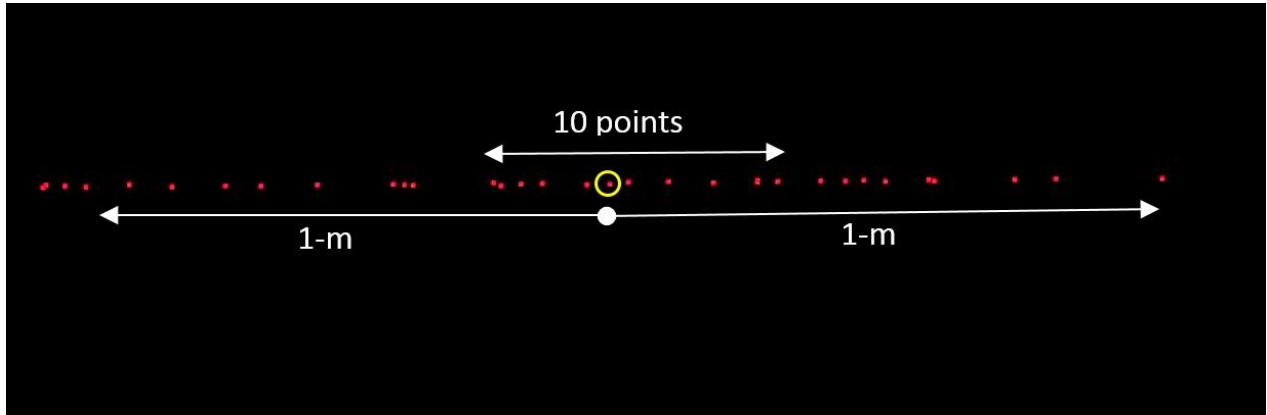
Figure 44: Assessing the existence of other overhead points within the vicinity of the detected overhead point (Circled).

The average distance from cluster of 10 nearest points, p_n to the point p_i is determined and is assessed follows.

$$\overline{Y}_i < 1m \rightarrow \text{is an overhead object}$$
$$\overline{Y}_i \geq 1m \rightarrow \text{is noise}$$

(19)

where $\overline{Y}_i$ is the mean distance from the 10 nearest neighbouring points p_n to the original overhead point p_i. It is assumed here that if the points are scattered more than 1m away then it is highly unlikely that these points belong to the same overhead object and, hence, the detected point does not represent an overhead object.

The reason a 1m and 10-point threshold was chosen is because the minimum point density of data used in this thesis is approximately 100 points per square meter. Assuming the points are evenly distributed along either end of the square meter, this translates to approximately 10pts/m. It is worth noting here that sensitivity analysis was conducted for the distance and point density thresholds and it was found that these thresholds did not impact detection accuracy. It is also worth emphasizing that this is an additional filter that is only applied to help distinguish overhead objects with a low point density from noise, if they exist.

6.2.2 OBJECT CLUSTERING & CLASSIFICATION

To identify the number of overhead structures determined on a segment, trajectory points along the roads surface for which a match was found are clustered using the DBSCAN (Density-Based Spatial Clustering of Applications with Noise) clustering algorithm [143].
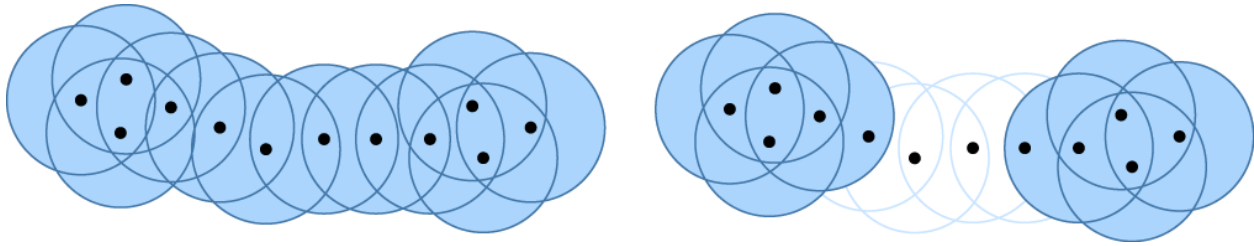
Figure 45: Density-based spatial clustering of applications with noise (DBSCAN)[144]

The DBSCAN algorithm is a density-based algorithm that works on grouping points based on proximity (ε) and hit count as illustrated in Figure 45. The proximity measure defines how close multiple points within a cluster are to one another. Hit count is a measure of the minimum number of points required for those points to be considered a cluster. If the distance between points exceeds the minimum proximity (ε) and the number of points exceeds the minimum hit count, it is likely that these points do not represent a cluster. A minimum hit count of 4 and a proximity (ε) of 1m were used to group of points into clusters, or in this case, an overhead object.

DBSCAN was selected for two main reasons. (i) DBSCAN does not require specifying the number of clusters in advance, which is extremely important for this application since we assume the number of overhead objects is unknown. (ii) DBSCAN has the ability to account for noise and does not require that all points are assigned to clusters, which means that outliers are ignored. This helps improve the accuracy of the detection and classification process by removing erroneous points.

Classification of clusters into bridges and non-bridges is done by applying two different statistical filters that are related to the density and spread of points in a cluster. Before discussing the filters, it is worth noting that objects were only classified into bridges and non-bridges since this is the most important distinction for transportation agencies interested in obtaining clearance information for bridge inspections.
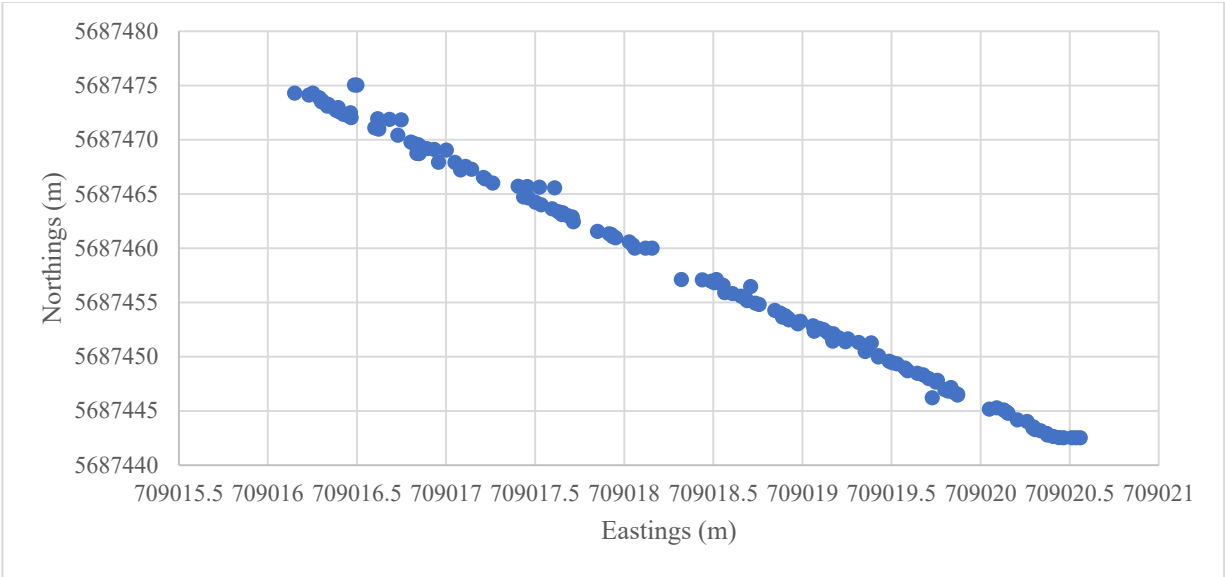
(a)   Detected Points on Bridge
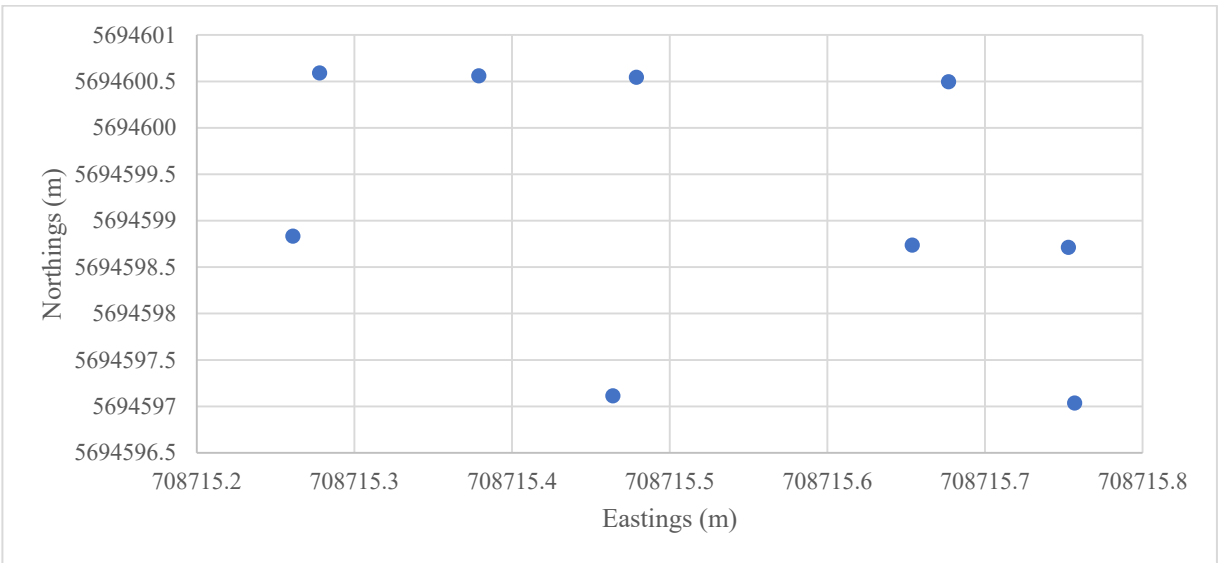
(b)   Detected Points on a Powerline
Figure 46: Points Detected on Overhead Object

Due to the wide span on bridges, point density of clusters detected along their cross sections is relatively high compared to other overhead objects such as power lines. As a result, it is expected that points along a bridge's cross section in the x-y plane would fit very well to a linear model, as evident in Figure 46. In contrast, the sparse and random nature of points along a power line's cross section means that they would generally fit poorly to a linear model. Therefore, the first classification filter is based on how well the points in a cluster fit a linear model in the x-y plane.

For objects where model fit is high (i.e., R-squared > 0.7) [145], these objects are bridge candidates however, they are subject to a second filter before they could be classified as bridges.

The second classification filter is related to the geometric distribution of the residuals of the regression model. As evident in Figure 47, the high density of points detected along a bridge's cross sections results in the probability density plot of the residuals peaking at the mean of zero. The Kurtosis, which is also known as the 4th central moment around the mean, is used to assess the peak in the residual density plot. Kurtosis parameter (γ) can be quantified as follows:

$$\gamma = \frac{n\sum_{i=1}^{n}(x_i - \overline{X})^4}{\left(\sum_{i=1}^{n}(x_i - \overline{X})^2\right)^2} \tag{20}$$

Where, x_i is the residual of point (i), $\overline{X}$ is the mean of all residuals, n denotes the number of observations in the cluster.

A sample with a parameter = 3 is considered normally distributed. If $\gamma < 3$ then the sample is a leptokurtic (peaked) sample, on the other hand, if $\gamma > 3$ then the sample is a platykurtic (flat) sample [146]. Therefore, clusters with a high linear model fit and a high kurtosis ($\gamma > 3$) are considered bridge clusters.
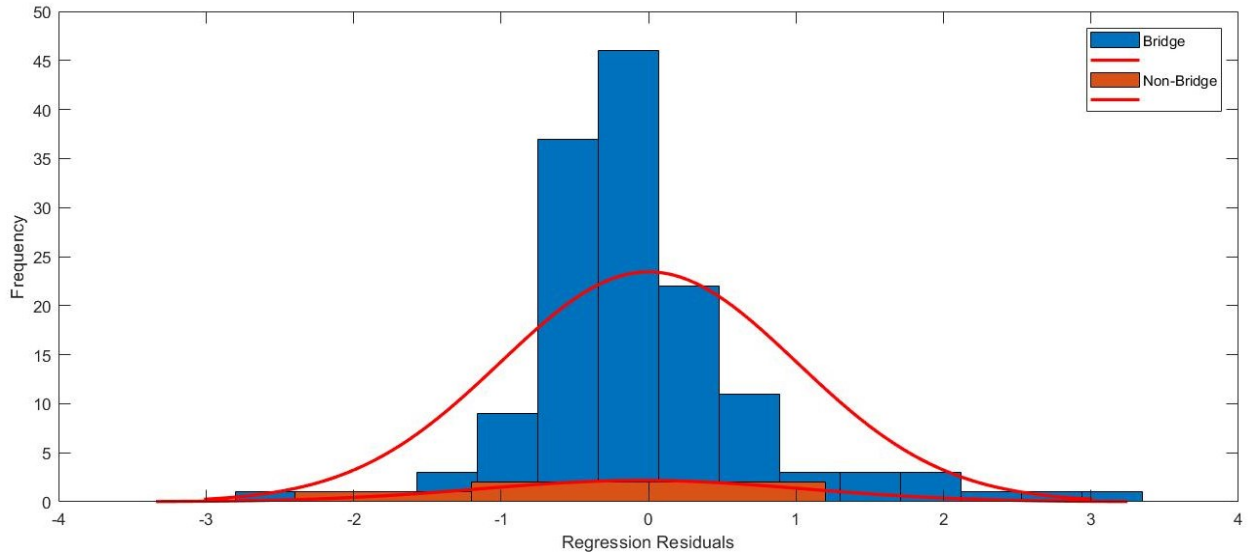
Figure 47: Histogram of Residuals (Bridge vs Non-bridge)

Finally, for all clusters that are determined to be overhead objects, the algorithm returns a clearance measurement at the point of detection. Although this measurement does not cover the all spans of the overhead object, it gives the user an estimate of the vertical clearance of the object in question.

6.2.3 DETAILED CLEARANCE ASSESSMENT

To obtain a more detailed estimate of clearance on bridge structures where vertical clearance could vary at different points along the bridge's span, a detailed clearance assessment is recommended. The detailed assessment involves replicating the trajectory points used in the overhead object detection across the width of the road and matching the new set of trajectory points with points on the bridge structure using nearest neighbor search. As seen in Figure 48, this guarantees accurate clearance measurements when the pavement surface has a high cross slope or when then road has a high grade.

Since different agencies require clearance measurements at different locations below a bridge structure, the specific points at which the clearance is assessed are left for the user to specify. In the example presented as part of the results (section 6.4.2.2), clearance is assessed in different lanes, on different approaches, and in shoulder lanes, since this is the information that is typically required by AT in bridge inspections conducted in the province.
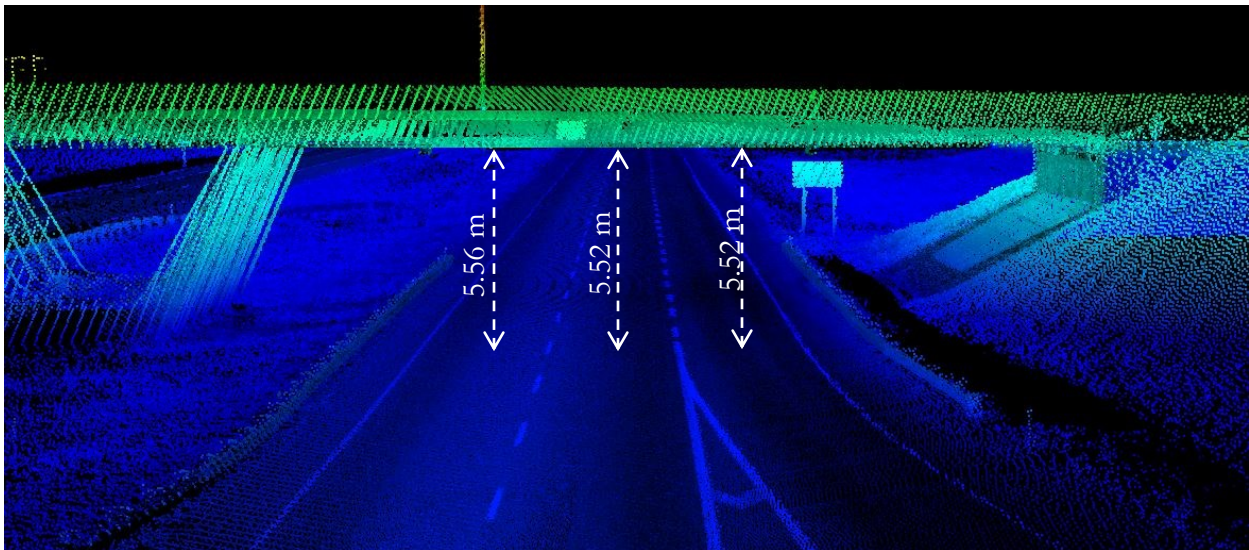
Figure 48: Detailed Clearance Assessment Highway 1 Bridge B

6.3   TEST DATA

The developed algorithm was tested on three different highways in the Province of Alberta, Canada. The segments were all divided highway segments that included a variety of overhead

structures including bridges, power lines, cables and overhead signs. The segments had differing levels of vegetation and tree density as well as different horizontal and vertical alignments. The next few paragraphs provide information about the three highways on which the proposed algorithm was tested.

LiDAR data was collected on the three different segments shown in Figure 49 using the REIGL VMX-450 laser scanning system. For more information on the scanning systems, readers are referred to Chapter 3 of this dissertation.

For two of the test highways, the extracted information was compared to clearance information posted at bridges. For a short segment on the third highway (Highway 2), the extracted information was compared to clearance information obtained in bridge inspections conducted by AT.

6.3.1   HIGHWAY 1

The portion of Highway 1 (also known as the Trans-Canada Highway) considered in the analysis extends a length of 4km and lies in the western part of the Province of Alberta, Canada. The segment is part of a 4-lane divided highway located west of the City of Calgary. The speed limit on the segment is 110km/h and it is highly travelled due to its proximity to the Banff National Park. The segment also has a high density of trees and vegetation on either side of the road as seen in Figure 49a. In addition, there is physical separation of the two travel approaches. The type of median varies along the segment (depressed vs. raised) as does the horizontal alignment of the segment. Two interchanges exist on the segment. The point cloud file of this segment consisted of over 17 million points. Overhead structures on this segment included two bridges in addition to several power lines.
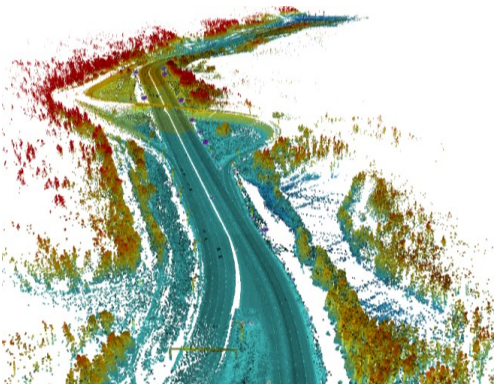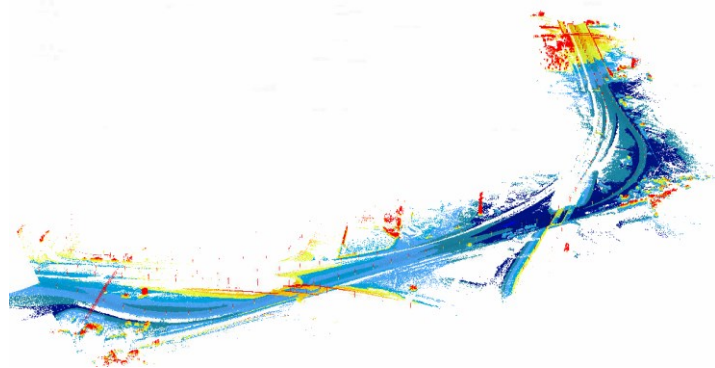
(a)   Highway 1   *(b)   Highway 14*
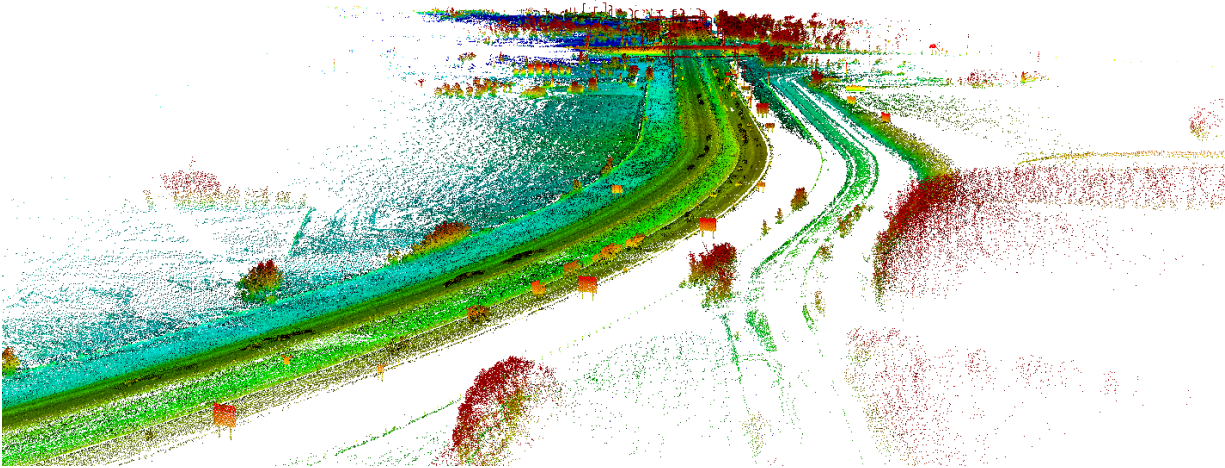
(c)   Highway 2 Corridor
Figure 49: Point Cloud Data at Test Highways

6.3.2   HIGHWAY 14

The Highway 14 segment extended a length of 4km. This segment was also a 4-lane divided rural road. The highway is located southeast of the City of Edmonton in Alberta, Canada. The travel approaches are separated by a depressed median with moderate vegetation and tree density on the side of the road as seen in Figure 49b. It is worth noting that part of this segment has travel approaches which are completely separated as the highway merges into the Anthony Henday Drive, which is a major ring-road encircling the City of Edmonton. The LiDAR point cloud file for this segment consisted of 31.7 million points. The speed limit on the road is 100km/h. Four different bridges exist on the analyzed portion of this segment as well as a number of power lines. It is worth noting here that the reason test segments on Highway 1 and Highway 14 were both 4km in length is because LiDAR scans collected by AT were segmented into 4km sections. This does not mean that the proposed algorithm is only applicable on 4km segments. In fact, the algorithm was tested on multiple highway corridors including Highway 2.

6.3.3   HIGHWAY 2 (CORRIDOR ASSESSMENT)

The section of Highway 2 (also known as the Queen Elizabeth II Highway) considered in the analysis lies in the central part of the Province of Alberta. The segment is part of a four-lane divided highway located in between the cities of Calgary and Edmonton. The speed limit on the segment is 110km/h and it is highly travelled as it is the main transportation route connecting Northern and Southern Alberta. The segment is primarily bordered by low vegetation as seen in

106

Figure 49c. In addition, there is physical separation of the two travel approaches. The median varies along the segment (depressed vs. raised) as does the horizontal alignment of the segment. This Highway was used for two purposes, first, the proposed algorithm was used to estimate clearance and detect overhead objects for the entire highway corridor which extended a length of 242km. The 242-km segment consists of over 1 billion points resulting in 41 GB of raw LiDAR data. Second, clearance information collected by AT in a Bridge inspection report was available on a selection of bridges along the highway, hence, this information was used to validate the clearance information obtained using the proposed algorithm.

6.3.4 RESULT ASSESSMENT METRICS

To numerically assess the validity of the detection results, three metrics (precision, detection rate, and accuracy) were calculated. The metrics were calculated as follows:

$$\text{Precision} = \frac{TP}{TP + FP} \tag{21}$$

$$\text{Detection Rate} = \frac{TP}{TP + FN} \tag{22}$$

$$\text{Accuracy} = \frac{TP + TN}{TP + FN + FP + TN} \tag{23}$$

where, TP and TN denote the number of true positives and the true negatives. FP denotes the number of false positives and FN denotes the number of false negatives.

Accuracy measures how effective the algorithm is in the valid classification of both true positives and true negatives, this measure is also known as *quality* and provides a compound performance metric that balances detection rate and precision [147]. *Detection rate*, also known as *completeness*, measures how effective the algorithm is in the valid identification of true positives only. Finally, *Precision*, also known as *correctness*, measures how successful the algorithm is in applying the classification filters.

6.4 RESULTS AND DISCUSSION

6.4.1 OVERHEAD OBJECT DETECTION

As already discussed the algorithm was tested on LiDAR data collected on Highways 1, 2, and 14. On Highway 1 and 14, testing was conducted on short subsegments of the highways (around 4km

each), whereas for Highway 2 testing was carried out on the entire highway corridor that extended 242km between Alberta's most populous cities Edmonton and Calgary.

6.4.1.1 SHORT TEST SEGMENTS

Figure 50 and Figure 51 show the results of the overhead structure detection performed on both Highway 1 and 14, respectively. For each highway, two different figures are displayed. The top figures (Figure 50a and Figure 51a) represent a plot of the detected clusters and the bottom figures (Figure 50b and Figure 51b) represents a plan view of the point cloud data. The horizontal axis on the plots represents the Universal Transverse Mercator (UTM) easting coordinates while the vertical axis represents the UTM northing coordinates. Each diamond on the plots represents a cluster of points which, in turn, represent a single overhead structure. If the cluster on Figure 50a and Figure 51a are traced down to Figure 50b and Figure 51b the overhead object can be seen on the plan view of the LiDAR highway.

Table 5 and Table 6 also show the overhead structure detection results for Highways 1 and 14, respectively. For each of the detected clusters, the tables show the cluster ID, the overhead object each cluster represents, the coordinates of the object, the minimum elevation and the points per cluster.

Table 5: Overhead Object Detection Results (Highway 1)

Cluster ID	Object	Eastings	Northings	Min Clearance	Points Per Cluster
1	Bridge A	5665281	612324.3	5.56	79
3	Cable A	5664144	613526.5	6.91	24
4	Cable B	5663579	613972.6	6.91	15
5	Bridge B	5663332	614171.5	5.46	66

Table 6: Overhead Object Detection Results (Highway 14)

Cluster ID	Object	Eastings	Northings	Clearance	Points Per Cluster
1	Cable	344291.6	5926148	15.77	45
2	Bridge A1	344345.6	5925679	6.03	154
3	Bridge A2	344380.2	5925623	6.65	146
4	Bridge B1	344869.3	5924822	5.76	158
5	Bridge B2	344895.9	5924779	5.85	173
6	Cable	346752.7	5924438	14.3	33
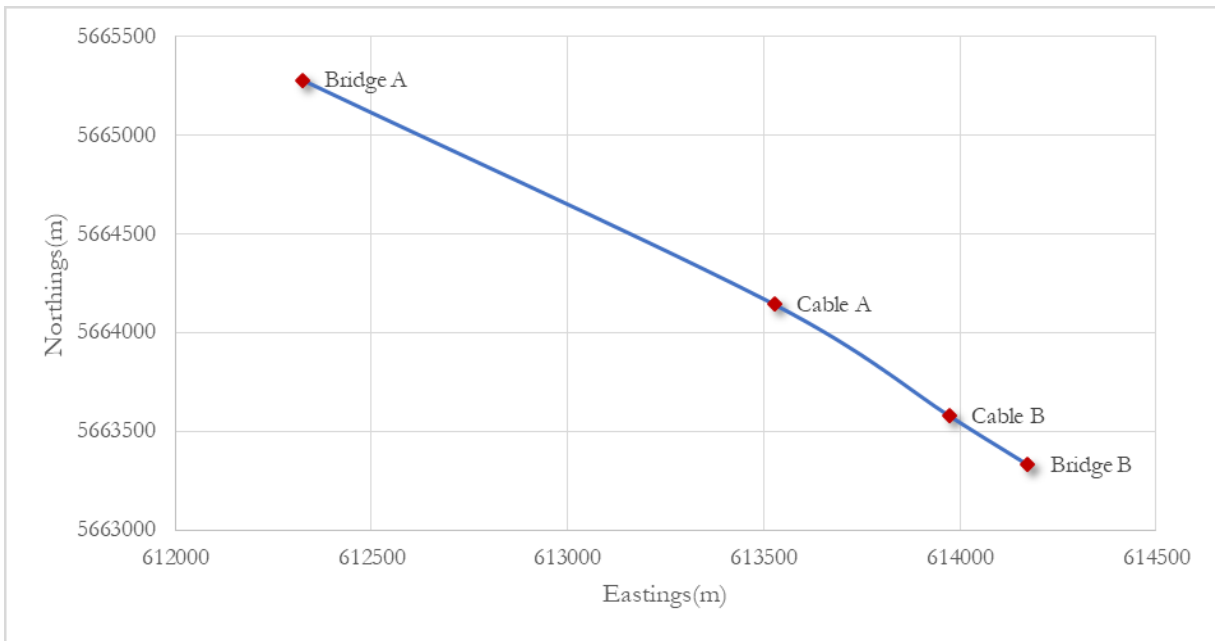
(a) Detection Results
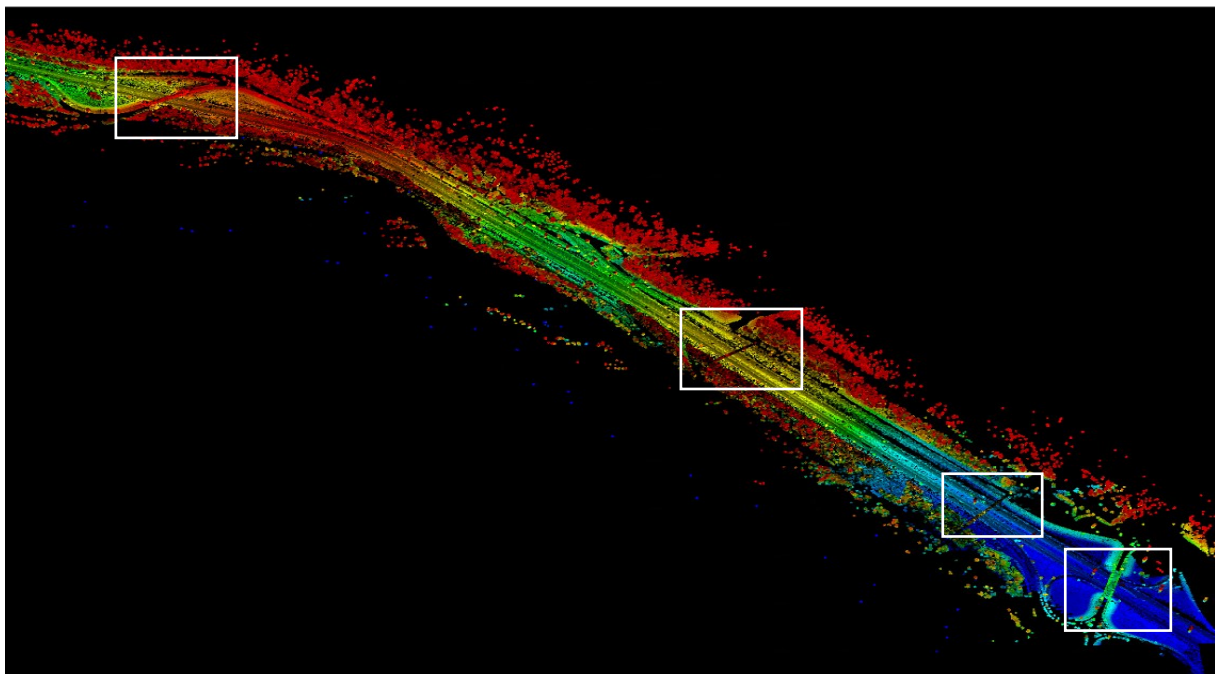
(b) Plan view of LiDAR segment
Figure 50: Overhead Structures Detected on Highway 1
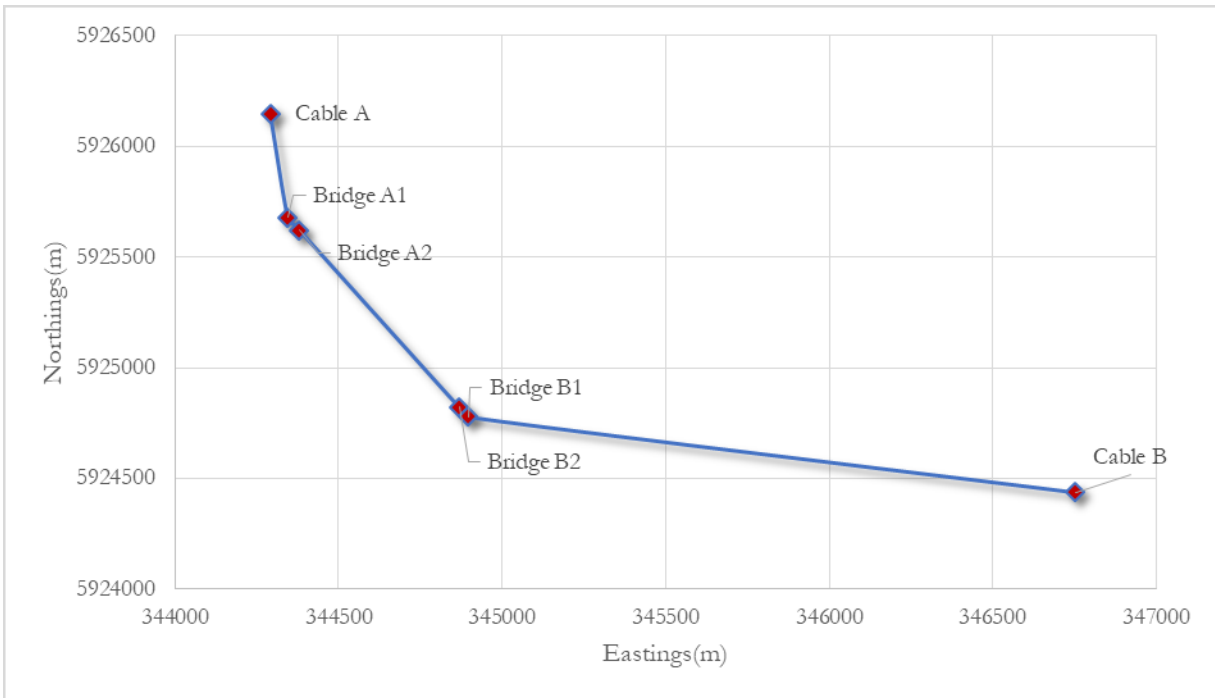
(a) Detection Results
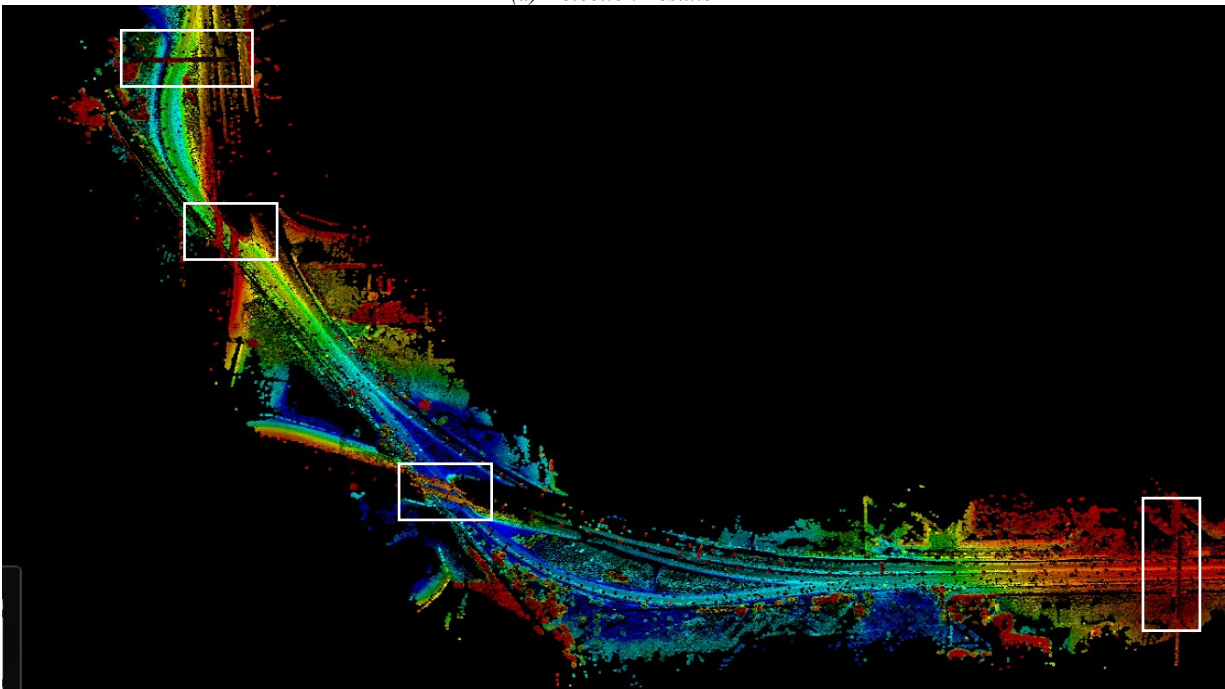
(b) Plan view of LiDAR segment
Figure 51: Overhead Structures Detected on Highway 14

On the analyzed segment of Highway 1, four different overhead structures existed, namely; two bridges and two power lines. On Highway 14, there were six different overhead objects on the

analyzed segment - two pairs of bridges and two power lines. As evident in Table 5 and Table 6, the algorithm successfully detected all overhead structures on both test segments.

6.4.1.2 LONG HIGHWAY CORRIDOR

To demonstrate the repeatability of the proposed method and its efficiency in a large-scale assessment, the algorithm was used to detect overhead objects along the Highway 2 Corridor in central Alberta. The algorithm was successful in detecting all 152 objects that existed on the analyzed segment without any False Positives. This included single cable power lines, multi-cable power lines, overhead signs, and bridges. Although no false positives were detected (i.e., all 152 objects were accurately detected), the detection process did result in two false negatives (i.e., overhead objects that were not detected). These were a virtual weigh station cantilever and an overhead sign that extended onto a single lane of the highway. It is worth noting here that detecting those objects is possible by simply offsetting the trajectory defined in section 6.2.1.1 to the lane of interest.

In addition to the accurate detection of objects, the algorithm was also successful in accurately classifying overhead objects into bridges and non-bridges. Out of 32 bridge structures on the 242km of the highway, the classification process yielded four false negatives and two false positives. Two of the false negatives (i.e., overhead objects that were classified into non-bridges despite representing bridge structure) were incomplete bridges that were split between two LiDAR segments due to the way the LAS files were stored. This causes the number of points on the bridge structure to get split between two sections. Another false negative was a pedestrian footbridge, which did not have a span as wide as traffic bridges. As for the false positives, one of those was a power line that consisted of over 10 cables, which resulted in a point density similar to that of a bridge. Although these power lines are rare, they could be distinguished from bridges due to the high clearance at those objects (typically > 11m).

To numerically assess the validity of the results, three metrics (precision, detection rate, and accuracy) were calculated. These metrics were computed to assess the validity of both the detection process (i.e., the accuracy of the proposed algorithm in detecting all overhead objects on the test highway), and the classification process (i.e., the ability of the proposed method in accurately classifying detected overhead objects into bridges and non-bridges). The metrics for detection and classification are presented in Table 7.

Table 7: Result Validity Assessment

Metric	Detection of Overhead Objects	Classification of Objects
Precision (%)	100	93.8
Detection Rate (%)	98.7	88.2
Accuracy (%)	98.7	96.3

The high percentages in table, combined with the fact that these results were obtained on a long highway corridor illustrate the robustness of the proposed method in detecting and classifying overhead objects. The results show the ability of the algorithm in accurately detecting and classifying overhead objects regardless of the length of the highway, or the type of overhead objects that exist on the highway.

6.4.2   CLEARANCE ASSESSMENT

6.4.2.1   PRELIMINARY CLEARANCE ESTIMATE

As already noted, a preliminary estimate for clearance at each overhead object is obtained as part of the detection process described in section 6.2.1.3. The preliminary clearance estimates obtained on the Highway 1 and Highway 14 test segments are presented in Table 5 and Table 6 are first explored. For Highway 1, the minimum bridge clearance based on the detection results is 5.56mand 5.46mfor Bridges A and B, respectively. On Highway 14, the minimum clearance was 5.76mand 5.85mfor Bridges A1 and A2 and 6.65mand 6.03mfor the two Bridges B1 and B2.

The posted minimum clearance at the analyzed bridges, as shown in Table 10 (columns 6) ranges from 5.2 meters to 6.5 meters. It is worth noting that AT require that the posted minimum clearance is 0.1m less than the minimum height measured between the lowest point on the overhead structure and the surface of the roadway. After subtracting the 0.1m tolerance, the number is also rounded down to the nearest 0.1 m. This means that if the minimum clearance measured at a bridge is 5.32m, the posted minimum clearance beneath the bridge should be 5.2m.

After comparing the minimum clearance based on the posted information to that obtained from the detection, the results reveal that the percentage difference ranges from 0.69 to 3% with an average difference of 0.92% for all bridges. This indicates that even the clearance estimate obtained in the detection process is a good representation of the measured clearance at the bridge.

With regards to the power lines, the minimum clearances are also summarized in Table 5 and Table 6. Clearance information about those objects is not known and not posted, however, clearance at

power lines typically ranges from 6m to 20mdepending on the voltage being carried in the cable [148]. This was indeed the case for all the power lines that were detected on the test highways.

6.4.2.2 DETAILED CLEARANCE ASSESSMENT

As highlighted in the last few paragraphs, the detection process proposed in this Chapter yielded accurate clearance estimates at all the detected objects. These measurements eliminate the likelihood of human error associated with traditional surveying practice and result in a more reliable clearance estimate. Nonetheless, if the absolute minimum clearance across the span of an overhead object is desired, a detailed clearance assessment is still required. Accordingly, the detailed assessment was performed at all the detected bridges due to their long span.

Clearance Information Validation

Before the detailed clearance assessment was conducted on Highway 1 and Highway 14, the clearance assessment algorithm was tested along a subsegment of the Highway 2 corridor where ground truth clearance measurements were available. This was a 4km segment that lies north of the town of Lacombe, Alberta. The point cloud file for this segment consisted of 29.5 million points. Only one bridge existed on the analyzed segment, however, a power lines and an overhead sign were also present. For verification purposes, the results of the detailed clearance assessment obtained using the proposed method were compared to the information obtained by AT in bridge inspections. Table 8 shows the results of the comparison.

Table 8: Clearance Verification Results

Lane Position[a]	Span Direction/Number[b]	Clearance Measured During Bridge Inspection	Clearance Obtained Using Proposed Method	Difference (cm)
L1	S3N	6.41	6.396	1.4
LS	S3N	6.65	6.619	3.1
RS	S3N	6.17	6.155	1.5
L1	S3S	6.4	6.396	0.4
LS	S3S	6.65	6.619	3.1
RS	S3S	6.13	6.132	-0.2

[a]L: Left, R: Right, S:Shoulder
[b] For span orientation, letter indicates span direction and number further specifies the location on the bridge, for further information see Chapter 7 of Alberta Transportation's Bridge Inspection Manual[149]

The differences in vertical clearance between the values measured in bridge inspection and those obtained using the proposed algorithm suggest that the methodology is accurate in determining the vertical clearance. The differences in clearance range from 0.4cm to 3.1cm, which could be caused by human error or potential imperfections when conducting manual field measurements. These

differences translate to percent differences that range from 0.03 to 0.47%, which indicates a high level of accuracy.

<p align="center">*Table 9: Result Validation Other Bridges*</p>

	Location		Lane		
	Located On	**Highway 2 Section Overpassed**	**LS**	**L1**	**RS**
LiDAR Assessment	597	2:26	5.888	5.792	5.762
Bridge Inspection			5.920	5.770	5.770
% Diff			-0.005	0.004	-0.001
LiDAR Assessment	HW42	2:24	5.530	5.570	5.674
Bridge Inspection			5.490	5.510	5.650
% Diff			0.007	0.011	0.004
LiDAR Assessment	32 St	2:24	5.978	5.907	5.955
Bridge Inspection			5.990	5.900	5.950
% Diff			-0.002	0.001	0.001
LiDAR Assessment	HW 616	2:30	5.370	5.380	5.440
Bridge Inspection			5.370	5.320	5.390
% Diff			0.000	0.011	0.009
LiDAR Assessment	HW 611	2:28	5.950	5.920	5.820
Bridge Inspection			5.960	5.860	5.820
% Diff			-0.002	0.010	0.000
LiDAR Assessment	HW 27	2:22	5.890	5.820	5.490
Bridge Inspection			6.000	5.900	5.580
% Diff			-0.018	-0.014	-0.016
LiDAR Assessment	HW 590	2:22	5.420	5.450	5.570
Bridge Inspection			5.400	5.410	5.570
% Diff			0.004	0.007	0.000
LiDAR Assessment	HW 54	2:22	5.700	5.710	5.820
Bridge Inspection			5.800	5.690	5.700
% Diff			-0.017	0.004	0.021
LiDAR Assessment	HW 27	2:20	5.900	5.820	5.610
Bridge Inspection			5.920	5.820	5.460
% Diff			-0.003	0.000	0.027

For further validation, clearance information obtained at other bridges on Highway 2 where ground truth information was available, was also compared to clearance measurements obtained in bridge inspections. Table 9 shows a summary of the comparison for the different bridges and the percent difference between the measurements for each bridge in three different lanes.

As apparent in the table, the differences ranged from a maximum percent difference of 2.7% at one bridge to 0% at other bridges. To understand whether those differences were statistically

significant or not, a paired t-test was conducted between measurements obtained in the LiDAR assessment and measurements obtained in the bridge inspections conducted by AT.

The t-test yielded a *p*-value of 0.4907, which indicates that there is not enough evidence to reject the null hypothesis. In other words, the *t*-test shows that there are no statistically significant differences between measurements obtained using the LiDAR Assessment and those obtained in the manual Bridge Inspections, which highlights the robustness of the proposed method.

Clearance Compared to Posted Clearance Information

The results of the detailed clearance assessment on Highways 1 and 14 are shown in Table 10. For these bridges ground truth information was not available since no bridge inspections took place at those locations, however, the results were compared to the posted clearance information. Table 10 shows the average clearance obtained from multiple points across each bridge's deck, the average of the minimum 10%, the average of the minimum 5% and the absolute minimum clearance value.

As evident by the difference between the average clearance (column 2) and the absolute minimum clearance (column 5) in Table 10, the clearance observations vary significantly beneath the bridges. The lower deck of the bridge contains steel girders, which cause the observed variations in the vertical clearance, as seen in Figure 52. The variation is also due to the slopes of the roadway or the overpass itself. Such variations highlight the importance of obtaining multiple clearance observations below a bridge's deck to increase the likelihood of finding the 'true' minimum clearance.

The actual minimum clearance obtained using the LiDAR assessment on all highways was conservative (i.e., the posted clearance was still less than the actual minimum obtained from the LiDAR analysis). Nonetheless, the differences between the absolute minimum clearance obtained at some of the bridges and the minimum clearance sign posted at those bridges was relatively close. For instance, at Bridge B1 on Highway 14 the posted clearance was only 4 cm lower than the absolute minimum obtained in the assessment algorithm. While such a difference might be acceptable, it shows that DOTs must be extra cautions when posting minimum clearance signs.

As already noted, AT requires that a 10 cm margin of safety is used when deciding on the minimum clearance that must be posted at a particular bridge. Accordingly, the posted clearance is expected to be 10 to 15 cm less than the absolute minimum clearance measured at the bridge. While this is

the case for most of the detected bridges, the fact that this is not the case for Bridges B1 and B2 on Highway 14 indicates that the posted clearance was based on a clearance value which was not the absolute minimum at the bridge.
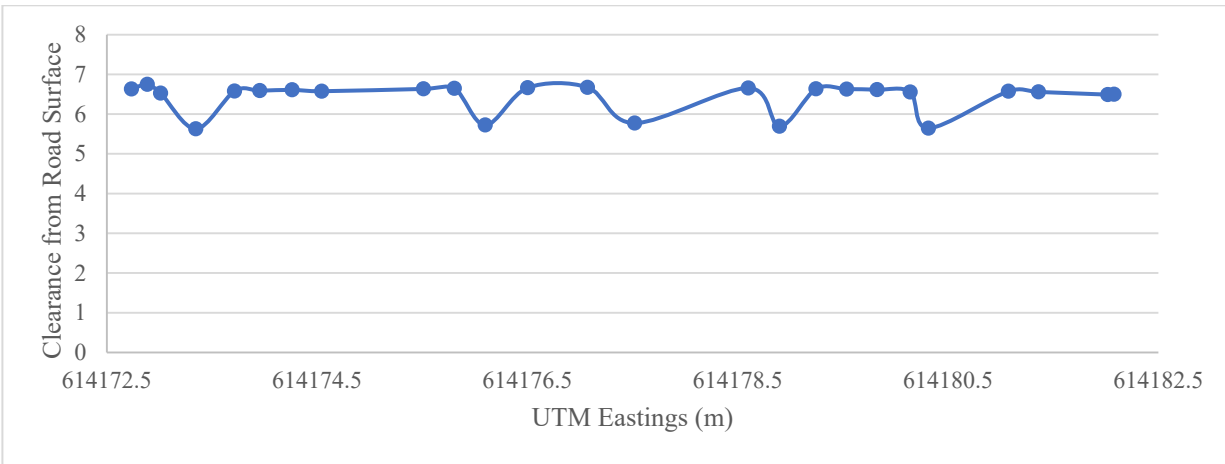
Figure 52: Steel Girders Below Bridge Deck

This finding demonstrates the importance of performing a detailed assessment of clearance before posting clearance signs as an error of 5 to 10 cm in the posted clearance might be the difference between a truck driving smoothly beneath a bridge and a collision costing hundreds of thousands of dollars in repairs.

The assessment also shows that, if it is evident that on multiple bridges the posted clearance is not based on the absolute minimum due to limitations in conventional clearance measurement tool, DOT's still using those tools might need to revise the margin of error used when posting minimum clearance signs.

Table 10: Clearance Assessment Results

	LiDAR Detailed Assessment				Conventional Measure		Difference in Clearance
	Average	Min 10%	Min 5%	Min	Posted	Calculated	Posted – Detailed Clearance Measure (cm)
HWY 1 Bridge A	6.31	5.54	5.49	5.45	5.30	5.40	15.30
HWY 1 Bridge B	6.33	5.61	5.58	5.52	5.30	5.40	21.70
HWY 14 Bridge A1	7.51	6.10	6.05	6.03	5.90	6.00	13.20
HWY 14 Bridge A2	8.10	6.73	6.67	6.65	6.50	6.60	15.10
HWY 14 Bridge B1	7.07	5.78	5.77	5.74	5.70	5.80	4.00
HWY 14 Bridge B2	7.16	5.85	5.84	5.79	5.70	5.80	8.70

6.4.3 PROCESSING TIME

The process proposed in this study for overhead object detection, classification and clearance assessment takes approximately one minute per kilometer for a Desktop PC with Intel i7 CPU and 16 GB RAM. This could vary depending on the number of overhead objects on a segment, however, the estimate is based on analysis conducted in this study, which includes 242km of the Highway 2 corridor (the longest and busiest highway in the province of Alberta) where 152 overhead objects exist (0.62 objects per km). It has been reported in previous research, based on data from Washington State DOT, that manual clearance assessment of a single bridge can take up to 1.5 hours, which excludes relocation time from one structure to another, lodging time and expenses for surveying crew [17]. Therefore, the proposed method creates significant time savings for agencies interested in assessing clearance information along highways. Furthermore, the fact that the same LiDAR dataset could be used for multiple applications helps save time spent in field visits collecting other information about road infrastructure[150].

6.4.4 CHALLENGES AND RECOMMENDATIONS

One limitation of the proposed method lies in its inability to detect power lines with a very low point density. Although the algorithm is programmed to check for LiDAR points within the lateral vicinity of power lines where point density is low (section 6.2.1.3), there are some instances where even lateral point density (i.e., the point density across the length of the power line) is sparse. This makes it difficult to distinguish such objects from noise in the data. Although this did not significantly impact the quality of the results, future studies might need to consider region growing techniques to overcome the issue of sparse point density along those power lines. Another challenge that may hinder the assessment process in some cases is the existence of incomplete overhead objects (see for example Figure 53). This could be caused by object occlusion during data collection (which is highly unlikely since the main source of occlusion is typically vehicles travelling on the highway which cannot obstruct overhead objects due to the difference in height) or LiDAR scan segmentation (which was the case in this study). LiDAR data collected on a highway is often broken down into several subsegments of manageable size. Breaking down those segments sometimes occurs at interchanges and results in the bridges at those interchanges getting split into two segments. This impacts the accuracy of the classification process of the detected

overhead asset. Therefore, it is recommended that such segmentation is avoided if the datasets are to be used for clearance assessment.
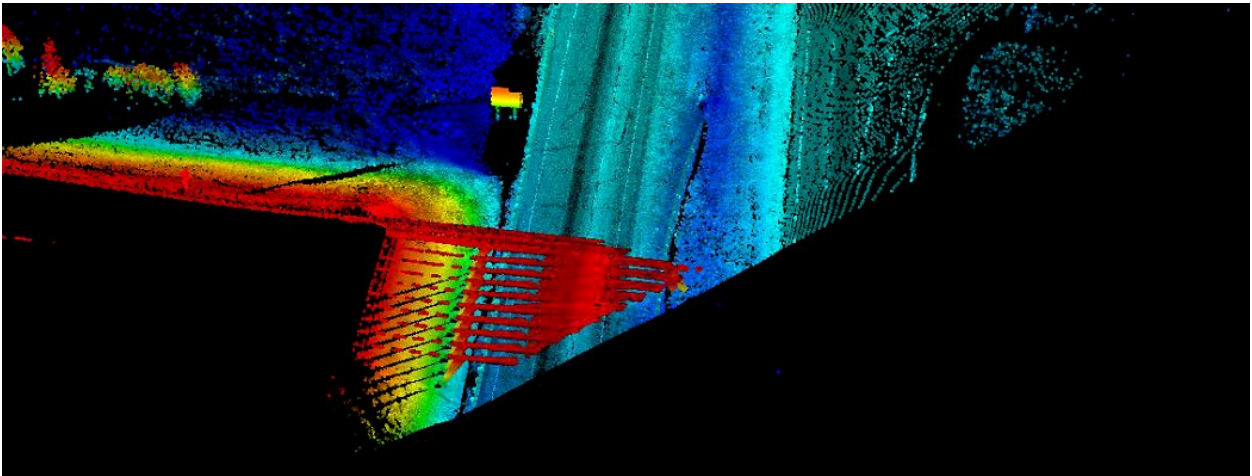
(a)   Top View
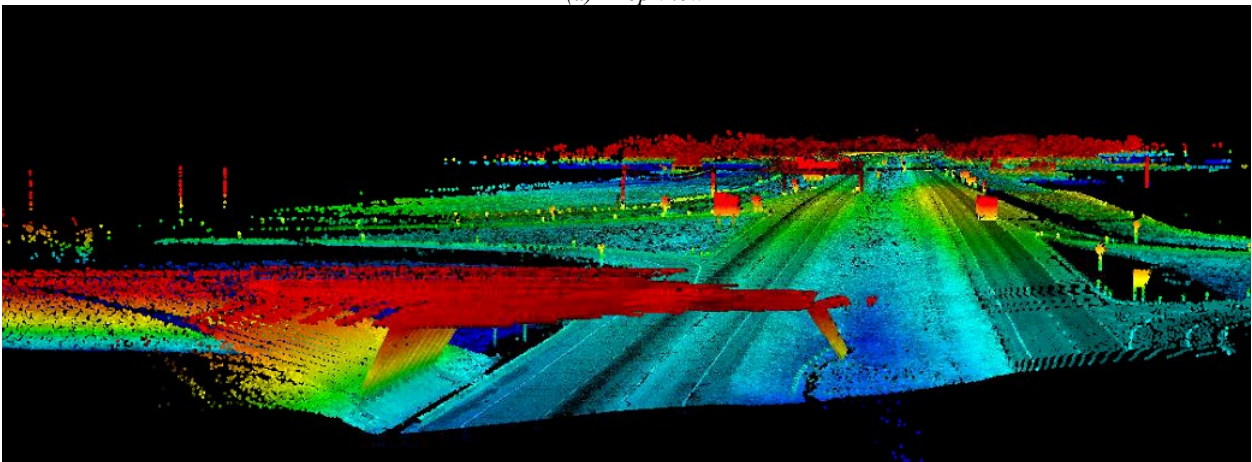
(b)   Side View
Figure 53: Incomplete Bridge

Despite these challenges, the algorithm is of great value for transportation agencies looking to automatically inventory and classify overhead objects on an entire highway network with minimal effort.

6.5   SUMMARY AND CONCLUSIONS

This Chapter proposes a novel algorithm which can be used to efficiently assess vertical clearance on a highway network using mobile LiDAR data. The algorithm involves automatically detecting, classifying and assessing the vertical clearance at all overhead objects on a highway. The proposed algorithm provides an exhaustive and accurate method for the assessment of vertical clearance in much safer conditions than existing techniques.

119

The proposed algorithm was tested using data collected on three highways in the Province of Alberta, Canada, including a 242km highway corridor. The results of the analysis showed that the algorithm was successful in detecting the vast majority of overhead objects on all highways. This included the detection of power line cables, overhead signs and bridges. Furthermore, comparison of the clearance information obtained using the proposed method to those documented in bridge inspection reports revealed that the proposed method provides an extremely accurate clearance measurement, with percent differences of less than 0.47%.

The efficiency with which clearance can be assessed using the proposed algorithm makes it extremely valuable when network-level assessment of clearance is desired. Bridge management agencies can also use the extracted information as part of their routine inspection of bridges to help manage their rehabilitation and maintenance programs. The extracted information could help agencies prioritize structures with significant clearance problems which would lead to agencies addressing integrity concerns in a timely manner before irreversible damage occurs or safety problems arise. The proposed detailed clearance assessment of bridges also increases the likelihood of detecting the absolute minimum clearance beneath a structure, which is not always possible using manual procedures. As evident through the assessment, the absolute minimum clearance might be relatively close to the posted clearance in some cases. If this is observed at multiple locations on a highway network, agencies might consider updating design codes to incorporate higher margins of safety when posting clearance information based on manually measured clearance estimates.

7 SIGHT DISTANCE ASSESSMENT

7.1 BACKGROUND

One important aspect that must be considered when designing vertical and horizontal alignments on highways is the available sight distance. Sight distance is generally defined as the minimum distance required by a driver to complete a certain maneuver [151,152]. Minimum stopping sight distance, for instance, is the minimum distance required by a driver to come to a complete stop before hitting an obstruction on a roadway. This includes the perception reaction time required by the driver and the breaking distance required to come to a complete stop. Similarly, passing sight distance is the distance required for a driver to complete a passing maneuver on two-way undivided highway. Whether it is stopping sight distance, passing sight distance or even intersection sight distance, highway design guides require that recommended standards for those features are met when designing roads[152,153]. In fact, many researchers have found that those features have significant impacts on the traffic safety and the operation efficiency on a highway [154,155].

In design guidelines, minimum stopping sight distance is used to compute the length of vertical curves as well as determine the offset that must be provided along horizontal curves. Although, in theory, designing curves based on the minimum stopping sight distance requirements ensures that this distance is available at any point along the curve, the assumptions associated with the estimation procedure (including the 2-dimensional approach in which alignments are designed) and certain project constraints (financial or practical) mean that there may be locations along a highway where minimum requirements are not met. Moreover, highway features may change after construction, for instance, resurfacing of a highway or other maintenance activities could affect cause changes to the sight distance provided by the original design of the highway. Similarly, the addition of roadside structures such as buildings or trees may limit the available sight distance in the post construction stage.

To that end, frequent evaluation of sight distance on highways is necessary to ensure that guidelines are met throughout the service life of the highway. The issue here is that assessment of sight distance at every point on existing highways is a time-consuming process that is both labor intensive and, in most cases, impractical. Furthermore, the accuracy of performing manual graphical assessments of sight distance is questionable. The reason here is that these assessments

can only be performed in two-dimensions, which means that sight distance at horizontal curves and vertical alignments must be assessed independently. This is not an accurate representation of available sight distance in the field.

To save agencies the burden of conducting manual graphic assessments, interest has moved towards automating the sight distance assessment process. For that cause, procedures have been developed to assess available sight distance by importing surface models of highways into computer software [156]. Unfortunately, such software is often limited in the amount of data they can process, moreover, site visits to collect GPS data and generate the DEMs before are required before those software packages can be used.

Mobile LiDAR technology has huge potential in transforming the way sight distance assessments are conducted, due to its ability to produce highly detailed three-dimensional maps of road infrastructure such as that seen in Figure 54 in a single survey pass along a highway. Using mobile LiDAR scans, complex sight distance measurements along an entire highway corridor could be measured without the need to send crew to the field on multiple occasions. In fact, researchers have been exploring using LiDAR for such assessments in recent years, however, as already noted in Chapter 2 of the thesis, most work in this area has focused on using aerial LiDAR scans for the assessment, as opposed to mobile LiDAR. Furthermore, existing research also suffers from other limitations including the inability to account for the existence of overhanging objects and the assessment procedures involving some manual component.
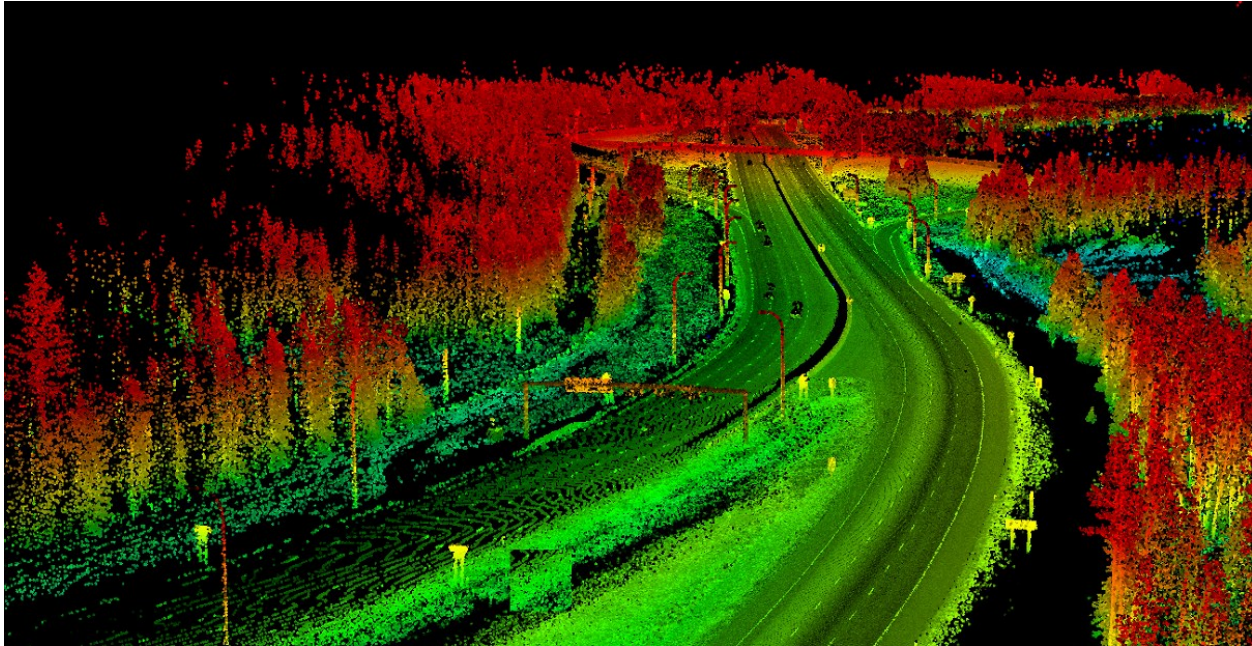
Figure 54: LiDAR point cloud

To overcome these limitations, this Chapter proposes a fully automated algorithm through which mobile LiDAR could be utilized for sight distance assessment. Unlike Aerial LiDAR scans, mobile LiDAR provides a more detailed scan of the roadway environment which ensures that all potential obstructions from a driver's perspective are represented in the dataset.

The method proposed in this Chapter first involves overlaying closely spaced points on the LiDAR highway segment. These are points of known coordinates aligned parallel to the road's axis and used to represent multiple observers and targets along the highway. The point cloud is then segmented and used to generate a DSM of the highway. Once that is achieved, the points representing observers and targets are overlaid onto the DSM and sight lines are constructed between all pairs of observers and targets. A line of sight assessment is then conducted to assess visibility along each of the sight lines and the outputs of the assessment were used to compute the available sight distance for each observer. Since ArcGIS is developed based on the Python Programming language, python scripts were written to perform the visibility assessment in ArcGIS in a fully automated manner. Further, MATLAB algorithms were used to calculate the available sight distance based on the outputs of the python script.

The MATLAB algorithm is also written to determine whether stopping sight distance requirements are met at each point along the highway by comparing the available stopping sight distance to the

theoretical stopping sight distance. The proposed methodology is tested on two short (4km) segments on a Highway in the Province of Alberta, Canada with results revealing obstructions to stopping sight distance on a small portion on one of the segments. Furthermore, to illustrate the efficiency and the repeatability of the proposed method, the algorithm was used to compute the available sight distance of a 50km highway corridor.

Unlike previous attempts to assess sight distance using LiDAR data in the literature [33,42], the method proposed in this Chapter is developed to perform the assessment on mobile LiDAR datasets and is highly efficient and fully automated. This efficiency makes it possible to assess multiple LiDAR segments simultaneously, which is required when performing network-level assessment of sight distance on an entire highway corridor. To the best of the author's knowledge, this has not been achieved in previous research. In addition, the algorithm proposed in this Chapter accounts for the existence of overhanging objects by segmenting the point cloud data before performing the sight distance assessment. This helps ensure that the surface models generated using the point cloud are not biased by the existence of such objects and that the sight distance measurements are an accurate representation of existing conditions along the highway.

7.2   ASSESSMENT ALGORITHM

The algorithm for sight distance assessment proposed in this Chapter involves (i) LiDAR point cloud segmentation, (ii) Generation of points of assessment, (iii) digital surface model creation, (iv) Sight line construction and line of sight assessment, and (v) Available sight distance estimation. The next few paragraphs provide a detailed discussion of each of those steps.

7.2.1   GENERATING OBSERVER AND TARGET POINTS

The first step of the process involves the extraction of observer and target points that run parallel to the road's axis. More information about how these points are extracted from the point cloud is provided in section 4.2.1 of the thesis.

The trajectory points are replicated with one set used as observer points $I = [i, i+1, i+2 ... n]$; and a set of targets $J= [j, j+1, j+2 ... m]$, which are aligned parallel to the road's axis. The number of the observer point (n) and target points (m) that are generated depends on how frequent the assessment is to be conducted. The higher the point density the more accurate the assessment is; however, processing times also increase as the number of observer and target points increase.

124

Hence, while an assessment of sight distances every 30-50m is recommended, this is a decision that is left to the designer.

To ensure that both sets of points are representative of actual observers and targets on a road, the height of points representing observers is adjusted to 1.05m. Similarly, for the points representing potential targets, heights are adjusted to 0.38m. These heights are recommended by the Alberta Highway Design Guide for stopping sight distance assessment, since it is assumed that the a driver's eye height (observer) is approximately 1.05m and the tail lights of a leading vehicle is approximately 0.38m[151]. It is worth noting the observer and target point are user defined, hence, alternative heights could be used. In fact, observer and target points could be probabilistically modelled to generate different levels of ASD.

7.2.2 LiDAR POINT CLOUD SEGMENTATION

The point cloud segmentation performed here is similar to that described in Chapter 6, Section 6.2.1.2 of this thesis, however, the aim of the segmentation for the sight distance assessment is to eliminate overhanging objects from the point cloud. It is worth noting here that the segmentation threshold was set such that only overhanging objects were eliminated and that all roadside features including vegetation were retained.

The reason such segmentation was required is because the elevation raster surface models are generated by averaging the elevation of points that fall within each raster cell. Therefore, the elevation of raster cells at locations where overhanging objects exist would be extremely high. Due to the way the line of sight assessment works, such cells are highlighted as locations where potential obstructions exist, despite there being no objects at those locations. Hence, it is important to eliminate such objects before creating the surface models used in the assessment.

7.2.3 DIGITAL SURFACE MODEL CREATION

The LiDAR data consists of a group of closely spaced points that represent a model of the road's surrounding environment. Unfortunately, no matter how dense the point cloud is, there is always a chance of a line of sight passing in between points representing a certain obstruction. Therefore, to ensure that a line of sight is actually blocked at locations where an obstruction exists, it is necessary to group the points within close proximity. This is done by using the point cloud data to generate a raster Digital Surface Model (DSM) in the form of a raster surface. The raster surface

is a grid of cells where the elevation of each cell is computed based on the average elevation of all the LiDAR points which fall in a particular cell. For this step, the python script written to automate the sight distance assessment uses ArcGIS's ArcPy Python module to perform "LAS dataset to Raster" conversion.

In addition to its value in grouping points within the point cloud and ensuring obstructions are detected, creating a raster surface also simplifies the analysis procedure since each cell in the raster surface is a representation of multiple points, hence the amount of data is reduced. Although Digital Terrain Models (DTMs) can be used as a representation of the LiDAR point cloud as was the case in some previous studies [42], the fact that DTMs only represent the bare ground on a highway makes it difficult to account for potential obstructions to sight distance such as buildings or trees on the side of the road.

After creating DSM, the observer and target points of known x, y, z coordinates and generated in Section 7.2.1 are overlaid onto the surface as illustrated in Figure 55.
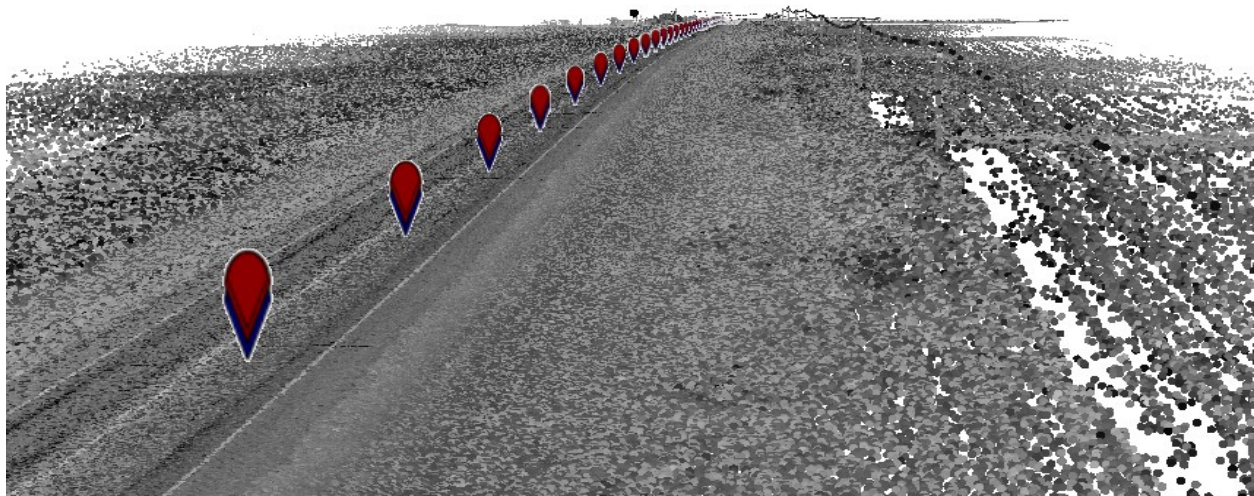
Figure 55: Observer (Red) and Target (Blue) Points (targets are slightly masked by the observers)

7.2.4   SIGHT LINE CONSTRUCTION AND LINE OF SIGHT ASSESSMENT

Once the observer and target points are imported and overlaid onto the raster surface, the Python code is used in the construction of sightlines, which create a direct link between pairs of observers (*I*) and targets (*J*). This is done using the "Construct Sight Line" tool in ArcGIS whereby for *n* observer points and *m* target points along the road's trajectory, $n \times m$ sight lines are created as illustrated in Figure 56. Similarly, the python code uses the arcpy module to automatically assess

the visibility along each of the constructed sightlines (i.e., from each observer to all targets) using ArcGIS's "Line of Sight" tool. For instance, to assess sight distance from observer i the tool would assess the visibility on the sight lines connecting observer i to all targets in set J.
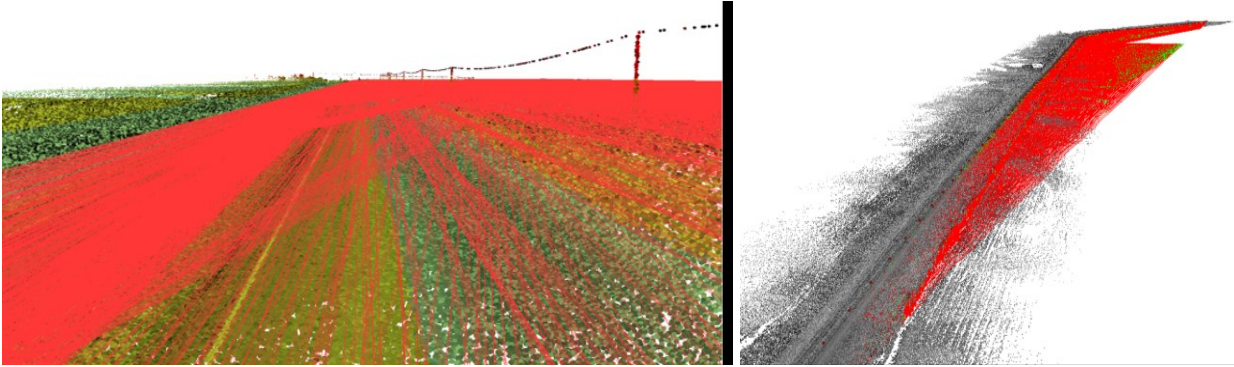
Figure 56: Line of Sight Assessment

The Line of Sight assessment procedure works by testing for the intersection of the sight lines with the raster surface. Any intersection between the sight line and the surface indicates that there is an object of higher elevation than the line, indicating that the target is not visible. Despite being able to assess obstructions along the sight line, the Line of Sight tool does output available sight distance information. Instead, the "Line Of Sight" tool outputs information about whether a target j is visible from an observer i. In addition, the output also includes information about the length of the sight line (Shape_Length) between the observer and target that is unobstructed. After constructing sight lines between pairs of observers and targets along the highway and assessing visibility along those sight lines, the python script exports the outputs from the "Construct Sight Line" and "Line of Sight" tools as *csv* tables. These output tables are then read into MATLAB for post processing to compute sight distance.

7.2.5 *AVAILABLE SIGHT DISTANCE COMPUTATION*

As already noted, two outputs are obtained from ArcGIS. The "Construct Sight Lines" tool outputs a table containing the ID's of all observers, all targets and the sight lines constructed between them. The output obtained from the "Line of Sight" tool includes information about the visibility of all target from each observer (i.e., whether a target j is visible from an observer i), and the portion of each sight line that is unobstructed. This data is available from all observers I to all targets J.

In order to compute the sight distance available along the segment, the outputs of the python code are analyzed in MATLAB. A MATLAB algorithm is written so that it loops through **all** target points (J) for **each** observer point (i) and checks the target visibility based on the outputs of the line of sight assessment discussed in the previous section. The algorithm finds the last visible target (j) from each observer; the distance between the observer and the last visible target is recorded as the available stopping sight distance for the observer (i). Given the design speed of the highway and other attributes, the code is also capable of computing the theoretical sight distance recommended in design guides. The code then compares the available sight distance to that required and highlights observers where sight distance requirements are not met. The flowchart in Figure 57 shows a summary of the logic followed by the MATLAB algorithm to compute the ASD.

The algorithm takes into account that, at the end of the LiDAR segment (i.e., the end of the LAS file), the sight distance calculated will not be representative of the actual available sight distance since no point cloud data exist beyond the end of the segment. This is done by locating the last local maximum within each road segment and truncating the computed available sight distance beyond this point. Alternatively, such a problem (i.e., ASD dropping towards the end of the LiDAR segment) could avoided if LiDAR data collected in surveys for sight distance analysis is stored with an overlap between consecutive LAS files.

Once, the ASD is calculated along the LiDAR segment, the algorithm plots the (ASD) as a function of distance along the roadway for all observer points along the road segment as seen in Figure 58.
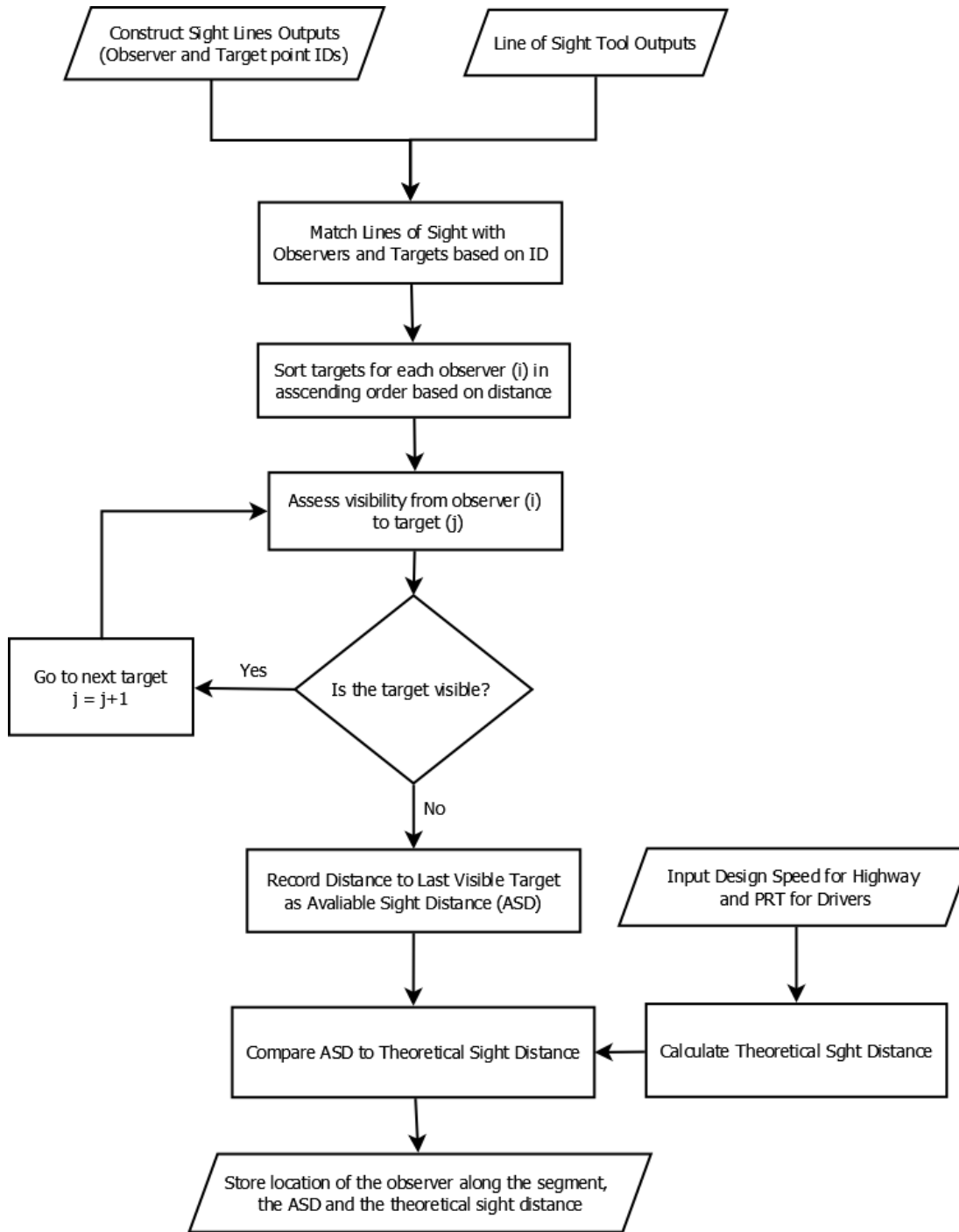
Figure 57: Available Sight Distance Computation
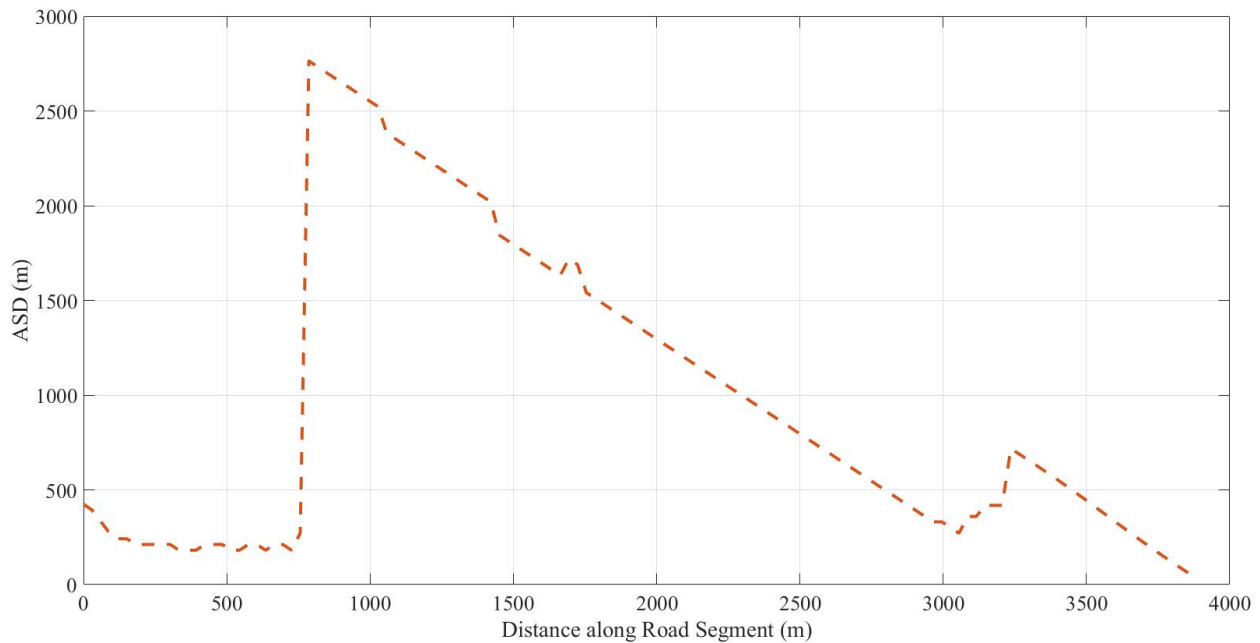
Figure 58 Sample of ASD Plot along a Segment of Highway 20, AB, Canada

7.3   TEST DATA

The developed algorithm was tested on two different highways segments along Highway 36 in Alberta. The two segments were chosen so that the alignment features along the road varied between the two segments. LiDAR data on the two test segments was also collected using the RIEGL VMX-450 Mobile Laser Scanning (MLS) system, which was introduced in Chapter 3 of the thesis.

Highway 36, also known as the Veteran's Memorial Highway, is a two-lane undivided rural road which lies in the eastern part of the province of Alberta. The southmost point on the highway lies east of the city of Lethbridge while the north most point is to the east of the City of Edmonton. The testing conducted in this Chapter was performed on 50km of Highway 36. In addition, testing was also conducted on two short segments (Segment A and Segment B) for validation purposes.

Segment A of Highway 36, seen in Figure 59, extends a length of 4km and has speed limit of 100km/h. Vertical alignment and horizontal alignments both vary along the segments posing potential limitations to sight distance. There is also at-grade stop-controlled intersection at one point along the segment. Unlike Segment A, Segment B is a fairly straight segment with limited variation in the horizontal and vertical alignments as evident in Figure 60. The segment extends

130

has more of a sub-urban setting and extends a length of 1.2km with a speed limit on the road is 50km/h. The reason such a flat short segment was selected for testing was is because it was easy to verify the accuracy of the estimated sight distance on such a segment with no obstructions.

LAS point elevation
- 962 - 983
- 960 - 962
- 958 -960
- 956 - 958
- 954 - 956
- 952 - 954
- 950 - 952
- 948 - 950
- 798- 948

Figure 59: Point Cloud Data at Highways 36 Segment A
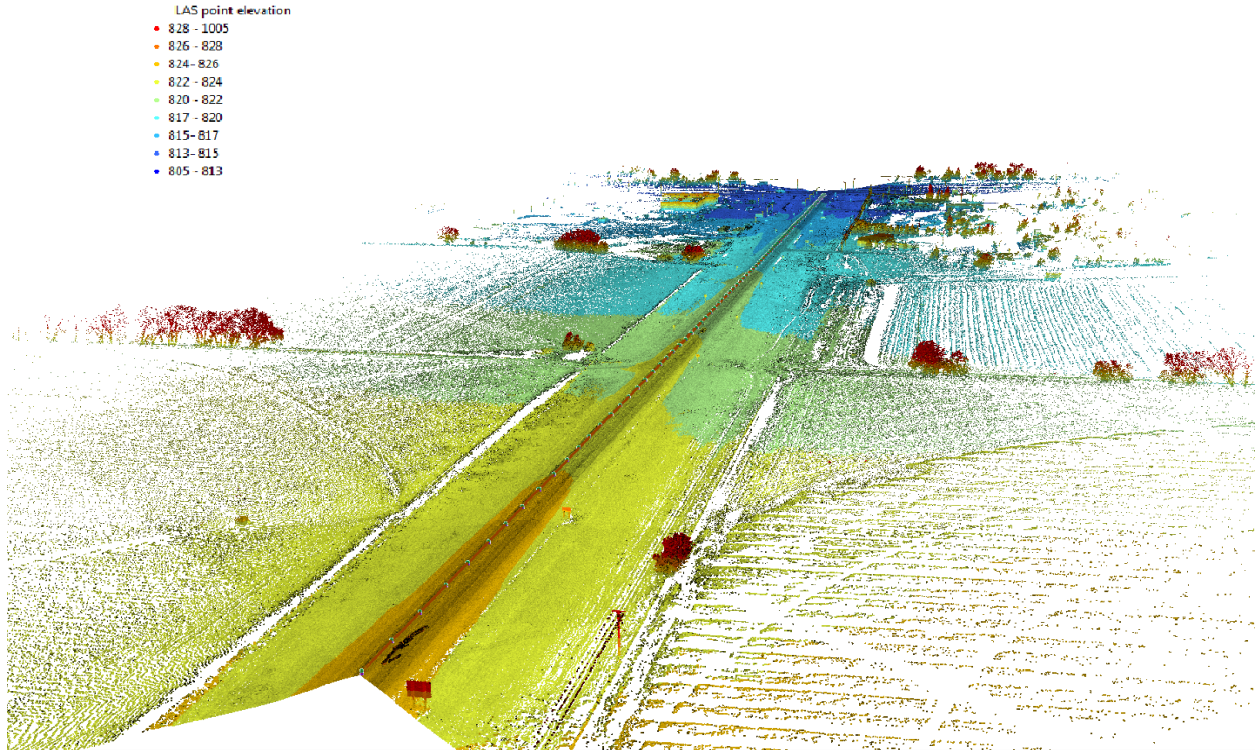
Figure 60: Point Cloud Data at Highways 36 Segment B

7.4 RESULTS AND DISCUSSION

This section discusses the results of testing the proposed sight distance assessment algorithm on the two road segments on Highway 36. Unfortunately, for this application, ground truth information was not available; therefore, validation of the results was done through manual inspection of the test segments. This was done be visiting locations where limitations in sight distance existed and identifying the causes of the obstructions. As already discussed and illustrated in Figure 59 and Figure 60, Segment A has higher variation in the vertical elevation along the road than Segment B, as a result, more limitations to sight distance are expected on this Segment.

Figure 61 and Figure 62 show the available sight distance computed along segments A and B, respectively. The *x*-axis represents the position of the observer along the segment and the *y*-axis represents the sight distance available to that observer. The dotted horizontal line drawn across the plots in on Figure 61 and Figure 62 represents the minimum stopping sight distance required in the AASHTO design guide and computed using the following equation:

132

$$SSD = 0.278Vt + \frac{V^2}{254(\frac{a}{g} \pm G)} \qquad (24)$$

where, V [km/h] denotes the design speed of the highway, t [sec] is the perception reaction time of the driver (AASHTO recommends using 2.5s), a [m/s^2] is the deceleration rate of the vehicle (AASHTO recommends using a deceleration rate of 3.4m/s^2), g [m/s^2] is the gravitational acceleration (9.81m/s^2) and G [%] is the grade of the highway (3% downgrade is used for tabulated SSD values in AASHTO).
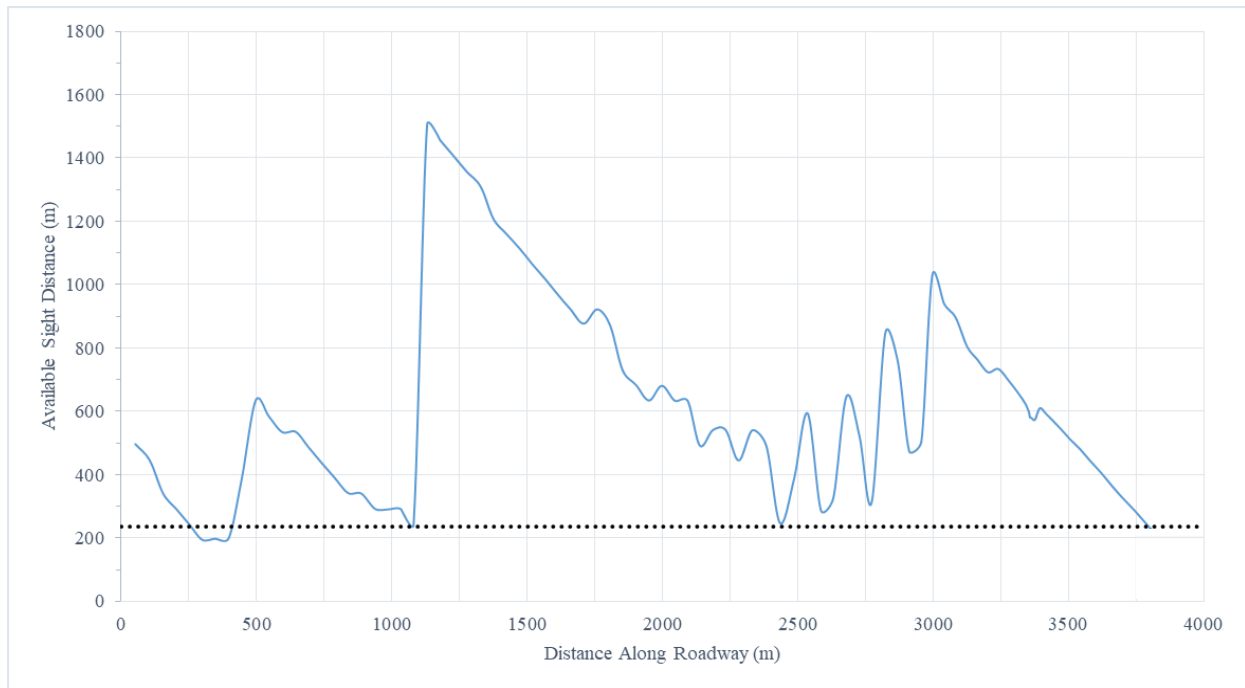
Figure 61: Available Sight Distance Along Highway 36 Segment A (Dashed Line Represent Theoretical SSD)
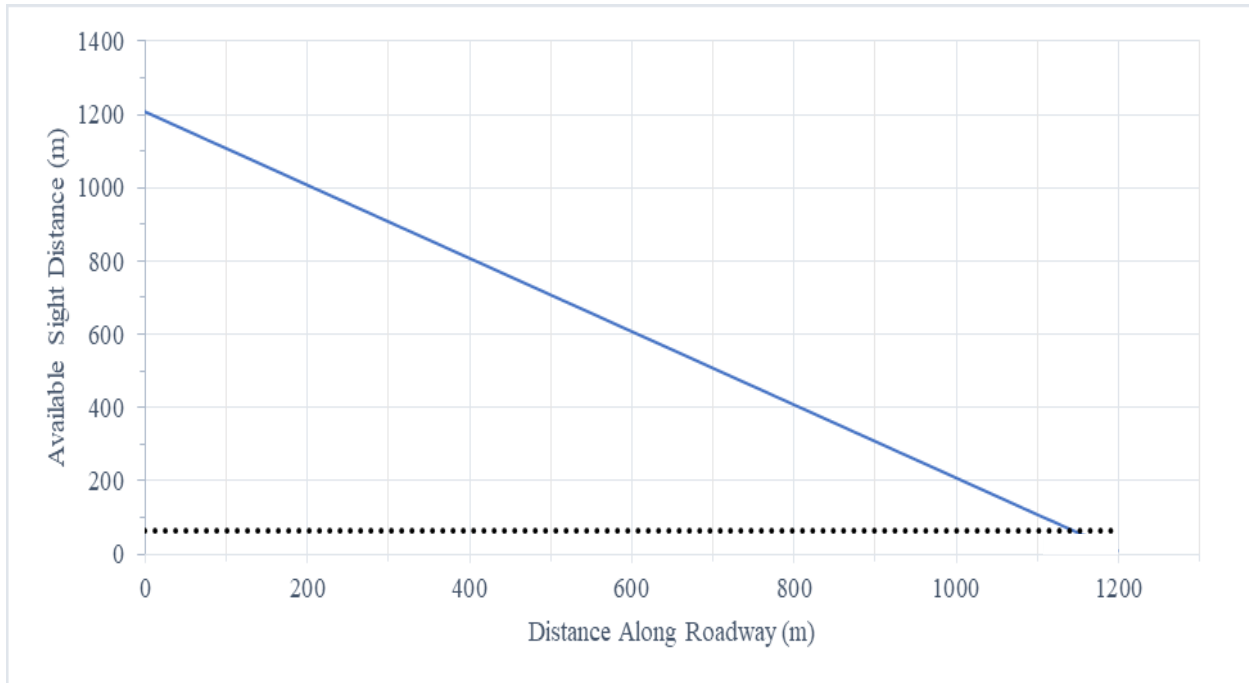
Figure 62: Available Sight Distance Along Highway 36 Segment B (Dashed Line Represent Theoretical SSD)

On Segment A, the figure shows that the available sight distance fluctuates as the observer is moved to different points along the segment. The sight distance on that segment ranges from a maximum of 1455m, available 1100m upstream the segment, to a minimum of 194 m, available 298m upstream the segment. In contrast to Segment A, on Segment B the minimum sight distance required is available throughout the segment. The reason the general trend is decreasing on both figures is because the further upstream the observer is moved, the closer to the end of the segment (i.e., the end of the point cloud file) that observer gets. In fact, these decreasing trends are actually a verification of the accuracy of the proposed procedure. Furthermore, the fact that the observer at the start of Segment B has an available sight distance (1200m) that is equal to the length of the segment is also a validation of the accuracy of the assessment procedure.

As already noted, the horizontal line drawn across the curve on Figure 61 and Figure 62 represents the minimum stopping sight distance required in AASHTO's design guide. Design guides including AASHTO and Alberta's Highway Design Guide obligate that these requirements are met throughout the length of a highway segment.

The minimum SSD on was calculated as 235m and 140m for Segment A and Segment B, respectively, based on the different speed limits along the two segments. When comparing the available sight distance to the minimum stopping sight distance required it is seen that the

134

minimum requirement was satisfied at all locations along Segment A except the region between 255m and 395m upstream. For Segment B, the minimum stopping sight distance requirements were met along the entire segment. The only location where the sight distance is limited is towards the end of the segment which, as already noted, is a matter of the remaining portion of the LiDAR segment not being long enough to perform the assessment. This has been integrated in the minimum sight distance assessment algorithm so that, in cases where the segment is not long enough to assess sight distance, the code would note that the sight distance was "not assessed" rather than "not met".

7.4.1 OBSTRUCTION ASSESSMENT

Figure 63 depicts the top view of a sight line where the target was not visible from the observer's location. The blue point represents the observer and the red point represents the target. As clear from the figure, the reason the target point is not visible from the observer location is because of the change in the vertical alignment between the pair of points. The sight line travels toward the target but, at one point, the line is not visible since it is overlaid by the road surface due to the change in the elevation of the surface (i.e., change in the vertical alignment). The side view, seen in Figure 64, also confirms that the sight line is obstructed by the change in vertical alignment.
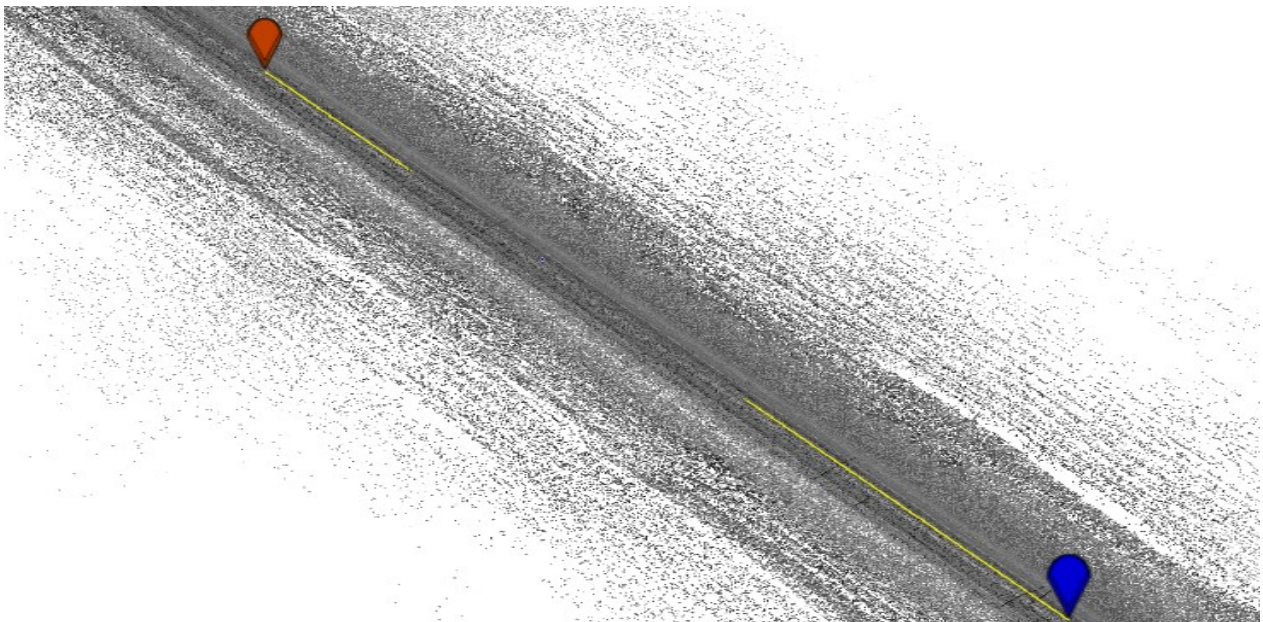
Figure 63: Observer and Target Points at Location of Limited Sight Distance (Plan View)
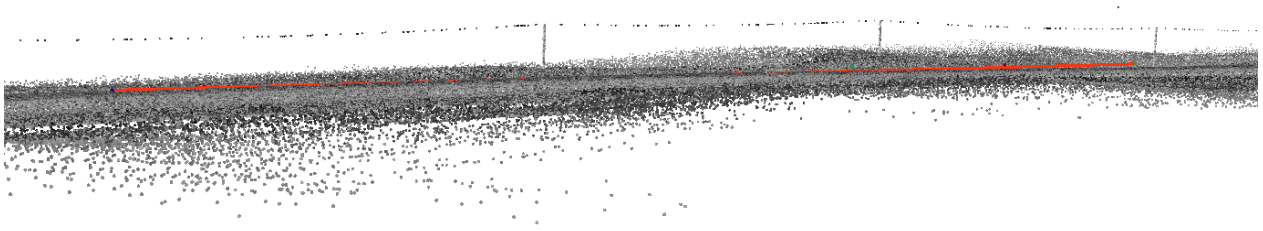
Figure 64: Sight Line Clearly Obstructed by Vertical Alignment of the Road (Profile View)

Figure 65: Limited Sight Distance Beyond Dashed Line (Google Street View©)

In order to verify that the sight distance was limited at points were the code detected obstructions, the corresponding sight lines at locations of obstruction were manually assessed. This assessment confirmed that the points were all obstructed due to changes in the vertical grade on the road. A street view image of the location where sight distance obstruction was detected is also shown in Figure 65. The figure clearly shows the limitations to sight distance caused by the crest curve that exists at the dashed red line. Figure 66 also shows a LiDAR view of the limitations at the beginning and the end of the region where ASD drops below SSD requirements, which extends for approximately 125m.
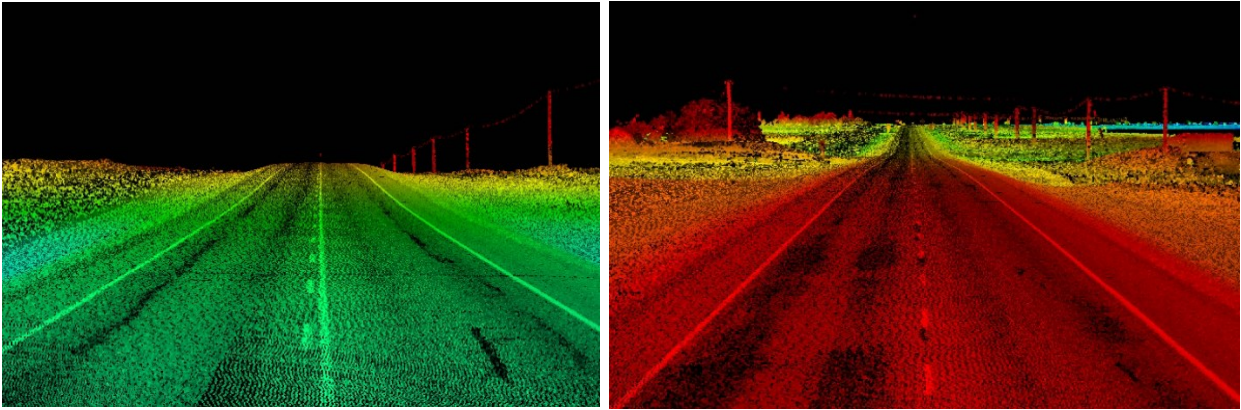
| (a) *Beginning of Limited Region* | (b) *End of Limited Region* |

Figure 66: Sight Distance Limitations (LiDAR View)

It is worth noting that in 3R/4R projects (i.e., projects which involve resurfacing, rehabilitation and restoration of existing roads), Alberta Highway Design Guide allows for the minimum allowable sight distance on a segment to drop to that of a segment where the speed is 20km/h lower than the current operating speed[151]. In other words, if the design speed is 110 km/h only, sight distance requirements for an 89km/h segment (165.75 m) need to be satisfied on this segment if it were analyzed as a 3R/4R project. Therefore, if this criterion were to be used in assessing Segment A, stopping sight distance requirements would be satisfied for the entire segment.

In order to demonstrate the value of the proposed algorithm in performing a network-level assessment of sight distance, the algorithm was tested on 50km of Highway 36. Multiple LAS files were processed and the available sight distance for the 50 kilometers was stored and plotted as illustrated in Figure 67. As evident in the figure not many limitations to sight distance exist on the segment, which is reasonable considering that Highway 36 lies in the eastern region of the province of Alberta where terrain is generally flat with very low vegetation.
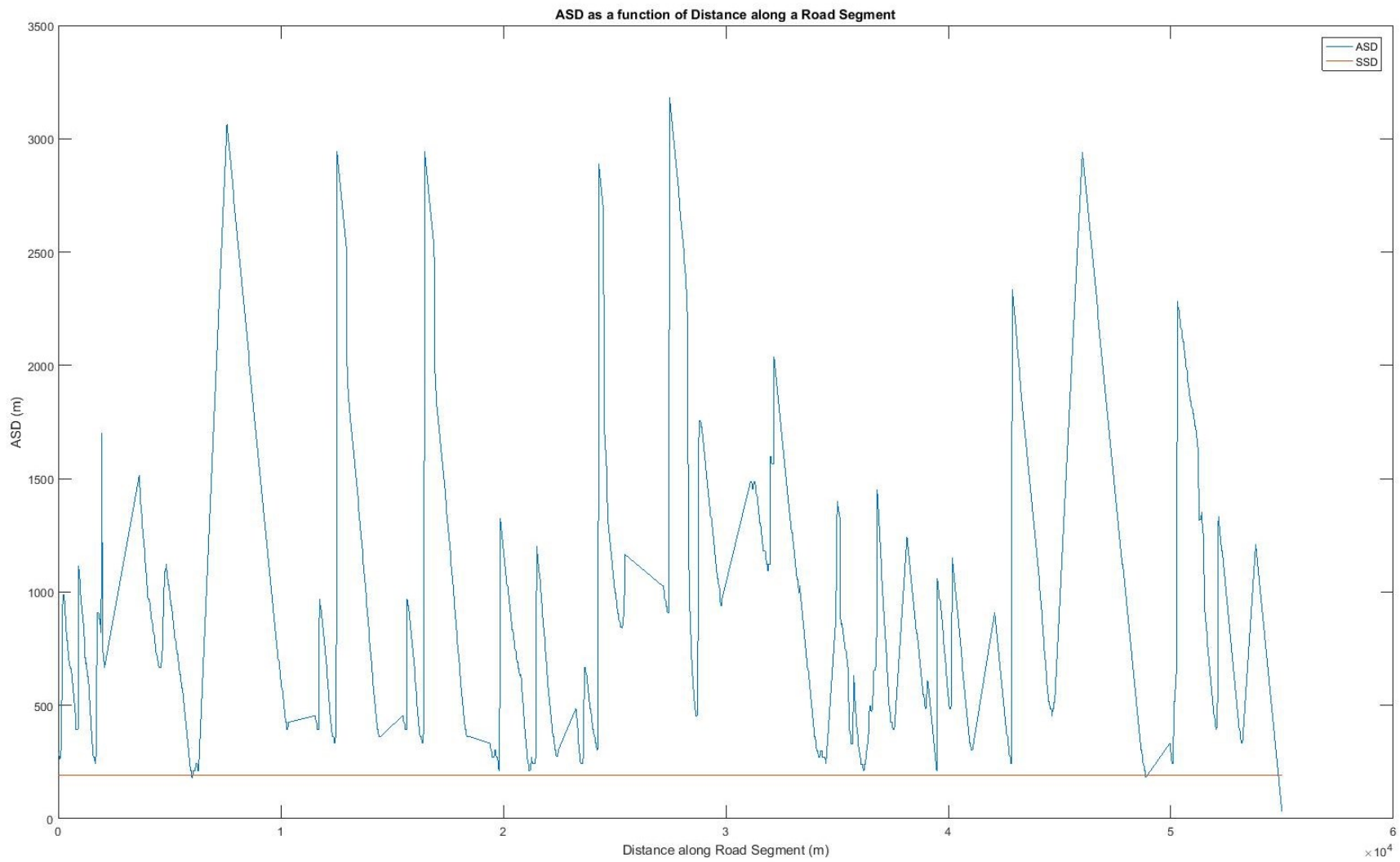
Figure 67: Available Sight Distance on 50km of Highway 36

7.4.2   PROCESSING TIME, CHALLENGES, AND LIMITATIONS

While the extraction algorithm was highly successful, a few challenges were encountered when conducting the assessment. The main challenge was the processing time when dealing with a high number of observer and target points. Highway design guides require that stopping sight distance is met at every position along a highway [151]. Although high point cloud density means that such an assessment is possible, increasing the number of observer and target points affects processing times. The reason here is that sight lines need to be created between each pair of lines and all combinations between those pairs must be considered. Hence, if 100 pairs are used, 9,800 sight lines need to be generated and assessed. That being said, processing times are still reasonable even with that amount of points. For a 4km segment, the algorithm is able to process the data and compute the available sight distance in 263.5" which is extremely efficient compared to the time required to perform manual assessment along a segment of that length.

7.5   CONCLUSIONS AND RECOMMENDATIONS

This Chapter proposes an algorithm that can be used to automatically assess sight distance along highway segments scanned using LiDAR technology. The LiDAR point cloud is first segmented to remove overhanging objects, observer and target points are then generated along the test highway, and sight lines between each pair of points are constructed. A raster model of the highway is then generated, and a line of sight assessment is then conducted to identify potential obstructions for a set observer along the highway segment. Information on potential obstructions was then used to compute the sight distance available to each observer. The developed algorithm was tested on two road segments on over 50km of Highway 36 in the province of Alberta, Canada. For a 4km portion of the test segments a 150m long region failed to satisfy minimum stopping sight distance requirements defined in design codes. Sight distance limitations were validated by comparing the obstructed sightlines against the vertical profile of the highway and using images from the field at obstruction locations.

The algorithm developed in this Chapter is highly effective in automated assessment of sight distance on highway segments. The only challenge associated with the assessment is specifying the number of observer points at which testing is required. Although a higher number of points is typically recommended, a slight trade-off between the number of points and the processing time exists.

8 SENSITIVITY ASSESSMENT OF THE IMPACTS OF POINT DENSITY ON THE EXTRACTIONS

8.1 BACKGROUND

Datasets collected using LiDAR technology often consist of dense point clouds. However, the density of the point cloud could vary depending on several different factors including the capabilities of the data collection equipment, the conditions in which data is collected, and other features such as range and angle of incidence. Although variation in point density is expected to influence the quality of the information extracted from LiDAR, the extent to which changes in density could impact the extraction is unknown. Understanding such impacts is essential for researchers looking to develop algorithms to extract information from LiDAR and for agencies looking to adopt LiDAR technology for infrastructure assessment. This Chapter focuses specifically on understanding the impacts of point density on extracting the features discussed in Chapters 4 through 7 of the thesis. The densities of the LiDAR point clouds were first reduced using stratified random sampling, and the different features were extracted at different levels of point density. The impacts of the point reduction on the detection and assessment of different features was then analyzed on a selection of different highway segment.

LiDAR data can be collected aerially, using helicopters or drones, or terrestrially. Terrestrial LiDAR data collection can either be static (scanning equipment is mounted on a tripod) or mobile (equipment is mounded onto vehicles in motion) [22]. Different laser scanning methods have different advantages and disadvantages. For instance, while a more detailed representation of the roadside features could be achieved using mobile laser scanning (MLS), aerial laser scanning (ALS) has a wider field of view (i.e., the extents of the spatial area covered in an aerial scan is wider) [22]. This wider range, however, comes at the expense of point density.

In fact, density is also a function of several other factors including the distance between the scanner and the scanned object (i.e., the range), the angle of incidence, the environment and weather conditions in which data is collected, and the speed of the data collection vehicle [104,157]. Another factor that impacts point cloud density is scanning system capabilities. Scanners vary in their scan rates, range, and the scanning mechanism [104]. Consequently, the quality of data obtained from different scanning systems, and the accuracy of measurements made using those

140

systems varies significantly [104]. Due to those factors and others, LiDAR point clouds could be prone to incompleteness of some features, noise, and density anisotropy [158].

Although information on the scan rates and the relative accuracy and density of point clouds achievable using different scanners is well documented by vendors, it does not help researchers and transportation agencies understand how extracting different features is affected by variations in the properties of the point cloud. In other words, the maximum scan rate or point density that can be acquired using a particular scanner does not help understand how this scanner would perform when extracting different elements of transportation infrastructure.

When using point cloud data for transportation applications, the point density required varies depending on the application. For instance, a higher point density might be required estimating cross slopes of a road compared to what might be required to measure lane widths. Although it is known that some application might require higher point density than others, these observations remain entirely speculative. Hence, the impacts of reducing point cloud density on the ability and the accuracy of extracting different transportation features are unknown.

This Chapter focuses on studying the impacts of LiDAR point cloud density on the extraction of road geometric elements for which procedures have been developed in this thesis, namely, cross and side slope estimation, horizontal curve extractions, overhead object detection and clearance assessments, and sight distance assessments.

8.2 PREVIOUS WORK

Previous work on the impacts of point density on transportation feature extraction from LiDAR has been limited. A large portion of previous work has focused on comparing the density of point clouds collected using different scanning systems, with less focus on the impacts of the reduced density on utilizing LiDAR for different applications.

Douillard, et al. [159] was one of the few papers that distinguished between the use of LiDAR point clouds of different density for an application in the field of transportation. The authors propose several ground segmentation techniques required when pre-processing LiDAR and split the segmentation methods into methods effective for dense point clouds, and others that are best used for sparse point clouds. Although the authors do not explicitly compare the impacts of

applying the same segmentation techniques to point clouds of different density, the distinction they make shows that it is sometimes necessary to process point clouds of various density differently.

Research on the effects of point density on extracting different forest canopy features from LiDAR points clouds has attracted more attention compared to transportation. Early work in this area speculated that higher pulse densities would improve the extraction of multiple features [160-162], however, contrary to expectations, further research proved that higher point density did not improve extraction for all features [163].

Thomas, et al. [164] found that low-density models were able to detect multiple canopy metrics at a higher level of correlation than high-density models. Other studies also found that certain features such as tree height and volume, were insensitive to point density [165-168]. The only cases where error in those measurements was found to grow exponentially was when densities were significantly reduced to very low levels (less than 0.004 p/m^2) [169]. Singh, et al. [170] found that even when the point density was reduced to 1% of the original dataset, decreases in the amount of variation explained in forest biomass was 14% and 11% for first and multiple return data, respectively. This led the authors to conclude that single-return LiDAR at reduced point density provided sufficient data for mapping urban forest biomass.

Impacts of point density reductions on the generation of Digital Elevation Models has also been explored. Liu, et al. [171] generated DEMs at 5m resolution using datasets where point density was reduced to 75%, 50%, 25%, 10%, 5%, and 1% of the original point cloud. They found that reductions in density of up to 50% did not impact the DEM accuracy.

Zhao, et al. [172] considered three different sampling techniques and drew LiDAR samples at 6 different levels of point density (20%, 10%, 5%, 1%, 0.2% and 0.1% of the original point cloud). The authors found that neither sampling technique nor point density had any significant impacts on the descriptive statistics of the elevations of the sampled data. Nonetheless, very sparse datasets (<2%) were found to impact the quality of the generated DEMs, variograms, and viewsheds. Anderson, et al. [173], produced a series of DEMs at different resolutions along a LiDAR point density gradient. The authors concluded that LiDAR datasets maintain adequate accuracy for elevation predictions even at substantial density reductions.

In a different application, Tomljenovic and Rousell [174] studied the impacts on automated extraction of building features from Aerial Laser Scans. The authors considered point density from 18 points-per-square-meter (ppsm) to 5 ppsm. The study found that reductions in density reduced the classification accuracy measured in both completeness and correctness of the extraction process. The authors also note that, although accuracy of the extraction also drops when reducing point density, significant drops in accuracy are only observed at densities below 5 ppsm.

Unlike in forestry, relationships between LiDAR point cloud density and the extraction of features of transportation infrastructure has not been explored in previous research. This leaves agencies interested in using LiDAR for transportation applications with limited information regarding point density requirements for different applications. Moreover, researchers developing algorithms to extract information from LiDAR remain uncertain about the impacts of reducing point cloud density on the accuracy and efficiency of their extraction algorithms.

8.3   POINT CLOUD SAMPLING

This chapter aims to understand the impacts of reducing point cloud density on the extraction of the geometric elements presented in Chapters 4 to 7 of this thesis. The first stage of the assessment procedure involved thinning the point cloud to lower point densities. This involved drawing random samples of the original point cloud to create a less dense dataset. The sampling technique used to achieve this was Stratified Random Sampling (SRS), which has been previously used in studies that attempted point cloud thinning for forestry applications [175,176].

8.3.1   STRATIFIED RANDOM SAMPLING

SRS is a two-step process where a dataset is first broken into 'Strats', where each Strata represents a subset of the original dataset. The second step involves drawing random samples from each Strata. These samples are then combined to embody a new less dense sample, which is representative of the original dataset. Although many statistical random sampling techniques exist in the literature, stratified random sampling was best suited to this problem since it ensures that sampling occurs evenly across the width and the length of the highway. To create the strata's of data, the point cloud was split into tiles of a 50 m^2 size. Tiling was achieved through 3D voxelization of the point cloud, already discussed in Section 6.2.1.2 of this thesis.

Once data tiles are created as illustrated in Figure 68, a random sample is drawn from each tile. The amount of points drawn for each sample was defined as a percentage of the original point density in each stratum. To capture the impacts of reducing point density across a wide range, samples were drawn at five different density levels (75%, 50%, 25%, 10%, and 5% of the original point cloud). Similar levels have been defined in previous research where the impacts of point cloud density on extracting forestry features was studied [176-179]. It is worth noting here that point cloud density (measured in points per square meter) varies across a highway segment since it depends primarily on the range (i.e., distance from the laser scanner to the scanned object) and the incidence angle. Despite this variation, the point cloud density on the pavement surface below the scanner was estimated for each of the test highways used in this Chapter to understand what the original point cloud density corresponds to in ppm^2. It was found that on the highways considered in this thesis, the point density on the road pavement surface was on average approximately 300 ppm^2.
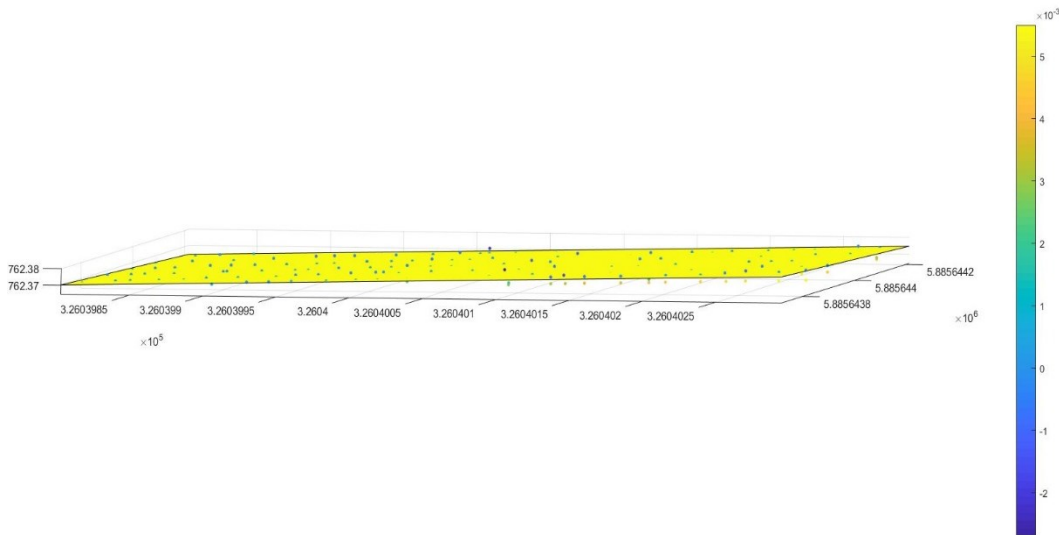
Figure 68: Data Strata Defined

The code for SRS was written in MATLAB and used to generate multiple LAS files of different point density for each of the test highway. Figure 69 (a) through (f) shows a test segment on Highway 36 at different point cloud densities.

As evident in the figures, the level of detail provided by the point cloud data drops significantly as the point density is reduced from 100% to 5%. For instance, pavement markings including the

'Stop Ahead' message and the warning sign on the side of the road are clearly visible at high point density but fade away at 5%.

(a)   100%

(b)   75%

(c)   50%

(d)   25%

(e)   10%

(f)   5%
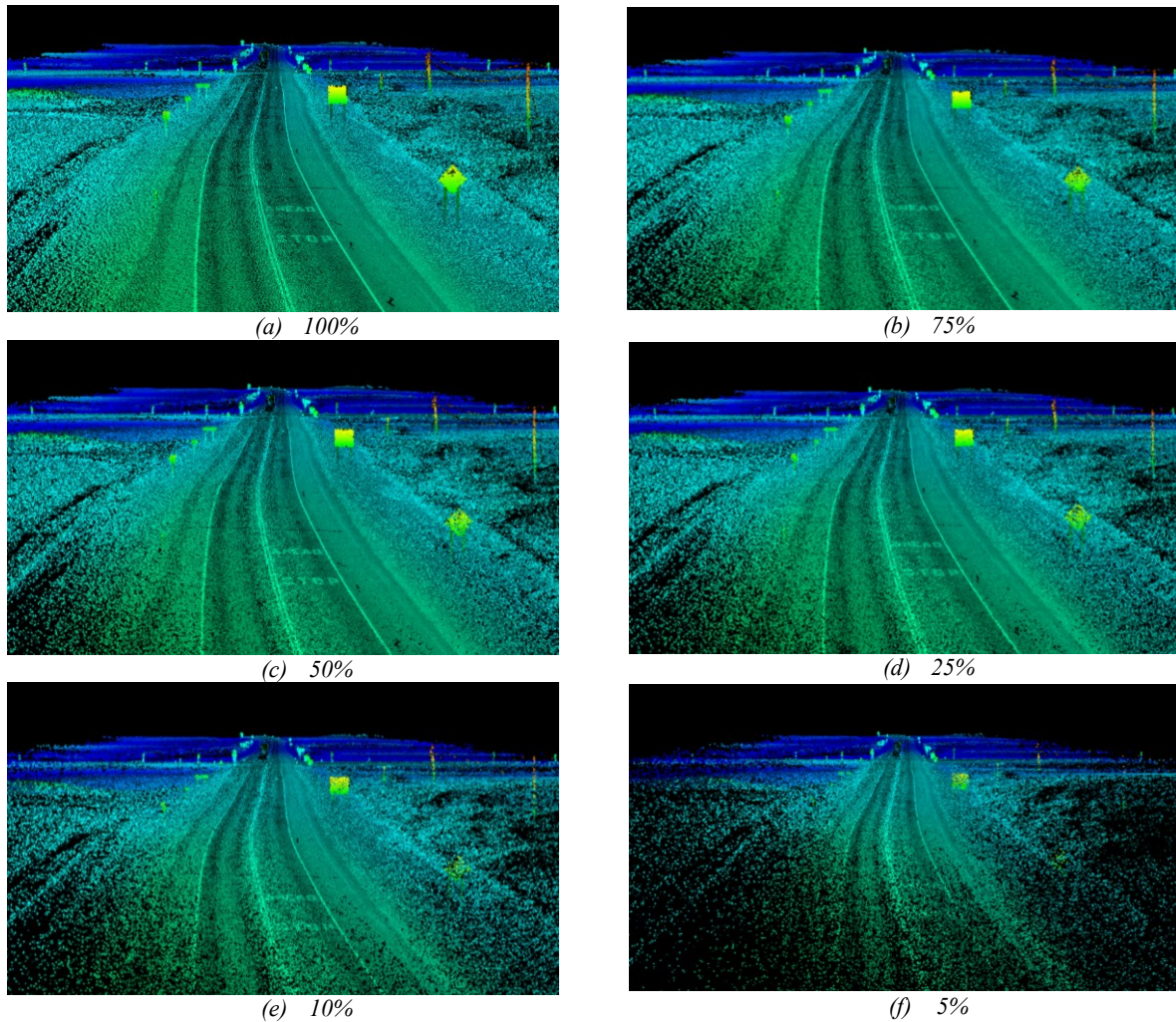
Figure 69: Highway Point Cloud Density Reduction

8.4   CROSS SECTION EXTRACTION AND SLOPE ASSESSMENT

In this section, the cross-section extraction algorithm developed in Chapter 4 of this thesis was tested on LiDAR highways while reducing the point density. The slope estimates obtained at different levels of point cloud density were compared to those obtained at 100% with the aims of identifying any variation. The assessment was conducted on six different cross sections extracted at randomly selected stations along two different test highway segments. The cross sections were extracted at the six different levels of point density (5% to 100%) and the slopes estimates were compared across the different levels.
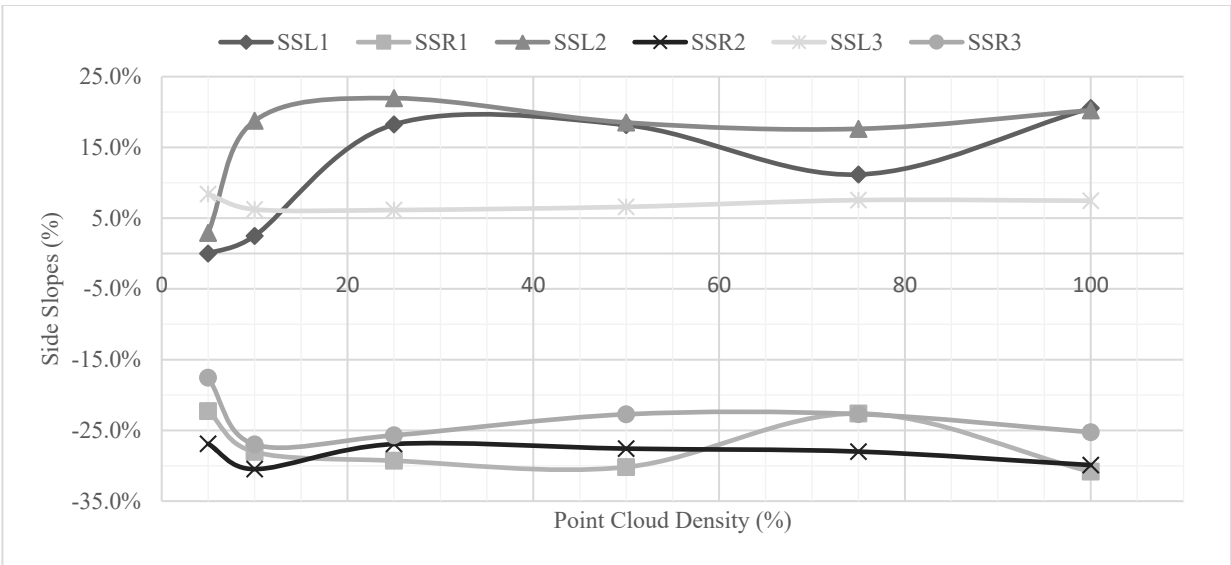
(a)   Highway 36 (Side Slopes)
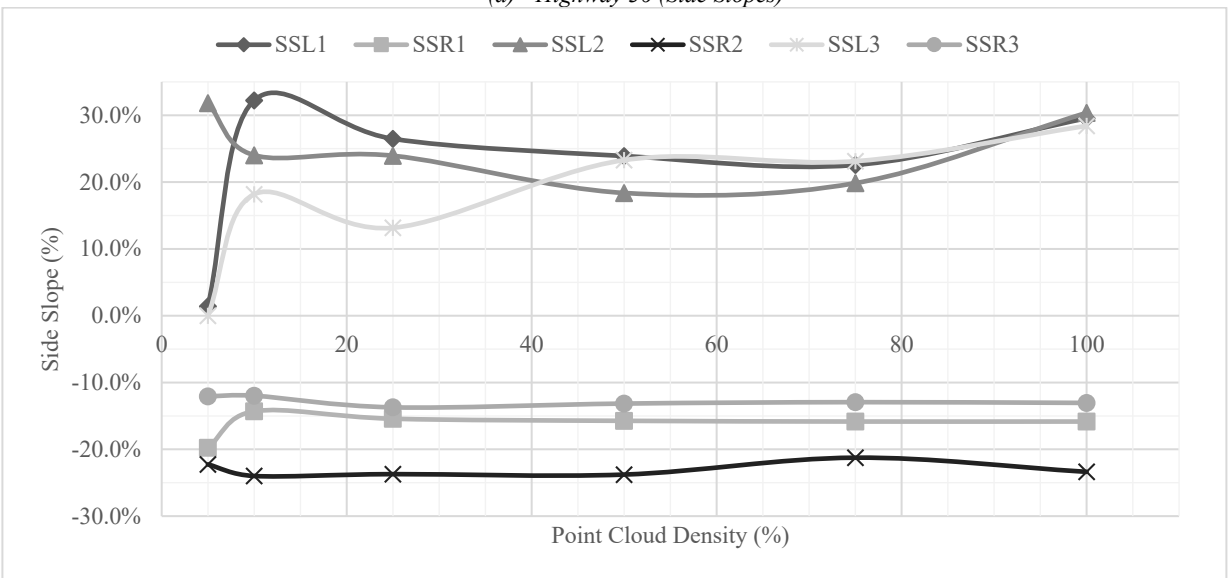
(b)   Highway 53 (Side Slopes)
Figure 70: Impacts of Point Density Reduction on Side Slope Estimates
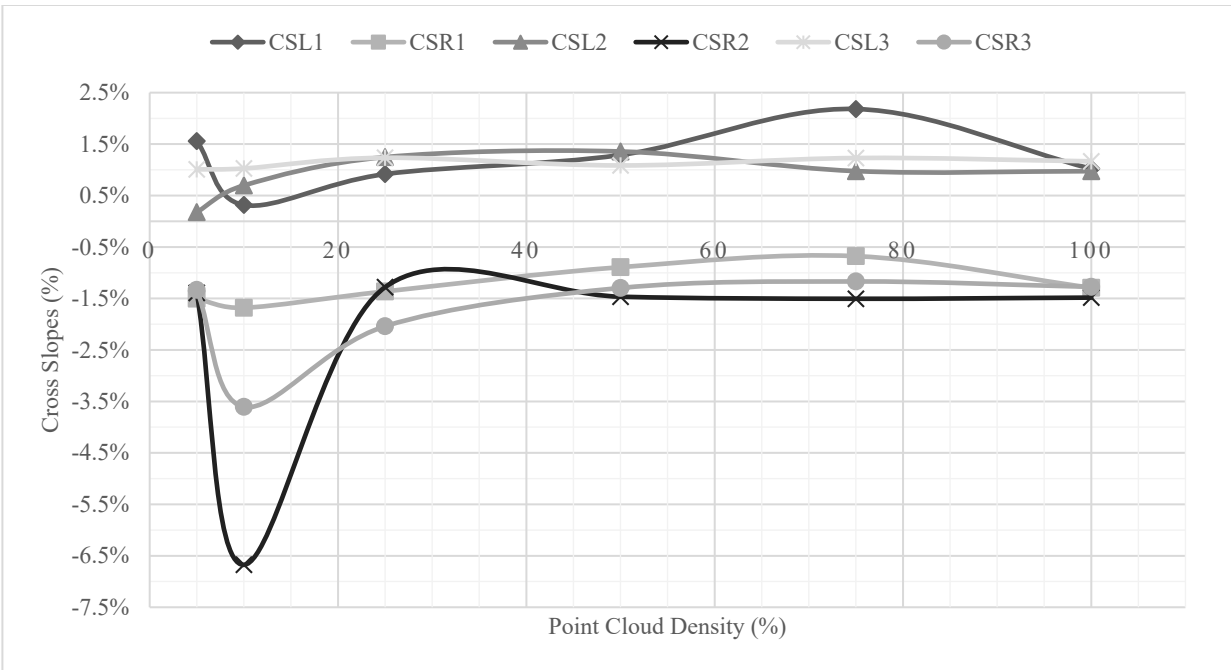
(a) Highway 36 (Cross Slopes)
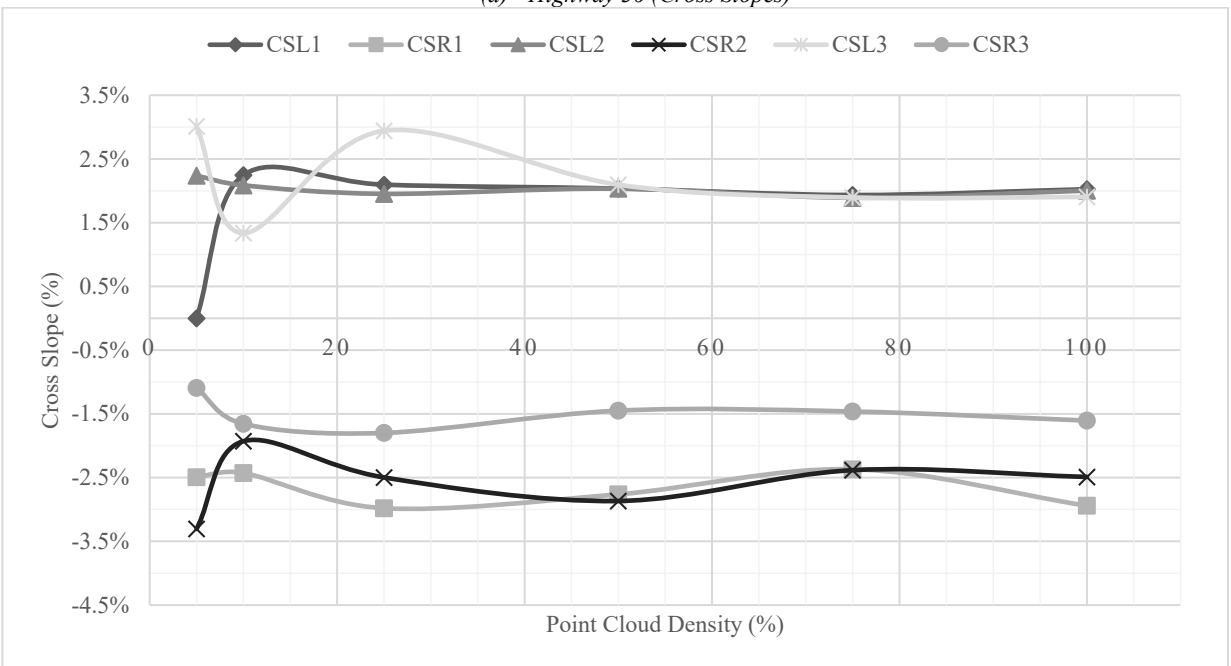
(b) Highway 53 (Cross Slopes)
Figure 71: Impacts of Point Density Reduction on Cross Slope Estimates

As evident by the results, it seems that fluctuation in the slope estimates are highest once the point density drops below 50%, this is particularly true for cross slopes as illustrated in Figure 71 a and b. Variations in the slope measurements resemble no specific trend though, which indicates that reduction in the point cloud density could result in either the overestimation or the underestimation in slope estimates.

One important observation to note for side slopes is that slope estimates obtained at the side further away from the laser scanner (i.e., on the approach opposite of the approach on which the data collection truck was travelling) had high variability in slope estimates when point density was reduced (see left side slopes, SSL, in Figure 70 a and b). The reason here is that point density is a function of the distance from the scanner and, as a result, side slopes further away from the scanner already have a lower point density than the slopes close to the scanner even at 100%-point density.

(a) Highway 36 (Cross Slope)

(b) Highway 36 (Side Slope)

(c) Highway 53 (Cross Slope)

(d) Highway 53 (Side Slope)
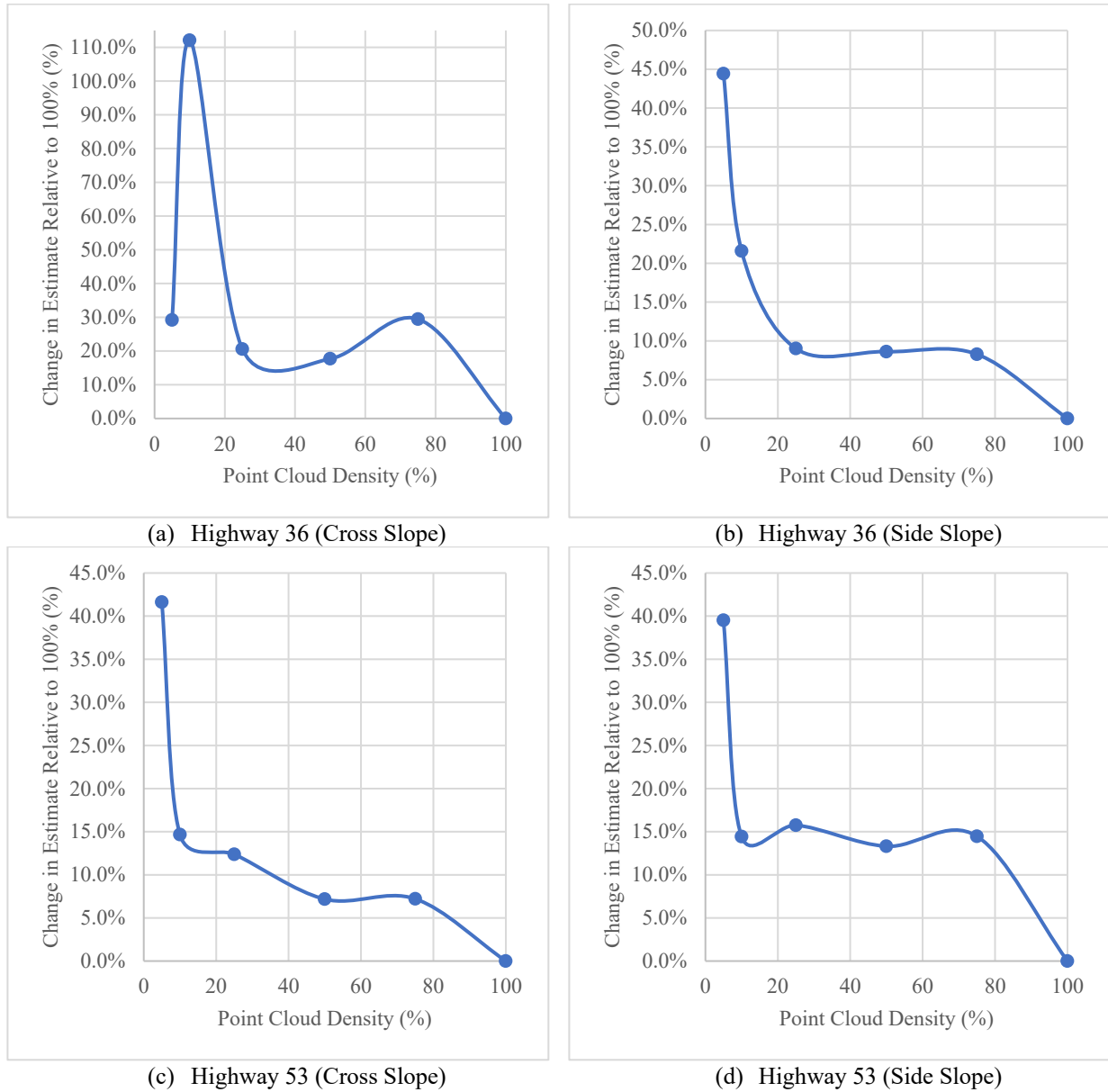
Figure 72: Changes in Slope Estimates Compared to 100 Percent Point Density

To further investigate the deviation in slope estimates compared to what was obtained at 100%-point density, the differences between the slopes obtained at 100% and those obtained at lower

point density (averaged across all cross sections) were plotted. These results are presented in Figure 72 a through d. As seen in the figures, deviation in the slope estimates peak at around 25% and are highest at 10-5% point density. However, it is worth noting that deviations as high as 15% of the original estimate exist even at point densities as high as 50% and 75%. Therefore, extracting cross sections for slope estimation at low point densities is not recommended. One exception to the observed trends was the average difference in slope estimate for cross slopes on Highway 36 at the 5% level. The error in that measurement was relatively low despite the low point density. The reason here is that the density reduction resulted in a few points that happen to fit well to a linear line and provide a relatively accurate estimate of the slope. This, however, is rearely the case at 5% point density, which is evident in the estimates for the other slopes and on the other highways.

8.5 HORIZONTAL CURVE DETECTION AND ATTRIBUTE ESTIMATION

To understand the impacts of point density on the performance of the horizontal curve detection algorithm, the algorithm was tested on three different highway segments at the eight levels of point density. The test segments were located on Highways 1, 2, and 9 and are seen in Figure 73 a, b, and c, respectively.
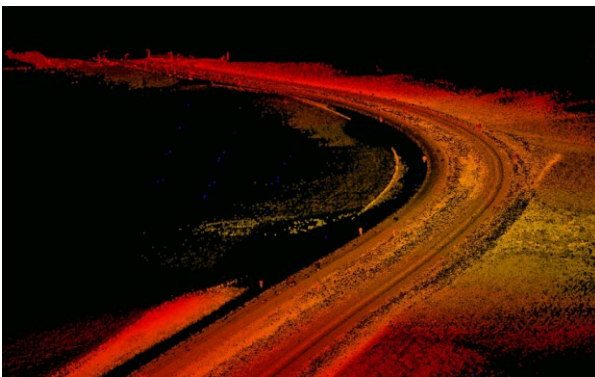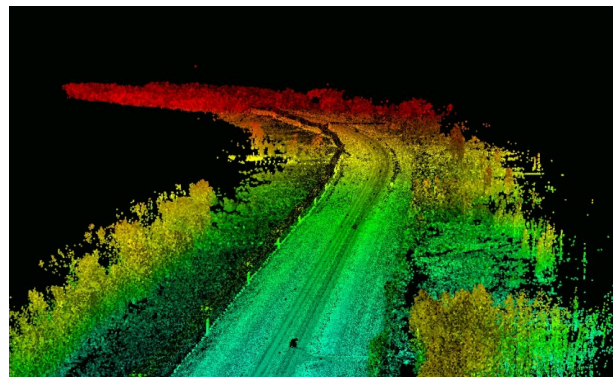
(a) Highway 1	*(b) Highway 2*
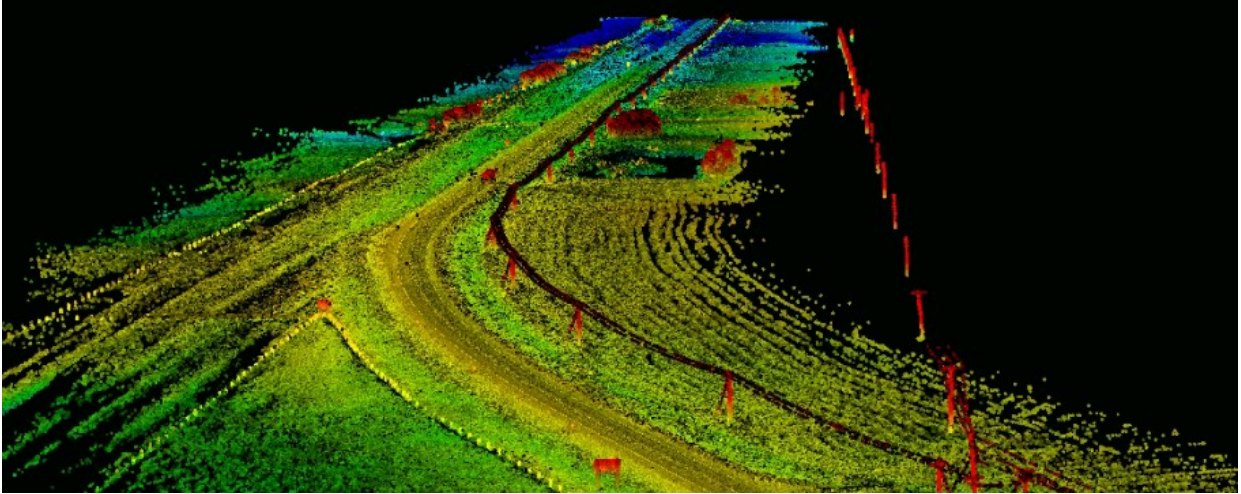
(c) Highway 9
Figure 73: Test Segment

The reason eight levels of point density were used for curves instead of the six levels defined for the other applications, was because the impacts were not apparent when only six levels were used. To quantify the impacts of point density reduction, the percent change between the attribute estimated at 100%-point density and that at the reduced level of point density was computed as follows.

$$\%Change = \frac{\left|Estimate\,at\,100\% - Estimate\,at\,p\%\right|}{Estimate\,at\,100\%} \times 100 \tag{25}$$

This was done at each level of point density (*p*) and the estimates were averaged across all three Highway segments. Figure 74 shows the percent change in the curve attributes estimated at point density of 90%, 80%, 75%, 50%, 25%, 10%, and 5% compared to the original (100%) point cloud. The figures show the impacts of varying point cloud density on the estimated Radius (Figure 74a), deflection angle (Figure 74b), and, Tangent (Figure 74c).

150
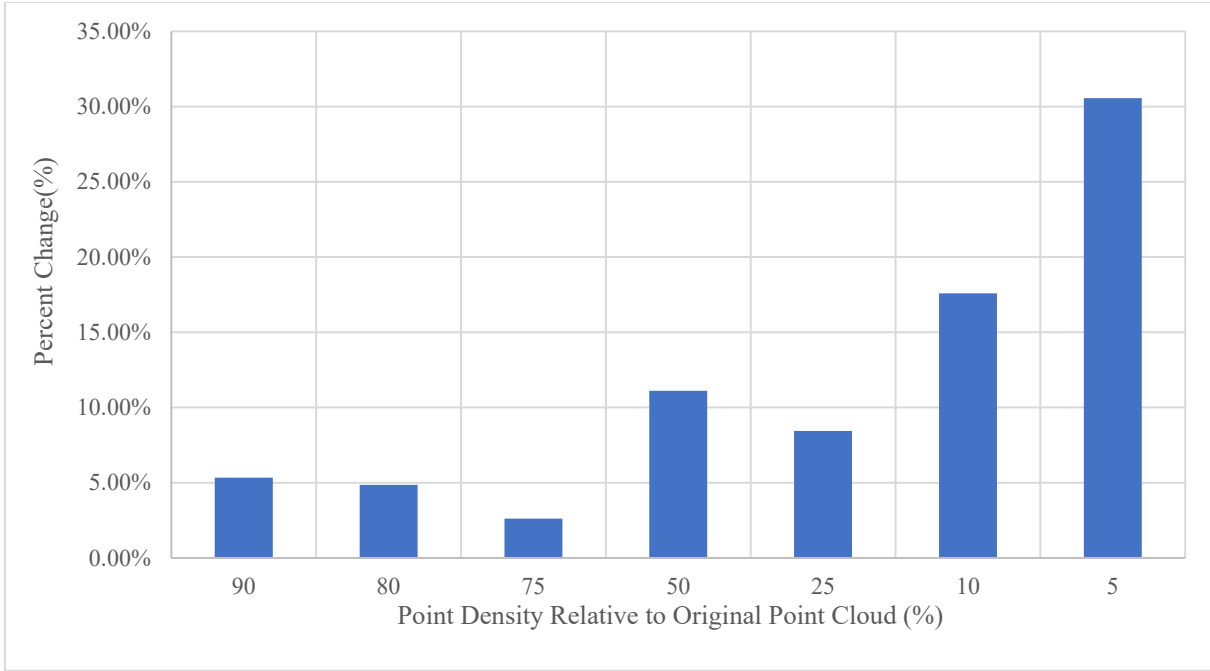
(a)   Radius
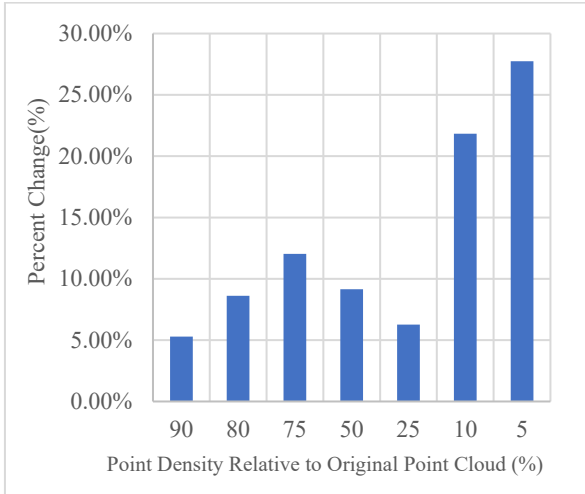
(b)   Deflection Angle
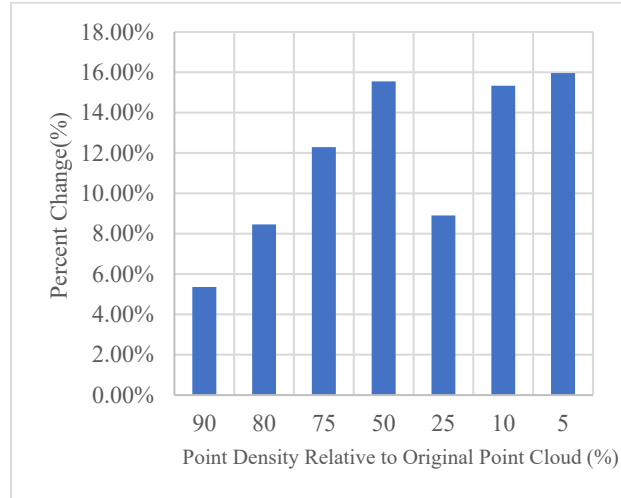
(c)   Tangent

Figure 74: Percent Change in Estimated Attribute Relative to that obtained at 100 percent density (Average Across All Test Segments)

Before discussing the impacts of reducing point density on the attribute estimation, it is worth noting that, as expected, reducing the point density did not have significant impacts on the detection of curves since the detection process is a vector-based detection that does not require an extremely high point density. Recall that, the most appropriate vector length for the detection of horizontal curves was found to be 20m. As a result, even reducing the point density by 95% still leaves us with a sufficient number of points to detect the curves. To understand this, it is worth considering the point density along the trajectory at both 100%- and 5%-point density. At 100%-

point density the number of points along the trajectory of a 4km road is anywhere between 20,000 and 30,000 points. Assuming it is 20,000 points, this means that there are approximately 5 points per meter of length along the road; assuming the points are evenly spread, this translates into a point spacing of 0.2m (i.e., 20cm) at 100%. If the number of points was reduced to 5% of the original point density, this would result in 1000 points along the 4km road (i.e., 0.25points/m); the point spacing in this case is 4m.

Unlike curve detection, point density reduction did impact the estimated attributes. In fact, an interesting finding in case of curves is that reducing point density seems to have impacts on the results even at point densities as high as 90% of the original point cloud. On average the percent change observed at that level across all four attributes was 5.27%. In other words, reducing point density by as low as 10% could result in 5% change in the estimated attributes. It is important to note here that, for a curve radius of 400m, a 5% change translates to a 20m difference in the estimated radius, which may not be considered significant.

Percent change does not seem to grow much as point density is further reduced. As seen in Figure 74a, the results show that for curve radius, the percent change seems to be within 10% for point densities of as low as 25% of the original point cloud. It is only at point densities of 10% and 5% where changes of over 20% are observed.

The point densities of 10 and 5% are also associated with the highest percent change for deflection angle too. As evident in Figure 74b, the results show that percent changes in excess of 20% are observed at 5- and 10%-point density, while for other levels of point density the changes are within 10%.

In case of curve tangent, the changes are less consistent compared to curve radii and deflection angle. Although, the highest change was still observed at 10%- and 5%-point density, high changes (> 8%) were also observed for point densities of as high as 80% of the original point cloud.

One reason the reduction in point density impacts the estimated attributes is because of its impacts on the fit of the regression lines estimated to detect the locations of both the point of intersection (PI) and the origin of the curve, which both impact the estimates of the radius and the tangent. The higher the density along the lines, the better the fit and the more accurate the estimates are. These

results further highlight the value of using dense LiDAR scans as opposed to sparse GPS points when estimating that attributes of horizontal curves

Based on the results presented in this section, it is not advised that point clouds of a density lower that 50% (i.e., less than 150 ppm^2) are used for the detecting or estimating attributes of horizontal curves. Although detection might be possible at such a low point density, estimated attributes might be erroneous.

8.6   VERTICAL CLEARANCE ASSESSMENT

In case of overhead objects, the effects of reducing point cloud density on the performance of the proposed algorithm were assessed on two different highways. The impacts of point density reduction were similar for all overhead objects on both highways.

Figure 75, Figure 76, and Figure 77 show the results of the running the algorithm across different point cloud densities for bridges and power lines. In case of bridges, the code was capable of detecting bridge structures even at point density as low as 5%. Furthermore, clearance estimates were also fairly consistent regardless of the point cloud density. These results demonstrate the robustness of the algorithm proposed when used for bridge clearance assessment. One reason the clearance estimates are fairly consistent even at very low point density is because the algorithm works on detecting overhead points then finds the nearest ground point to the detected overhead point. This increases the chances of the code finding a point on the ground that aligns perfectly with the point on the nonground object, which increases the accuracy of the clearance estimate at that point.
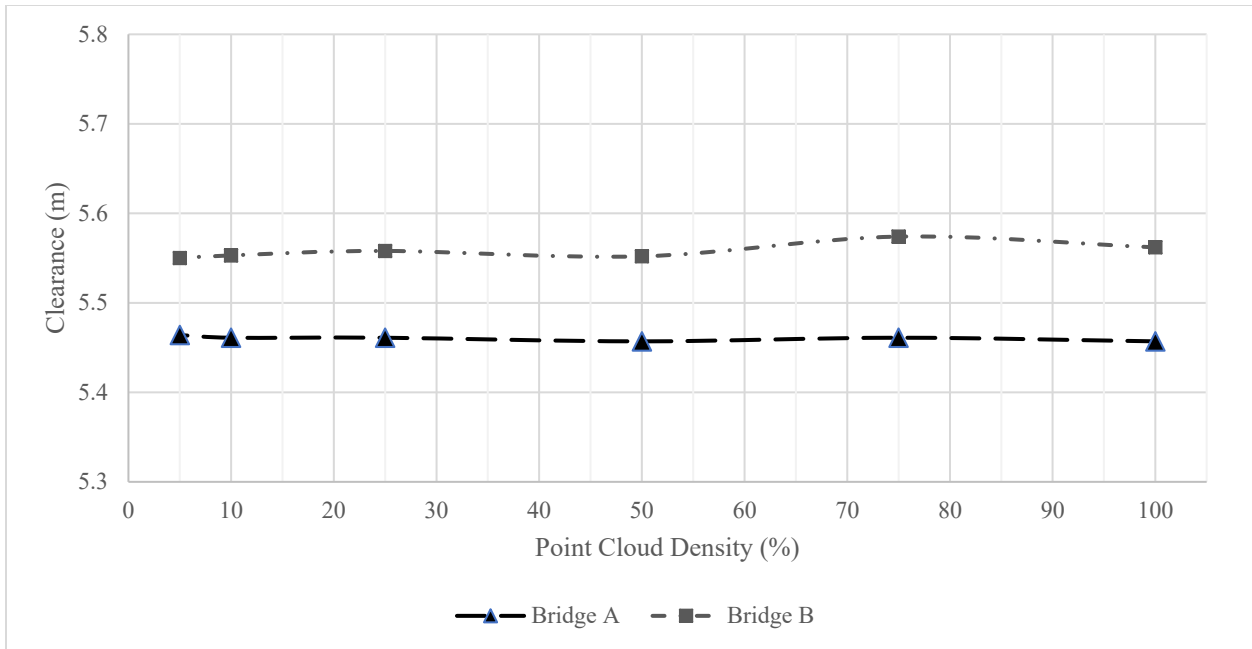
Figure 75: Bridge Clearance Estimates at Reduced Point Cloud Density (Highway 1)
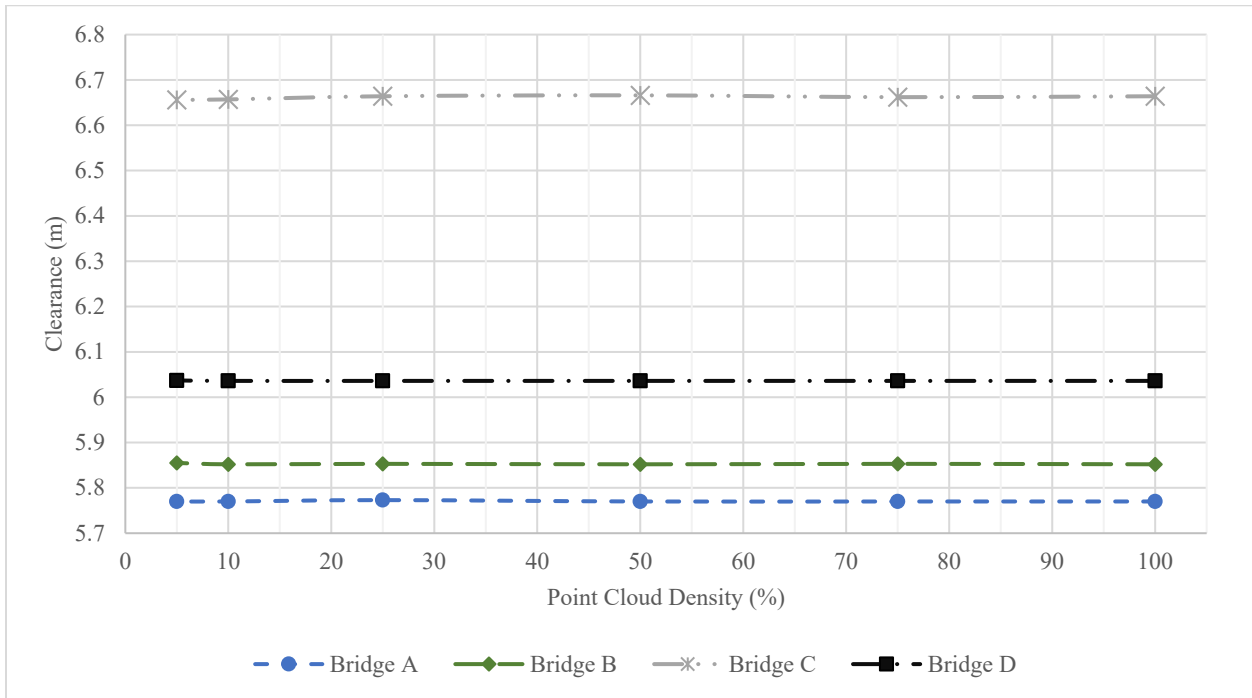
Figure 76: Bridge Clearance Estimates at Reduced Point Cloud Density (Highway 14)

In case of power lines, the results were slightly different. Due to the very low point density on power lines even in the original scans (i.e.,, 100%-point density), detecting some of those objects power lines was not possible at some of the reduced density scans. That being said, the algorithm was still effective in detecting 4 out of the 5 power lines at 10%-point density (i.e., 80% of the power lines). In contrast, none of the power lines were detectable at 5%-point-density. Clearance

154

estimates were also fairly accurate for most of the power lines detected at 10%-point density. Apart from power line B on Highway 1 where the clearance at 10% was overestimated by almost 3m, the average difference in clearance compared to 100%-point density and excluding power line B on Highway 1 was 5.5cm.
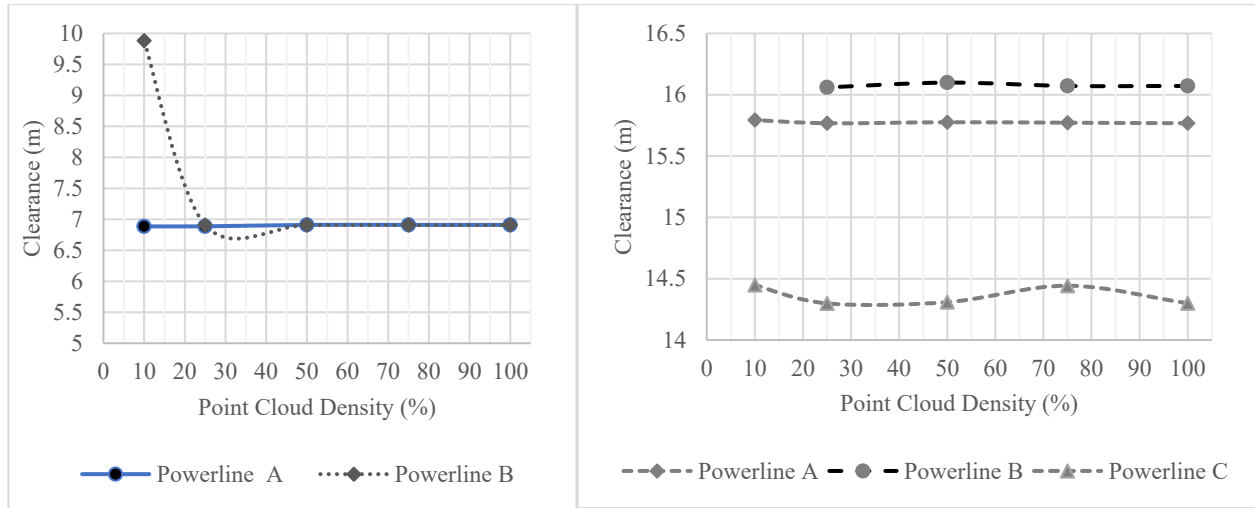
Figure 77: Power line Clearance Estimates at Reduced Point Cloud Density (Highway 1)

The reason clearance was overestimated by 3cm at Power line B on Highway 1 was because this was a 5-cable power line. After reducing the point density on the highway, only the point highlighted in Figure 78b was retained. Unfortunately, this point was not on the cable of the lowest clearance. Therefore, the clearance estimate obtained for this power line is still accurate, however, it is not a point on the cable of the lowest clearance.

(a)   100% Point Density
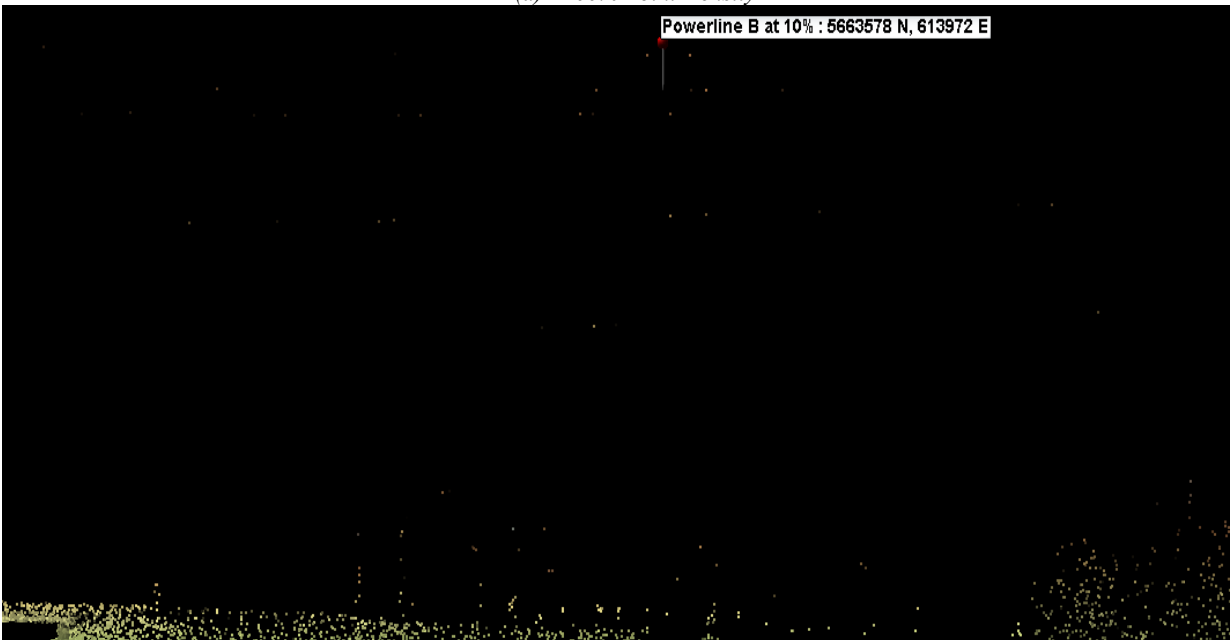
(b)   10% Point Density
Figure 78: Point Detected on the Multi-cable Power line

In general, point density reduction did not have any major impacts on the detection and clearance estimation of overhead objects. That being said, using datasets of very low point densities 10% or lower ($<$30ppm^2 on the pavement surface) for such purposes is not recommended. Very low point density could cause an inability of the code to detect some short span overhead objects. In addition,

156

very low point density reduction also causes slight variation in the clearance estimates at short span objects such as power lines.

8.7 SIGHT DISTANCE ASSESSMENT
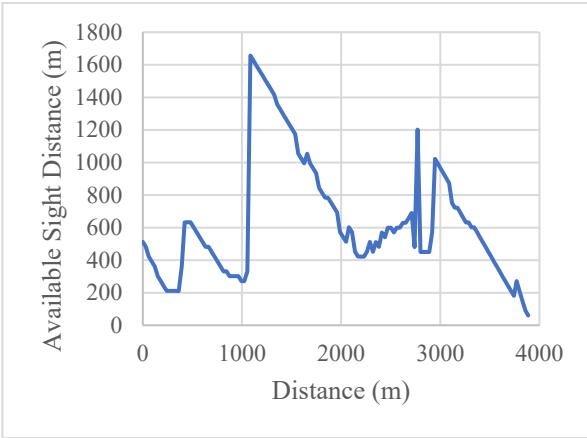
(a)   5% Point Density
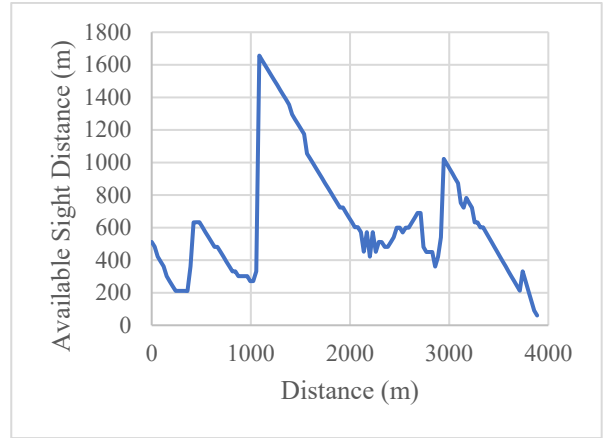
(b)   10% Point Density
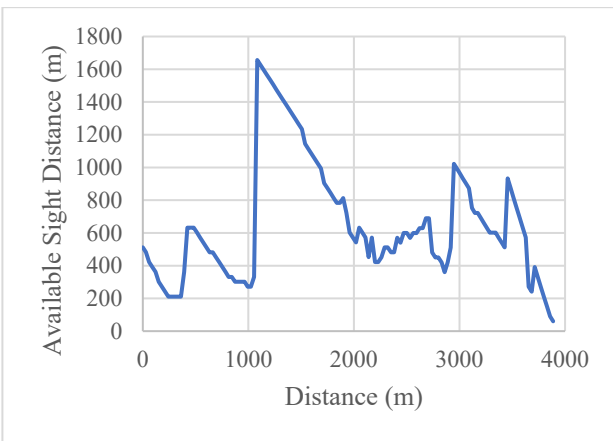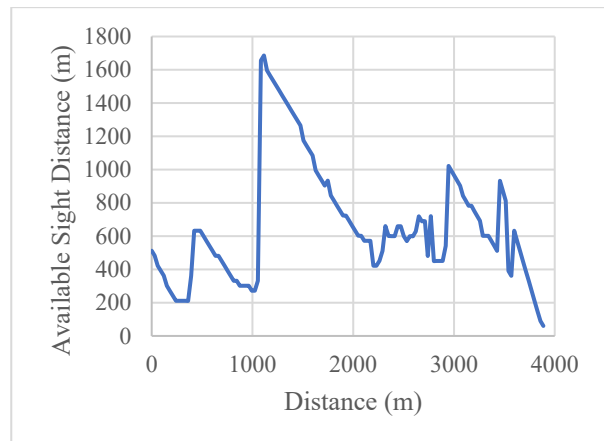
(c)   25% Point Density
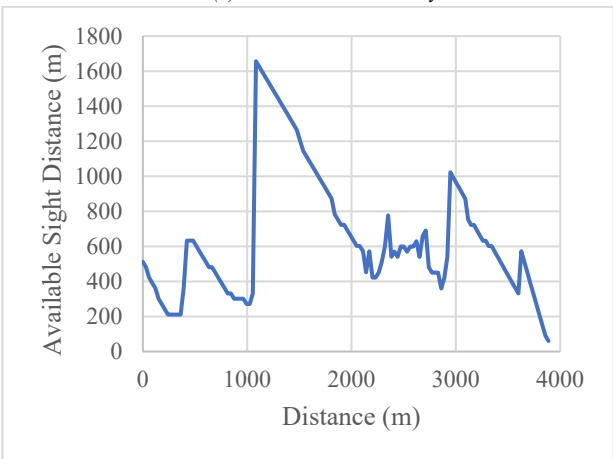
(d)   50% Point Density
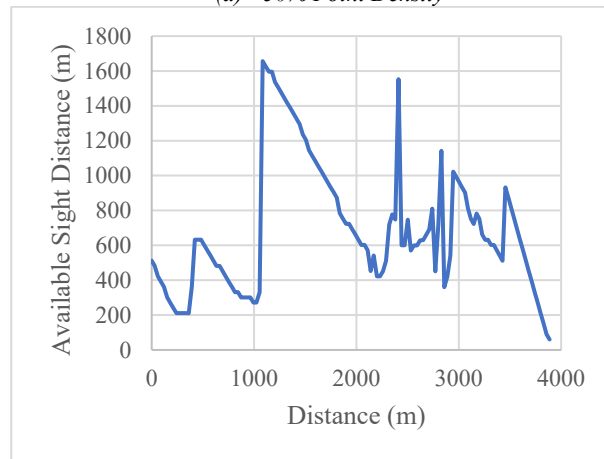
(e)   75% Point Density

(f)   100% Point Density

Figure 79: Available Sight Distance Estimated at Different Point Densities (Highway 36)

To identify impacts on reduction in point cloud density on the performance of the Sight Distance Assessment, the algorithm proposed in Chapter 7 of the thesis was used to estimate available sight distance along Highway 36 and Highway 53 at the different levels of point density. The plots in Figure 79, Figure 80, Figure 81, and Figure 82, show the available sight distance along the highway at different point cloud densities for the two highways. As seen in the plots, the general trend in available sight distance along the highway segment is almost identical regardless of the point density. This is the case for both highway segments where reduction in point cloud density was assessed.
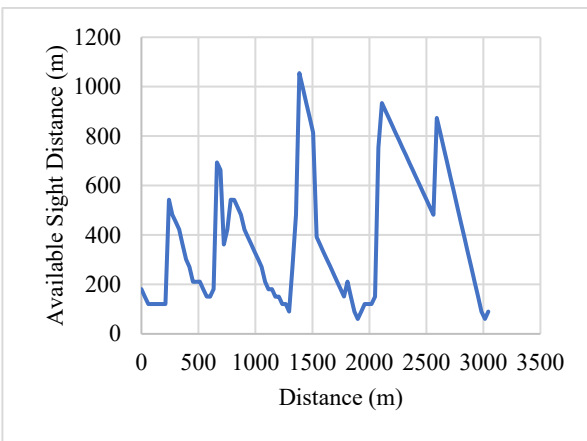
(a)   5% Point Density
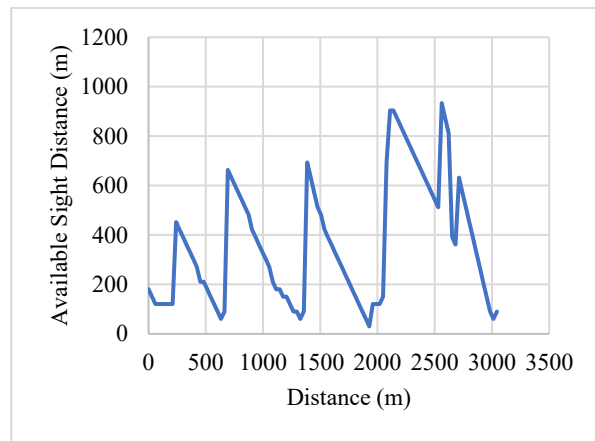
(b)   10% Point Density
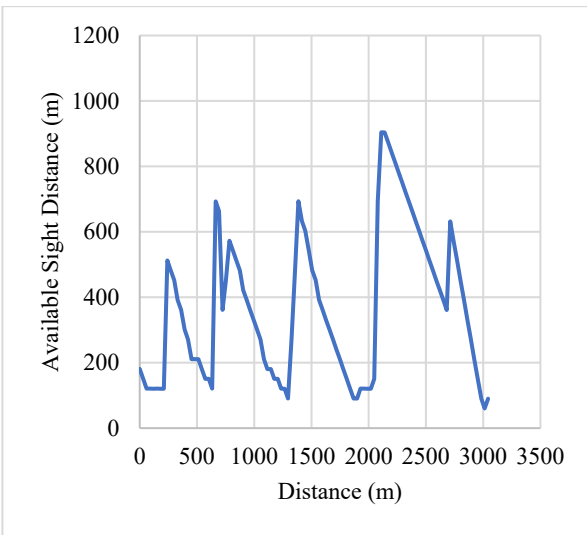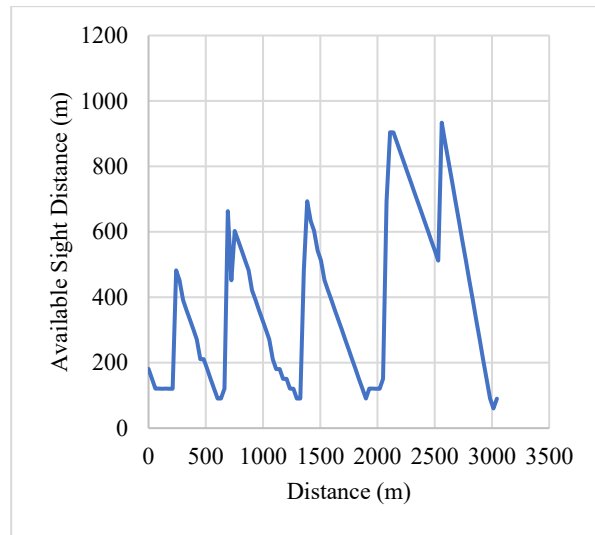
(c)   25% Point Density
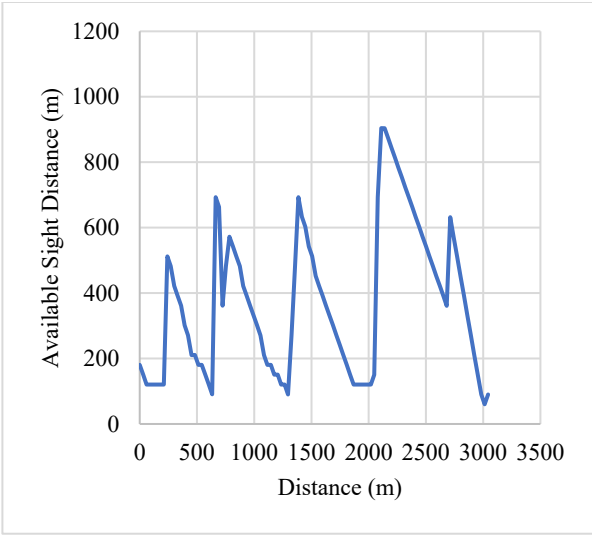
(d)   50% Point Density
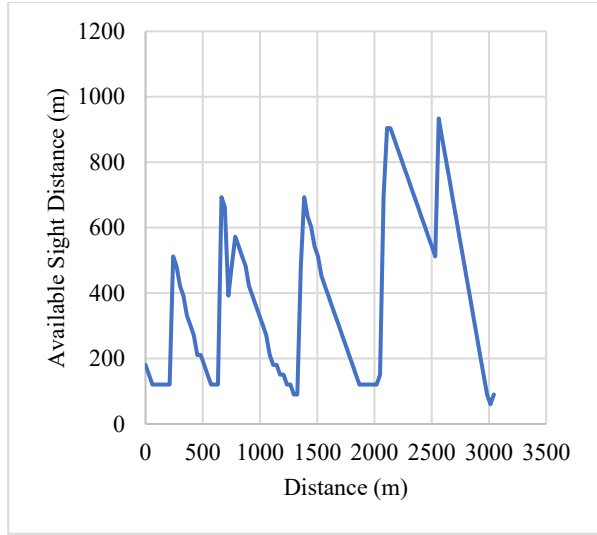
(e) 75% Point Density   *(f) 100% Point Density*

Figure 80: Available Sight Distance Estimated at Different Point Densities (Highway 53)
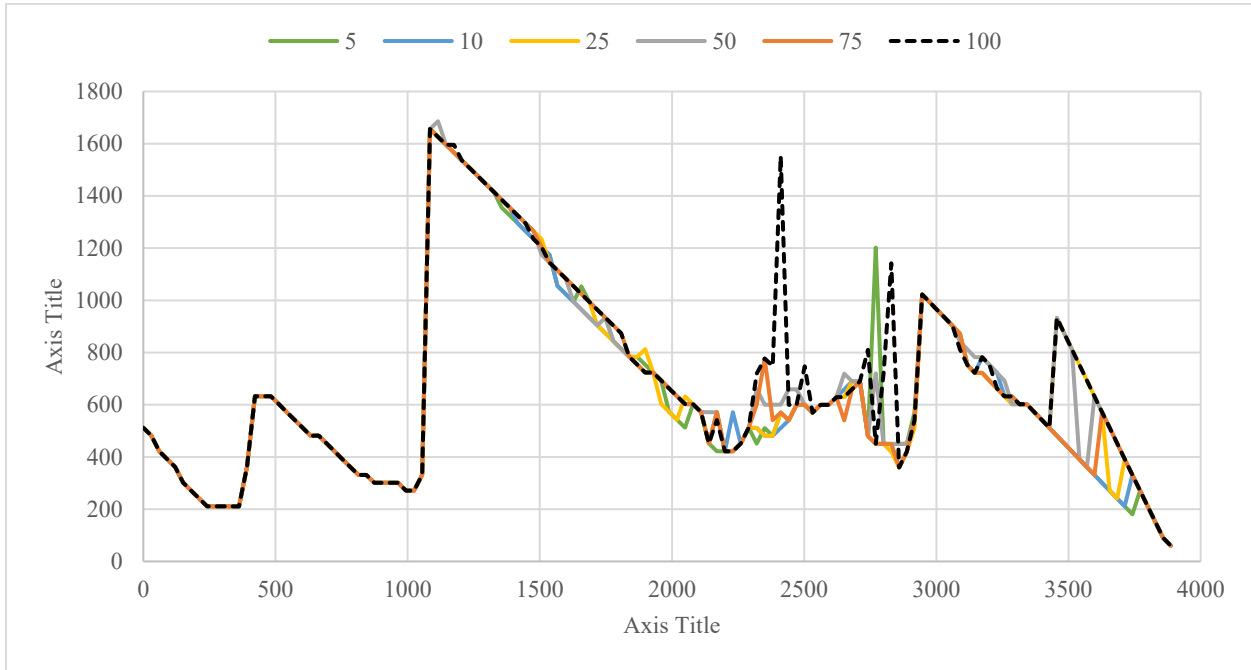
Figure 81: Available Sight Distance Multi-density Estimates (Highway 36)
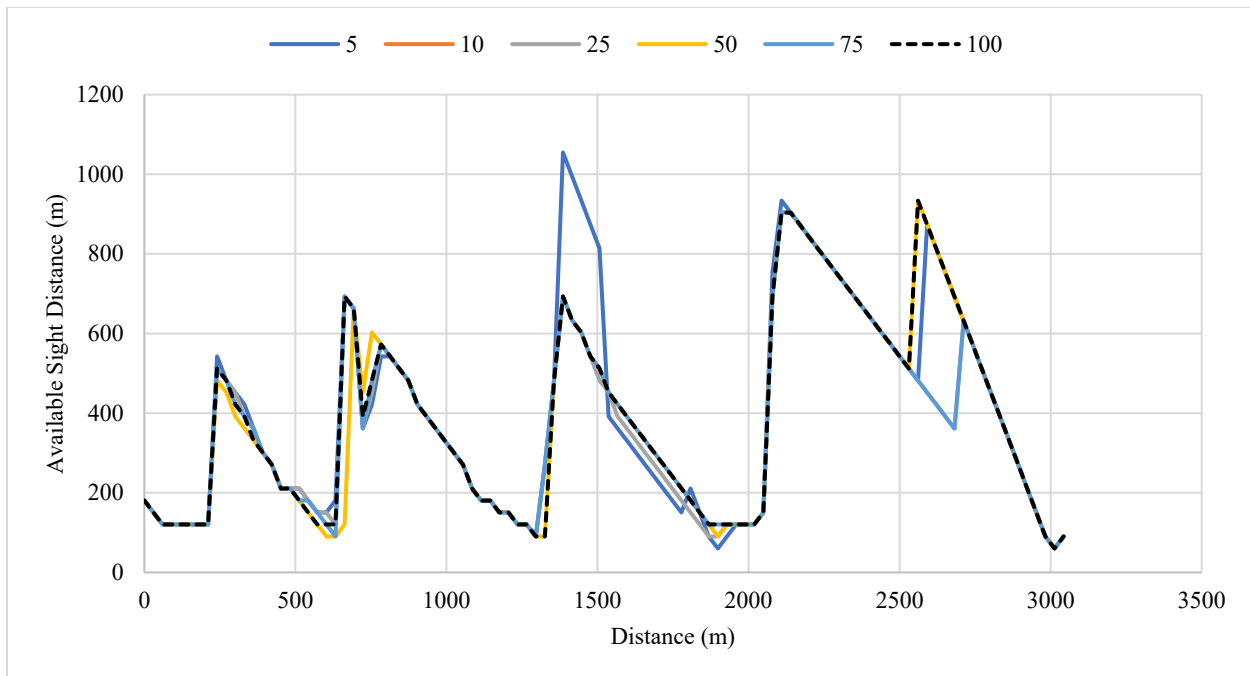
Figure 82: Available Sight Distance Multi-density Estimates (Highway 53)

Although the plots show that the trend in the estimated sight distance at different point densities was very similar, slight variations did exist. In order to quantify those variations and further understand the impacts of LiDAR point density on the assessment, the difference in the estimated sight distance for each observer along the segment at the thinned levels of point density was compared to that estimated at 100% density. The differences are plotted in Figure 83 and Figure 84 for both highways. Figure 83a and Figure 84a show the difference in estimated sight distance measured in meters at different point cloud densities. Figure 83b and Figure 84b show the difference converted into targets missed due to the reduced point density.
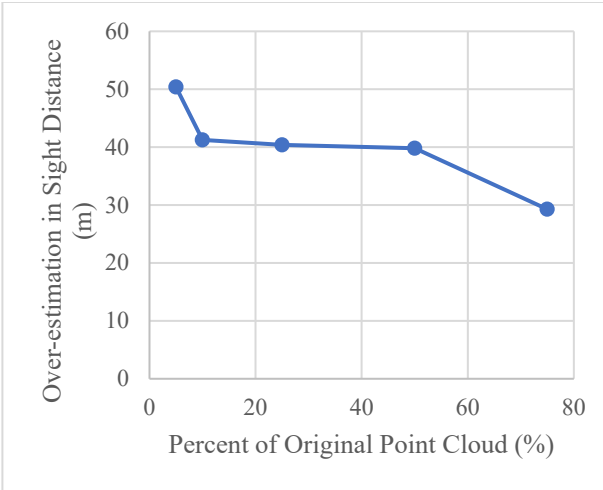
(a) Difference in Meters
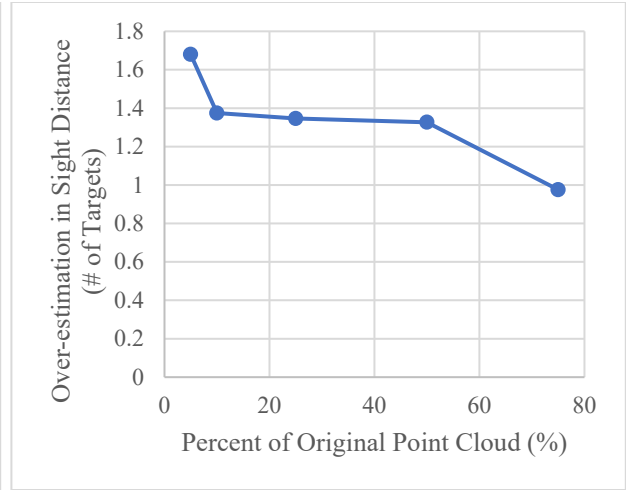
(b) Difference in Number of Targets

Figure 83: Average Difference In Estimated Sight Distance Compared to 100% (Highway 36)
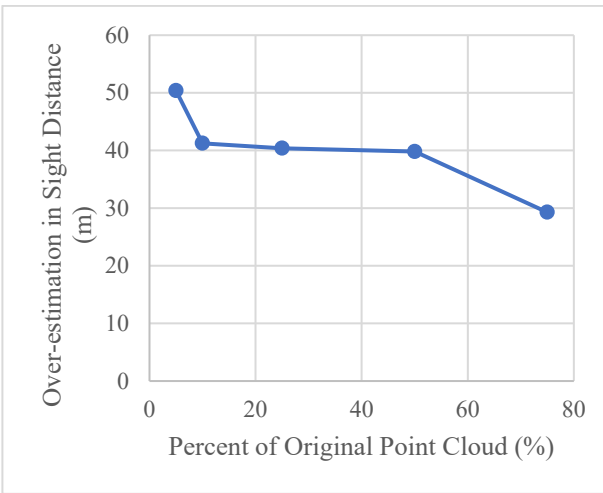
(a) Difference in Meters
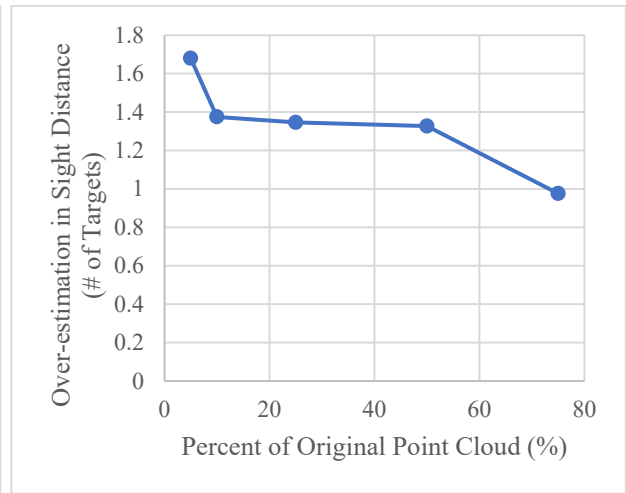
(b) Difference in Number of Targets

Figure 84: Average Difference In Estimated Sight Distance Compared to 100% (Highway 53)

The differences illustrate that the reduction in point density results in a slight overestimation in the available sight distance estimated at some observer locations. The overestimation varies depending on the level of reduction, however, on average the increase ranges from 29m to 50m on Highway 36 test segment and 24m to 44m on Highway 53. Furthermore, the increase seems to grow at lower point densities. This is highly intuitive considering that the reduction in point density results in the removal of points that could potentially represent obstructions to a driver's line of sight. In other words, less dense point clouds might not capture all potential obstructions along the road.

Since observer and target pairs were spaced at 30m for the sight distance assessment, it was important to convert the overestimation in sight distance into a number of targets. The conversion was simply done be dividing the distances by the 30m spacing between consecutive targets. This

161

resulted in the estimates in Figure 83b and Figure 84b. The results show that, on average, the reduction in point cloud density results in a shift of the last visible target by anywhere between 0.8 to 1.4 of a target, which is a minor shift.

One reason why the reduction in point density did not have major impacts on the sight distance assessment is the fact that the extraction algorithm involved rasterizing the point cloud, which uses a collection of points that fall within a raster cell to estimate the surface elevation properties at that location. This means that, even if the number of points that fall within a raster cell is reduced, the impacts of this reduction on the elevation estimate might not significant, as long as the remaining points accurately represent the existing conditions within the raster cell.

8.8   SUMMARY

This Chapter evaluates the impacts of reducing point cloud density on the accuracy of automatically extracting multiple geometric elements from LiDAR point cloud data. LiDAR point cloud density was first reduced to predefined percentages of the original point cloud and the different geometric attributes were then automatically extracted at the different densities. Specifically, this Chapter evaluated the impacts of reducing point cloud density on the following:

- The extraction of road cross sections and their slopes,
- The detection of horizontal curves and estimating their attributes,
- The detection of overhead objects including bridges and the assessment of vertical clearance at those objects,
- The assessment of available sight distance.

For each of those applications, different levels of point density were defined, and the algorithms were tested on LiDAR data collected on a selection of Highway segments in Alberta. In general, it was observed that impacts of point density varied with the variation of the application. Some applications had more apparent impacts on the accuracy and the quality of the extracted information than others. For instance, sight distance assessment and clearance assessment (at bridge structures) seemed to be the least sensitive to reductions in point cloud density. In contrast, cross sections slope estimation and horizontal curves attribute estimation seemed highly sensitive to reductions in point density.

Although, as already noted, the impacts of reducing point density vary depending on the application, reducing the point density to lower than 25% of the original point cloud (i.e., using point cloud density which is lower than 75 ppm^2 on the pavement surface) is not recommended regardless of the applications.

The outputs of this Chapter show that using extremely dense point clouds may not always be necessary. Furthermore, the robustness of the proposed algorithms and their ability to perform on datasets with lower point density is also demonstrated. This indicates that the algorithms could be effective in extracting features and performing assessments on Aerial LiDAR datasets or low-density point clouds obtained using photogrammetric techniques, without significant impacts on the quality of the information extracted. Using point clouds of lower density could also reduce the processing times required to extract information, although this was not a major issue for any of the applications. The findings of this Chapter are extremely valuable for transportation agencies with a limited budget, who are interested in purchasing laser scanning equipment.

9 MULTI-LEVEL DETERMINISTIC PERFORMANCE BASED ASSESSMENT OF STOPPING SIGHT DISTANCE REQUIREMENTS

As already discussed in different parts of this thesis, one of the main objectives of this research effort is to facilitate the adoption of an evidence-based design approach through which the performance of design elements on existing highways is analyzed and integrated into the design process of new facilities. This is achieved through utilizing information extracted from LiDAR about the characteristics of different geometric elements and understanding the extent to which those elements satisfy driver needs and the safety impacts of failing to satisfy those needs.

The aim of this chapter and Chapter 10 of the thesis is to demonstrates how such a goal could be achieved by conducting a performance-based assessment of Stopping Sight Distance (SSD) requirements on Highways. The performance-based assessment is conducted with the aim of understanding the underlying links between demand for sight distance, geometric integrity, and safety performance. In this Chapter the performance-based assessment is conducted at different levels of deterministically defined driver demand, while in Chapter 10, driver demand is modelled probabilistically. The assessment conducted in these two Chapters represents a general framework that can be adopted to conduct a performance-based assessment of any other geometric element.

9.1 BACKGROUND

As previously introduced in Chapter 7, minimum SSD is the distance required by a driver to come to a complete stop when a hazard or obstruction presents itself on a roadway. In order to ensure safe and efficient operation of a roadway, design guidelines require that ASD exceeds the minimum SSD requirements at all points along a roadway. Minimum design requirements for SSD are calculated using equations derived based on the laws of physics and presented in design guides (see Equation 24, Section 7.4). These equations are typically a function of speed, the road's grade, the driver's perception reaction time (i.e., the time required for the driver to perceive and respond to the hazard that creates the stopping requirement), and a vehicle's deceleration rate.

Variables like PRT and deceleration rate vary depending on driver capabilities, vehicular performance, and the situation on hand; however, most highway design guides use deterministic values for those variables. For instance, AASHTO's highway design guide recommends using 2.5s for a driver's PRT and a deceleration rate of 3.4m/s^2 [180]. These values are percentile values,

which were empirically derived based on the performance of a sample of drivers in an assessment conducted over two decades ago [181]. Despite that, it is assumed that roads designed to meet SSD requirements computed based on those values would adequately serve a significant proportion of the driving population. Unfortunately, this is an assumption that is not backed with any evidence. In fact, one critical limitation of the traditional design approach is that the proportion of drivers impacted by meeting or deviating from certain design requirements (including SSD) is unknown. Furthermore, the safety impacts of designing roads to meet those deterministic values is also unknown.

Although designing highways to meet SSD requirements recommended in design codes might ensure that sufficient sight distance is available for some drivers, other drivers including old drivers and drivers with limited abilities who have longer PRT or lower deceleration rates might not find the available sight distance adequate. A large portion of old drivers are typically slower in both their perception of risk and the manner in which they react to hazards on the road. This is due to many factors, including reduced visual acuity, reduced flexibility and motion range, narrower field of vision, greater sensitivity to glare and reduced muscle strength[182]. All these factors result in drivers having longer perception reaction time, hence, requiring longer sight distances. This issue is aggravated when considering the fact that the age structure of the population in most developed countries is changing. Statistics in Canada show that the average age of the driving population is on the rise with projections predicting that by 2030 around 20% of all drivers will be over the age of 65 [183].

Deceleration rate is another factor that affects sight distance requirements on highways and one which may vary among drivers of different ages and drivers with different capabilities. Old drivers and drivers with limited abilities are less likely to apply similar pressure to brake pedals as young drivers, hence, occasional differences in deceleration rates may appear. The length of the time in which a driver sustains a maximum comfortable deceleration rate also varies from one driver to another[184]. Furthermore, in places of adverse weather conditions surface traction might not always be best and may result in a reduction in deceleration rates.

Whether it is reaction time, deceleration rates, or environmental conditions, all these factors affect the amount of sight distance required by drivers on a highway segment. Although integrating all factors into design might not be economically feasible, it is critical to ensure that existing highway

infrastructure satisfies the demands of the majority of the driving population. In other words, it is important to understand how much of our existing highway infrastructure is able to accommodate the needs of different categories of drivers. Furthermore, it is equally as important to understand the safety impacts of failing to meet those requirements. All this information helps ensure that design requirements for future highway facilities are formulated based on the performance observed on existing facilities and based on the demands of the existing driving population. These principles are critical to the adoption of a performance-based design approach that would help create a safe system that is forgiving to driver error and caters to driver needs.

In this Chapter a multi-level deterministic performance-based assessment of SSD is conducted. Three different levels of required SSD are first defined with each level representing a specific category of drivers. The performance of a selection of crash prone highways in Alberta was assessed at each of those levels. Specifically, the assessment focuses on analyzing the relationships between the level of conformance to stopping sight distance requirements under the different levels of demands and the relationships between noncompliance to SSD requirements and safety performance on each of the test segments.

9.2 PREVIOUS WORK

Before discussing the details of the assessment, literature on how different variables in the SSD equation vary among different categories of the driving population is first reviewed. This was done to help define different levels of SSD requirements for the multi-level deterministic assessment. In addition, previous attempts that assess the difference between available sight distance on existing roads and the theoretical sight distance requirements are also reviewed in this section.

9.2.1 VARIABLES AFFECTING SSD REQUIREMENTS

In an early study, which conducted a thorough review of factors affecting PRT, Green [185], identified *driver age*, *expectation of hazard*, and the *urgency of the hazardous situation* as the main variables. In case of driver age, the study concludes that older drivers have a longer PRT than younger drivers. However, the study states that in order to establish a sound relationship between aging and change in PRT, more controlled studies are required.

In the case of the degree of expectation of various hazards, the same study divides the expectation into three levels (expected signals, common but uncertain signals and surprise intrusion). For

expected signals, such as break lights of a lead vehicle, the paper reports the mean perception reaction time of drivers typically ranges from 0.70 - 0.75 second. For common but uncertain signals such as brake lights of a vehicle ahead in traffic, it found that PRT was in the range of 1.2 – 1.35 seconds. Finally, for surprise intrusion such as animals running onto the road, Green [185]concludes that the PRT typically increases to 1.5s which is twice that of expected signals (0.75s).

For the final factor affecting PRT, defined as the "urgency of the situation", Green [185] found that the relationship between this factor and PRT is a U-shaped relationship such that at very short, and very long, time-to-collision correspond to long PRT. Unlike the values recommended by AASHTO, which represent the 85th percentiles, the estimates provided in Green's paper for perception reaction times are mean values estimated based on the outputs of other studies.

In a report by the NCHRP investigating the impacts of human factors on design equations, Campbell [186] explores the variation in PRT under favorable and unfavorable conditions and the effects of that on SSD. A number of drivers were asked to drive under those two conditions while being subject to unexpected roadway hazards. The mean PRT and deceleration rates for drivers were measured. The report defines favorable conditions (i.e., good visibility) for the PRT as driving during the daytime with the hazard being clearly visible and directly in the line of sight of the driver. During night-time, the report states that favorable conditions for the PRT include self-illuminated or retro-reflectorized hazards that are immediately recognizable and near the driver's line of sight. Unfavorable conditions (i.e., poor visibility) for the PRT in daytime consist of hazards that are hidden or camouflaged by the surrounding background, unreflectorized, not self-illuminated and initially off the line of sight of the driver. Furthermore, during night-time, unfavorable conditions for the PRT exist for low beam headlights with or without street lighting as well as if glare exists from oncoming vehicles. In good visibility, the mean PRT was estimated to be 1.6s while, for poor visibility, it was 5.0s.

In addition to PRT, the study also explores the effects of favorable and unfavorable conditions on deceleration rates. Favorable conditions (i.e., good traction conditions) were defined as straight road segments, dry or wet pavement, vehicle tires in good condition, and the vehicle being a passenger car. Unfavorable conditions (i.e., poor traction conditions) were defined as conditions when the stopping requirement happen in a curve or downgrade and where surface conditions were

poor. For good traction conditions a 5.4 m/s^2 deceleration rate was estimated while for poor traction conditions the rate was d 4.2 m/s^2.

Realizing that there is an element of uncertainty in some of the variables in design equations such as the equation of SSD, many researchers have attempted using reliability analysis to integrate uncertainties into safety analysis of sight distance on segments [14,154]. The principles applied in reliability analysis follow the limit states design approach where variables in the design equations are treated as random variables, which are expressed as probability distributions rather than constant values. In attempts to model the statistical distribution of PRT and deceleration rate, Ismail and Sayed [187] used the perception reaction time and deceleration rate from various studies. The mean perception reaction time was found to be lognormally distributed with a mean of 1.5s and a standard deviation of 0.4s. Similarly, deceleration rate was assumed to follow a normal distribution with a mean of 4.2 m/s^2 and a standard deviation of 0.6 m/s^2. Several other studies reviewed by Ismail and Sayed [187] estimated mean PRTs between 1.21s and 1.4s with standard deviations from 0.74s to 0.15s.

As evident in the review, variables used to predict required SSD on a highway segment vary depending on many factors. PRT is affected by visibility conditions, age, hazard expectancy and situation urgency. Similarly, surface conditions, the driver and vehicle driven all affect the deceleration rate.

The next section explores the studies which have analyzed the difference between available stopping sight distance on existing roads and the theoretical sight distance requirements while taking variation in different variables in the sight distance equation.

9.2.2 AVAILABLE SIGHT DISTANCE

The assessment of available sight distance on highways has been an interest for many researchers in recent years. Gavran, et al. [188], studied the differences between ASD and theoretical sight distance while addressing the importance of integrating operating speed into sight distance assessment. In addition to the ASD and the SSD the authores define another type of sight distance which they name Required Sight Distance (RSD). RSD was mathematically derived using the operating speed instead of the design speed used to compute SSD. To measure the ASD, a triangulated 3D model of the road was imported into a 3D CAD environment. The ASD was then plotted against the RSD. Although the authors do not provide much discussion of the results or

any validation of the method used to measure ASD, it is mentioned that the ASD exceeded the RSD on most of the test segments. However, the authors do argue the importance of using operating speeds when computing SSD requirements.

SSD and the horizontal line of sight offset, when approaching a horizontal curve and within the horizontal curve, were also studied in [189]. These two cases (i.e., when approaching the curve and when driving on the curve) were investigated in six different theoretical combinations of speed limit, curve radius, and superelevation. Using previous speed prediction models and reliability theory, the probability of noncompliance (i.e., the probability of a driver not having sufficient SSD to perceive, react, and brake before reaching an object on the curve) was calculated. The results showed that the probability of noncompliance when approaching the curve was greater than within the curve. This led the authors to suggest that the same SSD and line of sight offset should be used within the curve and near the end of the curve.

Sarhan and Hassan [190] also estimated the probability of noncompliance (referred as the probability of hazard) on a hypothetical roadway segment using a computer program. This computer program was developed to calculate and compare the available and required sight distances profiles in 2D and 3D. The program was used to estimate the probability of hazard on a horizontal curve with flat grade in a cut section and on horizontal curves combined with different crest and sag vertical curves. The results showed that the maximum probability of hazard value of all the cases was around 1%. The authors concluded that the deterministic approach of SSD was conservative in terms of safety, due to the low values of the probability of hazard, while this approach might be uneconomic from their point of view.

Ismail and Sayed [187] performed a reliability assessment of SSD on crest vertical curves as part of a paper where they propose a framework to incorporate uncertainty into the design of geometric elements on highways. The proposed framework involved calibrating a design value that satisfies a predefined probability of noncompliance, which is deemed acceptable by the designer. In other work, Hussein, et al. [191]used the proposed framework to calibrated design charts for the middle ordinate on horizontal curves. This ordinate plays a significant role in the sight distance available on horizontal curves. It is worth noting here that in both studies the available sight distance on the test segments was estimated using empirical equations. In both studies, the authors concluded that calibrated values were generally lower than those derived from AASHTO.

Ismail and Sayed [192] used reliability analysis to estimate the risk associated with adopting different design alternatives that were being considered for a set road segments with restricted sight distance in a mountainous region. The risk was assessed by comparing the probability of noncompliance for a range of values of design values. The study concluded that the design alternatives considered were associated with a relatively high risk of limited sight distance.

The probability of noncompliance was also assessed on horizontal curves by Ibrahim and Sayed [14] using the reliability theory. In this paper, ASD was estimated as a function of lane width, clearance, and the radius of the curve. Required stopping sight distance was simulated and the probability of noncompliance was computed. Among other findings, the study reported that 50% of the analyzed curves had a probability of noncompliance greater than 0.457. Similar reliability assessment of Sight Distance was also conducted in [193], however in this study three different methods were used to compute the ASD on a larger sample of curves on 12 different highway segments. Although one of the methods used in this study to quantify ASD was a 3D LiDAR based assessment, it only considered sight distance at isolated curve locations.

In more recent work, Wood and Donnell [194] assessed the needs of incorporating the distance from the front of the car to the driver's eye as a variable when computing the minimum stopping sight distance required on curves. The authors computed ASD on vertical curves based on the geometry of a parabola. Similarly, the ASD on horizontal curves was graphically computed based on their geometric attributes. The authors then developed a simulation model to estimate the sight distance required while incorporating the new variable to understand its impacts on the probability of non-compliance to sight distance requirements on a selection of vertical and horizontal curves.

In general, many studies in the literature acknowledge that available sight distance might vary along a road segment and that SSD requirements also vary among different drivers. Despite that, not much has been done to assess the extent to which existing roads (i.e., roads designed based on deterministic design standards) take those variations into account on an aggregate segment-level. Most of existing work focuses on analyzing a selection of curves or a single highway segment. The main reason here is that the supply (e.g., available stopping sight distance) is predicted using an empirical equation which is a function of certain road features or measured off dated design drawings. Consequently, reliability assessment is limited to locations where supply can be quantified (where empirical equations are derived, or where as-builts exist). Another common

limitation in previous studies is that most of those studies limit their assessments to evaluating the probability of noncompliance, which is an estimate of how often the supply is expected to fall below the demand[187]. Although such an assessment is important, it does not provide much information on the safety impacts of failing to satisfy the demand for SSD.

9.3 MODELLING

The aim of the multi-level deterministic analysis is twofold. The first aim is to determine the extent to which existing highways are able to meet different levels of SSD requirements, this is called the geometric performance assessment as illustrated in Figure 85. The second aim is to determine the safety impact of not meeting those SSD requirements, which is called the safety performance assessment.

To achieve those aims it was first necessary to quantify the available sight distance on test highways. This was done using the algorithm proposed in Chapter 7 of this thesis. After that three different levels for SSD requirements were defined considering driver capabilities and driving conditions and SSD was quantified at each of those levels as detailed in Figure 85. In particular, PRT and deceleration rate are used as a proxy for driver capabilities and driving conditions. The different levels for those two variables were identified based on the outcomes of previous research.
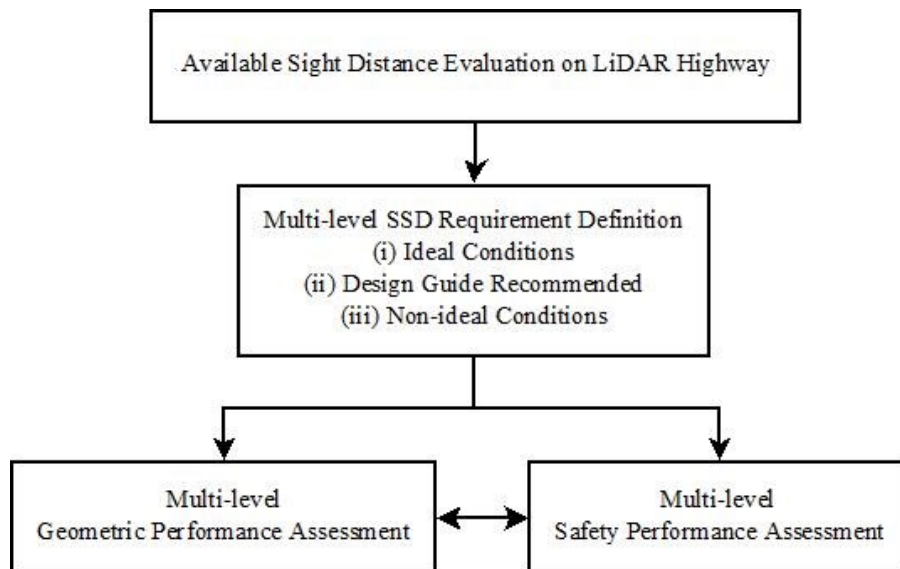
Figure 85: Multi-Level Deterministic Analysis Framework

For perception-reaction time, two levels were defined. Drivers with limited ability who are driving in poor conditions were assumed to have long PRT. In contrast, highly skillful drivers with high

cognitive ability driving in clear conditions were assumed to have very short PRT. In order to be consistent with the PRT values defined in the literature, a short PRT was assumed to be 1.6s and a long PRT was assumed to be 5.0s [195]. It is worth noting here that these values were previously defined in research conducted under the NCHRP and published by the TRB in a report titled "*Human Factors Guidelines for Road Systems*" [195].

Similar to PRT, for deceleration rate, two levels were defined. Deceleration rate under poor conditions was defined as conditions where a driver only applied slight pressure to the brake pedal and where surface traction conditions were poor. Deceleration rate under good conditions, on the other hand, is when a driver applies severe pressure to the brakes and where surface traction is good. For these two conditions deceleration rates of 5.4m/s^2 and 3.4m/s^2 were used for good and poor conditions, respectively [195].

The three levels of theoretical SSD are defined based on the conditions discussed in the previous paragraphs. For *Ideal Case* SSD was calculated based on a PRT of 1.6s and a deceleration rate of 5.4 m/s^2. For *Non-ideal Case*, SSD was calculated using a PRT of 5.0s and a deceleration rate of 3.4 m/s^2. In addition to the SSD values, which take into account variations in driving conditions and human factors, the SSD based on AASHTO's recommendation (PRT = 2.5s and Deceleration rate = 3.4m/s^2) was also calculated.

After identifying the available SSD on the test highways and after calculating SSD requirements at the different levels, the ASD and required SSD were plotted along the length of each segment on all the test highways. Moreover, the length of noncompliance (i.e., the portion of the test segment where the segment's geometric elements fail to accommodate the demand expected on that segment) was quantified under the different levels of demand. In addition, collisions that had occurred along each of the test segments were mapped onto the SSD plot. This information was used for the safety assessment where links between limitations in sight distance and collision performance were investigated.

9.4   TEST SEGMENTS

The multi-level assessment performed in this Chapter was conducted on seven different crash prone highway segments in the Province of Alberta, Canada. The test segments were identified as crash prone segments using the Empirical Bayes method. In the first stage of the Safety

Management Process, *Network Screening* is used to identify crash prone locations. This involves identifying locations that are deemed unsafe and ranking those locations based on the potential for crash reduction. The literature includes several methods to identify and rank these locations as part of the network screening process. Among the different crash identification and ranking methods, the Empirical Bayes method is considered to be the most consistent crash prone identification method and provides the most reliable results when compared to the other methods [196].

In brief, the Empirical Bayes method combines the observed number of crashes and the estimated number of crashes to provide an unbiased prediction of the true safety at a location. The observed number of crashes is usually extracted from historical crash data. The estimated number of crashes is computed from sites with similar traffic and geometric characteristics to the sites being analyzed using crash prediction models. The sites are then ranked using the Empirical Bayes method, where sites with higher Empirical Bayes values will have more potential for safety improvement.

In a comprehensive assessment of 17,355 two-way two-lane segments in the Province of Alberta[197], highways 5, 20, 22, 28, 55, 63, and 88 were identified as the top crash prone locations at a 5% significance level and, hence, they were considered as ideal candidates for the performance-based sight distance assessment.

All seven highway segments were 2-lane undivided rural segments with a speed limit of 100km/h. The length of the test segments ranged from 2.5km on highway 63 to 9.55km on highway 20. The average length of all segments was 6.23km. The seven highways spread across different parts of the province as seen in Figure 86. Table 11 shows a summary of information on the length and traffic information on the seven test segments.
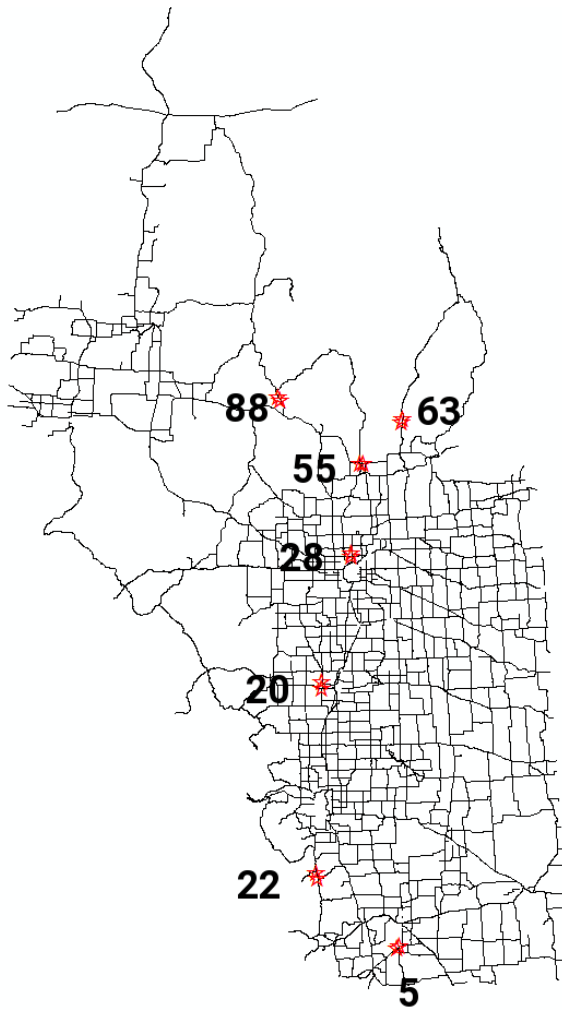
Figure 86: Test Locations

Table 11: Geometric and Traffic Information on Test Segments

Highway	Total Length (km)	AADT (veh/day)	Heavy Vehicles (%)
5	6.219	4535	6.9
20	9.554	8755	6.45
22	9.661	4403	9.58
28	5.334	7270	5.2
55	3.957	4893	8.73
63	2.514	3988	27.63
88	6.363	2340	27.73

It is worth noting that LiDAR data along the test segments was collected using RIEGL VMX-450 MLS system. More information about the capabilities of this unit are provided in Chapter 3 of the thesis.

174

9.5 RESULTS AND DISCUSSION

Figure 87 shows samples of the plots produced by the MATLAB algorithm which display the ASD for the test segments. The y-axis on the plots represents the available sight distance and the x-axis represents the distance along the segment. In addition to the available sight distance, two different horizontal lines are drawn across the plots one representing AASHTO's SSD requirements and the other representing the non-ideal conditions. If at any point along the segment the ASD falls below one of the horizontal lines this indicates that SSD requirements are not met at that location.

For all the highway segments analyzed, the ASD rarely dropped below the sight distance requirements under ideal conditions (i.e., the threshold defined for drivers with short PRT, high skill and high cognitive ability). Accordingly, the discussion of the results presented in the next few subsections will focus on whether or not ASD meets the AASHTO requirements and the sight distance requirements defined for non-ideal conditions and drivers with limited skills and low cognitive ability (i.e., sight distance requirements that take limitations in human factors into account).

9.5.1 GEOMETRIC PERFORMANCE (NON-COMPLIANCE RATES)

Table 12 presents the total length of each of the analyzed highway segments and the portion of that length where SSD requirements were not met (i.e., the length of the noncompliant regions). The ratio of the length of the noncompliant region to the total length of each segment (i.e., percent noncompliance) is also computed and shown in the table. The results are shown for the SSD requirements under AASHTO and under the non-ideal conditions.

175
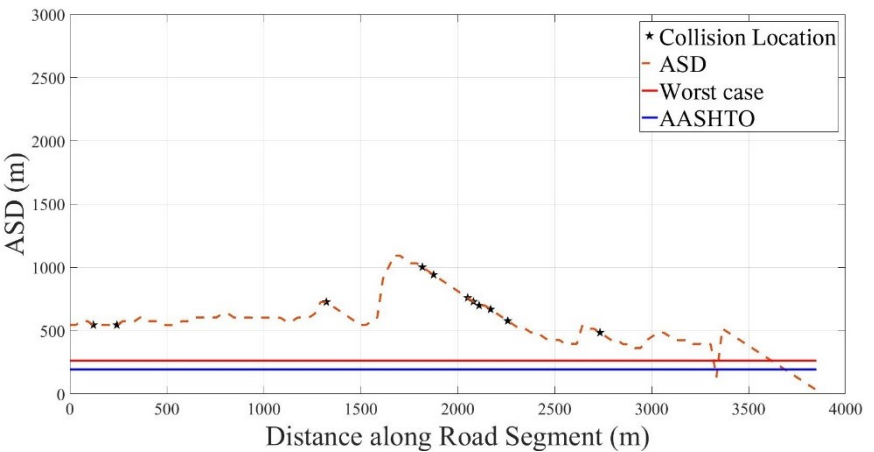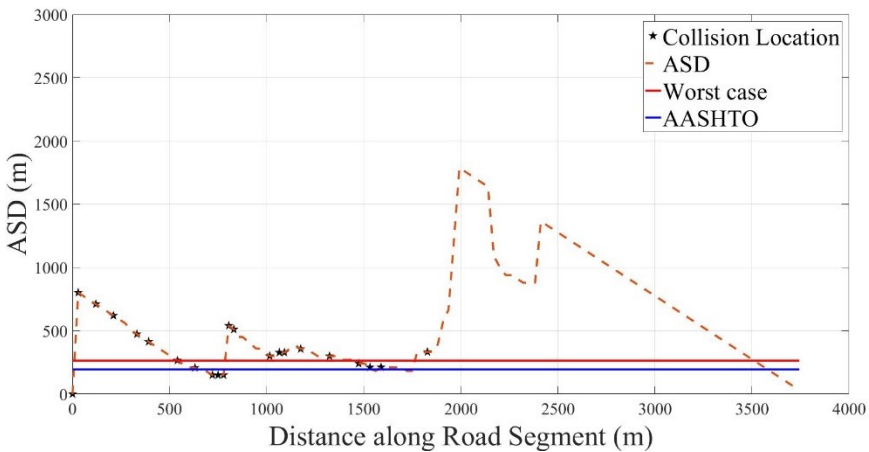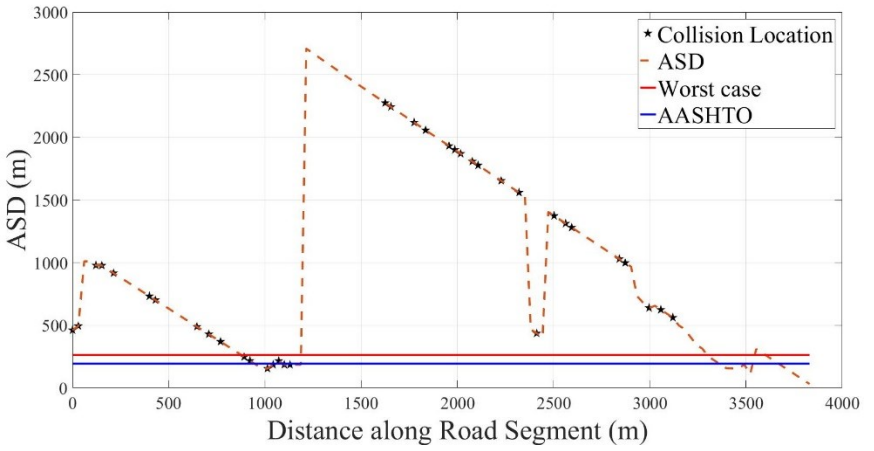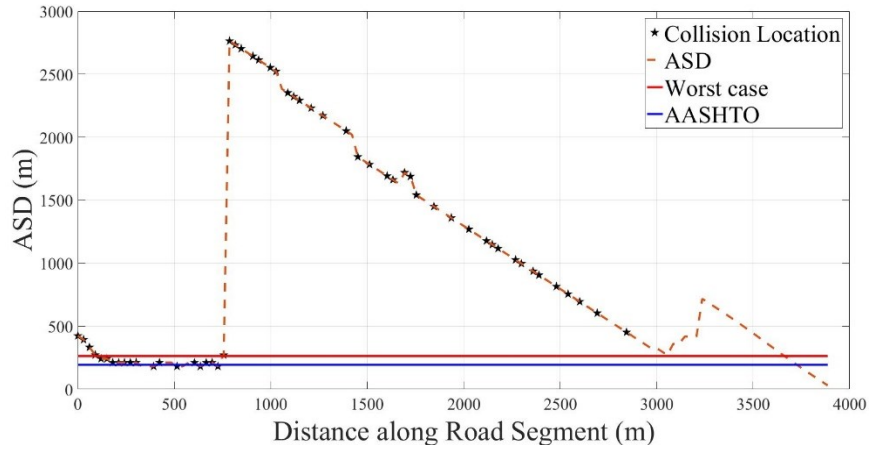
Figure 87: Plots Samples of the ASD with the different SSD Cases for Segments of Highways 20 (Top Left), 28 (Top Right), 55 (Bottom Left), and 88 (Bottom Right)

Note: y-axis represents available sight distance (ASD) in meters and x-axis represents the distance along the segment in meters

176

Table 12: Noncompliance Rates Compared

Highway	Non-ideal Conditions (Worst Case)			AASHTO		
	Length of NC* Region (m)	Total Length (m)	Percent NC (%)	Length of NC Region (m)	Total Length (m)	% NC (%)
5	260.2	6218.6	4.185	61.2	6218.6	0.984
20	1928.2	9554.1	20.181	630.8	9554.1	6.602
22	1054.4	9661.1	10.914	60.5	9661.1	0.626
28	513.3	5334.8	9.621	332.7	5334.8	6.236
55	694.8	3957.4	17.557	143.3	3957.4	3.622
63	393.5	2514.2	15.651	91.1	2514.2	3.625
88	30.4	6363.4	0.477	0.0	6363.4	0.000
Average	696.4	6229.1	11.2	188.5	6229.1	3.1

*NC: Noncompliance/Noncompliant

9.5.1.1 NON-IDEAL CONDITIONS (WORST CASE)
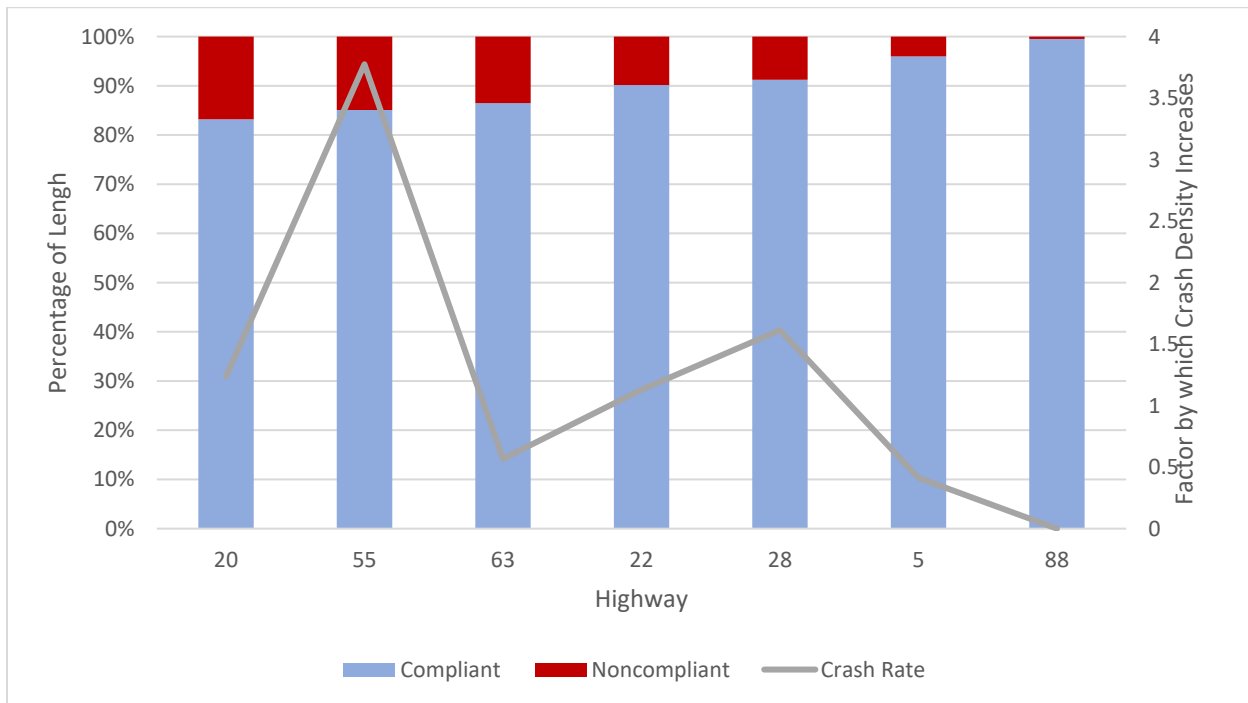
Figure 88: Percent Compliance/Noncompliance and Corresponding Change in Crash Density (Worst-Case)

Under non-ideal conditions (i.e., when the ASD is compared to the threshold which takes human factors into account) the results show that a substantial portion of the analyzed segments do not meet sight distance requirements. On 5 of the 7 analyzed segments noncompliance rate exceeds 9.62% with an average of 14.8% for the 5 segments. When considering all 7 segments average percent noncompliance drops to 11.2%. As seen in Figure 88, Highways 20 and 55 had the highest noncompliance rates. The percent noncompliance on Highway 20 was 20.2%. In terms of actual length, this translates to almost 2km of the 9.6km analyzed not meeting the sight distance

requirements. On Highway 55, noncompliance percent was 17.6% (almost 700m of the 4km analyzed).

Highway 88 was the highway with highest compliance rates. On this highway, sight distance requirements, under non-ideal conditions, were met on all but 30m of the segment (i.e., only 30m of the 6.3km analyzed were noncompliant). The segment with the second lowest percent noncompliance is Highway 5 where only 4.2% of the analyzed 6.2km did not meet sight distance requirements.

These numbers show that the ability of existing highways to accommodate drivers with low skills and low cognitive ability such as old drivers is restricted to only 80-85% of the road. In other words, those drivers spend 15-20% of their time driving on highways that are not designed to meet their needs, which puts them under an additional risk.

9.5.1.2   *DESIGN GUIDE RECOMMENDED (AASHTO)*
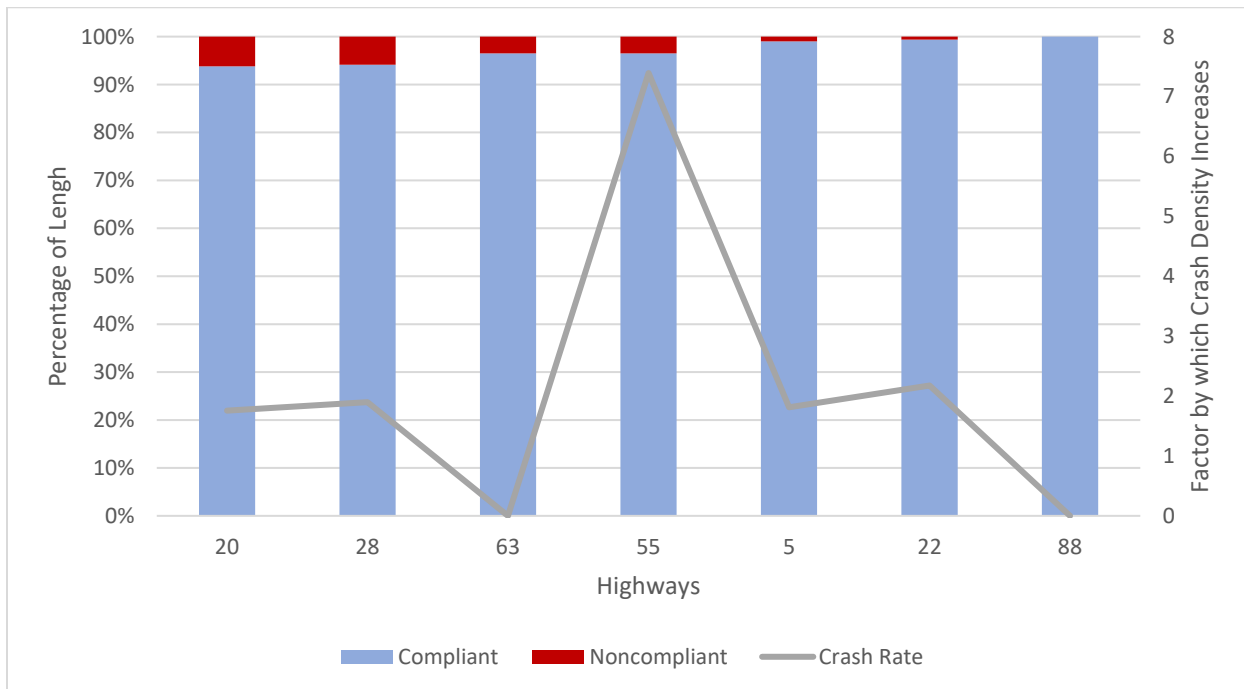
Figure 89: Percent Compliance/Noncompliance and Corresponding Change in Crash Density (AASHTO)

When compared to AASHTOs theoretical SSD requirements, the highest rate of noncompliance on the analyzed segments was 6.6%. This was observed on Highway 20. On average, percent noncompliance on the analyzed segments with respect to AASHTO was 3.1%. This is reasonable considering the fact that highways are designed to meet AASHTOs SSD requirements (Alberta

Design Guide recommends the same guidelines as AASHTO for SSD calculations). Out of the seven crash prone highway segments analyzed, Highway 88 was the only highway that was perfectly compliant to AASHTO's sight distance requirements as evident in Figure 89, although it is worth pointing out that the analyzed segments of Highway 5 and Highway 22 also had low noncompliance rates of 0.98% and 0.6%, respectively.

9.5.2 SAFETY PERFORMANCE

As evident by the results presented in the previous section, a substantial portion of the analyzed highway segments do not meet stopping sight distance requirements under the non-ideal conditions (i.e., when human factors and driving conditions are taken into account). Furthermore, the analysis shows that even AASHTO sight distance requirements were not met on some portions of the analyzed segments. To understand the impacts of such design deficiencies on safety, crash density at locations of noncompliance were compared to crash density on compliant regions on each of the analyzed segments. This process is known as the *Diagnosis Stage* of the Safety Management Process, in this stage different tools are used to analyse trends in the crash data before deciding on an appropriate countermeasure to treat the problem. Unlike the network screening stage where the EB method has been identified as the most accurate method, the HSM does not recommend a specific method for the diagnosis of crash sites.

Since the same traffic volume travels through both the compliant region and the noncompliant region of the same highway segment, crash frequency per length (crash densities) were used to compare safety at the two regions. Crash densities were calculated based on the collision data recorded on the test segments between 2009 and 2014. Moreover, the types of collisions and the demographics of drivers involved in collisions that occurred at locations of noncompliance were also explored to identify any links between design deficiencies and safety.

9.5.2.1 CRASH DENSITIES

Table 13 shows the crash densities (crashes per km) on the analyzed highway segments for the noncompliant and the compliant regions. The table also shows the change in crashes in the two regions expressed as a ratio and a percentage. As evident in the table, it is clear that on segments where non-compliant regions exist, these regions typically experience higher crash densities than compliant regions for both AASHTO and under non-ideal conditions. It is important to note here that the results presented here only examine the existence of a correlation between limitations in

179

sight distance and changes in crash density. The comparison of crash density on compliant and noncompliant regions of the same segment does help account for many confounding factors including geometric information such as number of lanes, lane widths, shoulder widths, pavement conditions, traffic volumes and many other factors.

Table 13: Crash Density Analysis

Highway	Non-Ideal Conditions				AASHTO			
	NC-CD[a]	C-CD[b]	Ratio (NC to C)	% Change	NC-CD	C-CD	Ratio (NC to C)	% Change
5	7.69	18.63	0.41	-58.7	32.67	18.03	1.81	81.2
20	42.53	34.36	1.24	23.8	60.24	34.29	1.76	75.7
22	8.54	7.55	1.13	13.0	16.54	7.60	2.17	117.5
28	33.12	20.53	1.61	61.3	39.08	20.59	1.90	89.8
55	59.01	15.63	3.77	277.5	139.54	18.88	7.39	639.2
63	5.08	8.96	0.57	-43.3	0.00	8.67	0.00	-100.0
88	0.00	6.32	0.00	-100.0	0.00	6.29	0.00	-100.0
Average	22.28	16.00	1.25	24.80	41.15	16.34	2.15	114.76

[a]NC-CD: Noncompliant Crash Density in Crashes/km, [b]C-CD: Compliant Crash Density in Crashes/km

Non-ideal Conditions (Worst Case)

When considering all analyzed crash prone segments, on average, the noncompliant regions under the non-ideal conditions experienced crash densities 24.8% higher than compliant regions. For crash prone segments where the percent noncompliance was higher than 9.6% (i.e., more than 9.6% of the length of the segment was noncompliant), crash densities in the noncompliant region were found to be higher than those in the compliant regions on all but one of the five segments. On average, for those highways, the noncompliant region experiences a crash density that is 66.5% higher than that of the compliant region. The highest increase in crash densities was observed on Highway 55. For this highway, the crash density increases from 15.6 crashes per km in the compliant region to 59 crashes per km in the noncompliant region (that is almost four times the rate). Highways 20 and 28 were also segments where there was a substantial increase in crash densities in the regions where sight distance did not meet the non-ideal theoretical requirements (i.e., regions of noncompliance). The increase was 23% and 61% for highways 20 and 28, respectively. Highway 63 was the only segment, of those analyzed, where crash densities were not higher in the noncompliant regions despite a relatively high percent of noncompliance. This could be down to the fact that only 2.5km of Highway 63 were analyzed (the shortest segment out of all highways).

180

In general, the findings demonstrate that when portions of a highway segment are noncompliant to sight distance requirements, which take into account limitations in driver abilities, it is likely that those portions of a highway will experience higher crash density. Considering the fact that the population of drivers with limited abilities is on the rise, this finding is quite concerning.

Design Guide Recommended (AASHTO)

When considering any part of a segment that does not meet AASHTO's SSD requirements as noncompliant the results are even more concerning. Although regions of noncompliance under AASHTO are short (i.e., the range from 0% to 6.6% of length), regions of noncompliance experience significantly higher crash densities. Out of the seven highways analyzed, five highways had higher crash densities in regions that were not compliant to AASHTO's SSD requirements. In fact, on those five highways noncompliant regions experienced a crash density which was, on average, 2.95 times higher than that in compliant regions. For the other two highways, Highway 88 meets AASHTO's SSD throughout (i.e., there were no noncompliant regions) and no crashes were recorded in the noncompliant regions on Highway 63. The highway that experienced the highest increase in crash densities in its noncompliant region compared to its compliant region is Highway 55. This highway was also the one with the highest increase in crash densities in its noncompliant region when considering sight distance requirements under the worst case.

When comparing the changes in crash densities between the noncompliant and the compliant regions, it is noted that, despite being shorter, noncompliant regions under AASHTO experience higher increases in crash densities when compared to noncompliant regions under the worst case SSD requirements. In other words, when the available sight distance dropped below AASHTO's sight distance threshold, the crash density increase was more critical than when the ASD dropped below the non-ideal threshold. This is highly intuitive considering that drops in ASD below the non-ideal threshold only affect drivers with limited abilities. In contrast to that, drops in ASD below AASHTO's requirements affect more drivers. In fact, the findings are in contrary to previous research where no correlation between SSD and crashes (all types, all severities) was found for up to 30% deficiency with respect to the AASHTO design guidelines [198,199].

To further verify the impacts of limitations in SSD on safety, a Chi-Squared test of association was used. The test was used to assess whether there was statistical correlation between a region being noncompliant to SSD requirements and crash densities increasing in that region. The tests

revealed that the association was statistically significant at the 10% level with p-values for the likelihood ratio of 0.08 (for AASHTO's case) and 0.104 (in case of the non-ideal conditions).

The more critical observations when AASHTO's requirements were violated are even more alarming when taking the ageing population into consideration. Currently, not many drivers have a longer perception reaction time (i.e., the majority of drivers today are comfortable driving on roads designed to meet AASHTO's sight distance requirements). When ASD drops below AASHTO's requirements, even for short periods, a large population of drivers is affected, which is reflected by the substantial increase in crash densities. The ageing population means that, over the next few years, more drivers will fall in the category of drivers with limited abilities, hence, drops in ASD below the SSD requirements that integrate driver ability and human factors will affect more drivers and the consequences will potentially be more critical, than the increases observed in this assessment.

Based on the outputs of the analysis performed in this study and the projections that predict increases in the ages of the driving population[183], over 10% of existing highways won't satisfy the needs of 20% driving population. This finding is highly critical to the future design of highways. Given the fact that the majority of developed countries have aging populations, authorities responsible for highway design must take such figures into consideration when designing new roads and when upgrading existing highways or when setting new speed limits.

9.5.2.2   AGE STRUCTURE

Table 14: Age Distribution of All Drivers Involved in Crashes

| | All Drivers | | | | Male Drivers Only | | | |
| | Noncompliant Region | | Compliant Region | | Noncompliant Region | | Compliant Region | |
Highway	Under 70	Over 70	Under 70	Over 70	Under 70	Over 70	Under 70	Over 70
5	4	0	302	23	2	0	159	17
20	324	6	1541	27	201	6	765	16
22	17	0	139	4	14	0	99	4
28	47	6	515	12	40	6	362	10
55	103	8	195	10	52	6	65	8
63	129	5	744	10	112	5	633	10
88	0	0	75	3	0	0	53	3
Total	624	25	3511	89	421	23	2136	68
Proportions	0.0385		0.0274		0.052		0.031	

To get more insight into whether drivers with limited abilities are overrepresented in the noncompliant regions, the age distribution of individuals involved in crashes that happened in the noncompliant region was compared to those that occurred in the compliant region on all the analyzed highway segments. It is important to emphasize here that dividing the segments into compliant and noncompliant sections was based on a PRT of 5s, as previously defined. This does not mean that all crashes that occurred in the noncompliant regions were because the drivers had a PRT of 5s or more, instead it is only a threshold used to divide the segments into portions of low ASD and high ASD. It is also worth stressing that, the reason 5s threshold was adopted is because that was previously defined in research conducted under the NCHRP and published by the TRB in the report titled "Human Factors Guidelines for Road Systems" [186].

Table 14 splits the number of drivers involved in crashes for the compliant and noncompliant regions into drivers above 70 and below 70. The table also shows the proportion of drivers over 70 in the compliant and the noncompliant regions. As seen in the table, when considering all seven of the analyzed highway segments, it is noted that the proportion of drivers over 70 who were involved in crashes in noncompliant regions (prop = 0.0385) is higher than that in compliant region (prop = 0.0274).

In an attempt to identify whether this difference was statistically significant, a test of proportions was run between the two samples. For more information about the test the reader is referred to [200,201]. The results of running the test revealed that the higher proportion of drivers over 70 in the noncompliant region was indeed statistically significant at the 90% confidence level (*p-value* = 0.06).

To further analyze the data, drivers were divided into two groups based on gender. Table 14 also shows the proportions for male drivers only. As seen in the table, the proportion of drivers over 70 in the noncompliant regions was, again, higher than that in the compliant regions. Statistical testing of the difference of proportions for male drivers revealed that the difference was statistically significant at a 99% confidence level (*p-value* = 0.01). When female drivers were analyzed separately, there was not enough statistical evidence that the proportion of drivers over 70 was higher in the noncompliant region, however, statistical significance at the 95% confidence level was observed when the drivers were divided into over 75 and under 75 age groups (*p-value* = 0.04). Overall, male drivers are usually more aggressive than female drivers and hence have higher

collision involvement. In Alberta, Transportation Traffic Collisions Statistics show that 4.9% of males over 65 are involved in collisions compared to only 2.7% of females [202].

In general, the results indicate that old drivers could be at a higher risk of collision in regions of a segment where limitations in sight distance are more prevalent. In other words, regions of highways that are not designed to account for the limited skills and the low cognitive abilities of over-age drivers may subject those drivers to a higher collision risk. This finding is perfectly consistent with previous research on the safety performance of older drivers [199,203-207]. In general, that work found that drivers over 70 years of age are at a higher risk of collision compared to other age groups [208].

In fact, the findings show that those drivers actually have a relatively low collision risk when driving on roads which take their limited abilities into account. This means that if roads were designed to accommodate those drivers this would help decrease their collision risk.

9.6   SUMMARY AND CONCLUSIONS

This Chapter assesses the extent to which existing roads are able to accommodate stopping sight distance requirements under different levels of demand, which were deterministically defined based on the outcomes of previous research. The algorithm proposed in Chapter 7 of the thesis is first used to evaluate the available sight distance on crash prone highways in the province of Alberta. The available sight distance on each of those highways is then compared to the theoretical SSD requirements at three different levels (AASHTO, ideal conditions and non-ideal conditions) and the percentage of the segment that is non-compliant to SSD requirements (i.e., the extent to which the analyzed segment meets SSD requirements) is analyzed. Sight distance requirements under the non-ideal conditions were defined for drivers with limited abilities driving in poor conditions, while ideal conditions represented drivers with high skill and high cognitive ability driving in good conditions. For the non-ideal conditions, it was found that ASD fell below the required SSD requirements for up to 20% of the length of the tested segments, while for AASHTO the percent noncompliance reached 6% on some of the segments. Such an observation indicates that high noncompliance rates are expected anywhere between a PRT of 2.5s and 5s.

 The safety analysis conducted revealed that, in general, regions of noncompliance had significantly higher crash density per km when compared to compliant regions of the same

segment. Furthermore, the analyses revealed that old drivers (over the age of 70) were overrepresented in crashes occurring in noncompliant regions compared to crashes in the compliant regions. This difference was statistically significant particularly among male drivers.

The performance-based assessment of stopping sight distance conducted in this Chapter revealed that portions of existing highways cannot accommodate the needs of specific portions of the driving population. Moreover, the results also show a link between design deficiencies on existing roads and crash occurrences. This is an extremely concerning matter that must be addressed in order to avoid future problems that could arise with the anticipated growth in the ages of the driving population. The finding reported in this Chapter indicate the importance of understanding the extent to which existing highways are able to accommodate driver demand and the need to update design guides to account for this information when designing new roads. One limitation of the performance-based assessment conducted in this Chapter is that the proportion of drivers included under the different levels of assessment is unknown. In other words, the proportion of drivers that fall under the category of drivers with limited abilities is unknown. Similarly, the proportion of drivers that are indeed satisfied by AASHTO's requirements is also unknown. These are common limitations when conducting a deterministic assessment. To overcome these limitations, Chapter 10 performs an assessment similar to that conducted in this Chapter but with stochastically modelled driver demand.

10 PROBABILISTIC PERFORMANCE BASED ASSESSMENT OF STOPPING SIGHT DISTANCE

10.1 BACKGROUND

Many components of the sight distance equation are traits of human behaviour, which cannot be modelled deterministically. Whether it is perception-reaction time, driver speed, or deceleration rate these attributes depend on driver capabilities, driving conditions, the situation on hand, personal preference, and age.

To appropriately reflect existing performance on roads, the different components of the sight distance equation must be modelled stochastically. In other words, the different variables in the sight distance equation should be treated as random variables that follow a certain statistical distribution as opposed to fixed variables of known value.

To that end, this Chapter focuses on conducting a stochastic performance-based assessment of stopping sight distance requirements. The analysis conducted in this Chapter is an extension of the multilevel deterministic analysis but one where required sight distance is probabilistically modelled. For instance, instead of using the speed limit or the design speed of the road as the variable representing driver speed to estimate the stopping sight distance required, this variable will be treated as a random variable, which is normally distributed with a mean μ and standard deviation σ. Before conducting such an assessment, it was essential to identify the appropriate statistical distribution that best fits the different components in the sight distance equation. This was done using information documented in the literature and analyzing driver performance observed on the test highways of similar characteristics. More discussion on the specific distributions that were chosen, and the properties of those distributions is provided in Section 10.3. The next section discusses the mathematical notation of Monte Carlo simulation used in the probabilistic assessment.

10.2 SIMULATION & MATHEMATICAL MODELLING

Monte Carlo simulation was used to identify the stopping sight distance requirements of different proportions of drivers on the different test segments. In a Monte Carlo Simulation, the independent

variable Y (required stopping sight distance in this case) is modelled as a random variable with an expected value of $\mu = E(Y)$. Let $Y = g(X)$, where $X \subseteq \mathfrak{R}^d$.

If each of the random variables in $X = (X_1, X_2, X_3 ..... X_n)$ follows a certain probability density function $p(x)$ which is greater than zero on a set of values χ. The expected value of the $g(X)$ can then be noted as follows:

$$E(g(X)) = \sum_{x \in X} g(x)p(x) \tag{26}$$

In cases where the dependent variable is continuous such as the sight distance equation, the expected value of the $g(X)$ is expressed as follows:

$$E(g(X)) = \int_{x \in X} g(x)p(x)dx \tag{27}$$

The Monte Carlo estimator of the random variable is:

$$\tilde{g}_n(X) = \frac{1}{n}\sum_{i=1}^{n} g(X) \tag{28}$$

If $E(g(X))$ exists, then the weak law of large numbers tells us that the probability of $\tilde{g}_n(X)$ deviating from the expected value $E(g(X))$ is close to zero. For any arbitrarily small ε this is denoted as follows:

$$\lim_{n \to \infty} P(|\tilde{g}_n(X) - E(g(X))| \geq \varepsilon) = 0 \tag{29}$$

The Monte Carlo estimator of a random variable is obtained by sampling multiple observations from the test distributions and estimating the expected value and distribution for the response variable.

10.3 STATISTICAL DISTRIBUTION OF RANDOM VARIABLES

As already indicated, stochastic modelling of driver performance on Highways requires identifying the most appropriate statistical distribution to model that behavior and estimating the parameters of that distribution. This must be achieved for all the variables that represent traits of driver behavior and vary between different drivers. In the stopping sight distance equation, this includes, deceleration rates, perception reaction time, and speeds. Estimating the appropriate distribution

and its parameters is often achieved by collecting a sample of observations on the analyzed highways. However, in cases where it is not possible to sample those observations from the test highways, these distributions could be estimated based on the outcomes of similar studies or previous research. For instance, it is difficult to deliberately create hazardous situations on highways to measure the maximum emergency declaration rates or the perception reaction times of drivers in response to those hazards. Hence, for those two variables, information reported in previous studies was used for the simulation.

10.3.1 DECELERATION RATES

Most previous studies assume a normal distribution when modelling deceleration rates, however, there is significant variation in what it considered a reasonable estimated for the mean maximum deceleration rate. As already indicated, AASHTO assumes a 3.4m/s^2 deceleration rate assuming a driver recognizes the danger and decelerates strongly but comfortably before reaching the hazard. However, Fambro, et al. [181], reports that this value is the 10th percentile of the observations and that the mean of those observations was 4.2m/s^2. Lower maximum deceleration rates have also been reported in other research. The Institute of Transportation Engineering (ITE) recommends a deceleration rate of 3m/s^2 [209,210]. Other common rates recommended in previous research include 4.3m/s^2[211]; 3.2m/s^2 Chang, et al. [212]; 3.9 m/s^2[213], and 3.26m/s^2 El-Shawarby, et al. [214]. The variation in maximum deceleration rates estimated motivated researchers such as Gazis, et al. [215] to recommend using a range of values between 0.3–0.5g(2.9-4.9m/s^2) as the maximum deceleration.

In more recent work, Naito, et al. [216] and Miyajima, et al. [217] used a threshold deceleration rate of 0.3 g (2.94 m/s^2) for describing and categorizing deceleration events in emergency braking. Wu, et al. [218] set a lower threshold value of 2 m/s^2 for comfortable longitudinal deceleration (*13*). In Japan, the threshold for detecting deceleration events is usually between 0.2 g and 0.4 g (i.e.,, 1.96 m/s^2 and 3.9 m/s^2, respectively) [216].

Deligianni, et al. [184] also reported a maximum mean deceleration rate of 2.7m/s^2 in their analysis of driver deceleration rates from data collected on roads where the initial speed was 25mph. In another recent study where the authors analyzed the stopping behavior of drivers when trapped in a dilemma zone at a signalized intersection (i.e., hard braking), Li and Abbas [219] fitted a

parabolic model between time to intersection and deceleration rate. Based on the fitted model, the maximum deceleration rate observed was 3m/s^2.

In general, there seems to be a significant variation in what is assumed to be a comfortable maximum deceleration rate in the literature with mean values ranging from as low as 1.96m/s^2 to as high as 4.2m/s^2. Since multiple studies have shown that drivers only maintain the maximum deceleration rate for a short duration of the braking distance [184,219,220], it was decided that using a maximum mean deceleration rate of 4.2m/s^2 recommended by Fambro, et al. [181] was unrealistic. Moreover, the fact that more recent research has reported lower deceleration rates indicates that deceleration rates may have changed due to changes in population demographics or other environmental factors. To account for the aforementioned factors and to use a more conservative estimate for the deceleration rate (i.e., an estimate that does not overestimate the capabilities of the average driver), the values of mean maximum deceleration reported in previous studies were averaged resulting in a new mean maximum deceleration rate of 3.3m/s^2 and standard deviation of 0.85m/s^2.

10.3.2 REACTION TIME

In case of reaction time, previous research has shown that this variable is most appropriately modelled as a lognormal distribution [221-223]. Similar to deceleration rate, studies estimating reaction time for drivers are fairly scarce, however, there is less variability in the estimates.

In early work, Gazis, et al. [215] estimated the mean and standard deviation of the reaction time as 1.14s and 0.32s, respectively. Other values have also been estimated in other early work including (1.3s mean , 0.6 standard deviation) by Wortman and Matthias [224], (1.3, 0.74) by Chang, et al. [212], (1.21, 0.63), and Sivak, et al. [225] (mean 1.25s) have all been estimated in early studies.

In slightly more recent work, Lerner [221] estimated the mean reaction time as 1.5s with a standard deviation of 0.4s. Fambro, et al. [181] reported that the mean of reaction times for unexpected and expected stimuli are 1.3s and 0.7s respectively. Green [185] also defined different levels for reaction time based on expectancy of a hazard. For surprise intrusions the author measured a mean reaction time of 1.5 s. For more information about the range of perception reaction times under anticipated and unanticipated hazards, readers are referred to Section 9.2.1 of this thesis.

Ranjitkar, et al. [226] used data collected to develop a car-following model on a test track to estimate the average driver reaction time. The estimated mean reaction time for individual drivers ranged from 1.27s to 1.55s. Similar to Ranjitkar, et al. [226], Ahmed [222] used data collected to model driver acceleration and lane changing behavior when he estimated mean value of reaction times as 1.34s [14]. The NCHRP report investigating the impacts of human factors on design, estimated the mean reaction time in good visibility at 1.6 s [186].

In general, estimates of mean reaction time observed in previous research range between 1.2 and 1.6 seconds. Most previous studies agree that unanticipated hazards are often associated with longer reaction times. Therefore, for stopping sight distance assessment, it is more appropriate to assume a longer reaction time. In this thesis, a mean reaction time of 1.5s and a standard deviation of 0.4s were used in the analysis.

10.3.3 OPERATING SPEEDS

Operating speed was the other probabilistic variable in the sight distance equation that varies from one driver to another. Accordingly, this variable was also represented as a random variable that follows a probability distribution with a mean μ and a standard deviation σ. Unlike the other two variables, AT uses Weigh in Motion (WIM) stations to collect speed data on a selection of highways around the province.

Unfortunately, only one of the prone highways considered in this analysis (Highway 28) had a WIM station and, hence, speed data was only available on that highway among those considered in this assessment. To understand speed behavior on the test segment, speed observations over 12 months were analyzed and the mean and the standard deviation of speeds was computed. The mean speed was estimated at 110.2km/h and the standard deviation of speeds was estimated at 10.55km/h.

To overcome data limitations on other highways, data from all WIM stations located on 2-lane undivided segments in Alberta (Highway 14, 37, 44, and 35) was analyzed and the mean and standard deviation of speeds was computed. In case of Highway 88 and Highway 55, these highways were within close proximity of Highway 44. In fact, the analyzed segment on Highway 88 was an extension of Highway 44. As a result, the distribution of speeds on Highway 88 and Highway 55 was based on the speed behavior on Highway 44, where the mean speed was 108.4km/h and the standard deviation was 9.4m/s^2.

For the remaining highways, the most conservative estimate of the mean and the standard deviation observed on all highways was used where WIM stations existed. The assessment revealed that the mean of speeds on all highways varied between (107.6km/h - 110.2km/h), while the standard deviation varied between (10km/h and 10.55km/h). Therefore, the most conservative estimates were those obtained on Highway 28 and, as a result, these estimates were used on all highways, except Highways 88 and 55.

10.4 MODELLING

After identifying the most appropriate statistical distribution for each of the random variables in the sight distance equation and identifying the parameters for each of those distributions it was possible to run the Monte Carlo Simulation model. The simulation code was written in MATLAB and 10 million trials were conducted before identifying the distribution of the required sight distance on each of the test highways.

In each trial, the code estimates a value for each of the Random Variables in the sight distance equation and computes a corresponding value for the required stopping sight distance. The code then stores the value obtained for the required sight distance based on the inputs used in that trial and runs through 10 million iterations. The histograms of the three random variables (speed, deceleration rate, and reaction rime) generated as a result of the 10 million trials are shown in Figure 90 a, b. and c. Furthermore, the histogram of the estimated Sight Distance for the 10 million trials is plotted in Figure 91a. As evident in the figure, the distribution for sight distance information is more appropriately modeled as a lognormal distribution. This is can be validated by viewing the plot in Figure 91b which shows histogram of the log transformed sight distance estimates.
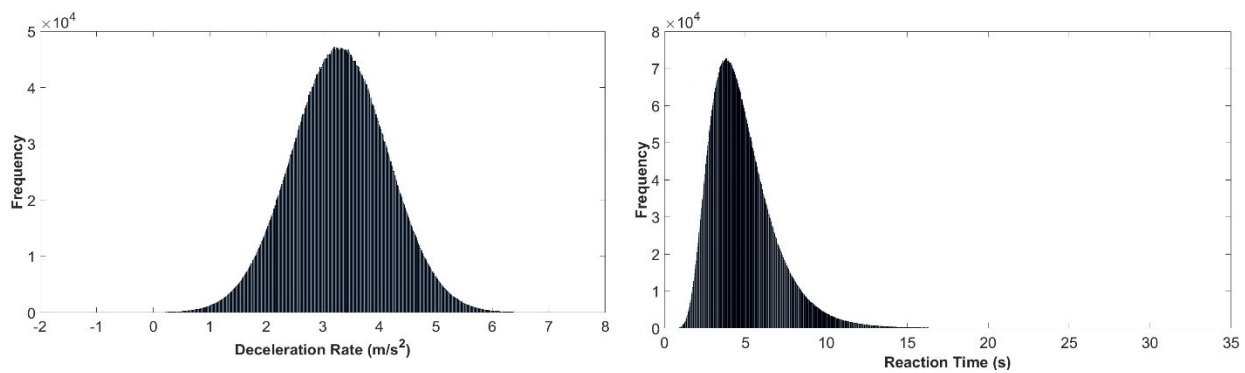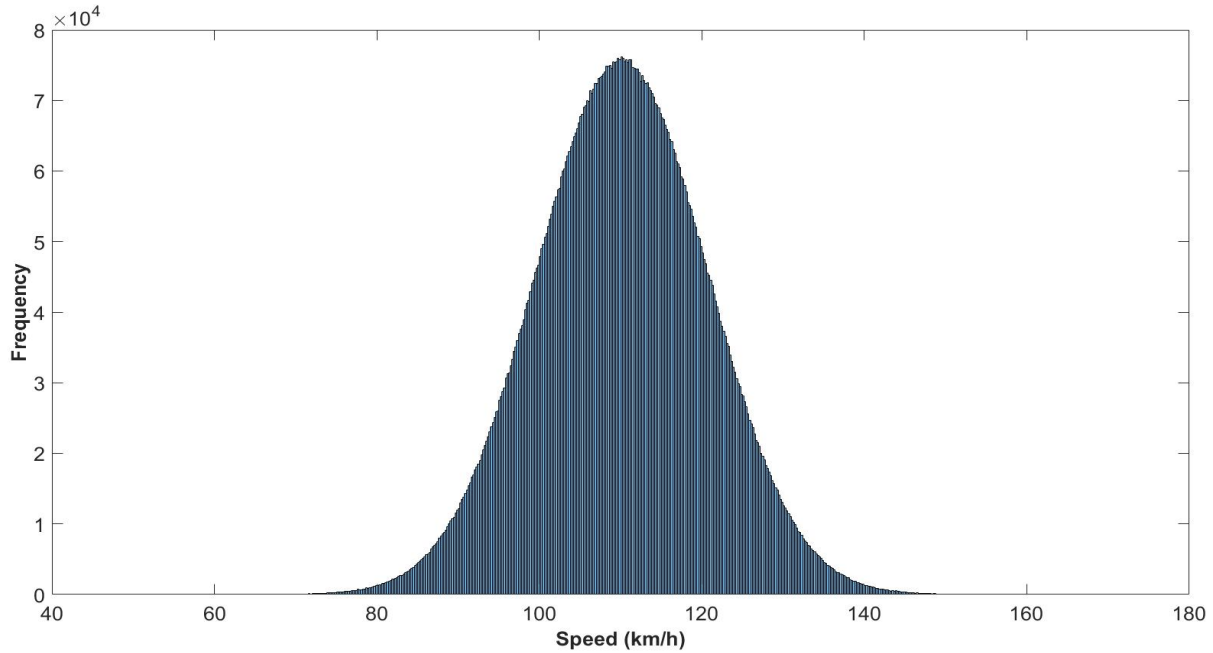
Figure 90: Frequency Distribution of Random Variables
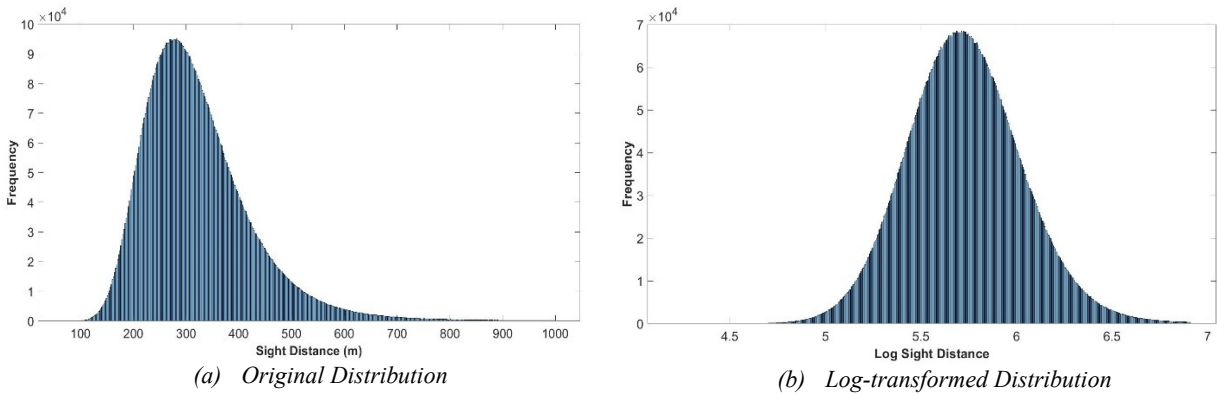
(a) Original Distribution *(b) Log-transformed Distribution*

Figure 91: Frequency Distribution of Simulated Stopping Sight Distance

To estimate the sight distance required by different proportions of drivers, the probability density function, the cumulative density function, and the inverse cumulative density function for required stopping sight distance were all estimated.

Let x represent a random variable that denotes the stopping sight distance required by a driver. If the stopping sight distance was lognormally distributed with a location parameter μ and a scale parameter σ then the probability of a driver requiring x amount of stopping sight distance can be estimated using the following probability density function.

$$f(x) = \frac{1}{\sqrt{2\pi}\sigma x}\exp\left(-\frac{(\ln x - \mu)^2}{2\sigma^2}\right) \text{ for } x \geq 0 \tag{30}$$

192

Similarly, the cumulative probability of the entire driving population requiring a stopping sight distance less than or equal to t can be estimated using the following cumulative distribution function.

$$F(x) = \int_0^x \frac{1}{\sqrt{2\pi}\sigma t} \exp\left(-\frac{(\ln t - \mu)^2}{2\sigma^2}\right) dt \text{ for } x > 0 \qquad (31)$$

Since we were interested in the stopping sight distance required by a specific proportion of drivers at a specific quantile, the inverse cumulative distribution function of the stopping sight distance, also known as the quantile function, had to be estimated. Let x_p represents the pth quantile of x, in that case, x_p can be denoted as follows.

$$x_p = F^{-1}(p \mid \mu, \sigma) = \{x : F(x \mid \mu, \sigma)\} \text{ for } 0 < p < 1 \qquad (32)$$

where p can be estimated using the following expression.

$$p = F(x \mid \mu, \sigma) = \frac{1}{\sigma\sqrt{2\pi}} \int_0^x \frac{e^{\frac{-(\ln(t)-\mu)}{2\sigma}}}{t} dt \qquad (33)$$

The inverse cumulative distribution function (CDF) was used to estimate the sight distance required by drivers at the 10th, 30th, 50th, 70th, and 90th quantiles.

Figure 92 a and b represent the probability density function (PDF) and the CDF of the estimated sight distance.
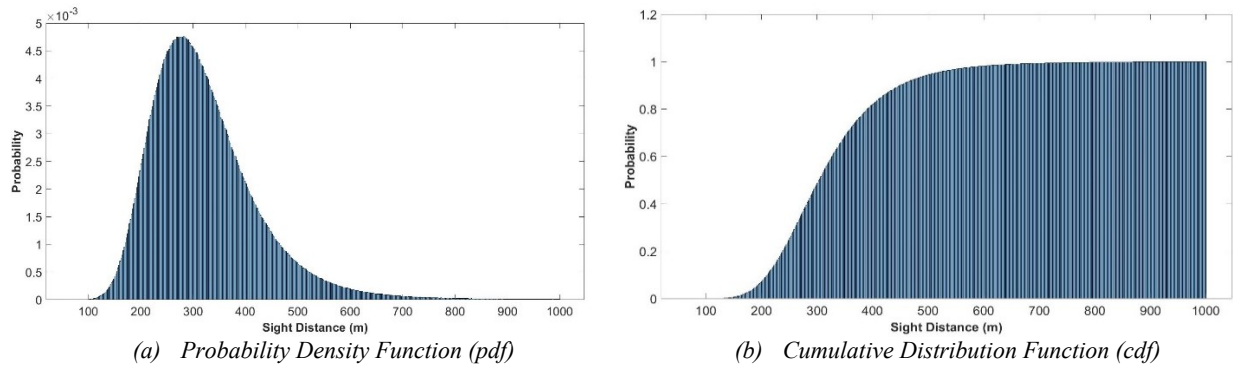
(a) *Probability Density Function (pdf)*   (b) *Cumulative Distribution Function (cdf)*
Figure 92: Distribution of Simulated Stopping Sight Distance

Using the simulation results, it was possible to understand the amount of sight distance demanded by different classes of the driving population and the ability of the existing road infrastructure to handle that demand. This was done by first estimating the available sight distance on the test

highways using the Sight Distance estimation algorithm proposed in Chapter 7 of this thesis. The sight distance required by different classes of drivers was then evaluated based on the simulation results and compared to the available sight distance.

An assessment similar to that presented in Chapter 9 of this dissertation was conducted whereby, if the available sight distance on a test highway fell below the theoretical sight distance then limitations in sight distance were flagged and the total length of the noncompliant region was computed. The main difference here is that the theoretical sight distance was not a value that was computed based on a deterministic equation, instead, the value represents the needs of a specific proportion of drivers. This helps identify the exact proportion of the driving population that would be impacted by limitations in sight distance at a particular location. For instance, if the available sight distance falls below 90% quantile, this indicates that the test segment fails to satisfy the sight distance requirements of 10% of the driving population. Similarly, if the available sight distance falls below the 30% quantile, this indicates that the test segment fails to satisfy the sight distance requirements of 70% of the driving population.

10.5 RESULTS AND DISCUSSION

Based on the simulation result and the quantiles estimated using the inverse CDF, it was found that 10% and 30% of the population require an SSD that is greater than 451m (437m on Highways 55 and 88) and 360m (350), respectively. Similarly, 70% and 90% of the driving population require a stopping sight distance that is greater than 263m (256) and 210m (206), respectively. Figure 93 shows a sample of the figures on that both the required stopping sight distance and the available sight distance are plotted. From top to bottom, the horizontal lines drawn across the plots show the following:

(i)   The dotted red line shows the minimum SSD demanded by 10% of the population (10% level or the 90% quantile),

(ii)   The dashed magenta line shows the minimum SSD demanded by 30% of the population (30% level),

(iii)   The black line shows the minimum SSD demanded by the 50% of the driving population (50% level),

(iv)   The dashed blue line shows the minimum SSD demanded by 70% of drivers (70% level)

(v)   The dotted green line shows the minimum SSD demanded by 90% of drivers (90% level).
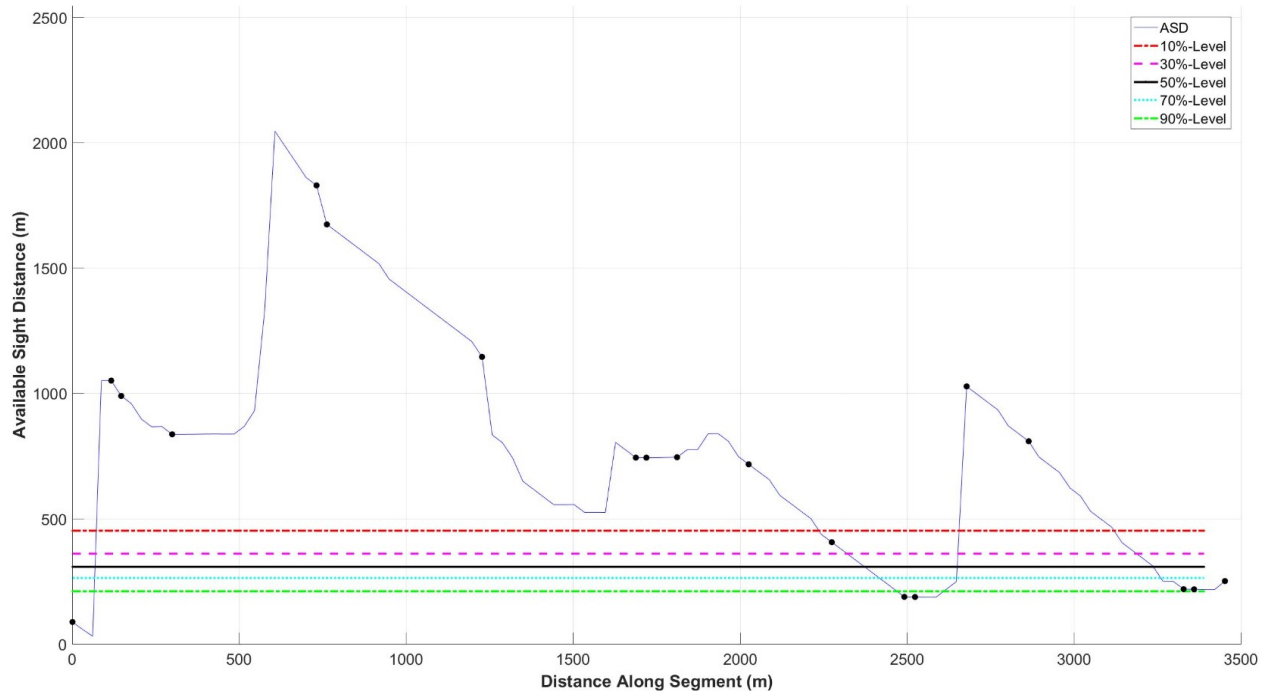
Figure 93: ASD Highway 20 Segment 4-8 (Black Dots Represent Collisions)

Before discussing the results, it is worth pointing out that the performance-based assessment conducted in this Chapter was conducted on the same Highways as in Chapter 9 with the exception of Highway 63, where data was only available on a short 2.5km section. Therefore, readers interested in more information about the test segments are referred to Section 9.4 of the thesis.

10.5.1 GEOMETRIC PERFORMANCE (NON-COMPLIANCE RATES)

Figure 94 represents the noncompliance rates expressed as a percent of the total length of the prone highway segments tested in this Chapter. The noncompliance rates were computed by dividing the length of the noncompliant region on the test segments by the total length of the analyzed segment. The length of the noncompliant region was the total length where the available sight distance fell below the required SSD at a certain level. The noncompliance rates were computed for all five bounds of assessment.
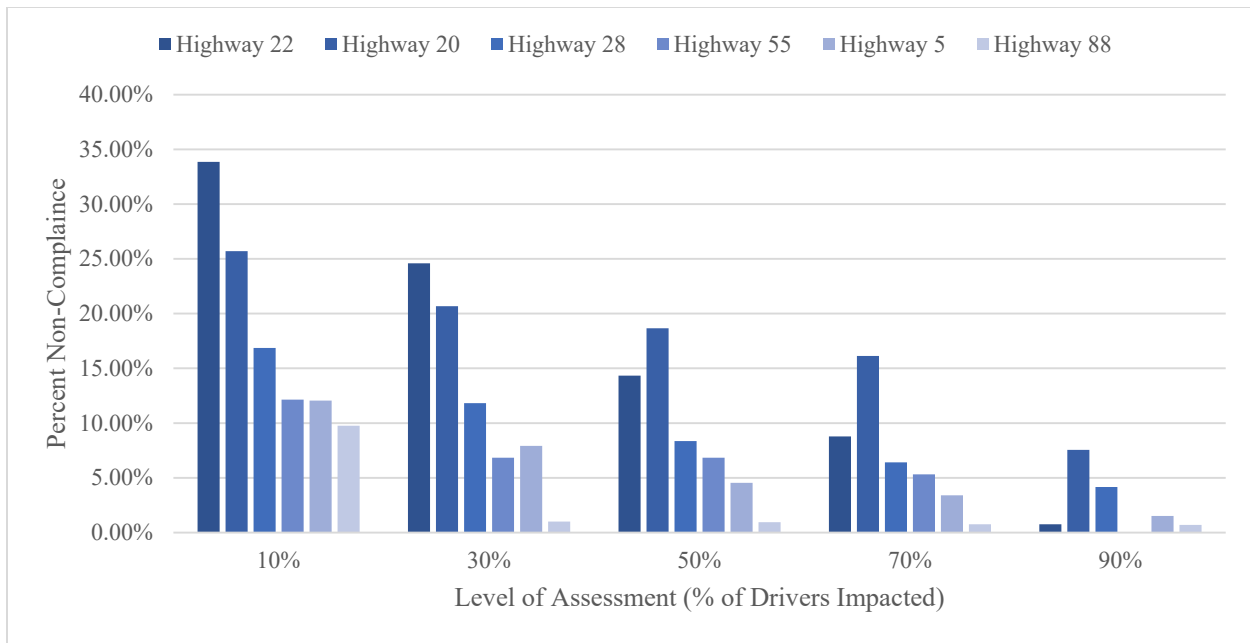
Figure 94: Percent Non-Compliance

As evident in the figure, noncompliance rates range from 0% to 34%. On average, the highest noncompliance rates across all levels of assessment were observed on Highway 22, which was closely followed by Highway 20 and Highway 28. In contrast, Highway 88 had the lowest levels of noncompliance to SSD requirements.

Figure 95, shows the average percent noncompliance observed across all segments at the different quantiles (i.e., the different levels of assessment). The average percent noncompliance on the test highways at the 10% level was 18%. This shows that, on average, 18% of the tested road segments are not able to satisfy the stopping sight distance requirements of 10% of the driving population. In other words, 10% of the driving population experience sight distance limitations on 18% of the length of the highway. This proportion of drivers could be older drivers or drivers with special needs.

196
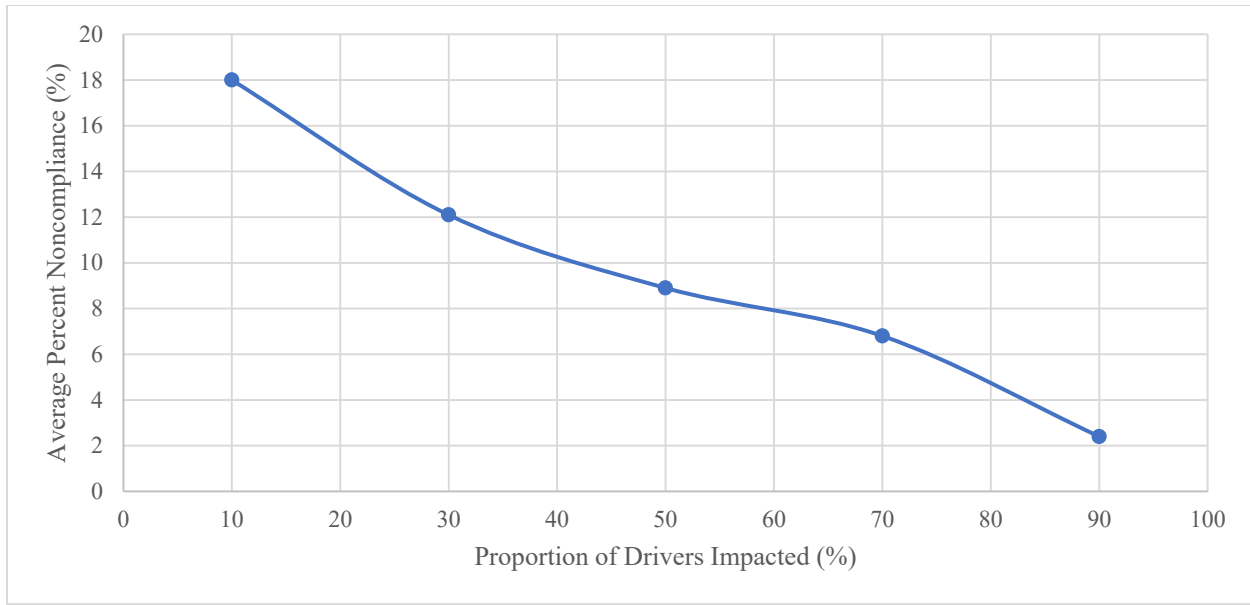
Figure 95: Average Percent Non-Compliance

At the 30% level, the average percent noncompliance on the tested highway segments stood at 12.1%, which indicates that, on average, 30% of the driving population experience limitations in SSD for 12.1% of their time driving on the test segments. It is worth noting here that the percent noncompliance at this level is similar to that estimated under the non-ideal case discussed in Chapter 9 of this thesis (11.2%). This indicates that the non-ideal level defined in the multi-level analysis represents the needs of 30% of the driving population.

On the 50% level, mean stood at 8.9%; the highest noncompliance rates at the 50% level as well as the 10% and 30% levels were observed on Highway 20 and Highway 22. It is worth noting that the total length analyzed on these two highways was 12km (the longest among all the other analyzed segment). At the 50% level, the noncompliance on Highway 20 and Highway 22 was 19% and 14%, respectively. In units of length, this means that 2.28km and 1.68km of the 12km on those highways failed to satisfy the SSD requirements for 50% of the driving population.

At the 70%-level (i.e., the level representing the minimum SSD required by 70% of the population, the average percent noncompliance to those requirements was 6.8%. This means that, on average, 6.8% of the test segments failed to satisfy the needs of 70% of the driving population. In terms of actual length, this translates into 3.5km of the 52km analyzed on all the test segments.

An interesting finding when observing the percent noncompliance approximated at the 85% level based on the trend (see Figure 95), is almost identical to that estimated when using the SSD

requirements defined by AASHTO's deterministic equation. This finding is extremely alarming since it indicates that, when designing roads to meet AASHTO's SSD requirements, the roads are actually designed to satisfy the requirements of only 15% of the driving population. Such a finding is only revealed by conducting the probabilistic assessment. That being said, it is worth emphasizing that, on average, 82% (100-18=82, from Figure 95) of existing road segments provided much more than the minimum requirements specified by AASHTO. In fact, this 82% satisfies the needs of 90% of the driving population (10% level).

The fact that AASHTO's requirements correspond to the needs of only 15% of the population is interesting since the values for deceleration rate and perception reaction time recommended in AASHTO, despite being deterministic, are supposedly based on the 10th and 90th percentile of drivers, respectively [181]. It is worth noting though that these values were estimated based on empirical studies conducted more than two decades ago. Hence, changes in the demographics of the driving population might have affected those values. Another potential cause is that the posted speed limit is often used to predict the SSD required using AASHTO's deterministic equation, which might not be appropriate. The speed data collected on two lane undivided segments including Highway 28, which was used to estimate speed data in the simulation, showed that the mean speed on those highways ranged from 107km/h and 110km/h, even though the speed limits on all those highways is 100km/h.

At the 90% level, the average percent noncompliance was 2.4%. In other words, the available sight distance only drops below that needed by 90% of the driving population for 2.4% (i.e., 1.25km) of the 52km analyzed.

10.5.2 SAFETY PERFORMANCE

The results presented in the previous section show that a substantial portion of the analyzed highway segments do not meet stopping sight distance requirements particularly at the 10%, 30% and 50% levels. Furthermore, the analysis shows that even at the 70% level (i.e., the level of SSD required by 70% of the driving population) percent noncompliance rates of up to 16% are observed on one of the highways. To understand the impacts of such design deficiencies in SSD requirements on safety, a similar assessment to that conducted in Chapter 9 of the thesis is carried out whereby crash densities at locations of noncompliance were compared to crash densities on compliant regions on each of the analyzed segments at the different levels of assessment.

Since the same traffic volume travels through both the compliant region and the noncompliant region of the same highway segment, crash densities per length were used to compare safety at the two regions. Crash densities were calculated considering crashes that occurred on each road segment in the period between 2009 and 2014.

Figure 96 represent the noncompliance rates and the corresponding changes in crash densities observed on each of the analyzed road segments at the five different levels of analysis. Increases in crash densities in the noncompliant regions measured as a ratio of noncompliant to compliant crash densities range from 0.98 to 18.8. The highest increases were observed on Highway 88 despite the segment having the lowest percent noncompliance. On Highway 88, noncompliant regions experienced a crash density that was, on average, 12 times higher than that in compliant regions. It is worth noting here that, unlike all the other highways analyzed, Highway 88 passes through a provincial park (Lesser Slave Lake Provincial Park). As a result, the existence of wildlife on the segment is much more likely than other segments, which explains the high proportion of animal collisions and the high crash densities in general on the segment and particularly in the noncompliant regions.

Highways 22, 20, and 28 (the highways with the highest noncompliance rates) experienced a change in crash densities in the noncompliant regions that ranged between 2 and 3.21 times that in the compliant regions. This indicates that, on most of the analyzed segments, crash densities in the regions noncompliant to SSD requirements are twice to three times as high as crash densities in the compliant regions. In fact, this was the case on four of the six analyzed segments.
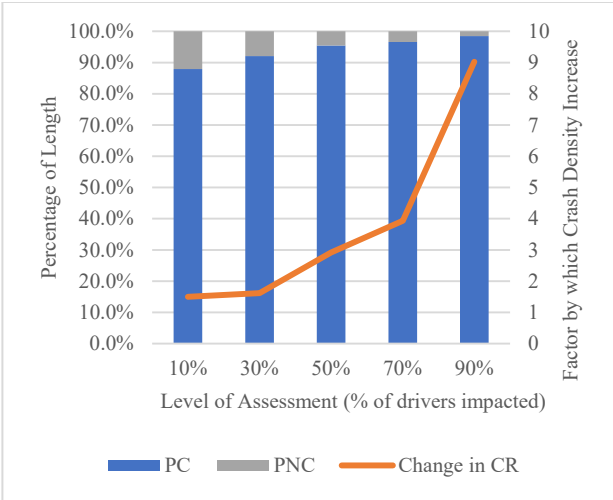
(a) Highway 5
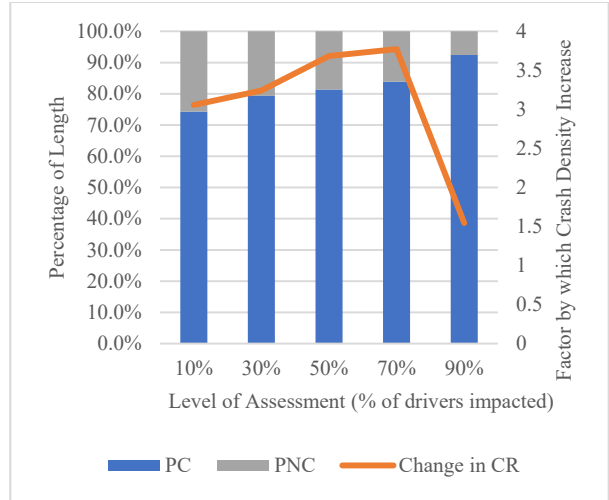
(b) Highway 20
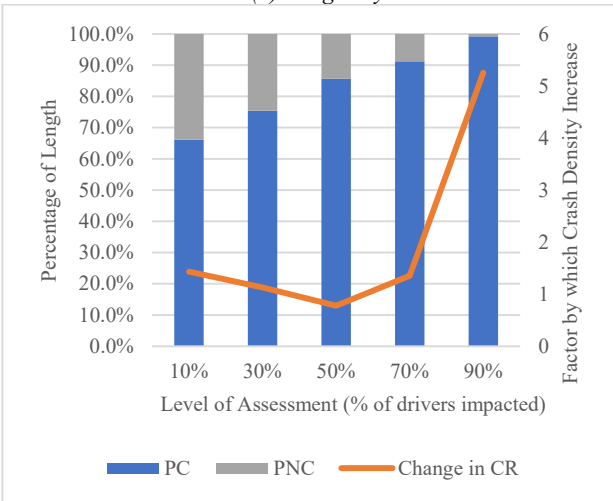
(c) Highway 22
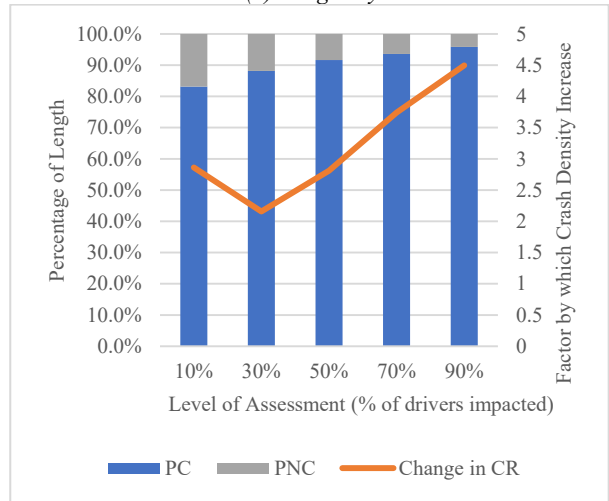
(d) Highway 28
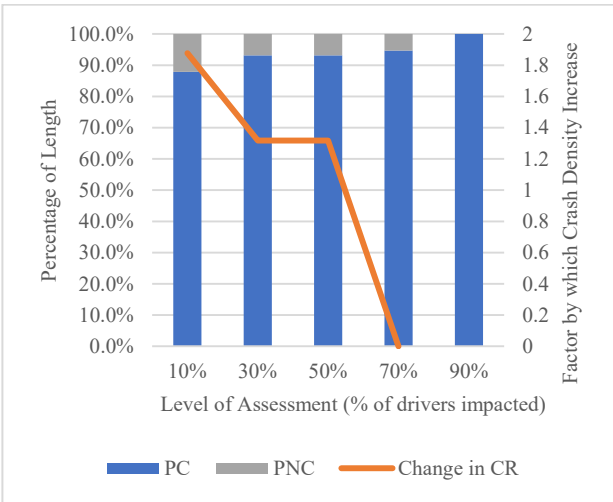
(e) Highway 55
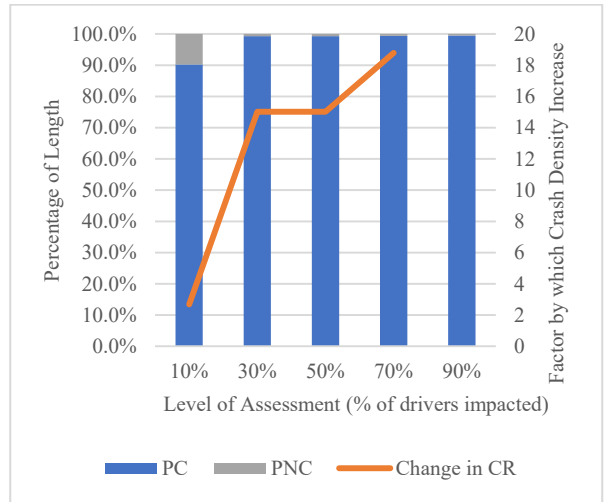
(f) Highway 88

Figure 96: Percent Non-Compliance and Corresponding Change in Crash Density

200

In general, the results show that the higher the population impacted by the limitations in sight distance the more critical the impacts are from a safety perspective (i.e.,, the higher the increase in the change in crash densities observed in the noncompliant region compared to the compliant region). This was observed on five of the six test segment as, evident in Figure 96, that represent a total length of 48km. For those segments, noncompliant regions at the 70% and 90% levels were associated with higher increases in crash densities compared to noncompliant regions at the 10% and 30% levels. This is the case even though the noncompliant regions impacting a higher population of drivers is significantly shorter than the noncompliant regions where a lower population of drivers is impacted.

The results presented in this section and the findings reported in Chapter 9 of the thesis indicate the importance of designing roads that meet the demand of as much of the driving population as possible. The simulation results indicate that, in order to meet the sight distance required by 70% of the population, a design stopping sight distance value close to 360m must be used, as opposed to the 193m recommended by AASHTO on highways with a speed limit of 100km/h. When observing the performance on existing infrastructure, it was found that, out of the six segments analyzed, sight distance requirements demanded by 70% of the population were only satisfied on a single highway, with two others coming close. On average, the results show that 12.14% of the analyzed segments do not meet the 360m requirements (6.3km of the 52km analyzed).

These findings are actually aggravated when considering the fact that the deterministic SSD equation assumes that drivers maintain the maximum deceleration rate for the entirely of the deceleration time, which has been proven untrue by other researchers [184]. Furthermore, it is also noteworthy that the SSD equations do not consider the impacts of adverse weather conditions, which are common in places like the province of Alberta. Adverse weather conditions can impact the ability of drivers to view hazards and respond to those hazards in a timely manner (i.e.,, braking distances). Although drivers are expected to compensate for those conditions by reducing speeds, these factors along with the potential changes in population demographics discussed in Chapter 9 must all be considered when the intention is to design forgiving highways that account for human errors.

To estimate the anticipated improvements in safety if 360m of sight distance were provided along the entirety of the test highways, the crash densities in the noncompliant region at the 30% level

were re-estimated assuming it would now become compliant. Here it was assumed that providing more sight distance in the noncompliant regions would bring crash density in those regions to a level similar to that in the compliant regions (i.e.,, that region would become compliant). Hence, the expected number of crashes in the noncompliant region after it became compliant were calculated as follows:

$$\text{Expected Collisions} = L_{\text{Non-Compliant}} \times CD_{\text{Compliant Region}} \qquad (30)$$

where, $L_{\text{Non-Compliant}}$ is the length in km of the region that is currently noncompliant at the 30% level (i.e., the region where the ASD is currently below 360m), and $CD_{\text{Compliant Region}}$ is the current crash density in crashes/km calculated in the compliant region at the 30% level.

Table 15: Expected Change in Collisions

Highway	Expected Collision Frequency	Percent Reduction
22	6.20	-0.11
55	2.28	-0.24
20	14.40	-0.71
28	5.10	-0.54
88	0.37	-0.93
5	3.09	-0.38

To quantify the changes in safety expected if such a change were to be implemented, the change in collisions was computed using the simple before after method [227]. Table 15 shows the changes in crashes expected on each of the highway test segments. As evident in the table, the reduction in collisions expected as a result of such a change range from 11.4% to 92.5%. On average, the change was estimated at 48.4% reduction in crashes. It is important to note that this is a simplified estimate of potential improvements on the test segments that does not account for many confounding factors, hence, it is only intended to give the reader a sense of the potential improvements that might occur.

10.6 Summary, Conclusions, And Recommendations

This chapter conducts a performance-based assessment of stopping sight distance on a selection of crash prone highways in Alberta. The Chapter utilizes tools developed in Chapter 7 of the thesis to assess available sight distance on the test segments (the supply). The demand for stopping sight distance is then modelled probabilistically using a Monte Carlo simulation, to accurately reflect the needs of the driving population. Failure to meet SSD required by drivers along each of the test

segments was then quantified and the safety impacts were estimated. The assessment revealed that a significant proportion of the analyzed highways did not satisfy the needs of up to 70% of driving population, with noncompliance rates reaching 16% of length on some of the segments. Moreover, the assessment also highlighted that crash densities in regions where SSD requirements were not met were, on average, two to three times higher than crash densities in compliant regions of the same segment.

The outcomes reported in this chapter must be taken into consideration when designing new highways to ensure that highway segments are able to accommodate the needs of as much of the driving population as possible. Moreover, the findings should also be used to take corrective action on existing highways. Although changing alignments to increase available sight distance on existing segments, might not be feasible due to the high costs associated with such changes, alternative approaches could be adopted. This includes simply reducing speeds on roads by changing speed limits or introducing variable speed limits along the segments to accommodate drivers in regions of noncompliance.

For the design of new highway segments, adopting the performance-based approach proposed in this chapter would involve replicating the probabilistic assessment to understand the extent to which highways similar to that which is being designed satisfy driver demands before deciding on an appropriate design value for SSD. It is worth noting here that the assessment framework adopted in this chapter is not limited to the assessment of Stopping Sight Distance. The same procedure could be adopted to identify the appropriate radius for the design of horizontal curves or any other design features.

10.7 PERFORMANCE BASED DESIGN FRAMEWORK

Results presented in this Chapter and in Chapter 9 demonstrate the importance of adopting a PBD approach when designing new components of highway infrastructure. This helps create a feedback loop whereby limitations in existing design are identified and accounted for in future design. PBD is essential for entities looking to adopt a driver-centric safe systems approach where roadway infrastructure is designed in a forgiving manner that accommodates driver error. This objective can only be achieved if driver demand for a particular design attribute and the ability of infrastructure to handle that demand (supply) are understood and appropriately modelled.

To assist in the adoption of a PBD approach, a framework that summarizes the design process is presented in Figure 97. As evident in the figure, the process is split into three key stages (i) Stage I involves defining performance metrics, which account for the demands of the driving population and estimating the design requirements that satisfy that demand. (ii) Stage II involves estimating the supply (i.e measuring design attribute on segments similar to that to be designed) this is done to assess the performance on existing segments and estimate the impacts of the proposed design. (iii) Stage III involves conducting the performance-based assessment whereby geometric performance improvements and the anticipated safety impacts of using the proposed design are estimated.

In the first stage of PBD, the performance metrics are converted into minimum design requirements through a probabilistic assessment of driver demands as demonstrated in Chapter 10, Section 10.3 of this thesis. In the second stage, large-scale assessment of the geometric element to be designed is conducted on a selection of existing highways to measure the 'supply'. Phase I (Chapters 4 through 7) of this thesis demonstrates how such information could be extracted in an efficient and accurate manner for a selection of geometric design elements on highways scanned using LiDAR technology. This step is integral to both the geometric and the safety assessments conducted in Stage III.

In Stage III, the performance-based assessment demonstrated in Phase II (Chapters 9 and 10) of the thesis is replicated whereby the ability of the existing infrastructure to handle that demand is first assessed and the safety impacts of the failure to do so are quantified.

The geometric and/or operational integrity of existing highways is assessed by estimating how often the supply measured on existing roads falls below the modelled demand. The potential improvements (could be geometric or operational improvements) the proposed design provides compared to existing conditions are then estimated. For instance, in case of the sight distance assessment conducted in Chapter 10, the improvements could be measured by quantifying the difference in percent noncompliance between AASHTO's design requirements and those formulated based on the performance metrics defined for the new design (i.e.,, at the 70% level). If the improvements are not satisfactory, the design requirements are adjusted, and the performance is reassessed.

Once the design team is satisfied with the geometric or operational improvements expected as a result of the proposed design, the safety impacts of the design are then assessed. Assessing safety performance is conducted on highways similar to the one to be designed where collision information is available. Similarity here includes many features such as the number of lanes, land use characteristics, traffic and roadside development. If the changes are expected to cause negative safety impacts, the design requirements can be updated, and the impacts can be reassessed.

Although it is important to ensure that performance metrics and the corresponding design requirements proposed by the design team do not have any negative safety impacts (see the lower end of the flowchart in Figure 97), the motivation when defining performance metrics does not always have to be to improve safety. In fact, setting a performance metric that is related to safety is an ethical dilemma that has for long challenged experts in the field (what is an acceptable level of safety). Therefore, the framework proposed in this thesis focuses on ensuring that the safety record anticipated on the proposed design represents an improvement on exiting conditions even if the performance metric selected is not related to safety. For instance, in case of vertical clearance requirements at a new bridge, the performance metrics could be to satisfy the demands of 70% of heavy vehicle traffic expected on the road (i.e., improve the throughput of commercial vehicles along a certain route). The minimum clearance required to satisfy that metric could then be estimated based on the distribution of the heights of heavy vehicles on existing highways. The next step would involve assessing the potential improvement in the level of service for heavy vehicles on a specific route or set of routes as a result of the change. The level of service assessment would take into account vertical clearance information at all existing bridges within close proximity of the proposed bridge, which could be quantified using the algorithm proposed in Chapter 6 of this thesis. The potential improvements in mobility as a result of the proposed design are then quantified.

Another factor that is important to integrate into the design process is the cost of the proposed design changes. However, in the driver-centric PBD approach proposed in this thesis, assessment of economic feasibility is only done after ensuring that the anticipated safety performance on the proposed design is satisfactory, as illustrated in final stage of Figure 97.
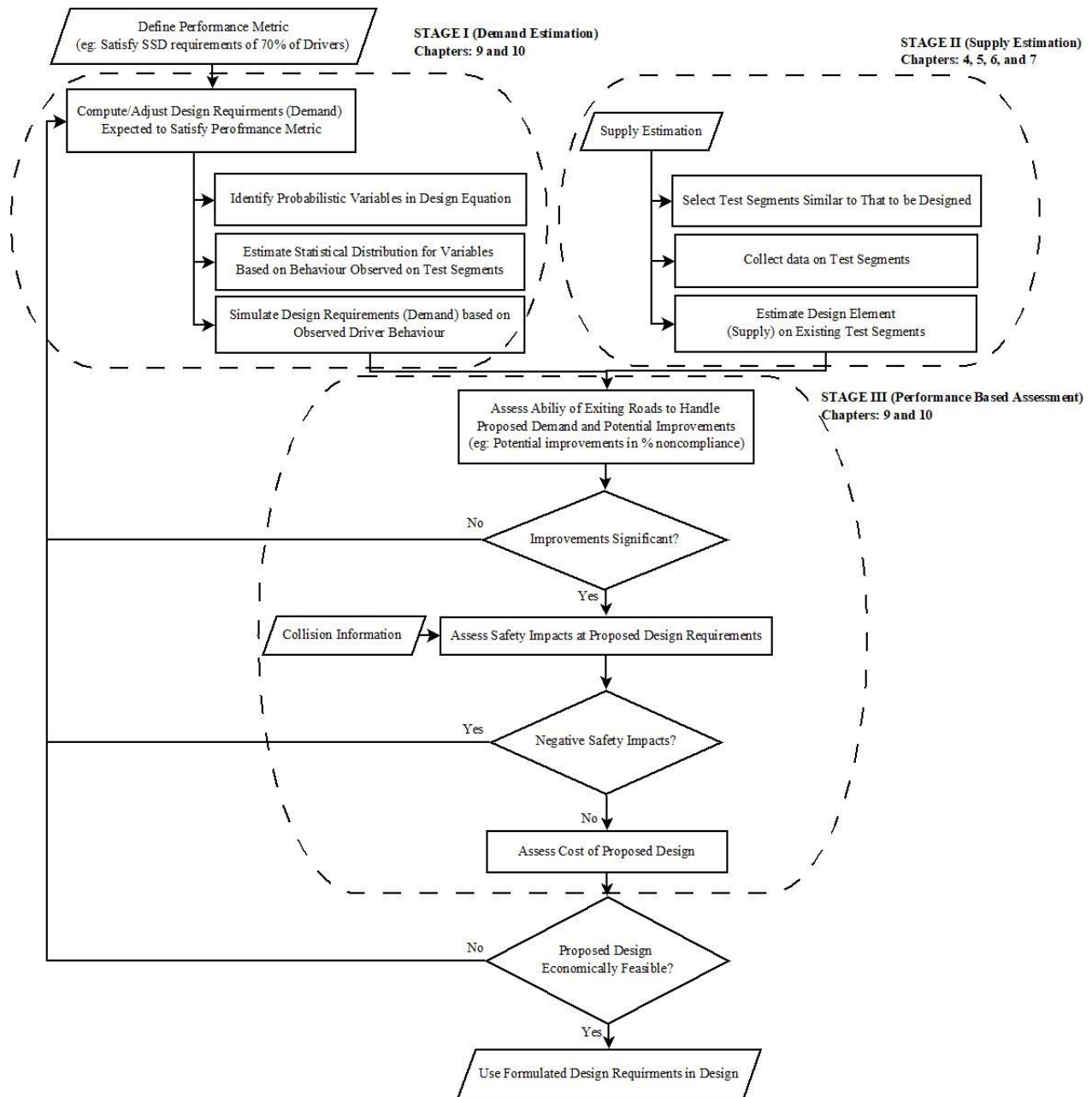
Figure 97: Performance Based Design Framework

Although this thesis presents a systematic framework and develops tools that could facilitate the adoption of a performance-based design approach, it is important to emphasize the challenges associated with adopting such an approach. Even with the existence of the tools that facilitate efficient assessment of geometric design elements and the abundance of information about collisions and safety, the expertise required to conduct advanced statistical assessments of the relationship between safety and design elements represents a challenge to some agencies. That

being said, a similar approach has been successfully implemented in seismic design, which demonstrates that the adoption of such an approach is practical.

11 CONCLUSIONS

11.1 RESEARCH SUMMARY

The first phase of this thesis develops a set of algorithms that facilitate efficient extraction and assessment of important road features from LiDAR point cloud data. Novel automated algorithms are developed to perform the following:

- Extract road cross sections and assess their slope.
- Detect horizontal curve and extract information about their attributes.
- Detect overhead objects including bridges and assess clearance at each of those objects.
- Perform three-dimensional assessment of available sight distance along highway corridors.

All these are all important elements of road infrastructure, which are extremely critical to the safe and efficient operation of Highways. In fact, highway design guides dedicate entire chapters to principles governing the design of alignments (vertical and horizontal) and road cross sections. Furthermore, in its review on the feasibility of conducting a performance based analysis of highways, the NCHRP identifies cross sectional slopes, vertical clearances, and sight distance as critical geometric features that cannot be efficiently assessed and linked to performance metrics using existing surveying tools [53].

Using the algorithms proposed in this thesis, information about these geometric elements, which is typically collected in long site visits or using error-prone graphical assessment, is made readily available to transportation agencies on an unprecedented scale. This provides transportation agencies with access to an abundant amount of information about highway infrastructure and creates huge opportunities in the areas of infrastructure management and highway design. In fact, the ultimate contribution of this research lies in facilitating the means by which the process of transportation infrastructure management and highway design could be transformed into one that is more informed and data-driven using the proposed algorithms.

The second phase of the thesis focuses on demonstrating how the algorithms developed in phase one of the thesis could be used to assess the ability of the road infrastructure to handle road user

207

demands and the safety impacts of the failure to do so. This done with the aims of facilitating the adoption of a novel performance-based design approach.

Specifically, phase two of the thesis is dedicated to conducting a performance-based assessment of SSD on top crash-prone highways in Alberta, Canada. To achieve this, the sight distance assessment method proposed in Chapter 7 of the thesis was first used to perform a large-scale assessment of available sight distance on a selection of test highways (measuring supply). The stopping sight distance for different categories of the driving population was then modelled in both a deterministic and a stochastic manner (quantifying the anticipated demand). The relationships between the level of conformance to stopping sight distance requirements at the different levels of demand were then assessed. Moreover, the relationships between noncompliance to SSD requirements and safety performance on each of the test segments was also investigated. Unfortunately, performing such an assessment was not possible in the past due to the lack of an efficient method that can be used in the large-scale assessment of road geometric elements (supply). As a result, previous work in this area was limited to assessments performed at specific locations along a highway where design information is either manually collected or estimated based on dated design drawings. In this thesis the data used in the performance-based assessment was collected along the entirety of the crash prone segment reflecting existing conditions on the segments. In fact, prior to this work, there has been a general lack of studies that assess the relationships between failure to meet SSD requirements and safety, with the most recent study performing in such capacity dating back to 1997 [228].

The performance-based assessment conducted in phase two of the thesis demonstrates how designers and engineers could analyses the integrity of existing road infrastructure and assess the interaction between variation in road design elements along highways and driver performance. Such an assessment provides insights into the ability of existing infrastructure to handle stochastically modelled demand. Moreover, such assessment also facilitates the adoption of a novel performance-based design approach whereby design requirements are formulated based on the demands of the driving population.

11.2 RESEARCH CONTRIBUTIONS

The contributions of this research span theory and practice to open new avenues in the field of transportation. The next few paragraphs consist of a detailed discussion of those contributions,

while focusing on the potential value of the work in the areas of transportation infrastructure management and highway design.

11.2.1 INFRASTRUCTURE MANAGEMENT

As already noted, the tools developed in this thesis can be used to help agencies responsible for infrastructure management in the efficient inventory and assessment of assets on their highway network. Whether it is bridge clearances, road slopes, or sight distances, efficiently gathering information about these elements is essential to the success of any infrastructure asset management program. In current practice, collecting such information is a tedious process where long site visits are required and where major disruption to traffic could occur due to road closure and mobilization of surveying equipment. Moreover, the process is also unsafe, labour intensive and error-prone since it requires surveying crew to be constantly present on-site while conducting manual measurements of different features.

The novel algorithms developed in this research make information about geometric elements of roads readily available to transportation agencies. Moreover, the efficiency of the developed algorithms means that inventorying different features can be achieved in a timely manner and on a network-level. This helps transportation agencies enrich their database with information on the location and attributes of each asset on the highway network. Having this information on such a large scale helps agencies optimize their resources when making decisions on the replacement or maintenance of different design elements on the highway network [17].

The proposed algorithms could be used to assess the conditions of different geometric design elements on a highway without experiencing the burden associated with conventional surveying methods. For instance, agencies concerned about changes in sight distance on a highway due to relaying or resurfacing a road could use the proposed methods to efficiently assess sight distance and identify any issues that could have ascended due to the resurfacing. Similarly, if an agency suspects that road slopes or superelevation might be ineffective, these features can be assessed using the developed algorithms to identify locations where corrective action might be required. The speedy assessment made possible using the proposed algorithms helps agencies take appropriate action to address geometric defects on roads in a proactive manner (i.e., before those defects become irreversible and before they start causing safety problems). In the long run, the

ability to extract geometric information about roads in such an efficient manner could create a paradigm shift in how road safety audits and geometric assessments of roads are conducted.

In addition to providing the tools to extract details about important road geometric elements from LiDAR, this thesis also provides insights into the impacts of using point clouds with a reduced point density on the feasibility of the extractions. As already noted, point cloud data can be collected using different LiDAR systems and even using photogrammetric techniques, however, data collected using different systems often result in point clouds of different density. Unfortunately, no work exists in the literature on the impacts of reducing point density on extracting transportation features on roads. To address this gap, this thesis dedicates an entire Chapter to studying the impacts reducing point cloud density on the quality and the consistency of extracted features. The value of this information lies in three different areas; (i) It helps researchers understand more about the feasibility of extracting different features of the road infrastructure from point clouds of different density, (ii) it provides insights on the robustness of the proposed algorithms, and (iii) it helps municipalities interested in acquiring LiDAR equipment to extract geometric attributes of highways with more information about the point density required for such extractions. This information helps entities make an informed decision regarding the quality of point cloud data required and the equipment that should be used to collect such data, which are factors that impact size of investment required.

11.2.2 EVIDENCE BASED HIGHWAY DESIGN

From a highway design perspective, research in this thesis paves the way for the adoption of a novel performance-based design approach in highway engineering. The thesis first develops the tools that facilitate the adoption of such an approach for a set of geometric elements and demonstrates the effectiveness of such an approach in linking safety performance observed on a highway to the highway's design elements. This is demonstrated through a probabilistic assessment of available sight distance on crash prone highways in Alberta, Canada.

An evidence-based design approach has countless advantages including the ability to understand the safety risks of designing a road to meet recommended design standards, and the risks of deviating from those standards. As a result, design guides could be enriched with such information, which ensures that previous experiences are considered when designing new highway facilities and makes the design process highly informed. For instance, the assessment conducted in Chapter

10 of the thesis revealed that a significant proportion of the analyzed highways did not satisfy the SSD requirements of up to 70% of the driving population on crash prone segments in Alberta. This indicates designing roads to meet deterministic design requirements in design codes is not always appropriate and highlights the need to consider such information when designing future highways.

To avoid designing highways where the safety impacts and the ability of the roadway to handle driver demands are unknown, this thesis proposes a framework for the adoption of a performance-based design approach whereby standards used in a particular design are formulated based on the anticipated demand instead of preset standards in design codes. The chances of failure under that demand are then assessed using information collected on local highways and a decision is made on whether such design is adequate [16]. The adoption of such an approach is critical to engineers in their attempts to design more forgiving roads that incorporate human fallibility, which is the cornerstone to creating a safe system and achieving the aims of vision zero.

In addition to helping design safer highways, the performance-based approach could also make the design process more economic. When the safety impacts of deviating from standards recommended for different design elements could be assessed and are fully understood, roads can be designed to meet the anticipated demand instead of preset standards defined in design guides. This helps agencies eliminate the need to meet requirements for nonessential design elements resulting in lower cost and improved value while still providing a safe highway. In a time when budgets are fairly limited due to high the transportation infrastructure deficits, estimated by the Federation of Canadian Municipalities to be around $21.7 billion [229], the US FHWA has recently been promoting the adoption of a PBD approach [54].

11.2.3 OTHER APPLICATIONS

Another important application where the outcomes of this research are useful is in applications developed for an autonomous vehicle. Many Autonomous Vehicle (AV) manufacturers including Google's Waymo have recently adopted LiDAR as an additional sensing technology onboard their fleet. LiDAR helps supplement existing sensors with the capability of surveying surrounding road features regardless of the time of day. Moreover, unlike cameras and other sensors onboard autonomous vehicles, LiDAR sensors are not limited by a field of view. This helps capture a more inclusive image of the surrounding highway at a high level of accuracy. Although point density varies among different LiDAR sensors, some of the procedures developed in this thesis could be

used to process LiDAR point clouds collected by autonomous vehicles. This would help AV recognize more features of their surrounding environment, which would result in more informed self-driving practice.

11.3 Limitations and Future Research

Work in this thesis can be extended in many directions including the following (i) using the proposed algorithms to assess performance of other road design features while estimating the reliability risk associated with those elements, (ii) enhancing the developed extraction algorithms to further improve their accuracy and ensure that they could perform in more complex environments (iii) the development of tools for the extraction of other geometric elements.

Chapters 9 and 10 of this thesis were dedicated to assessing the ability of existing crash prone highway segments to handle driver demand for stopping sight distance. Moreover, safety impacts of failure to meet the sight distance requirements were evaluated. Although the assessment did account for variability in reaction time, speed, and deceleration rates among different drivers, the assessment did not take into account potential variation in other attributes such as eye height (depending on the vehicle driven) and target height (depending on the type of target) could also be probabilistically modelled when estimating available sight distance. While major variations in those variables are not expected, it is recommended that future research integrate this variability into similar sight distance assessments. Another major challenge that is common when performing probabilistic assessments lies in the ability to identify a statistical distribution that accurately models the different probabilistic variables. Achieving this requires large scale observation of driver behavior which is not always possible. In this study, this was only achieved for speeds, however, future studies are encouraged to consider collecting such information for other probabilistic variables when replicating the assessment.

Another opportunity for future research is replicating the performance-based assessment conducted for SSD for other roadway design elements and other features of road infrastructure. For instance, the thesis proposes a LiDAR-based method to extract horizontal curve attributes, including curve radii. Similar to SSD, the minimum radius used to design horizontal curves is also a design variable that can be modelled stochastically since the choice of speed on a specific curve varies from one driver to another. Assessing whether existing horizontal curves meet the minimum radius required by drivers to safely negotiate curved segments on highways and the impacts of that

on the safety performance on different segments could be achieved in future research. Such assessments would help identify gaps that would result in the improvement of the Performance-Based Design framework that was proposed in this thesis.

The proposed algorithms could also be used to update roadside design guides with information on the design of clearzones based on a performance-based assessment of side slopes. In the AASHTO road side design guide, the design of clearzones is governed by the traffic volume anticipated on a particular segment, highway speeds, and the side slopes on the segment [230]. These guidelines were developed based on limited empirical evidence that dates back to the 1970s [230]. The algorithm proposed in Chapter 4 of this thesis for the extraction of side slopes could be used to develop an improved understanding of the relationships between side slopes and roadside safety based on the performance observed on existing road infrastructure.

The research could also be extended to preform reliability assessments of different road geometric design elements. In geometric design, reliability analysis is used to evaluate the risk of a particular design feature not meeting design requirements. Although research does exist in this area [14,154], most existing studies develop models where supply (e.g., available stopping sight distance) is predicted using an empirical equation which is a function of certain road features or measured off dated design drawings[14]. Using the algorithms proposed in this thesis, such an assessment could be conducted using information extracted from the LiDAR scans. This accurately reflects existing conditions in the field.

In addition to using the proposed algorithms to assess the integrity of existing road infrastructure and to help update information in design guides, work in this thesis could also be extended by improving the performance of the proposed algorithms and developing other algorithms for the extraction of other geometric elements. Furthermore, even the algorithms that were developed could benefit from some further research. Although the algorithms are effective in large scale extraction of multiple geometric elements, the algorithms suffer from a few limitations. In case of the cross-section extraction code, for instance, the algorithm is highly sensitive to the existence of road side vegetation. In fact, the existence of vegetation on the side of the road has been one of the main reasons the extraction of side slope information from LiDAR has not been attempted in previous research. One way in which future research could improve the extraction is by using machine learning techniques to train algorithms on the existence of roadside vegetation, which

enhances the algorithms ability to filter out those points. Machine learning algorithms could also be more effective in classifying overhead objects into bridges and non-bridges. In fact, further classification of objects into overhead signs, single cable powerlines, and multi-cable power lines might also be possible using machine learning tools. Another limitation of the overhead object detection algorithm that could be improved in future research is its inability to detect power lines with a very low point density. Although the algorithm is programmed to check for LiDAR points within the lateral vicinity of power lines where point density is low, there are some instances where even lateral point density is sparse; his could be resolved by adopting region growing techniques.

Future research could also explore the feasibility of extracting attributes of complex horizontal curves from LiDAR. While the proposed algorithm is effective in the estimation of the attributes of simple curves, complex curves such as reverse curves and curves with spiral transitions pose some challenges that impact the accuracy of the extractions.

The proposed algorithms could also be enhanced to perform in AV environments. Although, in this thesis, the focus was on the applications of LiDAR in the infrastructure assessments and roadway design, LiDAR datasets are usually processed in a similar manner when they are used to extract information for AVs. The main difference is that, in AV systems, focus shifts from processing of large quantities of data (e.g., a long segment or an entire highway corridor) in a short amount of time to real-time processing of small portions of data. In other words, the primary focus when developing the algorithms shifts from being able to assess as much of the road infrastructure as possible in a few seconds or minutes to assessing data within close proximity of a vehicle in the milliseconds (i.e., instantaneous assessment of small datasets). Most of the work that exists in this area has focused on extracting information that would help vehicles maintain their path such as road edges and lane markings. While this information is extremely important, information about geometric elements is also important for AV systems.

214

REFERENCES

[1]   C. Tingvall, N. Haworth, Vision Zero: an ethical approach to safety and mobility, 6th ITE international conference road safety & traffic enforcement: beyond, Vol. 1999, 2000, pp. 6-7.

[2]   Utires, New Road Safety Laws: Progress to Date, The Current State of Global Road Safety Vol. 2018, 2007.

[3]   L. Mooren, R. Grzebieta, S. Job, Safe system–comparisons of this approach in Australia.

[4]   P. Larsson, S.W. Dekker, C. Tingvall, The need for a systems theory approach to road safety, Safety science 48 (9) (2010) 1167-1174.

[5]   F. Wegman, F. Zhang, A. Dijkstra, How to make more cycling good for road safety?, Accident Analysis & Prevention 44 (1) (2012) 19-29.

[6]   J.N. Fahlquist, Responsibility ascriptions and vision zero, Accident Analysis & Prevention 38 (6) (2006) 1113-1118.

[7]   AASHTO, A Policy on Geometric Design of Highways and Streets, 2011, American Association of State Highway Transportation Officials, 2011.

[8]   TAC, Geometric design guide for Canadian roads, in: T.A.o. Canada (Ed.), Transportation Association of Canada, Ottawa, 1999.

[9]   A. Infrastructure;, Highway Geometric Design Guide, Edmonton, Alberta (1999).

[10]   E. Hauer, An exemplum and its road safety morals, Accident Analysis & Prevention 94 (2016) 168-179.

[11]   E. Hauer, SAFETY IN GEOMETRIC DESIGN STANDARDS I: THREE ANECDOTES, 2nd International Symposium on Highway Geometric Design, 2000.

[12]   E. Hauer, Safety in geometric design standards, University of Toronto, Department of Civil Engineering., 1999.

[13]   K. Bauer, D. Harwood, Safety effects of horizontal curve and grade combinations on rural two-lane highways, Transportation Research Record: Journal of the Transportation Research Board (2398) (2013) 37-49.

[14]   S.E.-B. Ibrahim, T. Sayed, Developing safety performance functions incorporating reliability-based risk measures, Accident Analysis & Prevention 43 (6) (2011) 2153-2159.

[15]   D.W. Harwood, C. Sun, Passing sight distance criteria, Transportation Research Board, 2008.

[16]   A. Ghobarah, Performance-based design in earthquake engineering: state of development, Engineering structures 23 (8) (2001) 878-884.

[17]   K.S. Yen, T.A. Lasky, B. Ravani, Cost-Benefit Analysis of Mobile Terrestrial Laser Scanning Applications for Highway Infrastructure, Journal of Infrastructure Systems 20 (4) (2014) 04014022.

[18]   J. Lee, F. Mannering, Impact of roadside features on the frequency and severity of run-off-roadway accidents: an empirical analysis, Accident Analysis & Prevention 34 (2) (2002) 149-161.

[19]   D.J. Findley, K.M. Tsai, Infrastructure Investment Protection with LiDAR, in: N.C.D.o. Transportation (Ed.), 2012.

[20]   B. Ravani, T.A. Lasky, LiDAR for Data Efficiency, in: W.S.D.o. Transport (Ed.), 2011.

[21]   M. Olsen, G. Roe, C. Glennie, F. Persi, M. Reedy, D. Hurwitz, K. Williams, H. Tuss, A. Squellati, M. Knodler, NCHRP 15-44 Guidelines for the Use of Mobile LiDAR in Transportation Applications, 2013, 2013.

[22]   K. Williams, M.J. Olsen, G.V. Roe, C. Glennie, Synthesis of transportation applications of mobile LiDAR, Remote Sensing 5 (9) (2013) 4652-4692.

[23]   B. Schwarz, LIDAR: Mapping the world in 3D, Nature Photonics 4 (7) (2010) 429-430.

[24]   M. Jalayer, J. Gong, H. Zhou, M. Grinter, Evaluation of remote sensing technologies for collecting roadside feature data to support highway safety manual implementation, Journal of Transportation Safety & Security 7 (4) (2015) 345-357.

[25]   B. Riveiro, L. Díaz-Vilariño, B. Conde-Carnero, M. Soilán, P. Arias, Automatic segmentation and shape-based classification of retro-reflective traffic signs from mobile LiDAR data, IEEE Journal of Selected Topics in Applied Earth Observations and Remote Sensing 9 (1) (2016) 295-303.

[26]   T.-A. Teo, C.-M. Chiu, Pole-like road object detection from mobile lidar system using a coarse-to-fine approach, IEEE Journal of Selected Topics in Applied Earth Observations and Remote Sensing 8 (10) (2015) 4805-4818.

[27]   C. Cabo, C. Ordoñez, S. García-Cortés, J. Martínez, An algorithm for automatic detection of pole-like street furniture objects from Mobile Laser Scanner point clouds, ISPRS Journal of Photogrammetry and Remote Sensing 87 (2014) 47-56.

[28]   S.I. El-Halawany, D.D. Lichti, Detection of road poles from mobile terrestrial laser scanner point cloud, Multi-Platform/Multi-Sensor Remote Sensing and Mapping (M2RSM), 2011 International Workshop on, IEEE, 2011, pp. 1-6.

[29]   W.Y. Yan, S. Morsy, A. Shaker, M. Tulloch, Automatic extraction of highway light poles and towers from mobile LiDAR data, Optics & Laser Technology 77 (2016) 162-168.

[30]   M. Lehtomäki, A. Jaakkola, J. Hyyppä, A. Kukko, H. Kaartinen, Detection of vertical pole-like objects in a road environment using vehicle-based laser scanning data, Remote Sensing 2 (3) (2010) 641-664.

[31]   S.A. Gargoum, K. El-Basyouny, J. Sabbagh, K. Froese, Automated Highway Sign Extraction Using Lidar Data, Transportation Research Record: Journal of the Transportation Research Board (2017).

[32]   M. Soilán, B. Riveiro, J. Martínez-Sánchez, P. Arias, Traffic sign detection in MLS acquired point clouds for geometric and image-based semantic inventory, ISPRS Journal of Photogrammetry and Remote Sensing 114 (2016) 92-101.

[33]   A.J. Khattak, H. Shamayleh, Highway safety assessment through geographic information system-based data visualization, Journal of Computing in Civil Engineering 19 (4) (2005) 407-411.

[34]   A. Holgado-Barco, D. González-Aguilera, P. Arias-Sanchez, J. Martinez-Sanchez, Semiautomatic extraction of road horizontal alignment from a mobile LiDAR system, Computer-Aided Civil and Infrastructure Engineering 30 (3) (2015) 217-228.

[35]   Y. Tsai, C. Ai, Z. Wang, E. Pitts, Mobile cross-slope measurement method using lidar technology, Transportation Research Record: Journal of the Transportation Research Board (2367) (2013) 53-59.

[36]   G. Haiyan, Automated Extraction of Road Information from Mobile Laser Scanning Data, Department of Geography and Environmental Management, University of Waterloo, 2014.

[37]   P. Kumar, Road features extraction using terrestrial mobile laser scanning system, National University of Ireland Maynooth, 2012.

[38]   C. Ai, A Sensing Methodology for an Intelligent Traffic Sign Inventory and Condition Assessment Using GPS/GIS, Computer Vision and Mobile LiDAR Technologies, Georgia Institute of Technology, 2013.

[39]   A.S. Huang, Lane estimation for autonomous vehicles using vision and lidar, Department of Electrical Engineering and Computer Science, MASSACHUSETTS INSTITUTE OF TECHNOLOGY, 2010.

[40]   W. Lu, Contributions to Lane Marking Based Localization for Intelligent Vehicles, Université Paris Sud-Paris XI, 2015.

[41]   M. Castro, J.A. Anta, L. Iglesias, J.A. Sánchez, GIS-based system for sight distance analysis of highways, Journal of Computing in Civil Engineering 28 (3) (2013) 04014005.

[42]   M. Castro, L. Iglesias, J.A. Sánchez, L. Ambrosio, Sight distance analysis of highways using GIS tools, Transportation research part C: emerging technologies 19 (6) (2011) 997-1005.

[43]   A. Holgado-Barco, B. Riveiro, D. González-Aguilera, P. Arias, Automatic inventory of road cross-sections from mobile laser scanning system, Computer-Aided Civil and Infrastructure Engineering 32 (1) (2017) 3-17.

[44]   R.O. Hamburger, The ATC-58 project: development of next-generation performance-based earthquake engineering design criteria for buildings, Structures Congress 2006: Structural Engineering and Public Safety, 2006, pp. 1-8.

[45]   S. Khan, J. Jiang, Performance-Based Seismic Design for the Vancouver Evergreen Line Rapid Transit Project—Process, Challenges, and Innovative Design Solutions, Structures Congress 2015, 2015, pp. 573-584.

[46]   M.L. Marsh, S.J. Stringer, Performance-based seismic bridge design, Transportation Research Board, 2013.

[47]   A.M. Billah, M.S. Alam, Performance-based seismic design of shape memory alloy–reinforced concrete bridge piers. I: Development of performance-based damage states, Journal of Structural Engineering 142 (12) (2016) 04016140.

[48]   A.M. Billah, M.S. Alam, Seismic performance evaluation of multi-column bridge bents retrofitted with different alternatives using incremental dynamic analysis, Engineering structures 62 (2014) 105-117.

[49]   K. Mackie, B. Stojadinović, Performance-based seismic bridge design for damage and loss limit states, Earthquake Engineering & Structural Dynamics 36 (13) (2007) 1953-1971.

[50]   M. Priestley, G. Calvi, M. Kowalsky, Direct displacement-based seismic design, 2005 NZSEE Conference, 2007.

[51]   S. Leelataviwat, S.C. Goel, B. Stojadinović, Energy-based seismic design of structures using yield mechanism and target drift, Journal of Structural Engineering 128 (8) (2002) 1046-1054.

[52]   J. Moehle, G.G. Deierlein, A framework methodology for performance-based earthquake engineering, 2004.

[53]   B.L. Ray, E.M. Ferguson, J.K. Knudsen, R.J. Porter, J. Mason, Performance-Based Analysis of Geometric Design of Highways and Streets, 2014.

[54]   FHWA, Performance-Based Practical Design, Vol. 2017, US Department of Transportation, Federal Highway Adminstration, 2017.

[55]   L. Zhou, Z. Deng, LIDAR and vision-based real-time traffic sign detection and recognition algorithm for intelligent vehicle, 17th International IEEE Conference on Intelligent Transportation Systems (ITSC), IEEE, 2014, pp. 578-583.

[56] W. Zhang, LIDAR-based road and road-edge detection, Intelligent Vehicles Symposium (IV), 2010 IEEE, IEEE, 2010, pp. 845-848.

[57] A. Serna, B. Marcotegui, Urban accessibility diagnosis from mobile laser scanning data, ISPRS Journal of Photogrammetry and Remote Sensing 84 (2013) 23-32.

[58] C. McElhinney, P. Kumar, C. Cahalane, T. McCarthy, Initial results from European Road Safety Inspection (EURSI) mobile mapping project, ISPRS Commission V Technical Symposium, Vol. 2007, 2010, pp. 440-445.

[59] A. Jaakkola, J. Hyyppä, H. Hyyppä, A. Kukko, Retrieval algorithms for road surface modelling using laser-based mobile mapping, Sensors 8 (9) (2008) 5238-5249.

[60] P. Kumar, C.P. McElhinney, P. Lewis, T. McCarthy, An automated algorithm for extracting road edges from terrestrial mobile LiDAR data, ISPRS Journal of Photogrammetry and Remote Sensing 85 (2013) 44-55.

[61] P. Kumar, C.P. McElhinney, P. Lewis, T. McCarthy, Automated road markings extraction from mobile laser scanning data, International Journal of Applied Earth Observation and Geoinformation 32 (2014) 125-137.

[62] H. Guan, J. Li, Y. Yu, C. Wang, M. Chapman, B. Yang, Using mobile laser scanning data for automated extraction of road markings, ISPRS Journal of Photogrammetry and Remote Sensing 87 (2014) 93-107.

[63] M. Thuy, F. León, Lane detection and tracking based on lidar data, Metrology and Measurement Systems 17 (3) (2010) 311-321.

[64] L. Yan, H. Liu, J. Tan, Z. Li, H. Xie, C. Chen, Scan line based road marking extraction from mobile LiDAR point clouds, Sensors 16 (6) (2016) 903.

[65] X. Chen, B. Kohlmeyer, M. Stroila, N. Alwar, R. Wang, J. Bach, Next generation map making: geo-referenced ground-level LIDAR point clouds for automatic retro-reflective road feature extraction, Proceedings of the 17th ACM SIGSPATIAL International Conference on Advances in Geographic Information Systems, ACM, 2009, pp. 488-491.

[66] A. Vu, Q. Yang, J.A. Farrell, M. Barth, Traffic sign detection, state estimation, and identification using onboard sensors, 16th International IEEE Conference on Intelligent Transportation Systems (ITSC 2013), IEEE, 2013, pp. 875-880.

[67] S. Weng, J. Li, Y. Chen, C. Wang, Road traffic sign detection and classification from mobile LiDAR point clouds, 2015 ISPRS International Conference on Computer Vision in Remote Sensing, International Society for Optics and Photonics, 2016, pp. 99010A-99010A-99017.

[68] C. Ai, Y.-C.J. Tsai, Critical assessment of an enhanced traffic sign detection method using mobile LiDAR and INS technologies, Journal of Transportation Engineering 141 (5) (2014) 04014096.

[69] J. Landa, D. Prochazka, Automatic road inventory using LiDAR, Procedia Economics and Finance 12 (2014) 363-370.

[70] S. Wu, C. Wen, H. Luo, Y. Chen, C. Wang, J. Li, Using mobile LiDAR point clouds for traffic sign detection and sign visibility estimation, 2015 IEEE International Geoscience and Remote Sensing Symposium (IGARSS), IEEE, 2015, pp. 565-568.

[71] C.V. Zegeer, D.W. Reinfurt, W.W. Hunter, J. Hummer, R. Stewart, L. Herf, Accident effects of sideslope and other roadside features on two-lane roads, Transportation Research Record (1195) (1988).

[72] H. Zheng, R. Wang, S. Xu, Recognizing Street Lighting Poles From Mobile LiDAR Data, IEEE Transactions on Geoscience and Remote Sensing 55 (1) (2017) 407.

[73]   S. Pu, M. Rutzinger, G. Vosselman, S.O. Elberink, Recognizing basic structures from mobile laser scanning data for road inventory studies, ISPRS Journal of Photogrammetry and Remote Sensing 66 (6) (2011) S28-S39.

[74]   G. Vosselman, B.G. Gorte, G. Sithole, T. Rabbani, Recognising structure in laser scanner point clouds, International Archives of Photogrammetry, Remote Sensing and Spatial Information Sciences 46 (8) (2004) 33-38.

[75]   B. Wu, B. Yu, W. Yue, S. Shu, W. Tan, C. Hu, Y. Huang, J. Wu, H. Liu, A voxel-based method for automated identification and morphological parameters estimation of individual street trees from mobile laser scanning data, Remote Sensing 5 (2) (2013) 584-611.

[76]   M. Lehtomäki, A. Jaakkola, J. Hyyppä, J. Lampinen, H. Kaartinen, A. Kukko, E. Puttonen, H. Hyyppä, Object classification and recognition from mobile laser scanning point clouds in a road environment, IEEE Transactions on Geoscience and Remote Sensing 54 (2) (2016) 1226-1239.

[77]   M. Lato, J. Hutchinson, M. Diederichs, D. Ball, R. Harrap, Engineering monitoring of rockfall hazards along transportation corridors: using mobile terrestrial LiDAR, Nat. Hazards Earth Syst. Sci 9 (3) (2009) 935-946.

[78]   P. Miller, J. Mills, S. Barr, M. Lim, D. Barber, G. Parkin, B. Clarke, S. Glendinning, J. Hall, Terrestrial laser scanning for assessing the risk of slope instability along transport corridors, (2008).

[79]   R. Souleyrette, S. Hallmark, S. Pattnaik, M. O'Brien, D. Veneziano, Grade and cross slope estimation from LiDAR-based surface models, 2003.

[80]   K. Zhang, H.C. Frey, Road grade estimation for on-road vehicle emissions modeling using light detection and ranging data, Journal of the Air & Waste Management Association 56 (6) (2006) 777-788.

[81]   J.J. Dawkins, Model based off-road terrain profile estimation, 2014 American Control Conference, IEEE, 2014, pp. 2792-2797.

[82]   C.-W. Wu, S.-H. Chio, 吳志文, 邱式鴻, Road surface modeling from vehicle-borne point cloud by profile analysis, 33rd Asian Conference on Remote Sensing 2012, ACRS 2012, Vol. 2, 2012, pp. 1031-1040.

[83]   J.-Y. Han, A. Chen, Y.-T. Lin, Image-Based Approach for Road Profile Analyses, Journal of Surveying Engineering 142 (1) (2015) 06015003.

[84]   S. Higuera de Frutos, M. Castro, A Method to Identify and Classify the Vertical Alignment of Existing Roads, Computer-Aided Civil and Infrastructure Engineering (2017).

[85]   P. Di Mascio, M. Di Vito, G. Loprencipe, A. Ragnoli, Procedure to determine the geometry of road alignment using GPS data, Procedia-Social and Behavioral Sciences 53 (2012) 1202-1215.

[86]   K. Baass, J. Vouland, DÉTERMINATION DE L'ALIGNEMENT ROUTIER À PARTIR DE TRACES GPS Transportation Association of Canada, Calgary, Alberta, 2005.

[87]   D.J. Findley, C.V. Zegeer, C.A. Sundstrom, J.E. Hummer, W. Rasdorf, T.J. Fowler, Finding and measuring horizontal curves in a large highway network: a GIS approach, Public Works Management & Policy 17 (2) (2012) 189-211.

[88]   W. Rasdorf, D.J. Findley, C.V. Zegeer, C.A. Sundstrom, J.E. Hummer, Evaluation of GIS applications for horizontal curve data collection, Journal of Computing in Civil Engineering 26 (2) (2011) 191-203.

[89]   M. Imran, Y. Hassan, D. Patterson, GPS–GIS-Based Procedure for Tracking Vehicle Path on Horizontal Alignments, Computer-Aided Civil and Infrastructure Engineering 21 (5) (2006) 383-394.

[90]   C. Ai, Y. Tsai, Automatic horizontal curve identification and measurement method using GPS data, Journal of Transportation Engineering 141 (2) (2014) 04014078.

[91]   Y.J. Tsai, J. Wu, Z. Wang, Z. Hu, Horizontal roadway curvature computation algorithm using vision technology, Computer-Aided Civil and Infrastructure Engineering 25 (2) (2010) 78-88.

[92]   J. Kim, J.-C. Lee, I.-J. Kang, S.-Y. Cha, H. Choi, T.-G. Lee, Extraction of geometric information on highway using terrestrial laser scanning technology, Int. Arch. Photogramm. Remote Sens. Spat. Inf. Sci 37 (2008) 539-544.

[93]   M. Castro, S. Lopez-Cuervo, M. Paréns-González, C. de Santos-Berbel, LIDAR-based roadway and roadside modelling for sight distance studies, Survey Review (2016) 1-7.

[94]   Y. Tsai, Q. Yang, Y. Wu, Use of Light Detection and Ranging Data to Identify and Quantify Intersection Obstruction and Its Severity, Transportation Research Record: Journal of the Transportation Research Board (2241) (2011) 99-108.

[95]   Alberta Transportation, Vertical Clearance Measurements (VCL2), Alberta Infrastructure and Transportation 2014, p. 13.

[96]   R.G. Lauzon, Automated vertical clearance measurement during photolog operations, 2000.

[97]   W. Liu, S.-e. Chen, E. Hasuer, Bridge Clearance Evaluation Based on Terrestrial LIDAR Scan, Journal of Performance of Constructed Facilities 26 (4) (2012).

[98]   I. Puente, B. Akinci, H. González-Jorge, L. Díaz-Vilariño, P. Arias, A semi-automated method for extracting vertical clearance and cross sections in tunnels using mobile LiDAR data, Tunnelling and Underground Space Technology 59 (2016) 48-54.

[99]   S.-E. Chen, W. Liu, H. Bian, B. Smith, 3D LiDAR scans for bridge damage evaluations, Bridges (2014).

[100]   H. Bian, L. Bai, S.-E. Chen, S.-G. Wang, Lidar based edge-detection for bridge defect identification, SPIE Smart Structures and Materials+ Nondestructive Evaluation and Health Monitoring, International Society for Optics and Photonics, 2012, pp. 83470X-83470X-83410.

[101]   B. Guldur, J.F. Hajjar, Laser-based structural sensing and surface damage detection, Department of Civil and Environmental Engineering Reports. Report No. NEU-CEE-2014-03. Department of Civil and Environmental Engineering, Northeastern University, Boston, Massachusetts. http://hdl. handle. net/2047/d20015559 (2014).

[102]   B. Jafari, A. Khaloo, D. Lattanzi, Long-term monitoring of structures through point cloud analysis, SPIE Smart Structures and Materials+ Nondestructive Evaluation and Health Monitoring, International Society for Optics and Photonics, 2016, pp. 98052K-98052K-98058.

[103]   M. Castro, S. Lopez-Cuervo, M. Paréns-González, C. de Santos-Berbel, LIDAR-based roadway and roadside modelling for sight distance studies, Survey Review 48 (350) (2016) 309-315.

[104]   H. Guan, J. Li, S. Cao, Y. Yu, Use of mobile LiDAR in road information inventory: a review, International Journal of Image and Data Fusion 7 (3) (2016) 219-242.

[105]   J. Kemeny, K. Turner, Ground-based LiDAR: rock slope mapping and assessment. Federal Highway Administration report, FHWA-CFL/TD-08-006., Available at http:// www. iaeg.

info/ portals/ 0/ Content/ Commissions/ Comm19/ GROUND-BASED LiDAR Rock Slope Mapping and Assessment. pdf, 2008.

[106] RIEGL, RIEGL VMX-450 Data Sheet, RIEGL Laser Measurment Systems, 2015.

[107] P. Steel, D. Mesher, J. Adamson, Development of a Road Safety Audit Network Screening Tool, Twenty-Fourth Canadian Multidisciplinary Road Safety Conference, 2014.

[108] S.A. Gargoum, K. El-Basyouny, J. Sabbagh, Assessing stopping and passing sight distance on highways using mobile lidar data, Journal of Computing in Civil Engineering 32 (4) (2018) 04018025.

[109] E. Hildebrand, P. Lougheed, T. Hanson, Relating roadside collisions to highway clear zone width, 2007.

[110] C. Liu, T.J. Ye, Run-off-road crashes: an on-scene perspective, 2011.

[111] FDOT, Florida's Design Criteria for Resurfacing, Restoration and Rehabilitation (RRR) of Streets and Highways in: F.D.o.T.P.P. Manual (Ed.), Vol. 1, 2012.

[112] D. Wang, Cross Slope: Revised Specification Highlights, in: F. DOT (Ed.), State Construction Office, Tallahassee, 2010.

[113] Holland, Holland Surveyors founder launches road slope measurement tool with Fowler Wyler Inclinometer, 2013.

[114] R. Singh, D. Artman, D. Brinton, L. Brown, Cross Slope Verification Surveys, in: O.D.o. Transport (Ed.), ODOT Surveyor's Conference, Oregon, 2002.

[115] R. Souleyrette, S. Hallmark, Grade and Cross-Slope FROM LIDAR DATA, National Consortia on Remote Sensing in Transportation, University of California, Santa Barbara, 2003.

[116] J.H. Friedman, Multivariate adaptive regression splines, The annals of statistics (1991) 1-67.

[117] M.S. Milborrow, Package 'earth', Citeseer.

[118] A. Infrastructure, Highway Geometric Design Guide, Edmonton, Alberta (1999).

[119] Digipas, Heavy Duty Digital Level, Vol. 2017, 2017.

[120] TAC, Geometric Design Guide for Canadian Roads, in: T. Canada (Ed.), Vol. 2, Transportation Association Canada, 2009.

[121] FDOT, HOT BITUMINOUS MIXTURES – GENERAL CONSTRUCTION REQUIREMENTS., in: F.D.o. Transport (Ed.), Florida, 2010.

[122] A. Holgado-Barco, D. Gonzalez-Aguilera, P. Arias-Sanchez, J. Martinez-Sanchez, An automated approach to vertical road characterisation using mobile LiDAR systems: Longitudinal profiles and cross-sections, ISPRS Journal of Photogrammetry and Remote Sensing 96 (2014) 28-37.

[123] FHWA, RDs and Curves_2005-2008, in: F.O.o. Safety (Ed.), 2010.

[124] S.M. Easa, Simple numerical method for solving horizontal circular curves, Journal of surveying engineering 120 (1) (1994) 44-48.

[125] R. Andrášik, M. Bíl, Efficient road geometry identification from digital vector data, Journal of Geographical Systems 18 (3) (2016) 249-264.

[126] H. Xu, D. Wei, Improved Identification and Calculation of Horizontal Curves with Geographic Information System Road Layers, Transportation Research Record: Journal of the Transportation Research Board (2595) (2016) 50-58.

[127] A.C. Estes, D.M. Frangopol, Updating bridge reliability based on bridge management systems visual inspection results, Journal of Bridge Engineering 8 (6) (2003) 374-382.

[128] B. Riveiro, D. Jauregui, P. Arias, J. Armesto, R. Jiang, An innovative method for remote measurement of minimum vertical underclearance in routine bridge inspection, Automation in Construction 25 (2012) 34-40.

[129] V. Gattulli, L. Chiaramonte, Condition Assessment by Visual Inspection for a Bridge Management System, Computer-Aided Civil and Infrastructure Engineering 20 (2) (2005) 95-107.

[130] S. Gargoum, L. Karsten, K. El-Basyouny, Network level clearance assessment using lidar to improve the reliability and efficiency of issuing over-height permits on highways, Transportation Research Record (2018) 0361198118758687.

[131] B. Nguyen, I. Brilakis, Understanding the problem of bridge and tunnel strikes caused by over-height vehicles, (2016).

[132] FHWA, Interstate System Conditions and Performance, in: F.H. Adminstration (Ed.), 2013.

[133] J. Wang, X. Ye, Application of laser collision avoidance system for crossroads, Beijing Evening 485 (2007).

[134] A.K. Agrawal, BRIDGE VEHICLE IMPACT ASSESSMENT, The City College of New York, New York, NY, 2011.

[135] Alberta Transportation, Budget 2016 Highlights, Vol. 2016, Alberta, 2016.

[136] T.F. Fwa, The handbook of highway engineering, CRC Press, 2005.

[137] B. Lipiner, Bridge underpass on Route 150 in Wallingford closing again this month, Vol. 2018, Wallingford, Oxfordshire, 2017.

[138] A. Hammad, J. Yan, B. Mostofi, Recent development of bridge management systems in Canada, 2007 Annual Conference and Exhibition of the Transportation Association of Canada: Transportation-An Economic Enabler (Les Transports: Un Levier Economique), 2007.

[139] A. Transportation, Existing Structures in the Provincial Highway Corridor, in: T.I.M. System (Ed.), Alberta, 2017, p. 328.

[140] FHWA, State Bridge Inspection Data, Structurally Deficient Ratings, in: N.B.I. U.S. Federal Highway Administration (Ed.), 2013.

[141] R. Zirbes, Scientific Visualization: Volume Surface Rendering, 2017.

[142] N.S. Altman, An introduction to kernel and nearest-neighbor nonparametric regression, The American Statistician 46 (3) (1992) 175-185.

[143] M. Ester, H.-P. Kriegel, J. Sander, X. Xu, A density-based algorithm for discovering clusters in large spatial databases with noise, Kdd, Vol. 96, 1996, pp. 226-231.

[144] J. Johnson, The Shape of Data Clusters and DBScan, WorldPress., 2013.

[145] D.S. Moore, S. Kirkland, The basic practice of statistics, WH Freeman New York, 2007.

[146] S.P. Washington, M.G. Karlaftis, F.L. Mannering, Statistical and econometric methods for transportation data analysis, 2003.

[147] M. Rutzinger, F. Rottensteiner, N. Pfeifer, A comparison of evaluation techniques for building extraction from airborne laser scanning, IEEE Journal of Selected Topics in Applied Earth Observations and Remote Sensing 2 (1) (2009) 11-20.

[148] OPSD, Minimum Vertical Clearances For Areial Cable System, in: O.P.S. Drawing (Ed.), Ontario Department of Transport, Ontario, 2011.

[149] A. Transportation, Bridge Inspection Manual - Vertical Clearance Measurements, in: A. Transportation (Ed.), 2004, pp. 7-8, 7-10.

[150] J. Chang, D. Findley, C. Cunningham, M. Tsai, Considerations for effective lidar deployment by transportation agencies, Transportation Research Record: Journal of the Transportation Research Board (2440) (2014) 1-8.

[151] Alberta Infrastructure, Highway Geometric Design Guide, in: A. Transportation (Ed.), Alberta, 1999.

[152] AASHTO, Policy on geometric design of highways and streets, American Association of State Highway and Transportation Officials, Washington, DC 1 (990) (2004) 158.

[153] TAC, TAC Geometric Design Guide for Canadian Roads, in: T.A.o. Canada (Ed.), 1999.

[154] S.E. Ibrahim, T. Sayed, K. Ismail, Methodology for safety optimization of highway cross-sections for horizontal curves with restricted sight distance, Accident Analysis & Prevention 49 (2012) 476-485.

[155] J. Glennon, Effect of sight distance on highway safety, State-of-the-Art Report (6) (1987).

[156] Y. Hassan, S.M. Easa, Sight distance on horizontal alignments with continuous lateral obstructions, Transportation Research Record 1500 31-42.

[157] S. Clancy, Mobile LiDAR Point Density – Part 2, LiDAR Magazine Spatial Media LLC, Fredrick, MD, 2012.

[158] Q. Wu, H. Yang, M. Wei, O. Remil, B. Wang, J. Wang, Automatic 3D reconstruction of electrical substation scene from LiDAR point cloud, ISPRS Journal of Photogrammetry and Remote Sensing (2018).

[159] B. Douillard, J. Underwood, N. Kuntz, V. Vlaskine, A. Quadros, P. Morton, A. Frenkel, On the segmentation of 3D LIDAR point clouds, Robotics and Automation (ICRA), 2011 IEEE International Conference on, IEEE, 2011, pp. 2798-2805.

[160] T. Brandtberg, T.A. Warner, R.E. Landenberger, J.B. McGraw, Detection and analysis of individual leaf-off tree crowns in small footprint, high sampling density lidar data from the eastern deciduous forest in North America, Remote sensing of Environment 85 (3) (2003) 290-303.

[161] M.L. Clark, D.B. Clark, D.A. Roberts, Small-footprint lidar estimation of sub-canopy elevation and tree height in a tropical rain forest landscape, Remote sensing of Environment 91 (1) (2004) 68-89.

[162] J. Lovell, D.L. Jupp, D. Culvenor, N. Coops, Using airborne and ground-based ranging lidar to measure canopy structure in Australian forests, Canadian Journal of Remote Sensing 29 (5) (2003) 607-622.

[163] S. Luo, J.M. Chen, C. Wang, X. Xi, H. Zeng, D. Peng, D. Li, Effects of LiDAR point density, sampling size and height threshold on estimation accuracy of crop biophysical parameters, Optics express 24 (11) (2016) 11578-11593.

[164] V. Thomas, P. Treitz, J. McCaughey, I. Morrison, Mapping stand-level forest biophysical variables for a mixedwood boreal forest using lidar: an examination of scanning density, Canadian Journal of Forest Research 36 (1) (2006) 34-47.

[165] S. Tesfamichael, J. Van Aardt, F. Ahmed, Estimating plot-level tree height and volume of Eucalyptus grandis plantations using small-footprint, discrete return lidar data, Progress in Physical Geography 34 (4) (2010) 515-540.

[166] N.R. Goodwin, N.C. Coops, D.S. Culvenor, Assessment of forest structure with airborne LiDAR and the effects of platform altitude, Remote sensing of Environment 103 (2) (2006) 140-152.

[167] T. Takahashi, Y. Awaya, Y. Hirata, N. Furuya, T. Sakai, A. Sakai, Stand volume estimation by combining low laser-sampling density LiDAR data with QuickBird panchromatic

imagery in closed-canopy Japanese cedar (Cryptomeria japonica) plantations, International Journal of Remote Sensing 31 (5) (2010) 1281-1301.

[168] M.K. Jakubowski, Q. Guo, M. Kelly, Tradeoffs between lidar pulse density and forest measurement accuracy, Remote sensing of Environment 130 (2013) 245-253.

[169] M. Magnusson, J.E. Fransson, J. Holmgren, Effects on estimation accuracy of forest variables using different pulse density of laser data, Forest Science 53 (6) (2007) 619-626.

[170] K.K. Singh, G. Chen, J.B. Vogler, R.K. Meentemeyer, When big data are too much: Effects of LiDAR returns and point density on estimation of forest biomass, IEEE Journal of Selected Topics in Applied Earth Observations and Remote Sensing 9 (7) (2016) 3210-3218.

[171] X. Liu, Z. Zhang, J. Peterson, S. Chandra, The effect of LiDAR data density on DEM accuracy, Proceedings of the International Congress on Modelling and Simulation (MODSIM07), Modelling and Simulation Society of Australia and New Zealand Inc., 2007, pp. 1363-1369.

[172] C. Zhao, J. Jensen, X. Deng, N. Dede-Bamfo, Impacts of LiDAR sampling methods and point spacing density on DEM generation, Papers in Applied Geography 2 (3) (2016) 261-270.

[173] E. Anderson, J. Thompson, R. Austin, LIDAR density and linear interpolator effects on elevation estimates, International Journal of Remote Sensing 26 (18) (2005) 3889-3900.

[174] I. Tomljenovic, A. Rousell, Influence of point cloud density on the results of automated Object-Based building extraction from ALS data, (2014).

[175] S. Magnussen, E. Næsset, T. Gobakken, Reliability of LiDAR derived predictors of forest inventory attributes: A case study with Norway spruce, Remote sensing of Environment 114 (4) (2010) 700-712.

[176] F. Pirotti, P. Tarolli, Suitability of LiDAR point density and derived landform curvature maps for channel network extraction, Hydrological Processes 24 (9) (2010) 1187-1197.

[177] E.S. Anderson, J.A. Thompson, D.A. Crouse, R.E. Austin, Horizontal resolution and data density effects on remotely sensed LIDAR-based DEM, Geoderma 132 (3-4) (2006) 406-415.

[178] Q. Guo, W. Li, H. Yu, O. Alvarez, Effects of topographic variability and lidar sampling density on several DEM interpolation methods, Photogrammetric Engineering & Remote Sensing 76 (6) (2010) 701-712.

[179] R.C. Olsen, A.M. Puetz, B. Anderson, Effects of lidar point density on bare earth extraction and DEM creation.

[180] AASHTO, Policy on geometric design of highways and streets, American Association of State Highway and Transportation Officials, Washington, DC 1 (990) (2011) 158.

[181] D. Fambro, R. Koppa, D. Picha, K. Fitzpatrick, Driver perception-brake response in stopping sight distance situations, Transportation Research Record: Journal of the Transportation Research Board (1628) (1998) 1-7.

[182] K.J. Anstey, J. Wood, S. Lord, J.G. Walker, Cognitive, sensory and physical factors enabling driving safety in older adults, Clinical psychology review 25 (1) (2005) 45-65.

[183] Road Safety Canada Consulting, Road Safety in Canada, 2011.

[184] S.P. Deligianni, M. Quddus, A. Morris, A. Anvuur, S. Reed, Analyzing and Modeling Drivers' Deceleration Behavior from Normal Driving, Transportation Research Record: Journal of the Transportation Research Board (2663) (2017) 134-141.

[185] M. Green, " How long does it take to stop?" Methodological analysis of driver perception-brake times, Transportation human factors 2 (3) (2000) 195-216.

[186] J.L. Campbell, Human factors guidelines for road systems, Transportation Research Board, 2012.

[187] K. Ismail, T. Sayed, Risk-based framework for accommodating uncertainty in highway geometric design, Canadian Journal of Civil Engineering 36 (5) (2009) 743-753.

[188] D. Gavran, S. Fric, V. Ilić, F. Trpčevski, Sight distance analyses in road design process: Serbian practice, Transport 31 (2) (2016) 250-259.

[189] J. Wood, E. Donnell, Stopping sight distance and horizontal sight line offsets at horizontal curves, Transportation Research Record: Journal of the Transportation Research Board (2436) (2014) 43-50.

[190] M. Sarhan, Y. Hassan, Three-dimensional, probabilistic highway design: sight distance application, Transportation Research Record: Journal of the Transportation Research Board (2060) (2008) 10-18.

[191] M. Hussein, T. Sayed, K. Ismail, A. Van Espen, Calibrating road design guides using risk-based reliability analysis, Journal of Transportation Engineering 140 (9) (2014) 04014041.

[192] K. Ismail, T. Sayed, Risk-based highway design: Case studies from British Columbia, Canada, Transportation Research Record: Journal of the Transportation Research Board (2195) (2010) 3-13.

[193] C. de Santos-Berbel, M. Essa, T. Sayed, M. Castro, Reliability-based analysis of sight distance modelling for traffic safety, Journal of advanced transportation 2017 (2017).

[194] J.S. Wood, E.T. Donnell, Stopping sight distance and available sight distance: new model and reliability analysis comparison, Transportation Research Record: Journal of the Transportation Research Board (2638) (2017) 1-9.

[195] J.L. Campbell, Lichty;, Brown;, Graving;, Richard;, Graham;, O'Laughlin;, Torbic;, Harwood;, Human factors guidelines for road systems, Transportation Research Board, 2012.

[196] A. Montella, A comparative analysis of hotspot identification methods, Accident Analysis & Prevention 42 (2) (2010) 571-581.

[197] M. Tawfeek, K. El-Basyouny, Safety Prediction Modelling and Deployment of Safety

Analyst Software, University of Alberta, 2017.

[198] D.B. Fambro, K. Fitzpatrick, R.J. Koppa, Determination of stopping sight distances, Transportation Research Board, 1997.

[199] C. Jurewicz, T. Makwasha, N. O'Callaghan, Verification of Austroads Road Design Criteria Based on Objective Safety Evidence, Austroads Ltd., Sydney NSW 2000 Australia, 2017.

[200] W.J. Dixon, F.J. Massey, Introduction to statistical analysis, McGraw-Hill New York, 1969.

[201] N.J. Garber, L.A. Hoel, Traffic and highway engineering, Cengage Learning, 2014.

[202] Alberta Transportation, Alberta Traffic Collision Statistics 2014, in: A.T.O.o.T. Safety (Ed.), 2014.

[203] M.K. Janke, Assessing older drivers: Two studies, Journal of Safety Research 32 (1) (2001) 43-74.

[204] J.M. Lyman, G. McGwin, R.V. Sims, Factors related to driving difficulty and habits in older drivers, Accident Analysis & Prevention 33 (3) (2001) 413-421.

[205]   G. McGwin Jr, D.B. Brown, Characteristics of traffic crashes among young, middle-aged, and older drivers, Accident Analysis & Prevention 31 (3) (1999) 181-198.

[206]   D.J. Foley, R.B. Wallace, J. Eberhard, Risk factors for motor vehicle crashes among older drivers in a rural community, Journal of the American Geriatrics Society 43 (7) (1995) 776-781.

[207]   R.A. Marottoli, L.M. Cooney, D.R. Wagner, J. Doucette, M.E. Tinetti, Predictors of automobile crashes and moving violations among elderly drivers, Annals of internal medicine 121 (11) (1994) 842-846.

[208]   G. Li, E.R. Braver, L.-H. Chen, Fragility versus excessive crash involvement as determinants of high death rates per vehicle-mile of travel among older drivers, Accident Analysis & Prevention 35 (2) (2003) 227-235.

[209]   A.K. Maurya, P.S. Bokare, STUDY OF DECELERATION BEHAVIOUR OF DIFFERENT VEHICLE TYPES, International Journal for Traffic & Transport Engineering 2 (3) (2012).

[210]   ITE, Traffic engineering handbook, 7th ed., John Wiley & Sons, 2016.

[211]   W.L. Williams, Driver behavior during the yellow interval, Transportation Research Record 644 (1977) 75-78.

[212]   M.-S. Chang, C.J. Messer, A.J. Santiago, Timing traffic signal change intervals based on driver behavior, (1985).

[213]   T.J. Gates, D.A. Noyce, L. Laracuente, E.V. Nordheim, Analysis of driver behavior in dilemma zones at signalized intersections, Transportation Research Record 2030 (1) (2007) 29-39.

[214]   I. El-Shawarby, H. Rakha, V. Inman, G. Davis, Evaluation of driver deceleration behavior at signalized intersections, Transportation Research Record: Journal of the Transportation Research Board (2018) (2007) 29-35.

[215]   D.C. Gazis, R. Herman, R.W. Rothery, Nonlinear follow-the-leader models of traffic flow, Operations research 9 (4) (1961) 545-567.

[216]   A. Naito, C. Miyajima, T. Nishino, N. Kitaoka, K. Takeda, Driver evaluation based on classification of rapid decelerating patterns, Vehicular Electronics and Safety (ICVES), 2009 IEEE International Conference on, IEEE, 2009, pp. 108-112.

[217]   C. Miyajima, H. Ukai, A. Naito, H. Amata, N. Kitaoka, K. Takeda, Driver risk evaluation based on acceleration, deceleration, and steering behavior, Acoustics, Speech and Signal Processing (ICASSP), 2011 IEEE International Conference on, IEEE, 2011, pp. 1829-1832.

[218]   Z. Wu, Y. Liu, G. Pan, A smart car control model for brake comfort based on car following, IEEE Transactions on Intelligent Transportation Systems 10 (1) (2009) 42-46.

[219]   P. Li, M. Abbas, Stochastic dilemma hazard model at high-speed signalized intersections, Journal of transportation engineering 136 (5) (2009) 448-456.

[220]   J. Wang, K. Dixon, H. Li, J. Ogle, Normal deceleration behavior of passenger vehicles at stop sign-controlled intersections evaluated with in-vehicle global positioning system data, Transportation Research Record: Journal of the Transportation Research Board (1937) (2005) 120-127.

[221]   N. Lerner, Age and driver perception-reaction time for sight distance design requirements, 1995 Compendium of Technical Papers. Institute of Transportation Engineers 65th Annual Meeting. Institute of Transportation Engineers, 1995.

[222] K.I. Ahmed, Modeling drivers' acceleration and lane changing behavior, Massachusetts Institute of Technology, 1999.

[223] G.T. Taoka, Brake reaction times of unalerted drivers, ITE journal 59 (3) (1989) 19-21.

[224] R.H. Wortman, J.S. Matthias, An evaluation of driver behavior at signalized intersections, Arizona Department of Transportation Phoenix, Arizona, 1983.

[225] M. Sivak, D.V. Post, P.L. Olson, R.J. Donohue, Automobile rear lights: Effects of the number, mounting height, and lateral position on reaction times of following drivers, Perceptual and Motor Skills 52 (3) (1981) 795-802.

[226] P. Ranjitkar, T. Nakatsuji, Y. Azuta, G. Gurusinghe, Stability analysis based on instantaneous driving behavior using car-following data, Transportation Research Record: Journal of the Transportation Research Board (1852) (2003) 140-151.

[227] AASHTO, Highway safety manual, AASHTO, National Research Council . Transportation Research Board. Task Force on Development of the Highway Safety Manual

Transportation Officials. Joint Task Force on the Highway Safety Manual, 2010.

[228] C. Jurewicz, T. Makwasha, N. O'Callaghan, Verification of Austroads road design criteria based on objective safety evidence, 2017.

[229] J.B.J.D.S. Mullin, Crisis and Opportunity: Time for a National Infrastructure Plan for Canada, Canada2020, 2014.

[230] T.O.T.F.f.R. Safety, Roadside design guide, AASHTO, 2011.